ON USING FILM BOILING TO PROMOTE CHEMICAL CHANGE OF ORGANIC LIQUIDS

by Sung Ryel Choi

This thesis/dissertation document has been electronically approved by the following individuals:

Avedisian,C Thomas (Chairperson)

Anton,Alan Brad (Minor Member)

Gouldin,Frederick Caskey (Minor Member)

ON USING FILM BOILING TO PROMOTE CHEMICAL CHANGE OF ORGANIC LIQUIDS

A Dissertation

Presented to the Faculty of the Graduate School

of Cornell University

In Partial Fulfillment of the Requirements for the Degree of

Doctor of Philosophy

by

Sung Ryel Choi

August 2010

© 2010 Sung Ryel Choi

ON USING FILM BOILING TO PROMOTE CHEMICAL CHANGE OF ORGANIC LIQUIDS

Sung Ryel Choi, Ph. D.

Cornell University 2010

This study presents an experimental demonstration of a chemical reactor based on film boiling. Film boiling is established around a horizontal tube that is immersed in a bulk organic reactant pool of pure methanol and ethylene glycol. Chemical reactions are promoted within the vapor layer due to a high temperature inherent to film boiling. Product gases are measured and analyzed to illustrate the efficacy of the reactor. Catalytic reactions using a platinum catalyst coating and thermal decomposition for a bare tube are investigated. The heater tube surface temperature is the primary parameter and results at various sub-coolings are reported.

Experimental results show the feasibility of film boiling to affect chemical change of methanol and ethylene glycol through catalytic and thermal decomposition. Catalytic conversion of methanol and ethylene glycol are observed below the heater temperature of approximately 1300K to avoid possible catalyst sintering at a higher temperature. Thermal decomposition of methanol and ethylene glycol started at approximately 1250K and 1050K respectively. The primary product is synthesis gas and is near stoichiometric proportions for methanol with a small quantity of CH_4 produced. For ethylene glycol, condensable by-products are found as well as gaseous products of CH_4, C_2H_2 and C_2H_4 suggesting various secondary reactions. Boiling curves are also reported which show higher fluxes with a catalyst compared to a bare

tube. Conversion efficiency is estimated by an energy rate balance on the control volume of the vapor film. The calculated efficiency resulted in the maximum conversion of 40% for methanol and 27% for ethylene glycol. Endurance tests are conducted to examine the catalyst's performance over prolonged exposure under the film boiling reactor's operating conditions. Carbon deposits forming on the catalyst tube appear to degrade performance. In addition, the experiments of ethylene glycol reveal bulk liquid sub-cooling effects of film boiling instability and low product yields.

BIOGRAPHICAL SKETCH

The author was born on February 25, 1974 to Daesik Choi and Bokja Shim in Seoul, Korea. After mandatory military service (from 1995 to 1997), he received his B.S. in Chemical Engineering from Chung-Ang University in 1999 and then a B.S. in Mechanical Engineering from Yonsei University in 2001. He continued to study Mechanical Engineering (specifically, cryogenics) at the advanced level through earning a M.S. in 2003 at Korea Advanced Institute of Science and Technology (KAIST).

The author started his research career as an engineer in an electronic company (SINDORICOH) and then transferred to the Fuel Cell Research Center in Korea Institute of Science and Technology (KIST) in 2004 to diversify his research career. He then moved to the United States in 2006 to pursue his passion for academia at Cornell University where he was a desperate research assistant and pursued studies toward from Fall of 2006 to Summer of 2010.

ACKNOWLEDGEMENTS

The challenging accomplishment of this research has been built on the help and support of many people. First and foremost, I would like to thank my advisor, Prof. C. Thomas Avedisian. He gave me one of the biggest life-changing opportunities with his continuous guidance and encouragement. He has not only taught me a wealth of technical knowledge but also developed my academic attitude as a future scientist or engineer. I would also like to thank the other three committee members. Dr. Wing Tsang, a scientist in the Physical and Chemical Properties Division of the National Institute of Standards and Technology (NIST), gave extremely valuable advices particularly regarding chemistry. Continuous support from Prof. Frederick C. Gouldin encouraged me to persevere through the tough Ph.D. program. Prof. A. Brad Anton's impressive insight and knowledge on chemical engineering was very precious to strengthen the basis of my research regarding chemical reactor design.

This research was supported by NSF grant no. CTS-05-00015 and CBET-09-33521 with Drs. Al Ortega and Ted Bergman as program managers. The grant provided tuitions and stipends for several years as well as funds for the research. I truly would like to thank for this generous supports.

Many thanks also should go to several specialists whose knowledge and skill were indispensible in my research. Dr. William B. Retallic, Vice President of Catacel Corporation, provided advanced catalyst coating techniques. Mr. Tim Brock in Cornell many times advised and assisted me regarding machining. I also thank Dr. Xia Zeng in the Department of Fiber Science & Apparel Design of Cornell for his assistance in GC-MS analysis of liquid reactant concentration.

Besides the technical support to my research, several staff and professors in the Sibley School of Mechanical and Aerospace Engineering at Cornell University

deserve gratitude. Mrs. Marcia Sawyer's constant assistance and encouragement helped me out during the toughest time of my Ph.D. program. I also thank Profs. Stephen B. Pope and Ke Max Zhang for their guidance in thermodynamic classes for the last two semesters of my TA duty.

I also thank my fellow graduate students in the Sibley School at Cornell, especially lab mates Michael S. Moorhead and Frank Yu-Cheng Liu for their friendly helps during my tough time. Special thanks should go to John W. Evangelista. He is one of my best friends. I remember that we always learned many things from each other through daily conversation over not only our research but also broad subjects. I would say that it would be impossible to finalize my research without his help.

Many undergraduate and M.Eng students helped me out on my research. Jens Notholt and Ziyan Huang have my special thanks for their efforts on designing the FIBOR chamber and LabVIEW program in the early time of my Ph.D. program. Matt Chao-Ting Hsueh, Alexander Naydich, Bojeong Kim, and Isaac Sung G. Lee helped me as undergraduate research assistants in the experimental portion of my research. I also send my thanks to Terence Davidovits and again Isaac Sung G. Lee for their efforts on the theoretical analysis portion.

The final but deepest acknowledgement of mine is for my parents, Bokja Shim and Daesik Choi. My achievement would never have been possible without their endless love and trust on me. Their encouragement from the long distance place, Korea, was the strongest motivation by which I was able to accomplish my Ph.D.

TABLE OF CONTENTS

LIST OF FIGURES

LIST OF TABLES

LIST OF SYMBOLS

A_c = cross sectional area of a tube, m^2

A_o = outer surface area of a tube, m^2

c_p = specific heat, J kg^{-1} K^{-1}

$\overline{c}_p$ = molar specific heat, J mol^{-1} K^{-1}

d_i = tube inner diameter, m

d_o = tube outer diameter, m

g = acceleration of gravity, m s^{-2}

h = enthalpy per unit of mole, J mol^{-1}

h_f = enthalpy of formation, J mol^{-1}

$\overline{h}$ = convective heat transfer coefficient, W m^{-2} K^{-1}

ΔH_{fg} = heat of vaporization, J mol^{-1}

ΔH_{rxn} = heat of reaction, J mol^{-1}

I =current, A

k = thermal conductivity, W m^{-1} K^{-1}

l = heater length, m

$\dot{N}$ = molar flow rate, mol sec^{-1}

N^* = molar flow rate per surface area, mol hr^{-1} m^{-2}

Pr = Prandtl number $\left(\nu_m/\alpha\right)$

$\dot{Q}$ = heat transfer rate from tube surface, W

$\dot{Q}_{evap}$ = rate of heat for evaporation of reactant, W

$\dot{Q}_{rxn}$ = rate of heat for chemical reaction, W

$\dot{Q}_{sens}$ = rate of heat for raising vapor temperature, W

$\dot{Q}_{sub}$ = rate of heat loss from liquid/vapor interface to bulk liquid by sub-cooling, W

$\Delta q''$ =heat flux difference of boiling curves, see Fig. 3.1, kW m^{-2}

r = radial coordinate

R = tube radius (d_o/2), m

Ra_{d_o} = Rayleigh number $\left(\frac{g\beta_e \left(T_{sat} - T_\infty\right) d_o^{\,3}}{v_m \alpha} \right)$

T = temperature, K

T_w = tube wall temperature, K

u = velocity, parallel to cylinder, m s^{-1}

V = voltage, V

X = conversion

Y_i = species mass fraction

Greek letters

α = thermal diffusivity, m^2 s^{-1}

α_i = stoichiometric coefficient of product species B_i

β_e =expansion coefficient, K^{-1}

δ = vapor film thickness, m

v = summation of stoichiometric coefficients of product gas

$\overline{v}$ = molar specific volume, L/mol

v_m = momentum diffusivity, m^2s^{-1}

μ = viscosity, kg m^{-1} s^{-1}

ϕ = angle from tube base

ρ = density, kg m^{-3}

ε = emissivity, dimensionless

σ = Stefan-Boltzmann constant, W m^{-2} K^{-4}

ω_i = reaction rate of species 'i', kg m^{-3} s^{-1}

ϖ_i = surface reaction rate parameter of species 'i', kg m^{-2} s^{-1}

Subscripts

in = control volume inlet

out = control volume outlet

P = product

R = reactant

sat = saturation condition

∞ = bulk liquid

v = vapor

l = liquid

CHAPTER 1

INTRODUCTION

1.1 Background and Motivation

Humanity is facing significant challenges of energy shortage caused by the depletion of fossil fuels. The fact has motivated many studies to find new, clean renewable energy sources (Turkenburg et al. 2001) and to find ways to convert low-valued substances, or even waste into useful more high valued fuel sources (Huber et al. 2007).

One example is heavy crude oil. Due to increased refining costs and high sulfur content, heavy crudes are often priced at a discount to lighter ones. The increased viscosity and density also makes production more difficult. But a recent growing demand for energy sources and increased oil prices are attracting interests to harness the low-valued energy source (Behura et al. 2007).

Another low-valued substance is glycerol which is a main byproduct from a renewable energy source, biomass. New ways to convert glycerol into a useful substance (Corma et al. 2007 and 2008) are being developed.

This thesis is relevant to the design of a new style chemical reactor that takes advantage of a heat transfer mechanism, film boiling, to promote chemical reaction. High temperatures generated by film boiling within a bulk liquid offer the opportunity to provide a unique reactor design concept with potential to convert heavier organic compounds, yet in a comparatively low temperature liquid.

Film boiling is a well known heat transfer mechanism that is usually associated with various thermal runaway scenarios in nuclear safety and thermal management of electronic component applications (Higgins 1955, Ruebsamen et al. 1952, Crooks et al. 1962, Lustman 1955). As such, research to understand mechanisms that control it is

typically designed to identify the control values under which film boiling is most likely to occur and, thus, to be avoided in application.

1.2 Physics and Characteristics of Film Boiling for Chemical Conversion

1.2.1 Physics of the Film Boiling Reactor

Pool boiling has four main regimes (Figure 1.1): free convection boiling, nuleate boiling, transition and film boiling. As a heated solid surface is in the nucleate boiling mode, numerous vapor bubbles form, break away from the surface, rise, and reach the free surface as shown in Figure 1.2 (a). Heat transfer from the surface is significant due to the turbulent bubbles and the surface temperature makes only a few degrees higher than the surrounding saturated liquid. When the solid surface is heated further, the boiling regime enters a transition mode. In this regime a vapor film forms around the surface due to bubble coalescence, and portions of this film break off forming bubbles that rise briefly exposing a portion of the surface. This film collapse and reformation is characteristic of the transition regime. When the surface temperature is further increased, the vapor film around the surfac becomes stable. This is the entrance of the film boiling regime. In the film boiling regime, the surface is completely covered by a stable vapor blanket as in Figure 1.2 (b). Comparably low thermal conductivity of the vapor creates a high wall temperature with a large temperature gradient across the vapor film. In this regime, the wall temperature is high enough to overcome the activation energy barrier, chemical reaction will occur around the wall. This high wall temperature is the chrateristic of film boiling that can be utilized to promote chemical reaction.

Chemical reaction in film boiling is most easily considered for the configuration of a horizontal tube. Figure 1.3 is an idealized schematic (cross-sectional view) of this configuration. A hozontal tube of radius R is immersed into a pool of

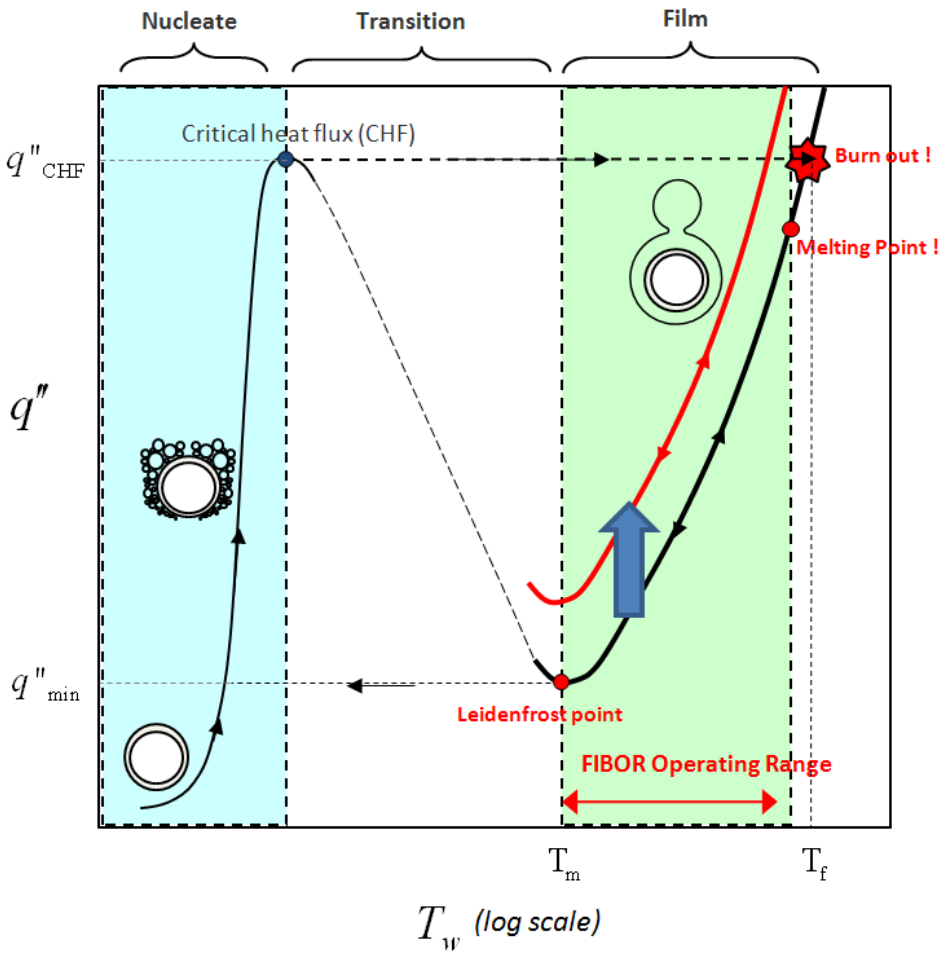

Figure 1.1 Boiling curve (FIBOR operating domain)

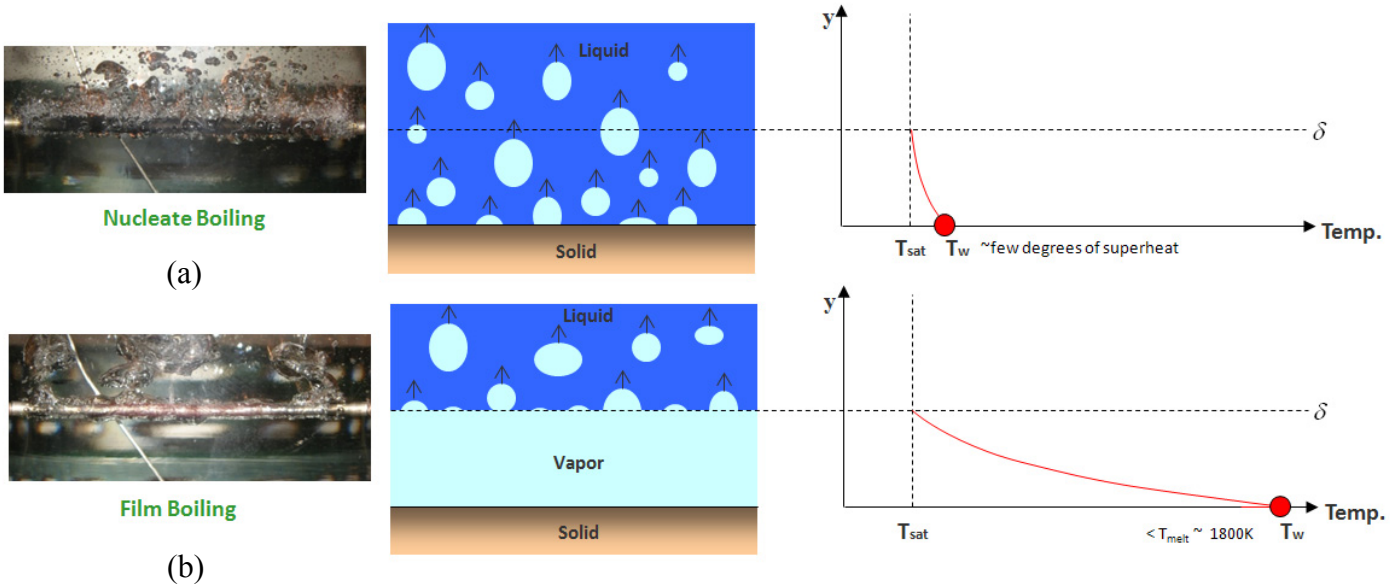

Figure 1.2 Two boiling modes of (a) nucleate boiling and (b) film boiling

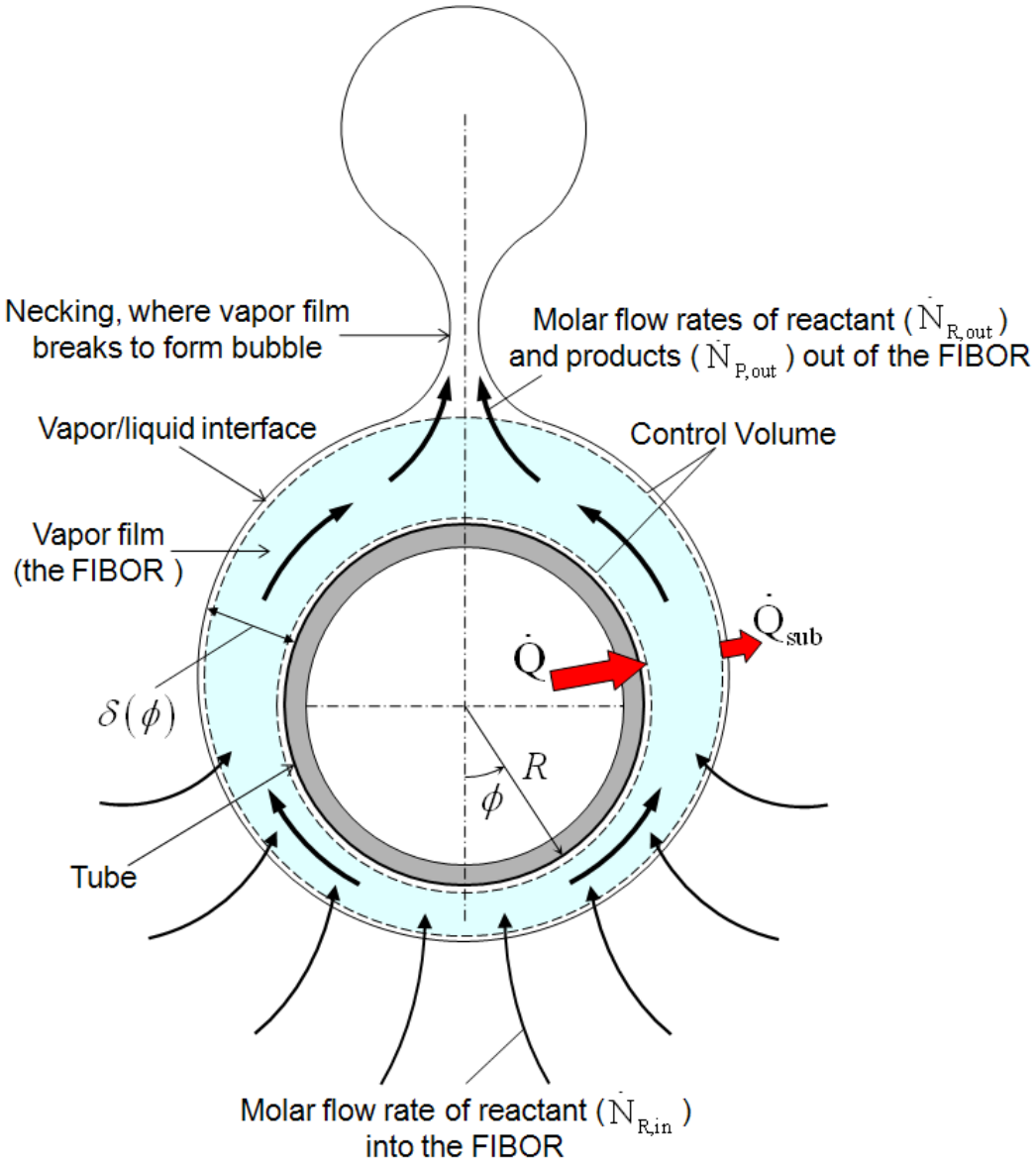

Figure 1.3 Concept and physics of film boiling reactor (not to scale: in practice δ<<R)

: Control volume of energy balance to estimate the conversion of FIBOR

reactant liquid and it is heated by electrical joule heating. As boiling around the tube is in the film boiling regime, a stable vapor film of thicknesss δ ultimately completely blankets the tube. Liquid evaporates at the liquid/vapor interface and the resulting vapors are transported around the tube under the action of buoyancy (for the configuration examined here experimentally, though a forced flow could accomplish the same effect perhaps more effectively). As the vapor flows around the tube, reactions may occur at rates appropriate to the gas temperature. Conversion by catalyic means (i.e., if the tube is coated with a suitable catalyst) or by thermal decomposition (i.e. if the tube is bare) forms product gases that are transported and collect at the top of the tube where vapor bubbles form: the catalytic reaction is by the mechanism of heterogeneous reaction with the wall material while the thermal deomposition is by the mechanism of homogeneous reaction in the gas phase (Cussler 2005). The bubbles percolate through the liquid pool in a manner typical of film boiling. The product gases are released as the bubbles break through the free liquid surface of the pool. We have termed this process of chemical reaction by the method as described above a Film Boiling Reactor (or FIBOR) (Urban et al. 2006). It can be created on any geometry and orientation, but in this research we employ a horizontal tube which is easy to fabricate film boiling. Many studies on film boiling (no chemical reaction) are besed on the geometry of a horizontal tube (Okuyama and Iida 1994; Avedisian et al. 2008; etc).

Figure 1.4 depicts the transport paths envisioned for film boiling and chemical reaction. Organic liquid evaporates (a) and diffuses to the surface or nearby (b). Part of the reactant is carried around the tube (c) in the vapor film (thickness) arising from flow (e) and part makes it to the wall (b), where it is adsorbed and reacts if the tube is coated with a catalyst (while thermal decompositin can occur near the tube if the temperature is high enough for the reaction). Products diffuse back into the film (d)

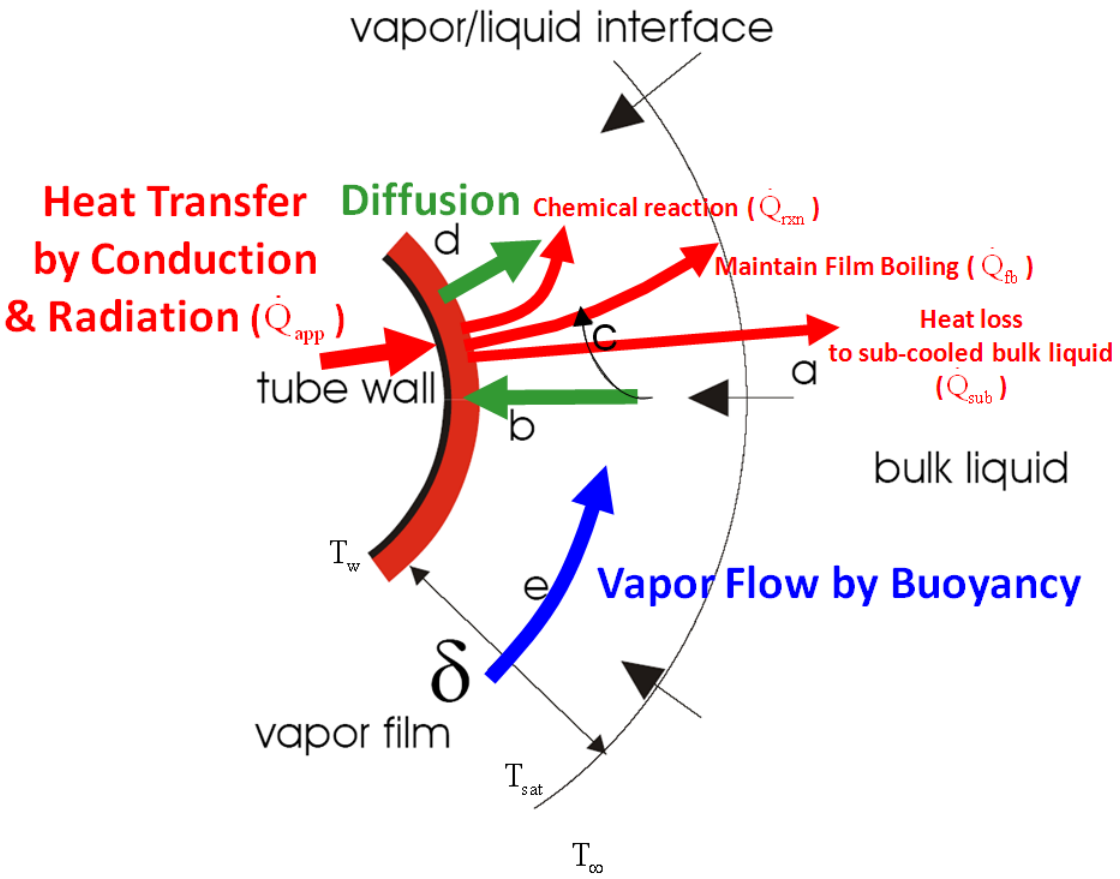

Figure 1.4 Transport phenomena in FIBOR

where they are carried around the tube surface and expelled through the percolating bubbles. In most instances we can expect that the composition of the bubble will contain both reactants and products. The FIBOR is a comprehensive chemical process including momentum transfer, heat transfer by conduction and radiation, and mass transfer of diffusion.

1.2.2 Operational Domain

The film boiling reactor has a limited operational domain of temperature where film boiling is stable. The operational limits of the FIBOR are governed by the boiling curve for a fluid, a general schematic of which is shown in Figure 1.1. To establish a vapor film, it is necessary that the wall temperature (T_w) be larger than the minimum film boiling temperature (Leidenfrost point [Incropera 2002], T_m). Various models for T_m (Avedisian et al. 1984 and 1986, Lienhard et al. 1981, Ohtake et al. 1965-1977, Sinha et al. 2003) result in values in the range of 400 to 500 K for methanol, independent of the transport situation for the fluid (models assume T_m sometimes is the same as the limit of superheat of a fluid). Increasing heat flux (or power) transitions nucleate boiling to the critical heat flux (CHF, q_{chf}) as indicated in Figure 1.1. Formulations for predicting CHF for horizontal tubes are well established (Lienhard 1987). After reaching the CHF, the tube enters to film boiling regime with a further heat flux increase. The absolute upper limit on T_w is the melting point of the tube material, such as 1800 K for stainless steel and 1673 K for Inconel 600. If T_f is larger than the melting point, the experimental configuration is physically destroyed upon reaching q''_{chf}.

If chemical reaction occues, the boiling curve of the film boiling region changes depending on the nature of chemical reaction (endothermic or exothermic) respectively as shown in Figure 1.1 for the case of an endothermic reaction. Since an

endothermic reaction requires heat input in addition to supporting a film boiling itself, the boiling curve representing the total required heat flux would shift up (Okuyama and Iida 1994). On the other hand, the heat release from an exothermic reaction offsets the one to maintain film boiling resulting in a shift-down of the boiling curve. In this thesis we have examined fluids for which the expected reaction is exothermic.

1.2.3 Liquids Examined and Associated Chemical Reactions

The reactant liquids are methanol (CH_4O, boiling point of 337.8K) and ethylene glycol ($C_2H_6O_2$, boiling point of 470K) because of their comparatively moderate boiling points, reasonably known decomposition chemistry and industrial relevance. Ethylene glycol is a common engine coolant and de-icer for aircraft that is often processed and recycled as a hazardous material, and it is representative of "heavier" organic compounds. Methanol also has energy relevance, and it is one of the simpliest organic liquid compounds and is relevant as a "light" substance.

Identifying the relevant chemical reaction mechanism is critical in examining the effectiveness of a FIBOR to promote chemical change. The primary conversion reactions for methanol and ethylene glycol are endothermic. For methanol,

$$CH_3OH \rightarrow CO + 2H_2 \qquad 1.1$$

with a heat of reaction (ΔH°_{rxn}) of 91 kJ/mol. For ethylene glycol,

$$C_2H_4(OH)_2 \rightarrow 2CO + 3H_2 \qquad 1.2$$

with ΔH°_{rxn} = 173 kJ/mol (Yaws 2003).

For methanol and ethylene glycol, secondary reactions may include water/gas shift and methanation reactions.

$$CO + H_2O \rightarrow CO_2 + H_2 \text{ (water/gas shift)} \quad 1.3$$

$$CO + 3H_2 \rightarrow CH_4 + H_2O \text{ (methanation)} \quad 1.4$$

Reactions in film boiling can also produce carbon or coke (Xun et al. 2009, Okuno et al. 2002) which can be detrimental to catalyst performance. Some possible pathways to carbon formation are through decomposition of methane and carbon monoxide as follows.

$$CH_4 \rightarrow 2H_2 + C \quad 1.5$$

$$2CO \rightarrow CO_2 + C \quad 1.6$$

$$CO + H_2 \rightarrow H_2O + C \quad 1.7$$

The above reactions are not all inclusive and the actual chemical reaction mechanism for a FIBOR is likely more complicated with even more pathways for generation of product species. For example steam reforming studies of ethylene glycol (Xun et al. 2009) have found that for certain operating conditions, traces of more exotic product species such as C_2H_2, C_2H_4 and C_2H_6 can be formed. These species were detected in this research with ethylene glycol as shown in Section 3.3. Furthermore, some condensable product species were detected in the reactant (Section 3.6). Our intent is however not to study the details of the kinetic mechanism for reaction in a FIBOR but to simply show its potential for chemical conversion and to suggest controlling mechanisms in the process. Gas chromatography (GC) analysis of the product gases will allow doing this. For example, if Eqs. 1.1 and 1.2 are controlling, we should expect that the CO to H_2 ratio, CO:H_2, is 1:2 for methanol and 2:3 for ethylene glycol. Formation of methane and carbon would indicate the potential of Eqs. 1.4, and Eqs. 1.5 to 1.7 respectively.

1.2.4 Advantages and Disadvantages of the Film Boiling Reactor

- *Advantages and Applications*

The unique mechanism of the film boiling reactor creates a variety of possible advantages and disadvantages over existing chemical reactors like a packed-bed reactor. With the concept as described above, high temperature reactions are accomplished by the natural separation of a high temperature surface in film boiling from the bulk liquid in which it is immersed. In this way, vapors of the pool liquid can achieve the high temperatures needed for reaction, while the bulk liquid remains relatively cold at a sub-cooled temperature (defined as $T_{sat} - T_{\infty}$ in Figure 1.5). It also operates at atmospheric pressure. The FIBOR therefore has no high temperature or high pressure liquid containment issues normally associated with other chemical reactor designs. Furthermore, a pump is not needed to move reactant liquid through the reaction zone because it is accomplished by the action of buoyancy (though a pump could be employed to enhance transport).

Another feature of the FIBOR is that the reactor would essentially build itself (i.e., it is self-assembled) as a consequence of the natural transition between nucleate and film boiling as the temperature of the heated surface is raised. The photograph (Figure 1.6 (a)) shows methanol in film boiling on a (nominal) 5 mm diameter by 140 mm long Inconel 600 tube. The reactor here - the FIBOR - is the vapor film that covers the hot surface. Chemical reaction occurs in the vapor film which is self-assembled without the aid of separate pumping and vaporization systems. It is thus extremely simple and compact and can be used in situ without transporting the reactant to the reactor. It could result in the mitigation of power requirements. On the other hand, for a typical chemical reactor such as the packed-bed reactor (Figure 1.6 (b)), reaction space is separated from a reactant liquid source chamber. Q_1 would be the energy required to maintain the tubular shell and catalytic material at a given

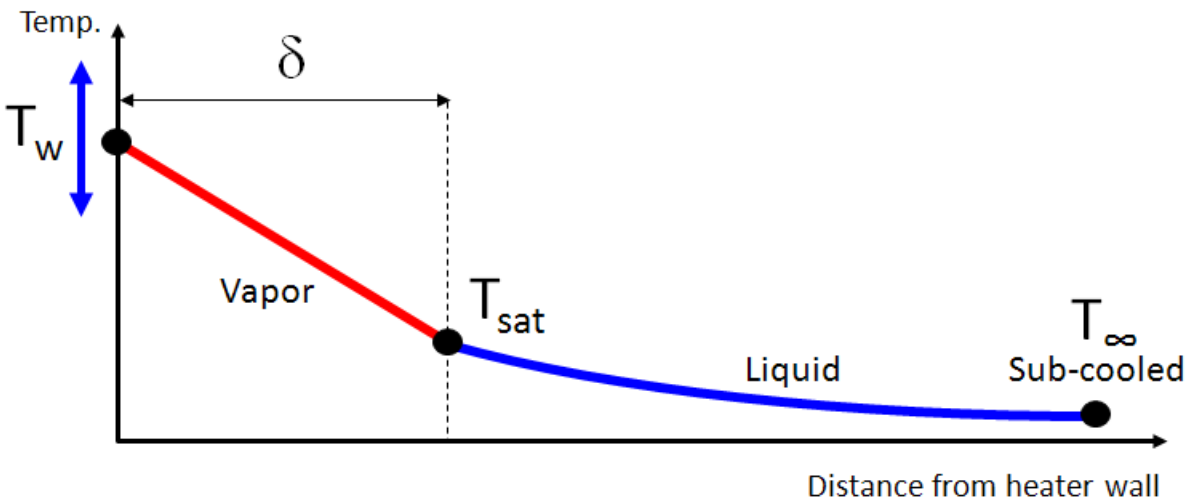

Figure 1.5 Temperature profile in FIBOR

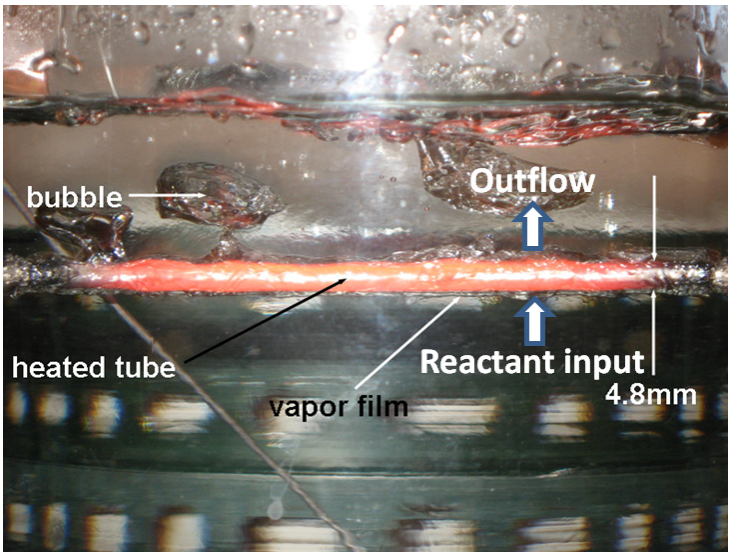

(a)

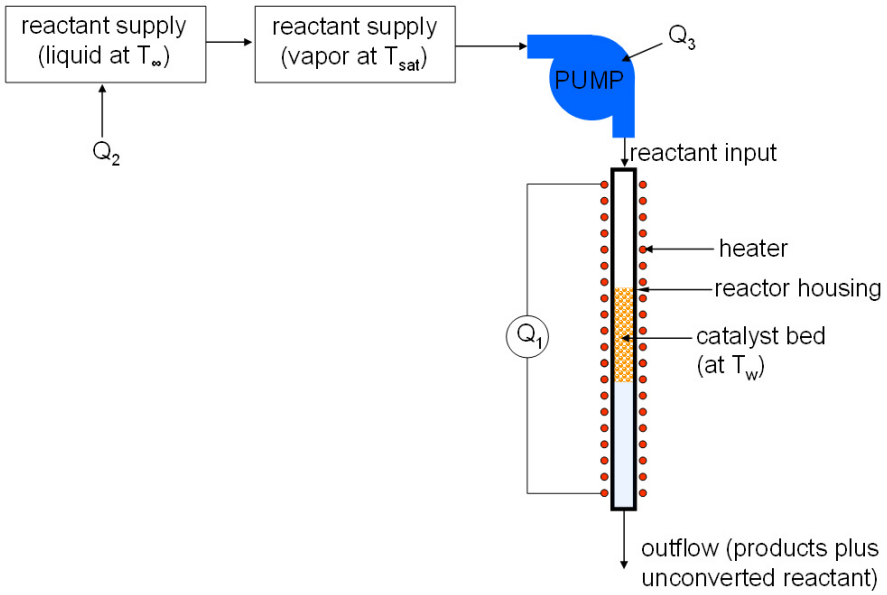

(b)

Figure 1.6 Comparison between (a) FIBOR and (b) packed-bed reactor

temperature, T_w. Q_1 for the FIBOR has a similar purpose: to maintain the reactor (tube) surface temperature at T_w against losses associated with evaporation of the liquid and the endothermicity of the liquid reactant. In a typical reactor where the reactant is a liquid, reactant is first transported through a vaporization unit and a pump which require additional power Q_2 and Q_3 respectively.

The FIBOR accomplishes the process of vaporization and transport together. Its structural simplicity of the FIBOR suggests a portability that would allow for on-site conversion, and its inherent scalability indicates a possibility for chemical conversion at heater scales ranging from the macroscale to the microscale (characteristic dimensions being on the order of microns, where arrays of such surfaces could be fabricated to increase the overall yields). But the present study will examine the ability of chemical reactions to occur only in macroscopic surfaces (dimensions on the order of millimeters).

A FIBOR could have the versatility to promote conversion by either thermal decomposition or catalytic reaction depending on whether or not heater surface is coated with catalyst. The FIBOR has a simpler construction to analyze physical and chemical mechanisms while reaction space of the packed bed reactor has a much more complicated structure filled with porous catalyst particles. The FIBOR can therefore be used for laboratory-scale study to investigate the mechanisms of organic compound catalytic or thermal cracking. Once physical and chemical mechanisms of the FIBOR are understood and analyzed mathematically, reaction constants like activation energy may be extracted. This point is further discussed in Appendix G.

Chemical reactors have been designed to produce synthesis gas (syngas) from organic compounds. Syngas consists primarily of hydrogen and carbon monoxide. Small amounts of carbon dioxide may be present. It is combustible and often used as a fuel source or as an intermediate for the production of other chemicals (Beychok

1975). The FIBOR might be also used for syngas production from organic compounds like other existing chemical reactors. Some of the features mentioned above for the FIBOR could make it more effective to convert heavy organic compounds into syngas than other reactors because the power to vaporize and transport heavy organic compounds required in the common chemical reactors is possibly mitigated by FIBOR.

- *Disadvantages*

The FIBOR has limited ability to control the reactant supply rate directly. The supply rate is determined indirectly by evaporation of liquid reactant. Even though the total power into a heater is measured or controlled, the portion of the power for evaporation must be computed, and it is in any case difficult to measure. This feature of the FIBOR will be mentioned again in Section 3.4 regarding conversion efficiency.

Another disadvantage of the FIBOR fitted with a catalyst is possible catalyst degradation, while would be a common problem for other reactors. Catalyst deactivation by various mechanisms such as sintering at high temperature, and coke (carbon) formation may occur (Baird et al. 1973; Okyuama and Iida 1994; Fogler 2006). The catalyst degradation and its possible reasons are further investigated in Section 3.5.

Even though recent theoretical work (Urban et al. 2006 and Avedisian et al. 2008) has shown the possibility that the film boiling process can be put to a useful purpose, there has not been an attempt to demonstrate the FIBOR's performance experimentally, in particular detail measurement of spcific gas species (CO and H_2). It is unknown whether the FIBOR will work properly in a controllable manner, what its product yields may be and what conversion efficieny it may have (we define "efficiency" in Section 3.4). These issue motivate this research and constitute the main objectives of this thesis.

1.3 Literature Review

1.3.1 Film Boiling without Chemical Reaction

Many studies of film boiling have been reported that do not include chemical reaction. Nukiyama's pioneering experimental work revealed the regimes of boiling heat transfer depicted by the boiling curve. Experiments were performed to measure "maximum values of heat, Q" or CHF (Nukiyama 1966).

Bromley (1950) was the first to provide a theoretical analysis of film boiling and provided a correlation to estimate the heat transfer coefficient for horizontal cylinder heaters that is reasonably accurate for heater diameters between 6.35mm to 19.05mm. Breen and Westwater (1962) later examined the effect of heater diameter and provided a modified treatment of Bromley's equation to account for both smaller and larger heaters. Interestingly, it was determined that for small heater diameters (less than 6.35mm) the heat transfer flux was independent of the heater diameter.

The flat plate geometry was investigated by Koh (1962) who analyzed film boiling on vertical surfaces. Lienhard et al. (1973) measured peak pool boiling heat flux on finite horizontal flat plates. Carey (1992) developed an analysis of film boiling for a vertical plate with analogy to film condensation. Lee (1997) reported the effect of liquid subcooling for both the nucleate and film boiling regimes of the boiling curve for methanol on an electrically heated tungsten wire (0.3~1.55mm) and his efforts revealed that as the liquid subcooling increases, the critical heat flux increases and the film boiling curve is shifted upward. However a negligible effect on the film boiling curve was found at either very high liquid subcoolings (>50K) or high wall superheats (>800K). Further extentions besides subcooling have been considered including importance of radiation and transport in the liquid and turbulent flow in the film, respectively for a horizontal tube (Sakurai et al. 1990 and Sarma et al. 2001).

Ede and Siviour (1975) introduced a method to avoid burnout of a metal surface during establishment of film boiling which can be caused by a direct increase of power. Sakurai et al. (1990) used the method in their experimental studies of film boiling of water whose critical heat flux is so high that the metal surface can have a property to burn out.

1.3.2 Film Boiling with Chemical Reaction

Studies of chemical reaction associated with film boiling originate in the context of nuclear reactor accident scenarios (e.g., Higgens 1955; Ruebsamen et al. 1952; Crooks et al. 1962; Baker and Just 1962; Lustman 1955). Most of these early studies provided only a phenomenological understanding of the interaction and were carried out in poorly controlled conditions.

Epstein et al. (1984) provided the first rigorous analysis of film boiling on a reactive, but noncatalytic, surface for stagnation point flow on a flat plate, again in the context of molten metal/water interactions (e.g., zirconium/water) and hydrogen production was mentioned. Anderson et al. (2001) also noted the production of hydrogen associated with the reactivity of molten lithium with water.

Film boiling with catalytic decomposition was first analyzed by Okyuama and Iida (1994) who studied film boiling with chemical reaction on a horizontal tube. They examined the effect of reactivity of methanol in film boiling on the heat transfer coefficient which was conjectured to be due to an enhancement of the heat flux associated with the endothermic reaction of methanol and the heat needed to sustain the vapor film. Many of the physics of film boiling were missing in the analysis, such as radiation across the vapor film and motion in the liquid as the result of non-zero shear at the vapor/liquid interface caused by vapor transport in the film. Product species were also not measured.

Zhukov et al. (2003) reported several observations that are directly applicable to the findings of this study. Most notable are their experimental findings that included thermal decomposition of a wide range of organic liquids through film boiling on a wire heater. Zhukov et al.'s results included measuring product flow rates with respect to heater temperature and detecting chemical species that consisted mainly of hydrogen (H_2), methane (CH_4), ethane (C_2H_6), ethylene (C_2H_4), and carbon monoxide (CO). Their observations also included the existence of surface reactions that created graphite-like compounds on the heater surface. These substances were analyzed further and determined to consist mainly of carbon and small amounts of hydrogen (less than 1%). Additional X-ray analysis found that the structure was similar to that of meteoric graphite. Zhukov et al. also found that the liquid phase can undergo chemical change through diffusion of contaminants consisting of aldehydes (mainly formaldehyde), various alcohols and ketones.

We also note the literature that has attempted to use surface boiling with chemical reaction as a means to grow carbon layers, or specifically pyrolytic graphite or carbon composite deposits on heated substrates (called the 'Kalamazoo' process (Bruneton et al. (1997); Okuno et al. 2002; Rovillain et al. (2001)). Zhang et al. (2002a, 2002b) showed the capability of chemical reaction with boiling to grow carbon nanotubes (CNT) on the heated surface. To promote CNT formation, the concept apparently requires placing an appropriate coating of a metal film of nanometer dimensions on the surface to serve as catalyst for CNT formation. Without such a coating, the deposit would simply be carbon as a by-product of pyrolysis.

The aforementioned investigations suggest the possibility for effecting chemical change by film boiling. Urban et al. (2006) attempted to establish film boiling in terms of its potential as a chemical reactor. The emphasis was on the influence of process variables and the identification of operating conditions to

optimize product formation. Methanol catalytic decomposition was analyzed as a test case because the conditions for conversion are not that much different from those of many other catalytic decompositions and a catalytic effect could be more easily analyzed with a boundary condition. It was shown that product gases from methanol – synthesis gas in particular – form at rates which are most influenced by tube wall temperature. The analysis neglected radiation, potential for bulk liquid motion and assumed no catalyst degradation during operation. Avedisian et al. (2008) extended the Urban et al. (2006) analysis to include the effects of radiation. Results indicated that volumetric emission was not an important factor, however surface emission played a role above temperatures of 1000K causing a larger vapor film thickness and higher product yields.

Thus far, the FIBOR's chemical process has been only theoretically analyzed without conclusive experimental verification. The present study is intended to fill this gap in our knowledge to show the feasibility of film boiling to promote chemical reaction on a laboratory scale.

1.4 Objectives

The main purpose of the present research is to demonstrate experimentally the feasibility of film boiling to affect chemical change of organic liquids in a controlled way. The designed FIBOR platform is described and its performance as a chemical reactor is evaluated. Specific objectives are the following:

1. Design and fabricate a laboratory scale FIBOR platform based on a horizontal tube configuration that allows for easy variation of parameters - tube wall temperature, tube diameter, bulk liquid temperature (sub-cooling) - to measure product yield and concentration from the film boiling reaction process.

2. Demonstrate the capability to use the FIBOR to convert two substances, methanol and ethylene glycol, into intermediate products through two chemical reaction modes: catalytic reaction and thermal decomposition.

3. Evaluate the FIBOR with turnover numbers like production yield and conversion.

4. Determine performance of the FIBOR for various sub-cooling and tube temperature.

CHAPTER 2

EXPERIMENTAL OVERVIEW

2.1 Construction of a FIBOR Platform

This section describes the design and construction of laboratory scale FIBOR that uses a horizontal cylindrical tube. This geometry has been often used for film boiling studies as remarked in Chapter 1 and facilitates theoretical analysis.

The platform should provide the following capabilities: film boiling establishment by controlling power through a technique that minimizes liquid contact with the surface during creation of the vapor film; control of temperature or power during operation; condensation and reflux of unreacted reactant; a computer data acquisition system to record product flow rate, temperatures of tube wall and bulk liquid reactant, and input electrical power; chemical analysis of product gas by gas chromatography, and flow rate measurement, to identify products and concentrations; flexibility to accommodate catalytic conversion or thermal decomposition.

2.2 Experimental Design and Instruments

2.2.1 A Schematic of Experimental Apparatus

A schematic of the experimental apparatus with the required capabilities mentioned in Section 2.1 is shown in Figure 2.1. It provides for development of film boiling on a horizontal tube, and it monitors and stores data relating to the FIBOR's overall performance and chemical species produced. The operational parameters include tube power input, and tube temperature. The design allows for measurement of all relevant temperatures including input power, tube wall and bulk liquid temperatures, and product species composition.

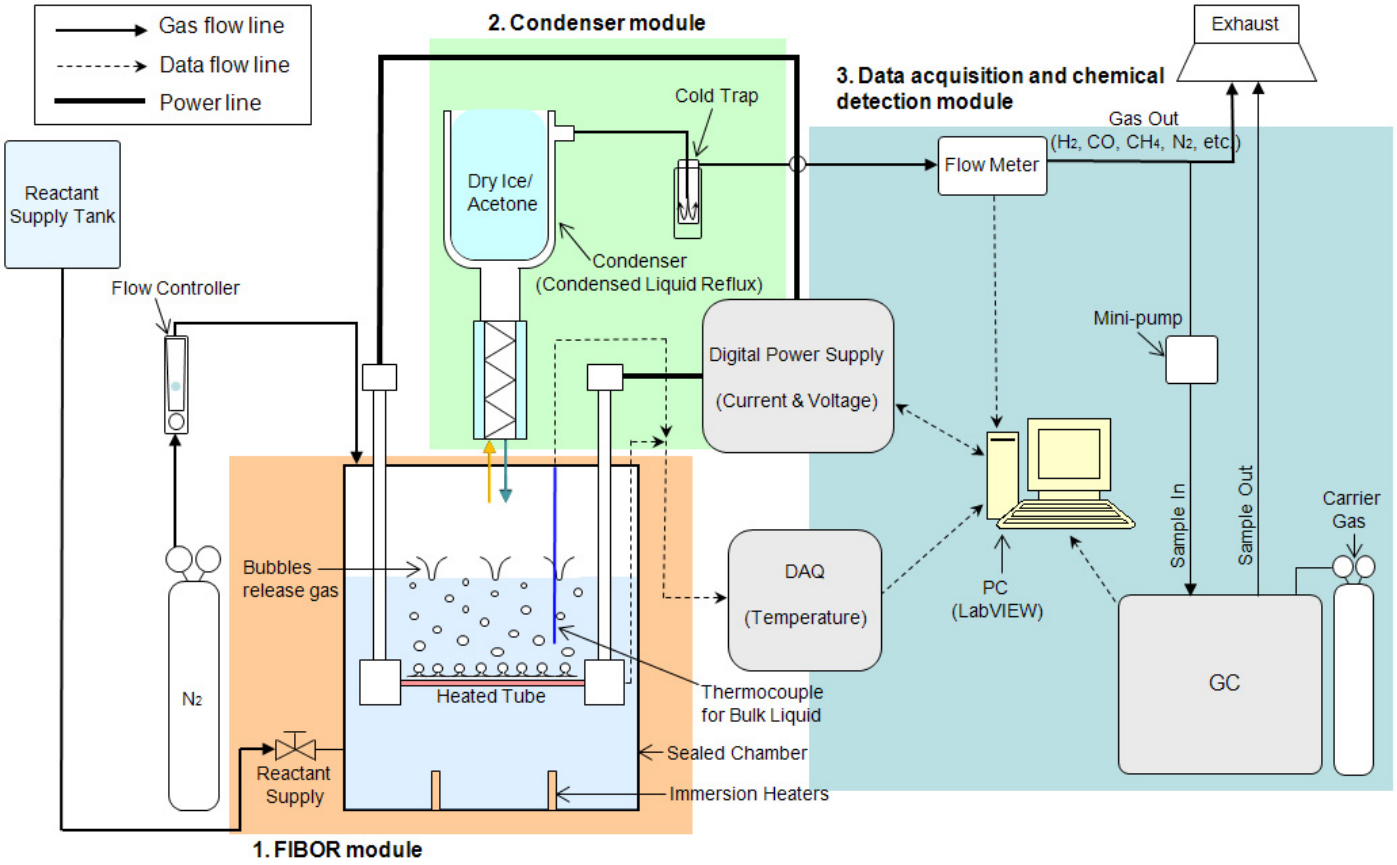

Figure 2.1: Experimental Apparatus

Considering the two main methods of establishing boiling – by controlling heater power or temperature - the design employs a power-controlled process because of its relative simplicity though certain portions of the boiling curve will be inaccessible when input power is controlled (i.e., the transition boiling regime). The components of the apparatus in Figure 2.1 and procedures are discussed below.

The apparatus consists of three basic modules. The first (FIBOR module) consists of a glass chamber (2L) to contain the reactant liquid and the tube around which the FIBOR is created. The second (Condenser module) consists of condensers and vapor traps that completely condense reactant vapors and separate then from the output gas stream. The third module (Data acquisition and chemical detection module) includes the data acquisition and control system assembly which consists of a programmable DC power supply (Agilent #6681A) for heating the tube, digital flow meter (Omega #FMA-A2309) for measuring product gas flow rates, and a mini-pump arrangement for product gases to be directly introduced into the GC (GOW-MAC Instrument Series 600–TCD). The GC we used targeted H_2, N_2, CO and CH_4 for product gases.

As the output gas is exhausted, a small volumetric flow (~30ccm) is withdrawn and introduced directly into the GC by a mini-pump. The GC analyzes product gases at steady state during an experiment. The experiment is controlled by LabVIEW which adjusts input voltage and current supplied to the heater, records the volumetric flow rate of product gases, the power to the tube (voltage and current) and all thermocouple outputs.

The apparatus has the capability to detect chemical reaction in the FIBOR in two ways. The first way is simply measuring a product flow rate. Non-zero value measured by the flow meter indicates chemical reaction in FIBOR because vaporized reactant is completely condensed through the condenser module before the flow meter.

The measured value though is not pure product flow rate since some condensable species might be generated by the chemical reaction as discussed in Chap 3.6. The second way is though GC analysis of the sampled product gas.

2.2.2 FIBOR Module

Figure 2.2 shows a FIBOR module which consists of the heater and chamber assemblies. The heater assembly is connected to the chamber assembly through two feed-through glands, 'j' (Conax Buffalo Tech. Inc., EG-500-A-23-T) in Figure 2.2. Figure 2.3 (a) shows the heater assembly which acts as a support for a heater and as a power delivery medium to the heater (a mechanical drawing is shown in Figures A.1 and A.2). It mainly consists of a heater tube, two copper buses, and two wet and dry clamps. Figure 2.3 (b) is the chamber assembly. It mostly consists of a glass middle chamber, aluminum top and bottom flanges, feed-through glands, immersion heaters, and small accessories. Mechanical drawings of the main three components (the glass middle chamber, the aluminum top and bottom flanges) are shown in Figure A.5, A.6, and A.7 respectively. All elements of the FIBOR module are described in detail in this section.

2.2.2.1 Heater Assembly

The heater tube for supporting the FIBOR is a thin-walled horizontal tube of nickel alloy (Inconel 600): 4.76 mm O.D, 3.34 mm I.D. and 140 mm long as shown in Figure 2.4 (a). Thermocouples (i.e., Omega #KMQXL-010G-18 thermocouples) are used to measure average tube temperature at the locations (seven points) shown in the figure. Figure 2.4 (b) is an example of a measured temperature distribution for the powers indicated for heating in methanol. The temperature is reasonably uniform along the central 60 mm of the tube. The decrease at the ends is due to heat losses

a – Aluminum top plate
b – Aluminum bottom plate
c - Glass middle chamber
d – Heater
e - Electrode wet clamps
f - Electrode dry clamps
g - Electrode buses
h – Heater tube thermocouples
i – Bulk liquid thermocouple
j – Feed-through for copper buses
k – Feed-through for thermocouples (big)
l - Feed-through for thermocouple (small)
m - 3/8" Hex bolts (x6)
n - Pressure gauge w/ release valve
o - Immersion heaters
p - Immersion heater connections
q - Insulation

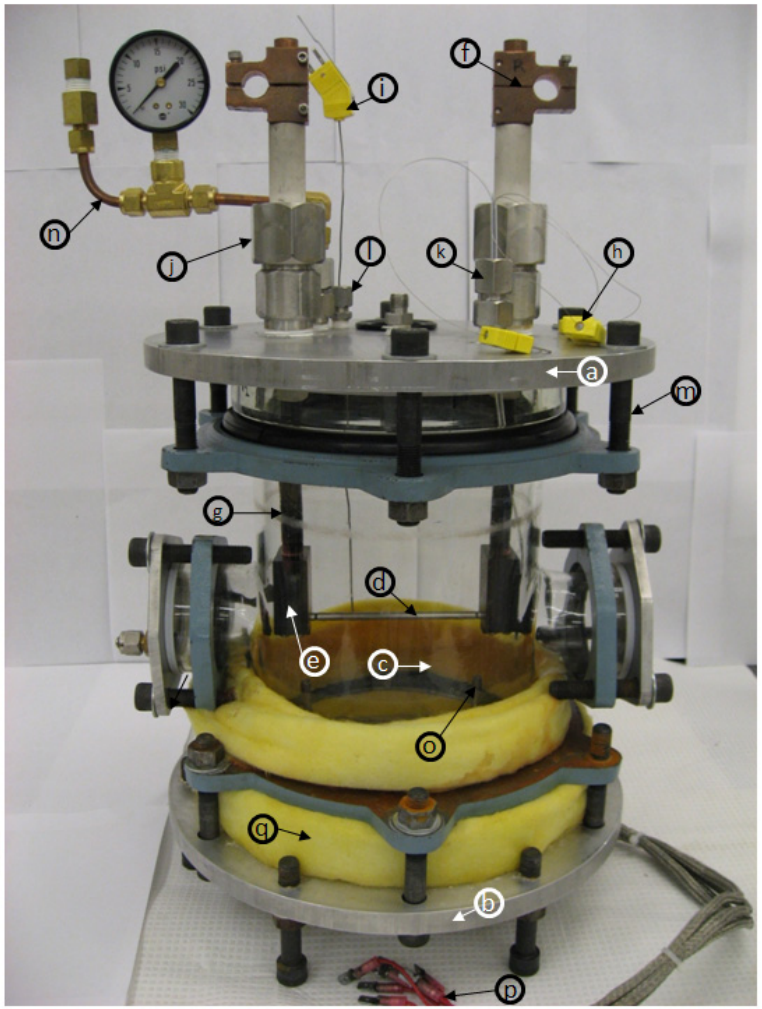

Figure 2.2: FIBOR Module

a – Aluminum top plate
b – Aluminum bottom plate
c - Glass middle chamber
d – Heater
e - Electrode wet clamps
f - Electrode dry clamps
g - Electrode buses
h – Heater tube thermocouples
i – Bulk liquid thermocouple
j – Feed-through for copper buses
k – Feed-through for thermocouples (big)
l - Feed-through for thermocouple (small)
m - Pressure gauge w/ release valve
n - Immersion heaters
o - Insulation

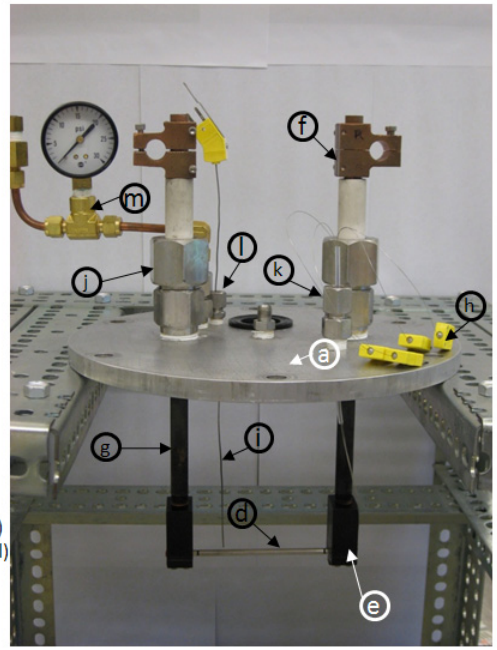

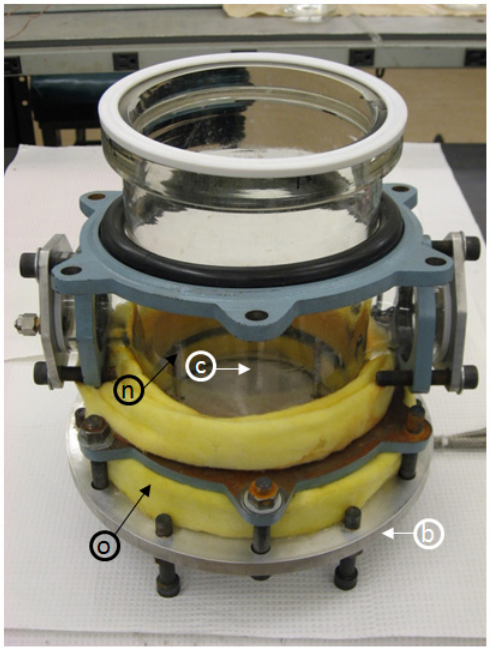

(a) **(b)**

Figure 2.3: (a) Heater and (b) chamber assemblies

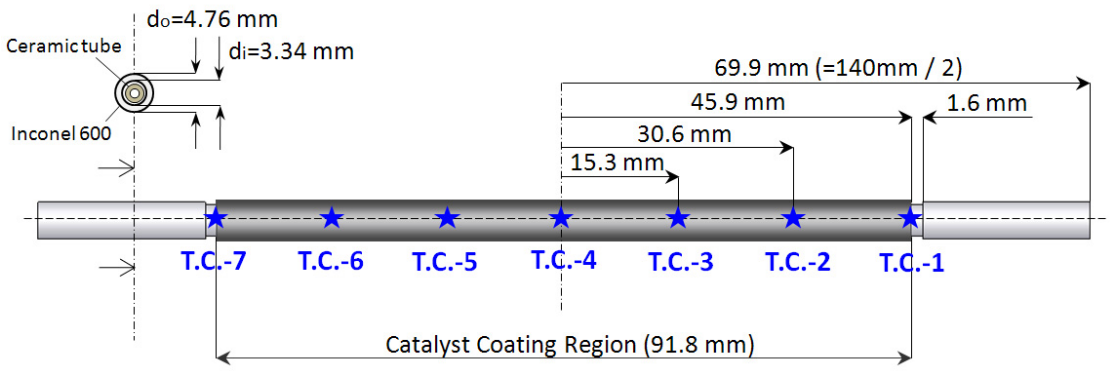

(a)

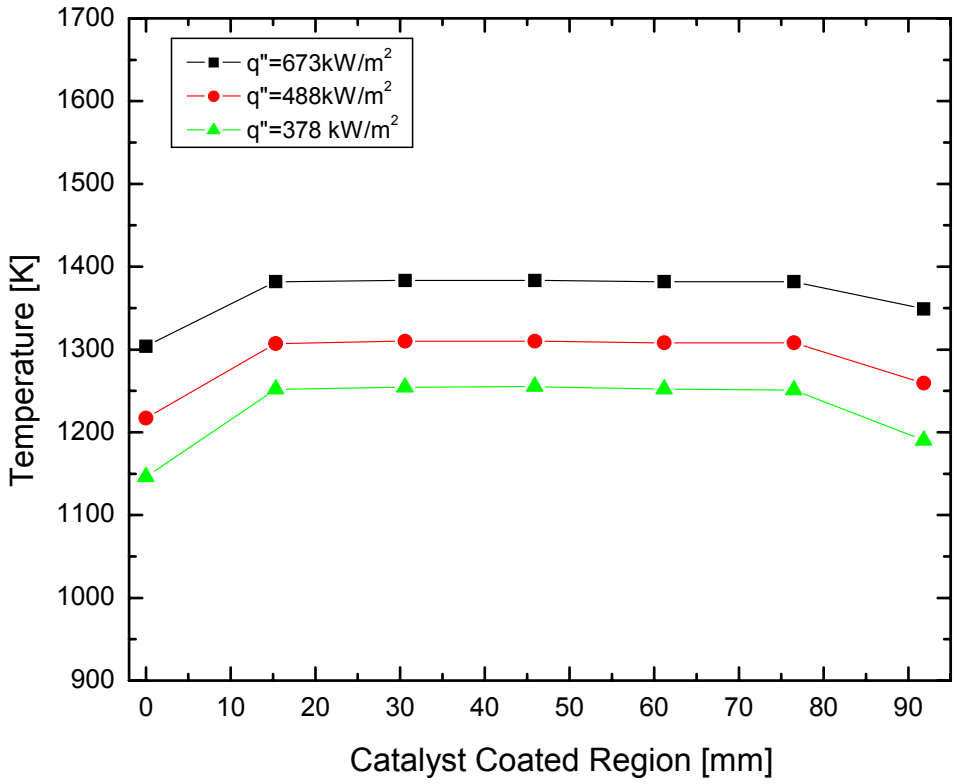

(b)

Figure 2.4: (a) Heater tube and (b) an example of temperature distribution

through the copper clamps, which created some issues with film boiling destabilization as further discussed in Section 3.1.

Electrical power is delivered to the tube by 13 mm diameter copper rod busses attached to two pairs of wet clamps at each end of the tube. The buses penetrate the top flange of the glass chamber through electrical feed-throughs and then connect to two cables from the power supply by two pairs of dry clamps. Figure 2.5 (a) and (b) show the elements of the dry clamps (4 parts) and wet clamps (4 parts) respectively. Each element is connected together by #6-32 thread screws. The mechanical drawings of the buses and clamps are also shown in Figure A.2, A.3, and A.4. Figure 2.6 shows the terminals of the cables which connect the dry clamps and the power supply. Thus, the heater assembly works as a series circuit with a power supply as shown in Figure 2.7. Naydich (2008) showed that total electrical resistance of the copper cables, clamps, and buses ($R_1 + R_2 + R_4 + R_5 < 0.001\Omega$) is negligible in comparison to that of the Inconel tube (R_3: 0.015Ω). It can therefore be assumed that the measured voltage by the power supply is almost equal to the voltage the tube ends.

The tube includes a single-hole ceramic rod insert (Omega, ORX-11618: OD 3.175mm, ID 1.588mm) through which the thermocouples are inserted to provide electrical isolation of the thermocouples from the tube wall and structural integrity to the tube, as prolonged heating at high temperatures can cause the tube to sag. All internal gaps between tube, ceramic rod and thermocouples are intended to be filled with aluminum oxide powder (Al_2O_3) of high thermal conductivity (18 W/m·K, Incropera 2002) to improve temperature uniformity inside the tube. The tube ends were sealed with heat resistant sealant (Dow Corning 736) which is rated up to 260°C. Catalyst coatings covered the central 92 mm of the tube for the experiment of catalytic reaction.

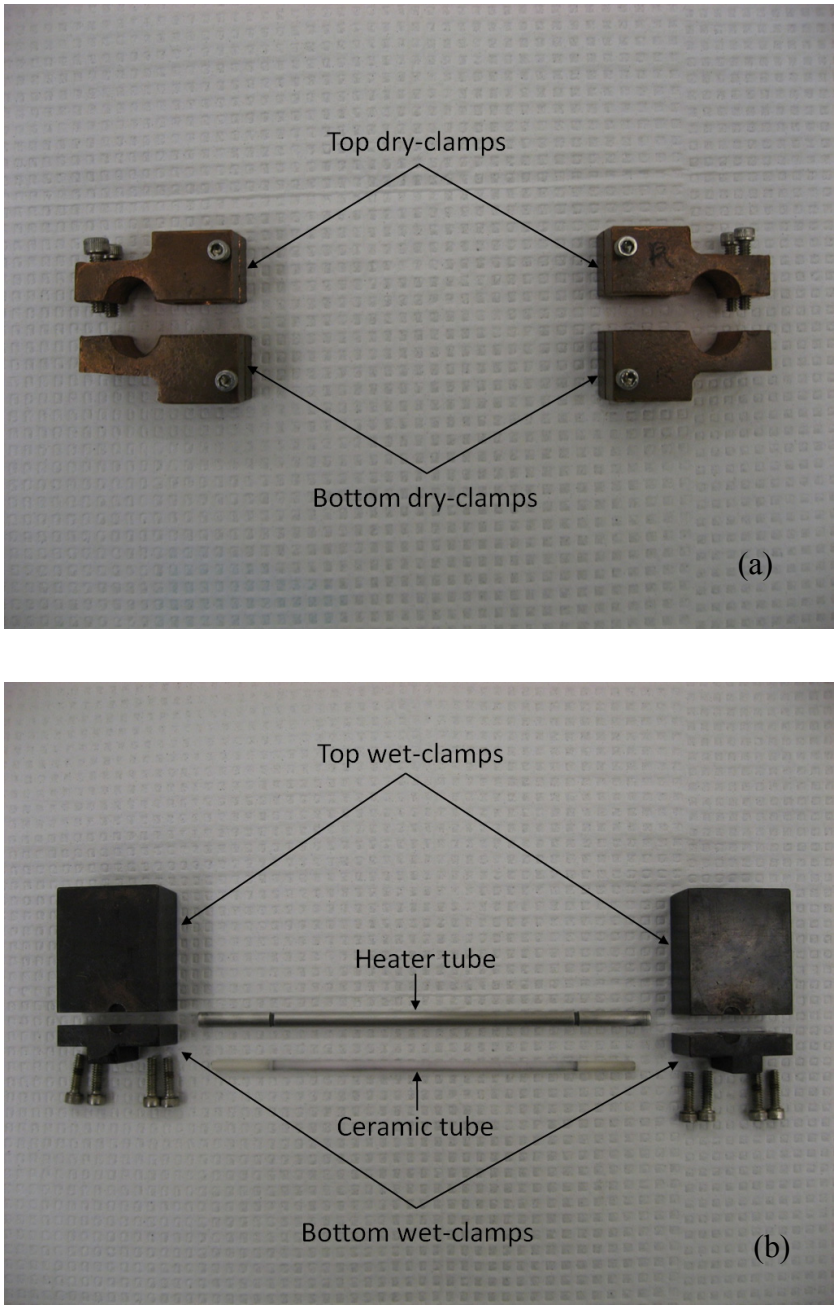

Figure 2.5: Elements of (a) dry and (b) wet clamps

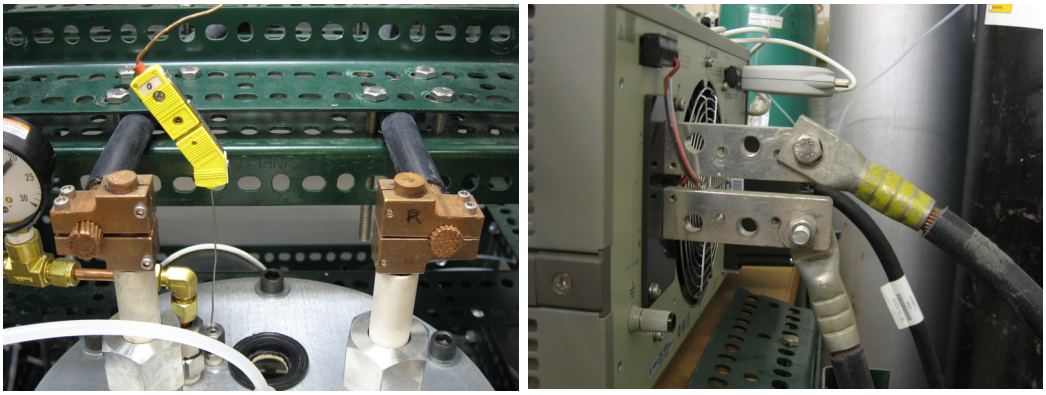

(a) (b)

Figure 2.6: Cable terminals of (a) dry clamp side and (b) power supply side

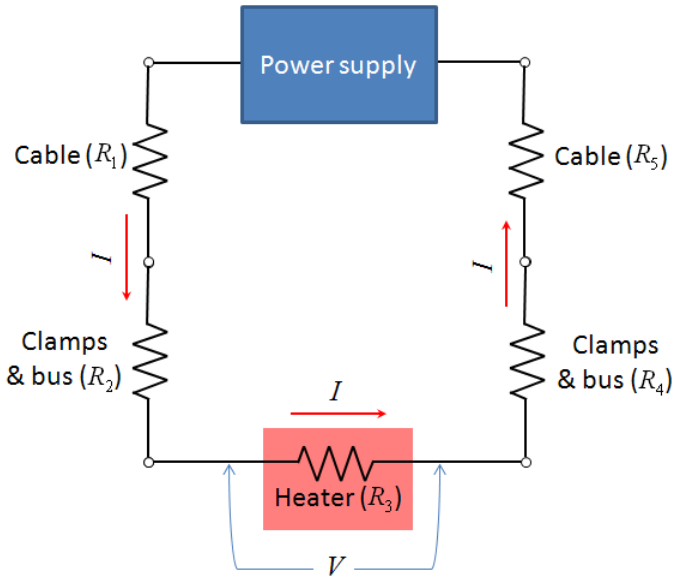

Figure 2.7: A series circuit of FIBOR

The primary design parameters are the dimensions of the heater tube (length and inner or outer diameters). The design task is therefore to determine the dimensions which can reach the critical heat flux or heat fluxes of the film boiling regime within the restricted specification of the power supply. Inconel 600 (Microgroup, 600F10188X028SL) is selected as a material of Joule heating because of its high electrical resistivity (ρ) compared to other metals as shown in Table 2.1 and its strong variation of ρ and T as shown in Figure 2.9. Table 2.2 (www.specialmetals.com) lists several physical properties of Inconel 600 such as electrical resistivity, thermal conductivity, and specific heat as well as the selected dimension.

Based on the selected tube dimension in Appendix B.1, material and CHF of water (126W/cm^2), the calculated current and voltage are the following: 407 [A] and 6.49 [V]. The dimension of Inconel 600 tube chosen of 4.76 mm O.D. , 3.34mm I.D., and 140mm length will be accessible with the power supply.

2.2.2.2 Chamber Assembly

The glass chamber is a crucial part of chamber assembly as it provides the fluid containment. The size of the chamber was determined based on the heater geometry mentioned above. The glass chamber was designed in the shape of a cross to provide the flexibility to allow a vertical or horizontal positioning of the heater though we only examined a horizontal FIBOR. Using glass also allows visual observation during experiments.

The two end flanges of the chamber (see Figure A.6 and A.7 for mechanical drawing) were designed to cap the openings of the glass chamber. Aluminum was selected because of its machineability and provided for feed-through for the two copper buses of the heater assembly. The flanges have circular grooves for the o-ring seals indicated as ‘Section B-B’ and ‘Section A-A’ in Figure A.6 and A.7 respectively.

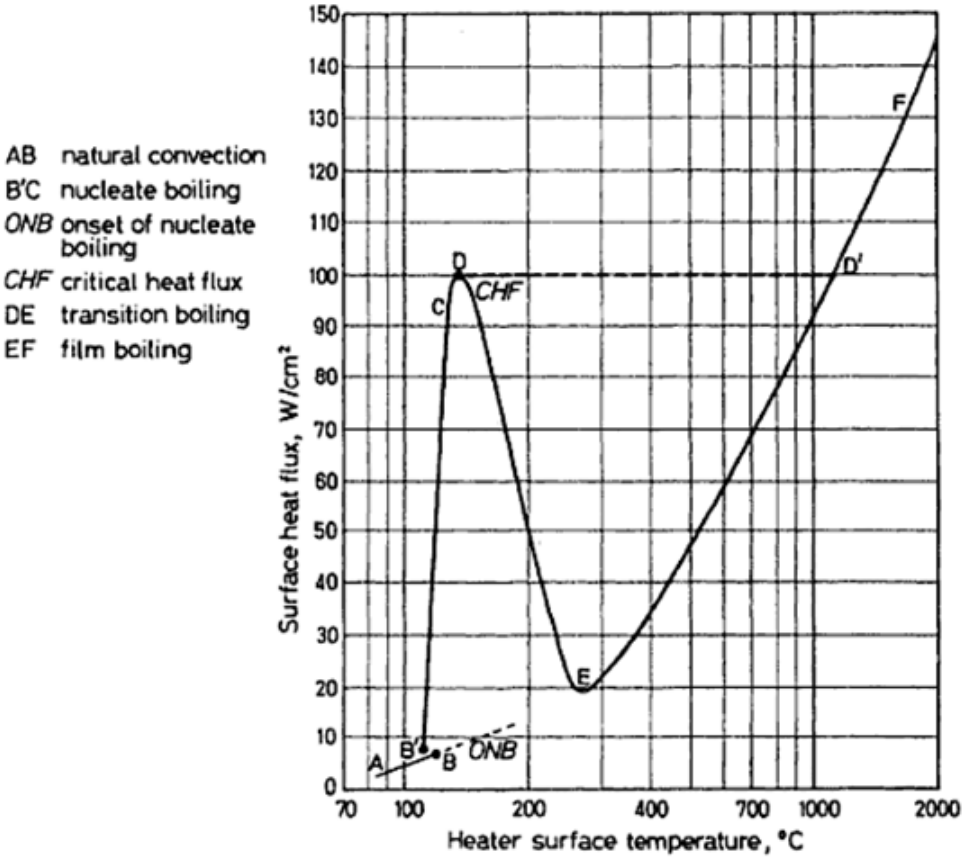

Figure 2.8: Pool boiling curve for water at atmospheric pressure (from Collier, pp. 122-123).

Table 2.1: Resistivity of metals at 20°C

Material	Resistivity ρ (ohm m) at 20 ˚C
Silver	1.59 x10^-8
Copper	1.68 x10^-8
Aluminum	2.65 x10^-8
Tungsten	5.60 x10^-8
Iron	9.71 x10^-8
Platinum	10.6 x10^-8
Manganin	48.2 x10^-8
Lead	22 x10^-8
Mercury	98 x10^-8
Nichrome	100 x10^-8
Constantan	49 x10^-8
Inconel 600	1.03 x10^-6

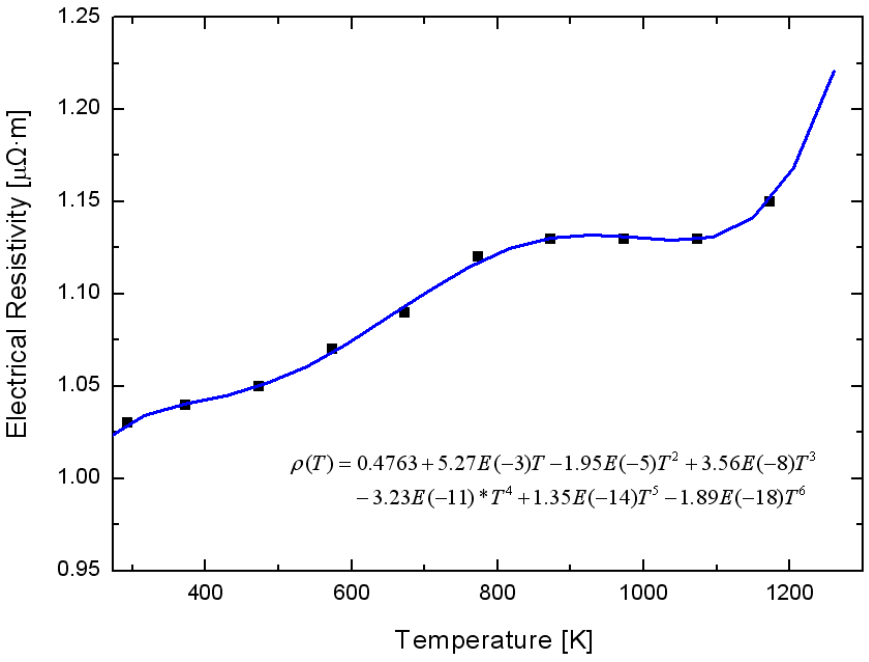

Figure 2.9: Resistivity of Inconel 600 vs. wall temperature (www.specialmetals.com)

Table 2.2: Heater Tube (Inconel 600) Properties (www.specialmetals.com)

Physical Properties (Microgroup, 2009)						
Material	Grade	Mfg Type	OD Max/Min [in]	ID Max/Min [in]	Length [in]	Melting Rg [ºC]
Nickel Alloy	600 (Inconel)	Seamless	0.1825/0.1925	0.1181/0.1449	5.5	1354-1413
Chemical Properties (Microgroup, 2009)						
C%	Mn%	S%	Si%	Ni%	Cr%	Cu%
0.023	0.77	0.001	0.32	72.4	16.27	0.01
Ti%	Cb%	Co%	Al%	N%	Fe%	Other%
0.31	0.01	0.02	0.18	0.023	9.49	0.173

Thermo-physical Properties (Special Metals Corporation)			
Temperature [K]	Electrical Resistivity [μΩ·m]	Thermal Conductivity [W/m·K]	Specific Heat [J/kg·K]
293	1.03	14.9	444
373	1.04	15.9	465
473	1.05	17.3	486
573	1.07	19	502
673	1.09	20.5	519
773	1.12	22.1	536
873	1.13	23.9	578
973	1.13	25.7	595
1073	1.13	27.5	611
1173	1.15	-	628

Leak proof sealings are developed using two pairs of an o-ring (Sealing Devices, Inc., O-RING AS-362 70-DURO NITRILE) and a rubber gaskets (Teflon) as shown in Figure 2.10. A condenser seal (Brinkmann Instruments, Inc., Vacuum Seal KD-22) is included in the chamber assembly to assure an adequate seal on a condenser connection hole. An o-ring and rubber gasket is inserted between the top plate and the middle glass chamber while another pair is located between the bottom plate and the middle chamber as the chamber is assembled.

Two copper buses of the heater assembly pass through the chamber via feed-through glands ('b' in Figure 2.11 (a), Conax Buffalo Tech. Inc., EG-500-A-12-T). Another two types of feed-through glands are used to provide impermeable seals for the thermocouples and a pressure relief valve. The bigger type 'c' and 'd' in Figure 2.11 (a) (Conax Buffalo Tech. Inc., #PG2-125-A-T) are used for thermocouples to measure heater wall temperatures and a pressure relief valve. On the other hand, the smaller type 'e' in Figure 2.11 (a) (Omega, Model #MFT-040-3) is used for a bulk liquid thermocouple. A pressure relief valve (STRA-VAL #N1167) is connected to the feed-through 'd' for safety as shown in Figure 2.11 (a), rated at 5 psi above the ambience.

Four immersion heaters (WATTCO WC20303001 300W 120V ¼"D x 3"L) are installed inside of the FIBOR chamber, especially on the bottom plate as shown in Figure 2.11 (b), to control liquid temperature. The power of 300W was selected based on the design calculation in Appendix B.2.

2.2.3 Condenser Module

The gases coming out of the FIBOR module include unconverted reactant and condensable contaminants, as well as product gases. A condenser module was designed to separate the vaporized reactant and contaminants from the product gases.

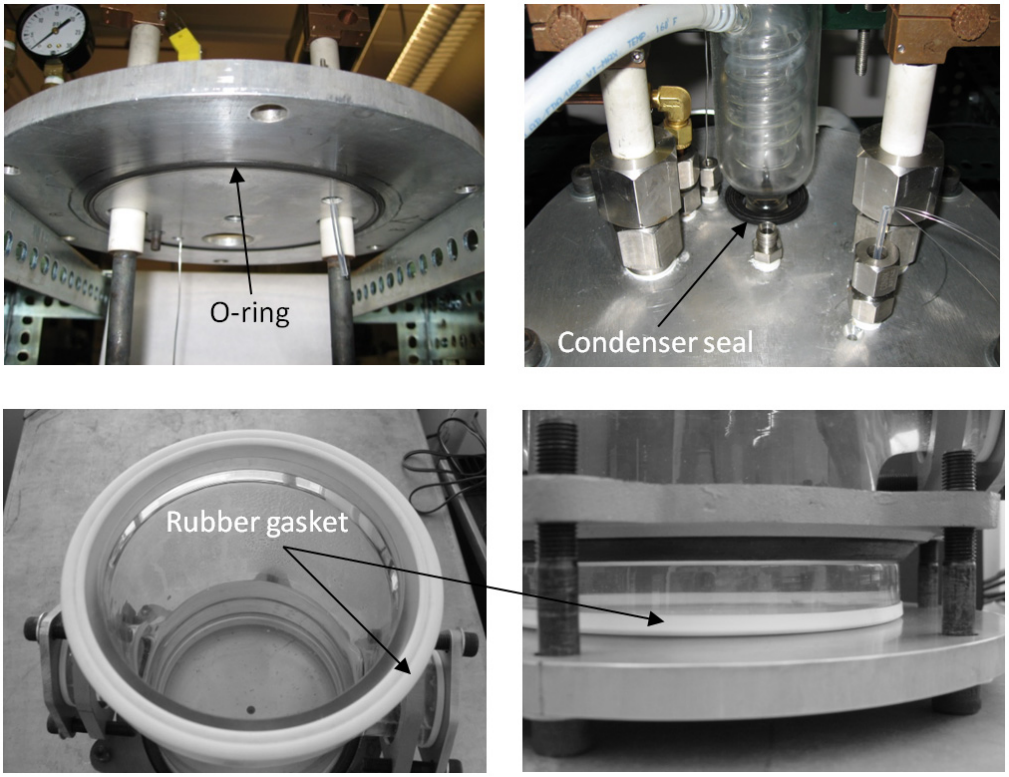

Figure 2.10: Seal of FIBOR module

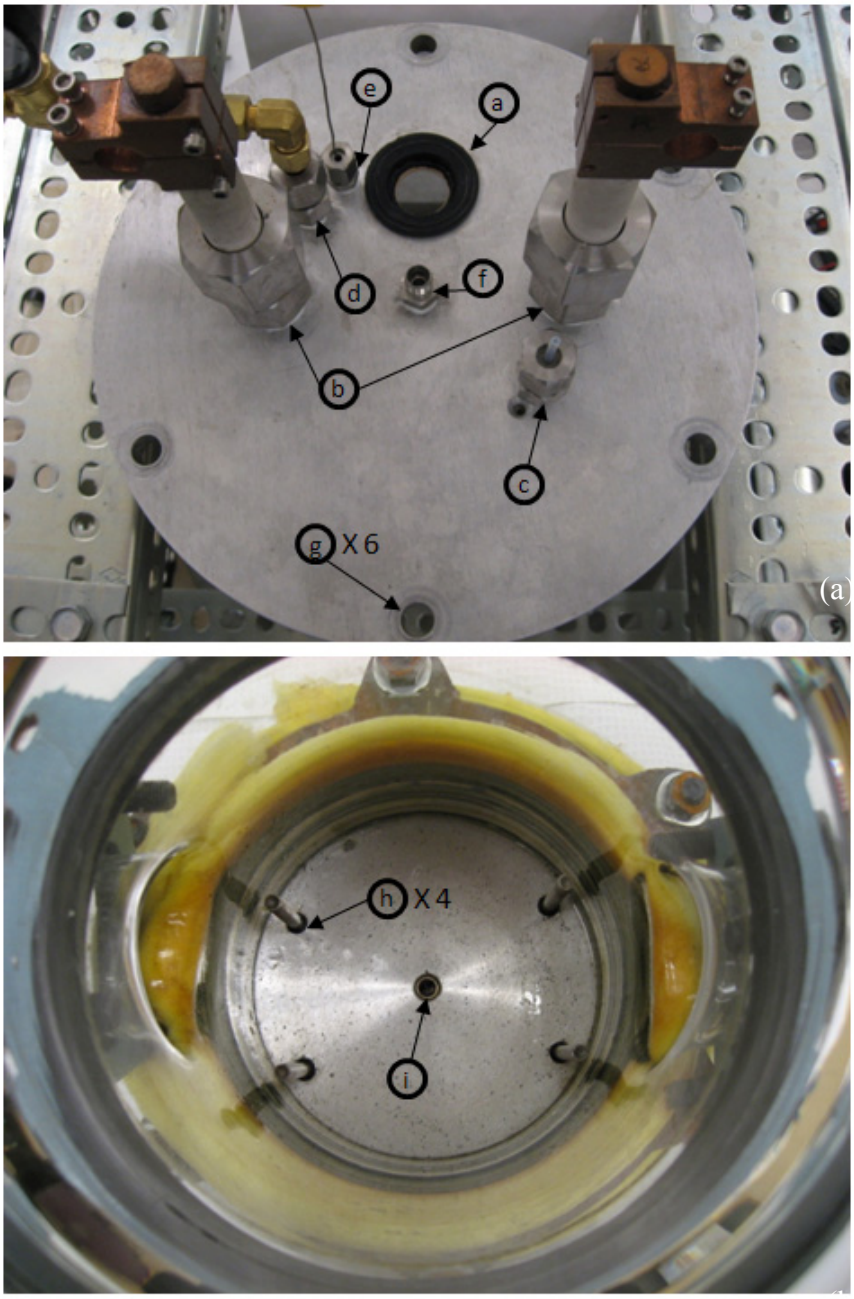

Figure 2.11: (a) Top and (b) bottom flanges of FIBOR chamber

This allows a flow meter positioned downstream of the condenser outlet to measure the product flow rates due to chemical reactions if only insoluble gaseous products are created by the reaction process. If the products contain soluble products, the flow rate will not then be indicative of all the products created. Figure 2.12 illustrates the mechanism of species transport and energy flow in the FIBOR and condenser modules. The bubbles generated from the FIBOR are composed of vaporized reactant and contaminants, and product gases. Some parts of the vaporized reactant and contaminants in the bubbles are directly condensed as they float up in the sub-cooled reactant liquid (see the right-down inset in Fig. 2.12). However, the other parts still remain in the gases coming out of the FIBOR module. If a condenser, which is connected to the outlet of the FIBOR module, works effectively, all of the remained vaporized reactant and contaminants will be condensed.

From the perspective of an energy balance, assume a system such that all power supplied by the heater tube and immersion heaters is consumed to vaporize the reactant liquid (no chemical reaction and no heat loss to the environment). Therefore, it is necessary to design a condenser whose cooling capacity is at least bigger than the sum of the heat inputs from the heater tube and the immersion heaters.

$$\dot{Q}_{\mathrm{FIBOR}} + \dot{Q}_{\mathrm{IH}} \le \dot{Q}_{\mathrm{Cond}} \qquad 2.1$$

where $\dot{Q}_{\mathrm{Cond}}$ is the cooling rate of the condenser module, $\dot{Q}_{\mathrm{FIBOR}}$ is the heat transfer rate from FIBOR, and $\dot{Q}_{\mathrm{IH}}$ is the heat transfer rate from immersion heaters (see Figure 2.12).

The condenser module consists of two condenser assemblies and two cold traps as shown in Figure 2.13. The first condenser assembly consists of two commercial products, Aldrich reflux condenser #Z517232 (Condenser S) and Aldrich

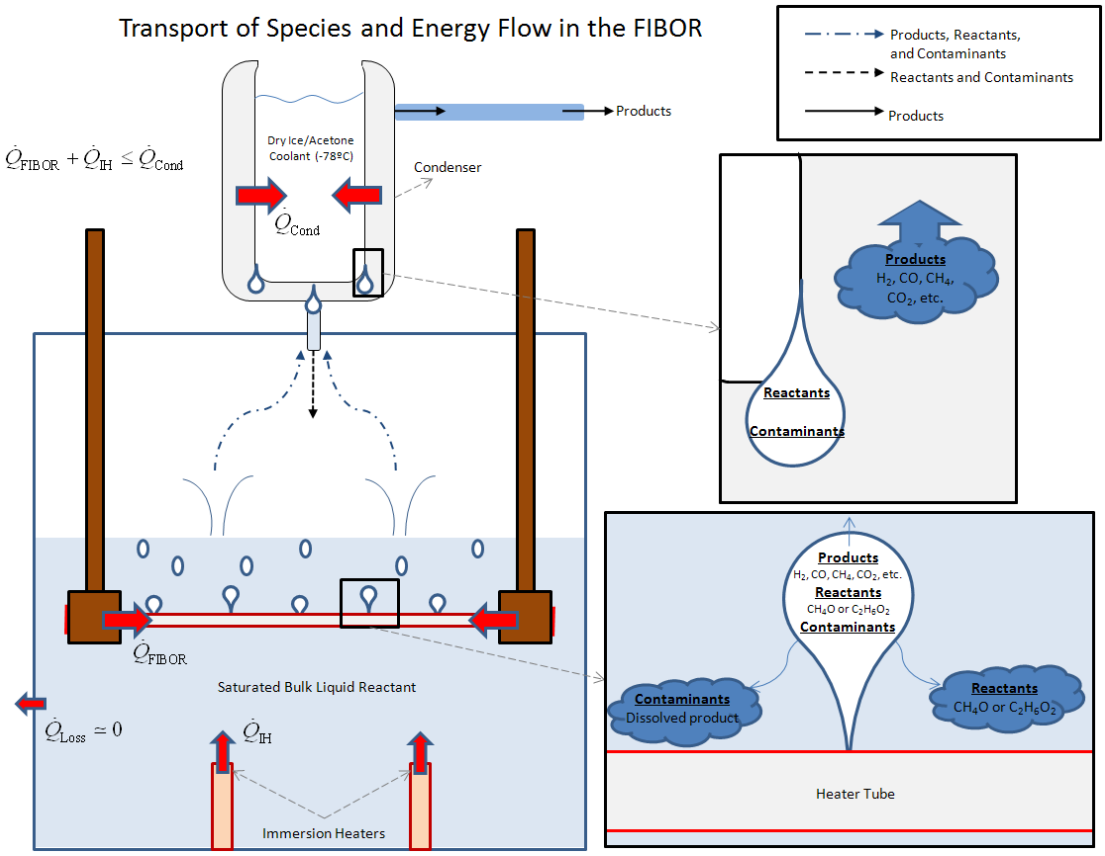

Figure 2.12: Species transport and energy flow in FIBOR apparatus

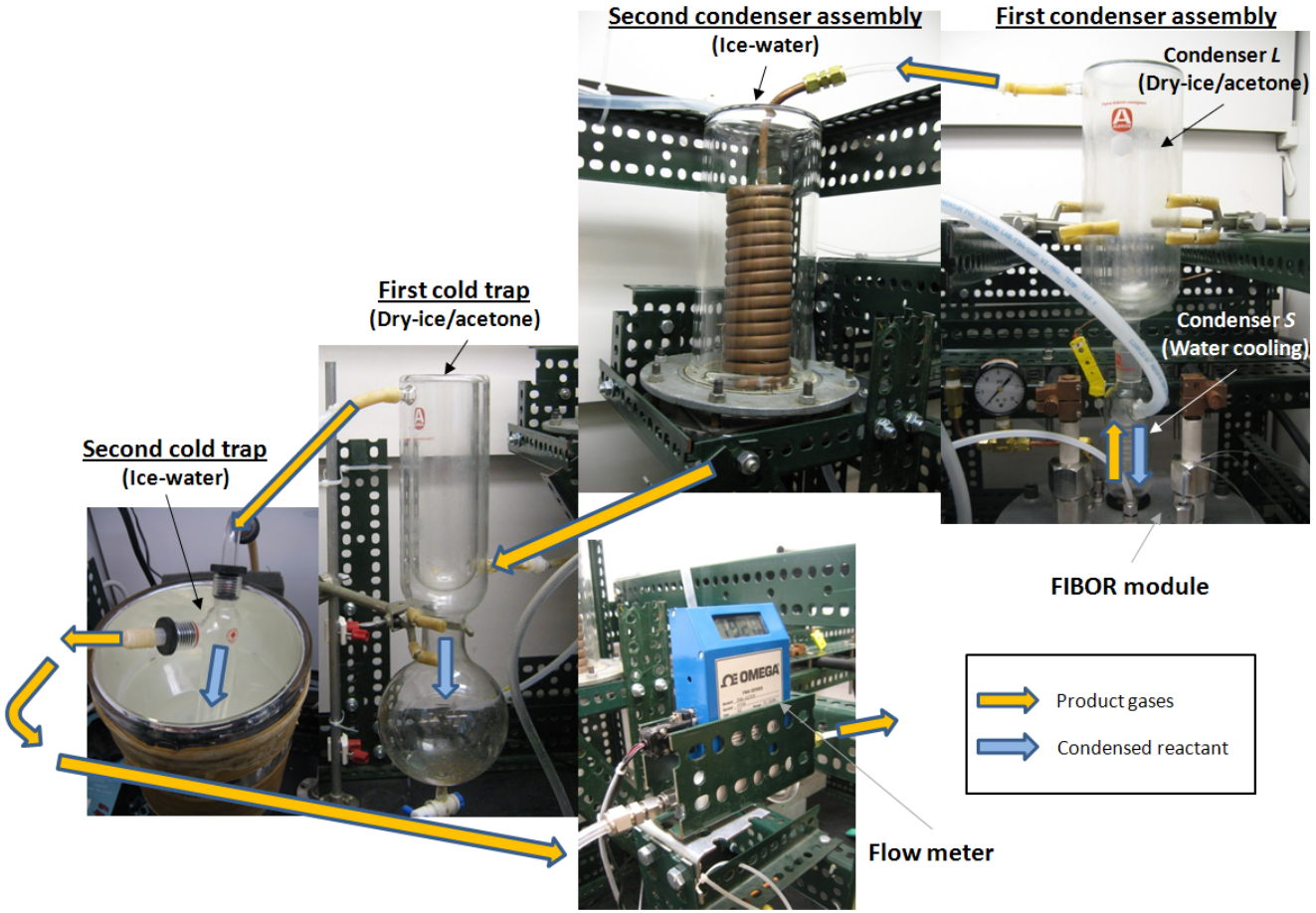

Figure 2.13: Condenser module set-up

cold-finger condenser #Z164038 (Condenser L). A coiled-type condenser was selected as the second condenser assembly to provide greater cooling surface area that was used in a prior study (Purdy 1987). Two cold traps were placed after the second condenser assembly (i.e. the coiled-type condenser) to assure more complete screening of reactant and condensable contaminants before entering the flow meter. Figure 2.13 shows the cold trap arrangement. If the outlet gases from the second condenser assembly include condensable components, the cold traps will screen and accumulate the components inside of the traps. Commercial products of Aldrich dry ice condenser trap (#Z422347) and Ace vacuum trap (#Z256870), which are marked as 'First cold trap' and 'Second cold trap' respectively in Figure 2.13, are used in this study. Design calculations conducted to select the condensers is shown in Appendix B.3.

2.2.4 Data Acquisition and Control Module

The data acquisition and control module consists of a digital power supply, data acquisition units for temperature and flow rate measurements, and a computer as shown in Figure 2.14. In total, there are five operating parameters that must be monitored and controlled. These include heater tube temperature, power supply settings to the heater tube, the bulk liquid temperature, the immersion heater power supply setting to the bulk liquid, and product gas flow rates. The GC must also have an integrated data acquisition system to generate and save chromatograms. This function performs separately under the internal settings of the GC.

Thermocouples monitor the temperature of both the bulk liquid and heater tube. Immersion heaters, connected to a manually adjusting AC/DC transformer, allow for manual control of the power input to maintain the bulk liquid at its saturation point. A DC power supply allows the user to manually control the heater tube temperature through "joule heating" or adjusting the current passed through the heater

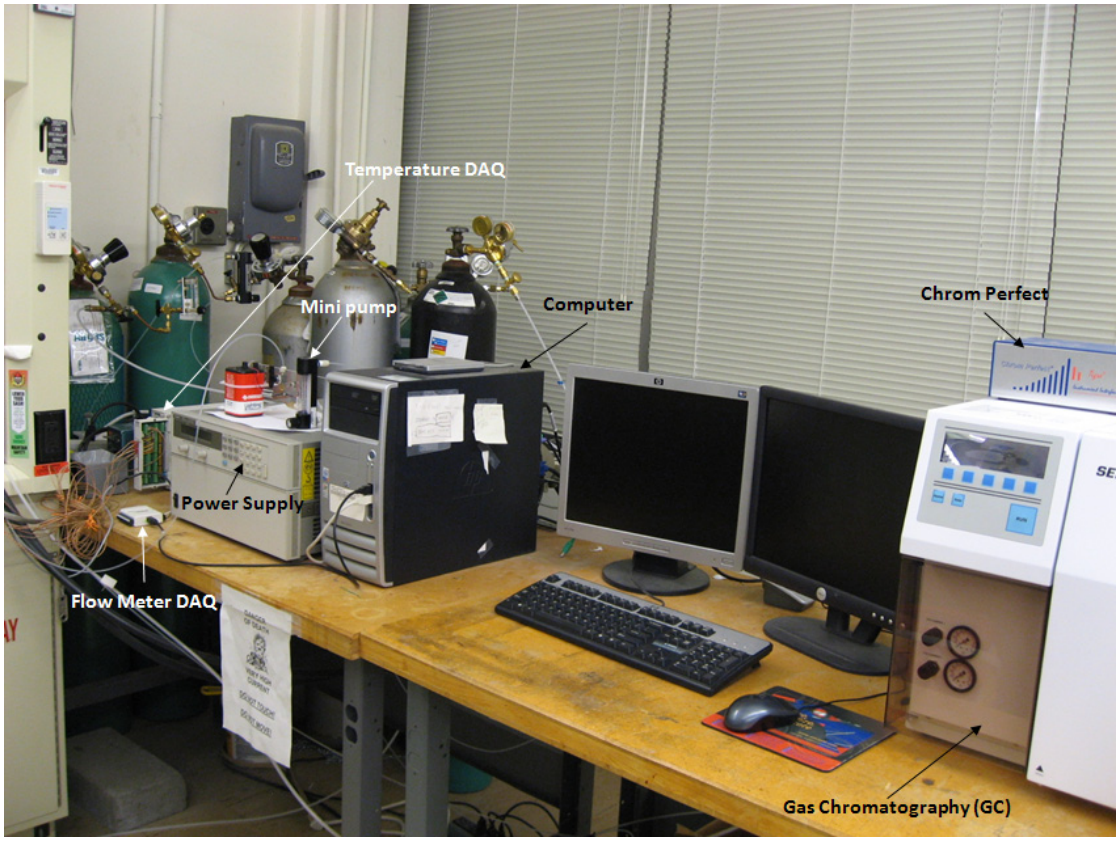

Figure 2.14: Data Acquisition and Control Module

tube. The product gas flow rate is monitored by a digital flow meter positioned downstream of the cold traps. A LabVIEW program acquires and store all temperature outputs from thermocouples, flow meter readings and allow the user to control power supply settings.

2.2.4.1 Power Supply and Temperature DAQ

The power supply provides the current and voltage required to the heater tube through a pair of cables previously shown in Figure 2.6. The power supply is shown in Figure 2.15 (a). The power supply provides a range of operation of 0 to 580 Amperes and 0 to 8 Volts, giving the flexibility to vary the power input from 0 to 4640W. The power supply is controlled by the PC via a GPIB (General Purpose Interface Bus) controller (Agilent Tech. #82357A USB/GPIB interface) shown in Figure 2.15 (b). A GPIB controller is used to control and communicate with one or more external instruments that have the GPIB interface.

Another important parameter in this study is temperature. A temperature data acquisition unit (DAQ) (Figure 2.16) receives the signals from the thermocouples located inside of the heater and also in the bulk liquid, converts them to a digital format and retransmits the signal to the PC. The selected DAQ unit consists of a National Instruments PCI-6220 (DAQ card), SCXI-1102C (Signal Conditioning Module with Gain and a 10 kHz filter for 32 channels) and an SCXI-1303 (Isothermal Terminal Block that connects thermocouples and signals to the SSCXI-1102 Modules). A photograph of the DAQ cards is given as Fig 2.16. It shows the signal conditioning module with the isothermal block attached at the front. This signal conditioning module is connected to the PCI-6220 in the PCI slot of the computer. Thermocouple junctions are connected to the isothermal block as shown in Fig 2.16 (b). A maximum of 32 thermocouples can be connected to this terminal block. The red wire will be

(a)

(b)

Figure 2.15: (a) Power supply and (b) USB-GPIB connector

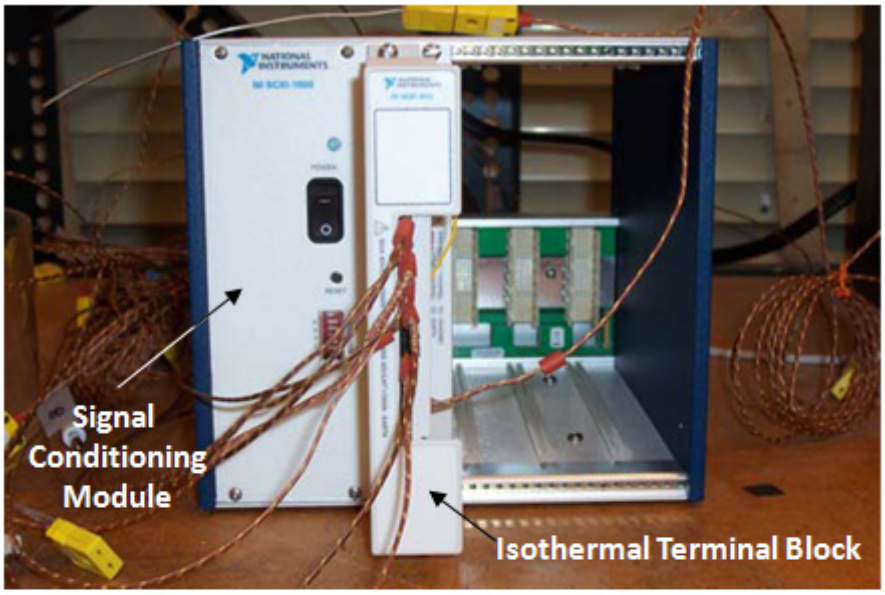

(a)

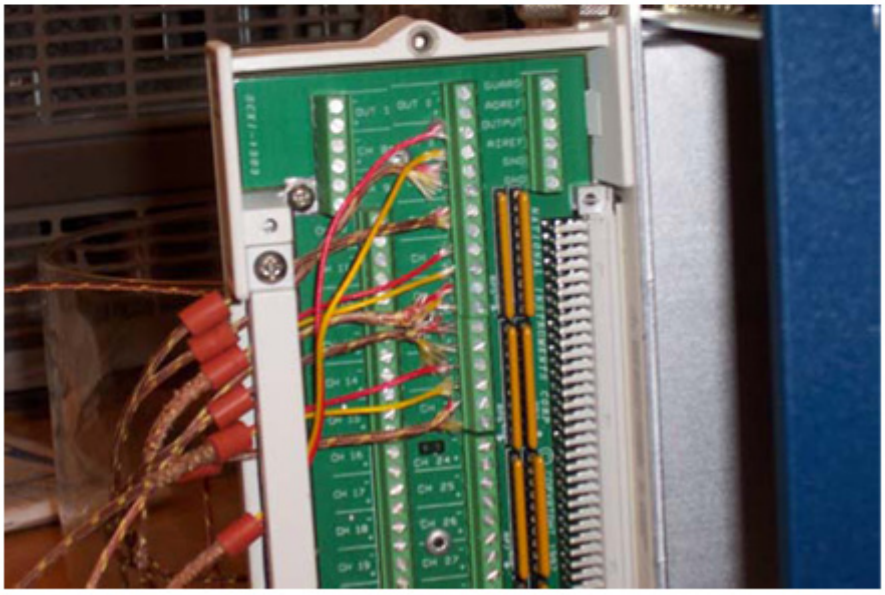

(b)

Figure 2.16: (a) Temperature DAQ and

(b) thermocouple connection to the isothermal block

wired into the negative terminal and the yellow one will be wired to the positive terminal.

A LabVIEW program is developed based on the following requirements: accurately monitor up to 8 thermocouples in the temperature range of 20°C-1300°C; record thermocouple outputs at a high enough frequency rate to be able to detect the sudden increase in temperature. The minimum sampling rate will be 100Hz (1/10ms); accurately control the output voltage and current of the power supply; decrease the output power of the power supply when burnout is about to occur; enable the computer to store all the temperature and power readings into the hard disk for data analysis after the experiment; program must be user-friendly to allow the user to run and stop the program; program must be expandable to allow for modifications for other specific experiments.

Figure 2.17 shows the main panel of the developed LabVIEW program. The panel has three windows for the purpose of monitoring temperature, flow rate, and power in real-time. The LabVIEW program can be started by clicking on the right-handed arrow at the top left of the control panel and clicking on the "stop" button will end the program. The user can set the output voltage and current by keying in the values under 'Set voltage' and 'Set current'. Note that the voltage is adjusted for the whole experiment because the power supply is set in the constant voltage mode. The current should be set to its maximum of 580A.

The power supply works in either the control voltage mode or the control current mode. For a set of V_{set} (voltage set) and I_{set} (current set), the actual output voltage and current will be determined by the limiting variable (V or I) which are related by the resistance across the terminals. If $V_{set}/R < I_{set}$, output voltage will be V_{set} and output current will be V_{set}/R, not I_{set}. So if we preset the current to its maximum possible (580A), the experiments will always be in the voltage control mode. Also

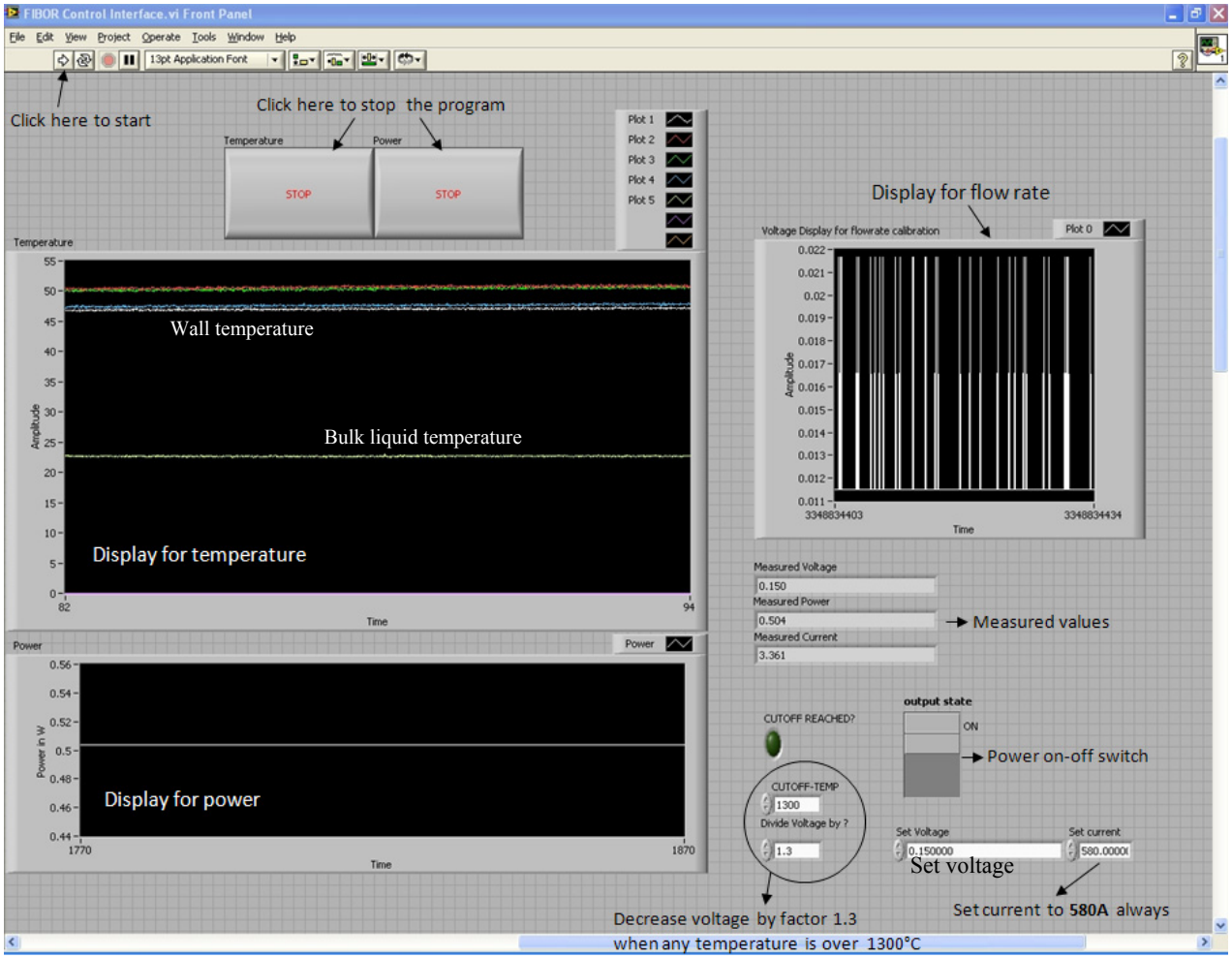

Figure 2.17: LabVIEW interface panel

note that when the VI (Virtual Instrumentation) is running, the power supply is controlled solely by the LabVIEW program and we can press the “Local” button to regain manual control for the power supply.

Two block diagrams of the developed LabVIEW program are presented in Appendix D. One block diagram (Figure D.1) is a temperature and flow rate measurement loop which communicates to two DAQs of temperature (NI PCI-6220) and flow rate (NI USB-6008, Figure 2.18 (b)). This VI can be modified easily to allow for more thermocouples. The array of temperatures from the DAQ assistant is channeled into this VI and the signals are split into 5 because the signal contains a cluster of 5 temperature readings. The VI allows for plotting temperature and flow rate against time in the main panel. The measured temperature and flow rate values are saved at the same time under c:\experiment\TEMPERATURE.lvm and \flowrates.lvm in PC. A timer is also applied in this VI to record the amount of time that has passed since we started to run the VI.

The other block diagram (Figure D.2) is a voltage and current control loop which communicates to the power supply, which was an assigned GPIB address of ‘5’ for this study. This block diagram includes the capability of setting voltage and current. Similar to the temperature and flow rate loop of Figure D.1, the second loop allows the measured power, voltage and current values to be displayed in real-time and to be saved under c:\experiment\POWER.lvm, \voltage.lvm, and \current.lvm in PC respectively. Both of the loops are equipped with a ‘CUTOFF-TEMP’ cluster to avoid burn-out of the heater tube.

For every acquisition loop, the LabVIEW program checks whether any of the thermocouple temperatures have exceeded a pre-set melting temperature of the heater material. If the largest temperature exceeds a certain temperature set (‘CUTOFF-TEMP’ in Figure 2.17) set by the user based on the material properties (melting point

of Inconel 600), this VI (Figure D.1) will send a trigger to power.vi (Figure D.2) and decrease the set voltage by a factor ('Divide Voltage by?' in Figure 2.17) determined by the user. The cut-off temperature and the voltage divider can be also modified by the user during an experiment.

A high sampling and data collection rate is required to minimize incurring burnout of the heater tube. The signal conditioning module (SCXI-1102C) has a sampling rate of 333 kHz for analog inputs while the DAQ card (PCI-6220) samples at a maximum rate of 250 kHz. There is a 10 kHz low-pass filter built into the SCXI-1102C that filters signals above 10 kHz, so the whole set-up can effectively sample up to a rate of 10 kHz. The actual sampling rate by the computer will be lower because there is a certain amount of processing time involved in one temperature acquisition loop. For every acquisition loop, the LabVIEW program takes 1 temperature reading from each thermocouple and checks whether any of them has exceeded the cut-off temperature. The amount of time needed to perform these operations will lower the actual sampling rate. The LabVIEW program in this study gives the sampling rate of 110Hz (Huang 2006).

The PC requirements to use LabVIEW software are 256 MB in RAM memory, 866 MHz of speed in the processor and 900 MB of hard disk space. The computer was selected to allow for considerable complication of the PC requirements in the future and to use up to date technology to operate the experiment. The specifications of the acquired PC are the follows: Windows XP; Intel Pentium 4 processor at 3 GHz; 1.49 GB of RAM memory; 75 GB of Hard disk drive space; 17" Flat screen dual monitors.

2.2.4.2 Flow Meter and Calibration

There are two ways of detecting if a chemical reaction occurs in a FIBOR as mentioned earlier: by measuring a nonzero flow rate of the gas output section using a

flow meter and assuming that none of the products are soluble in the reactant liquid; and by analyzing the output gas flow with a GC to identify the product gas species. Chemical detection by GC is discussed in the next section.

The product stream flow meter mentioned earlier accounts for a minor dependence on density, pressure, and fluid viscosity. The flow meter shown in Figure 2.1 measures the mass flow rate of gases in the range from 0 to 10 L/min while giving a linear output signal over 0-5 VDC. Figure 2.18 (a) shows the flow meter's mechanical drawing. Pin 1 and 7 are for power input while pin 4 is for the output signal. Pin 9 must be connected to pin 5. Voltage signal from pin 4 is transmitted to the PC through a flow meter DAQ (NI USB-6008) as shown in Figure 2.18 (b). The flow meter DAQ has eight analog inputs at 12-bit and 10 kS/s and it is compatible with LabVIEW. The LabVIEW program saves the collected voltage signal showing its change on the panel (Figures 2.17) at the same time.

The output signal in voltage from the flow meter is converted to flow rate values using an appropriate calibration correlation equation between voltage and volumetric flow rate. Calibration is accomplished by a DryCal Definer-220 flow meter (see Figure 2.19) to give absolute scale as there will be a significant error when the measured gas mixture contains a variety of species due to the density difference among the gas mixture. The manufacturer's calibration cannot then be used. GC analyses of the FIBOR product gases in this study found a variety of species as noted earlier.

We calibrated the OMEGA #FMA-A2309 flow meter (an accuracy of ±1%) against the DryCal absolute meter with three types of standard gases which have similar concentrations to the actual FIBOR product gases of three experimental cases. One calibration gas (#1) is a binary mixture with the molar concentration of H_2 66.66% and CO 33.34% which corresponds to the cases of catalytic reaction and

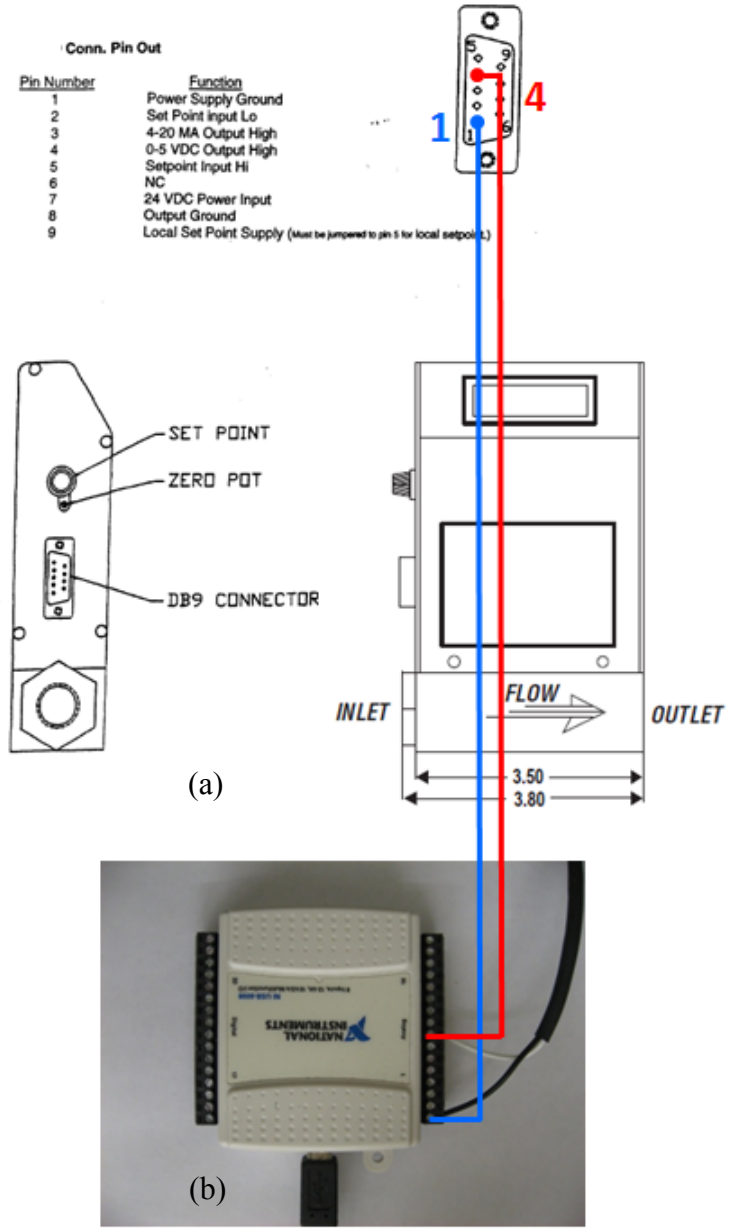

Figure 2.18: (a) Flow meter and (b) DAQ connection

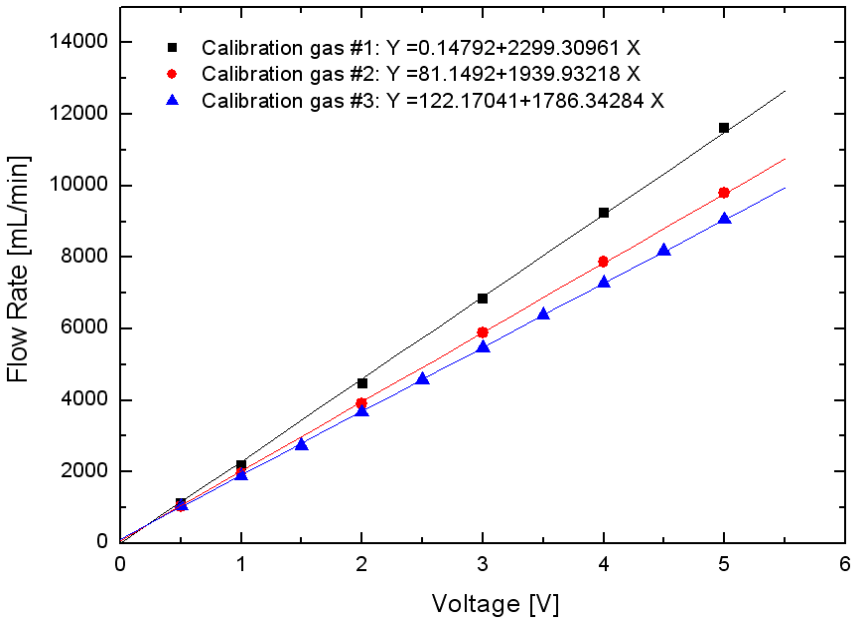

(a)

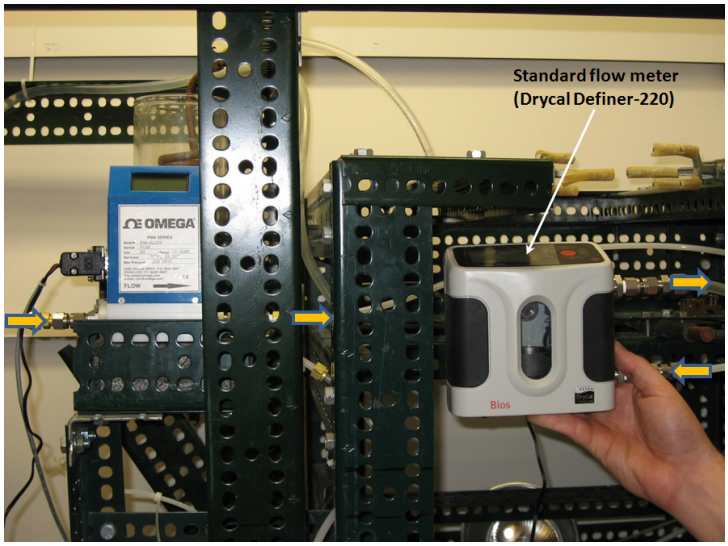

(b)

Figure 2.19: (a) Flow meter calibration lines and (b) calibration method

thermal decomposition of methanol. Another calibration gas (#2) has more species: 2% C_2H_2, 2% CO_2, 4% C_2H_4, 2% C_2H_6, 5% CH_4, 35% H_2, and 50% CO which is close to the product gases for ethylene glycol's catalytic reaction. A third calibration gas (#3) with concentration of 14% C_2H_4, 18% CH_4, 18% H_2, and 50% CO was used. This gas mixture corresponds to thermal decomposition of ethylene glycol.

Three calibration correlations from the three standard gases are shown in Figure 2.19 (a). The calibration equations are the following:

$$\text{Calibration gas \#1: } Y = 0.15 + 2299.31 \times X \tag{2.2}$$

$$\text{Calibration gas \#2: } Y = 81.15 + 1939.93 \times X \tag{2.3}$$

$$\text{Calibration gas \#3: } Y = 122.17 + 1786.34 \times X \tag{2.4}$$

where

X: voltage [V] and Y: flow rate [mL/min]

Each calibration correlation was used based on a similarity between the concentrations of the standard gas and the actual product gas measured by GC. Eq. 2.2 was used for methanol catalytic and thermal decomposition; Eq.2.3 for ethylene glycol catalytic reaction; and Eq. 2.4 for ethylene glycol thermal decomposition as discussed in Section 3.2 and 3.3. Specifically, the product gas concentrations for methanol catalytic and thermal decomposition were very close to hydrogen to carbon monoxide ratio (2:1) of calibration gas #1. The product concentration of ethylene glycol's thermal decomposition was also quite close to that of calibration gas #3. Even though the GC trace of ethylene glycol's catalytic reaction shows a difference from the concentration of calibration gas #2, the selection of the calibration gas #2 is justified due to little slope change between the correlation lines of the calibration gases #2 and #3 (see Figure 2.19 (a)) whose hydrogen compositions are quite different.

Figure 2.19 (b) illustrates how to acquire the flow meter calibration lines. The DryCal Definer-220 meter measures absolute flow rate in mL/min of the specific gas while the Omega flow meter provides only a voltage signal. The digital flow meter is calibrated by connecting it in series to the DryCal flow meter and the calibration gas flow rates. Voltage signals and their corresponding actual flow rates are measured by the Omega flow meter and the standard flow meter between 0 and 14 L/min from which the calibration correlations of Eqs.2.2 to 2.4 are obtained.

Noticeable noise is generated during collection of flow rate data. This is likely due to the pressure fluctuation or turbulent bubbling dynamics as gases are expelled from the bulk liquid. As a result, statistical averaging was performed to process the noise for easier analysis. OriginPro7 provides a statistical analysis tool called "Adjacent Averaging". Figures in Appendix G compare a sample analyzed data set (b) with original date (a). The polynomial fit is applied to the raw data (a) and overlaid with the adjacent average data (b) to show the accuracy.

2.2.5 Chemical Detection Module

2.2.5.1 Gas Chromatograph (GC)

The GC used in this study was capable of detecting H_2, CO, CH_4, C_2H_2, C_2H_4, CO_2, and C_1 to C_5 alkanes as these are the anticipated main product species. The GC used in this study is a temperature programmable gas chromatography with thermal conductivity detector (GOW-MAC 600 Series). The GC specification is as follows: model #: Gow-Mac GC600P00012801 (115VAC, 60Hz, 2000W); programming rate: 0.1°C to 40°C/min in 0.1°C increments; oven cooling rate: 300°C to 50°C in 5 minutes; 200 Thermal Conductivity Detector, 10-952 with WX filaments; 309 Pneumatically Actuated 6 Port Gas Sample Valve with 2 ml sample loop; 405 Interface PCB to activate TTL closure from external source.

The GC's capability to detect product species is largely dependent on the "column(s)" installed. A GC column is a narrow tube filled with packing material. Product species flow through the column with the aid of a "carrier gas" such as helium. Gases travel through certain columns in specific amounts of time, otherwise known as the "retention times." The retention time is related to the partition coefficient of the sample between the gas and condensed phase. An important variable in the partition coefficient is the molecular weight, and thus the composition of a gas mixture can be determined.

Columns are limited to how many different species they can detect based on their retention time. Our columns had the following specifications: serial #: C3211980032; size and material: 8'x1/8", ST.ST.600; type: Molecular Sieve 13x80/100 mesh; max. temperature: 375°C; allowable covering impurities: H_2, N_2, O_2, CH_4, & CO in He (carrier gas).

The GC is interfaced with data acquisition software (Chrom Perfect Software ® Spirit TM LSI ver.5.0) and a 32 Bit Chromatography Data System (Tigre III). The software supports batch reprocessing, multilevel internal or external standards, sequence files, ASCII files, graphical calibrations, comparison of up to 16 chromatograms, and graphic method development.

The configuration shown in Figure 2.20 allows for the extraction of a sample from the FIBOR product gas into GC analysis (The mechanical drawing is shown in Figure A.8). Downstream of the flow meter (Figure 2.20), product gases are extracted through a mini-pump set at 0.03 L/min (Figure 2.21). The relatively small rate of flow induced by the mini-pump prevents disturbance of the flow meter and also entrainment of air at the end of the exhaust line. The Chrom Perfect software is programmed to allow for an automated gas sample injection into Column A under control of the user.

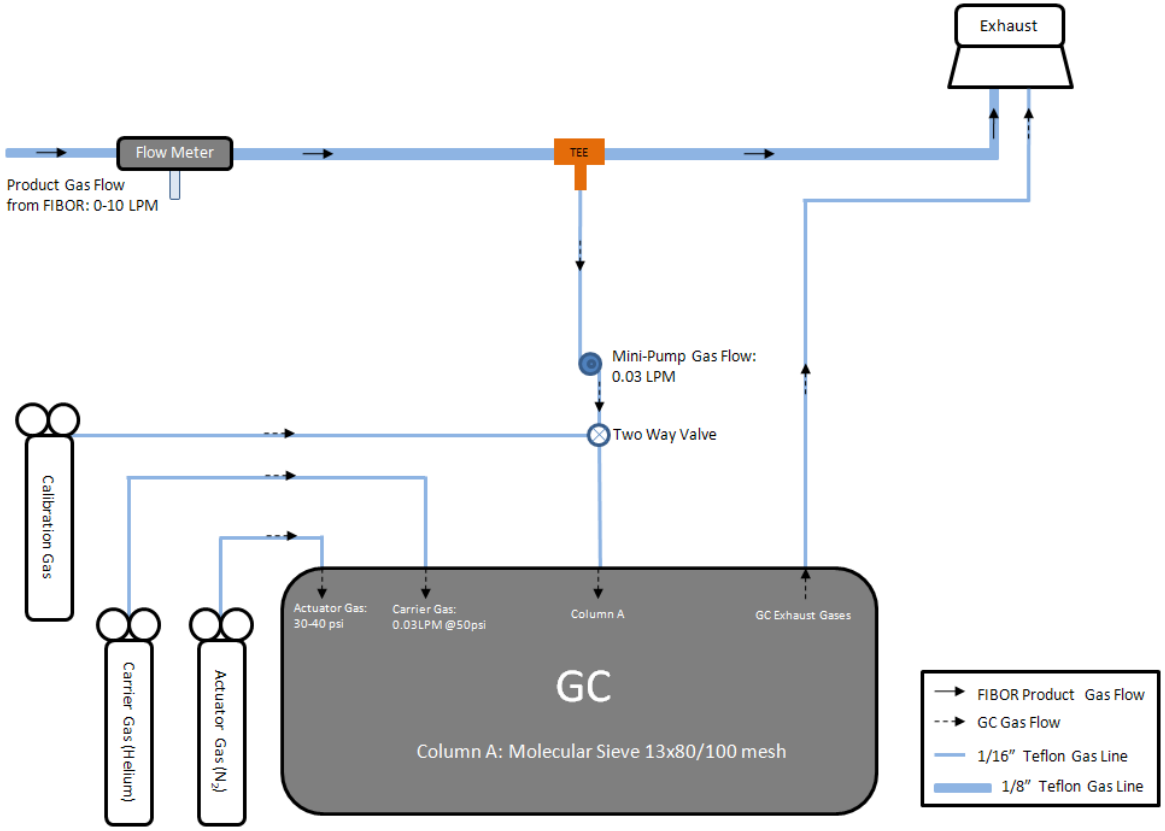

Figure 2.20: Configuration of the first version GC

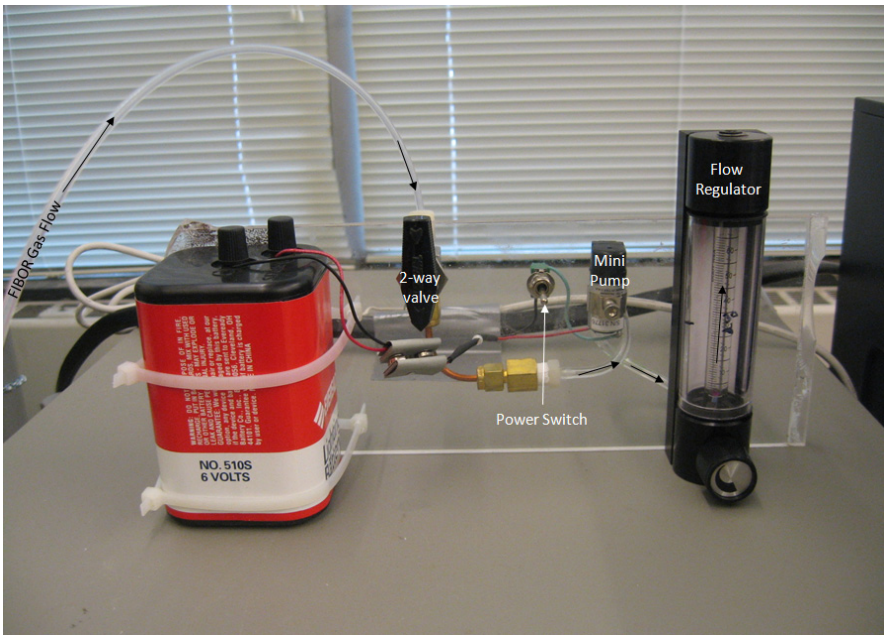

(a)

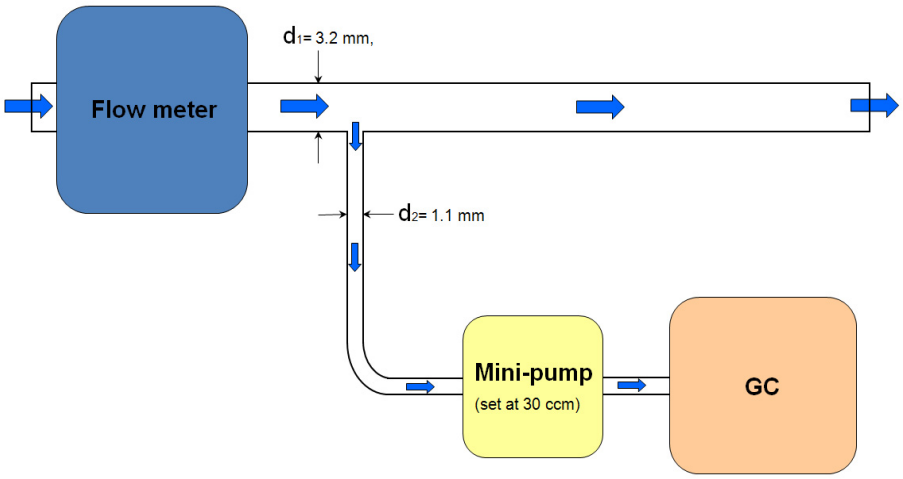

(b)

Figure 2.21: (a) Mini-pump for gas sampling and (b) the schematic

The actuator gas is compressed nitrogen set at 30-40 psi which provides pneumatic pressure (to a solenoid valve) to activate the gas sample injector valve. The carrier gas is compressed helium with a regulated pressure of 50 psi and a flow rate of 0.03 L/min.

Two columns were installed in parallel to detect product species of interest. Figure 2.22 shows the configuration of the upgraded GC installed with two columns and two liquid injection ports (Figure A.9 is the mechanical drawing). Two separate samples must be extracted after reactant vapors are condensed and separated. The first sample is injected into the first column capable of detecting H_2, O_2, N_2, CO and CH_4 (Column A is an 8ft. x 1/8in Molesieve 13x, 1ml Loop Column).

A second sample is injected into the second column capable of detecting CO_2 and hydrocarbons up to C5 (Column B is an 8ft. x 1/8in Haysep Q 13x, 1ml Loop Column). The GC is programmed with data acquisition software to generate a chromatogram for each column, and it is retrofitted with liquid injection ports for liquid chromatography, but this capability was not used in this study. Instead, actual liquid testing utilized a GC-MS (Agilent Technologies 6890N.5973 High Performance Combination) (though future research may utilize the GOW-MAC 600 Series GC for liquid testing). Further information of the GC upgrade is discussed by Evangelista (2010).

2.2.5.2 Isothermal and Temperature Programming Modes

It is possible that traces of higher hydrocarbons exist in the gas stream such as C_2H_2, C_2H_4 and C_2H_6 along with CO, H_2, and CH_4. The GC with a molecular sieve 13x column cannot detect higher hydrocarbons in an appropriate GC running time (i.e. around in 20 minutes) in the isothermal mode. The temperature programming mode available in the GOW-MAC 600 enables the detection of such higher hydrocarbons.

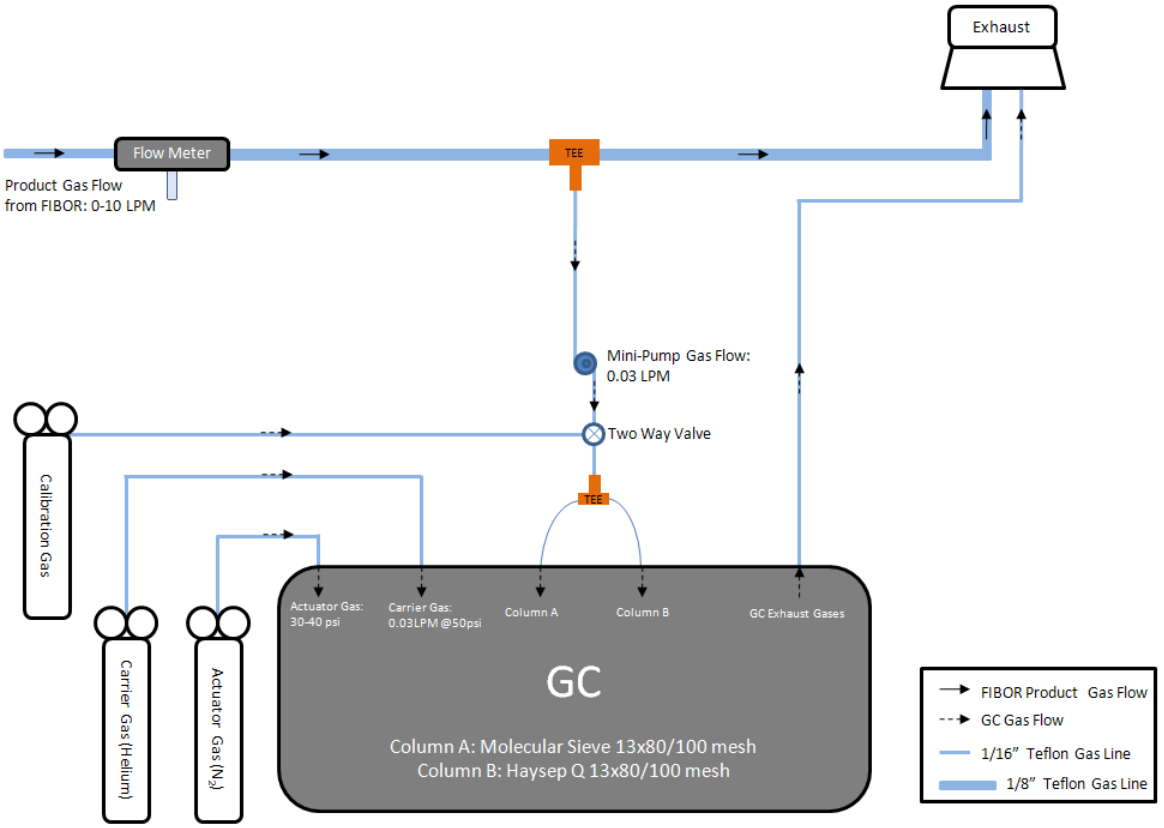

Figure 2.22: Configuration of the second version GC

The standard isothermal GC detection mode is used with a retention time of 5 minutes which is sufficient to detect CO, H_2, and CH_4 of main products for methanol when the column oven temperature is set at 95°C and the filament (Thermal Conductivity Detection: TCD) is set to 60°C as shown in Figure 2.23 (a).

On the other hand, the higher hydrocarbons (i.e. C_2H_2, C_2H_4, C_2H_6) can be detected in a comparatively longer time, 20 minutes, only at a higher oven temperature of 140°C while the common species (H_2, CO, CH_4) should be detected in the lower temperature of 60°C to avoid peak overlaps. Thus the oven temperature programming in Figure 2.23 (b) enables the detection of all suspected gaseous species in ethylene glycol experiments. TCD temperature should always be higher than the oven temperature for proper GC functionality.

2.3 Catalyst Fabrication

The catalyst fabrication process includes the following steps as illustrated in Figure 2.24: 1) oxidation of the tube surface; 2) creation of an aluminum oxide adhesion layer; and 3) application of the platinum catalyst by impregnating the alumina layer. In the first step, a cleared bare tube is roughened (with #320 grit paper) and then baked in an oven at 900°C for four hours. In the second step, a "washcoat" is applied to the tube using a pipette to drip it over the tube which is rotating at about 30rpm (the washcoat is an aqueous gamma alumina solution with pH 3). The washcoated tube is then baked at 800°C for five hours. The second step is repeated at least five times until a uniform alumina layer is deposited. A delicate balance exists when applying the adhesion layer on the surface as it is critical to establish a uniform catalyst coating to promote chemical reaction. If the layer is too thick it can increase the thermal resistance of the tube and possibly prevent film boiling. In the third step, a tetraamine platinum nitrate solution with pH 3 is applied by dripping from a pipette

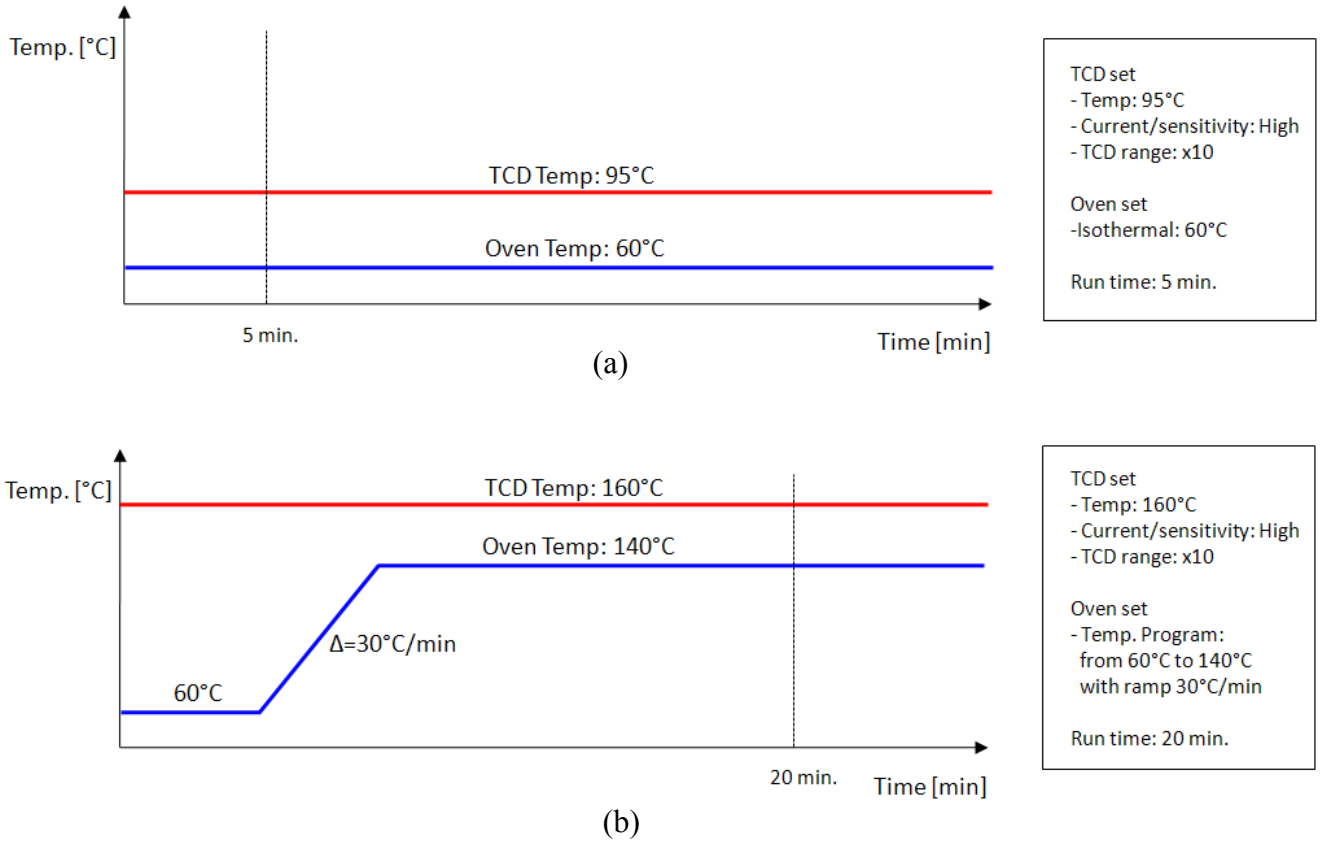

Figure 2.23: GC running modes: (a) Isothermal and (b) Temperature Programming modes

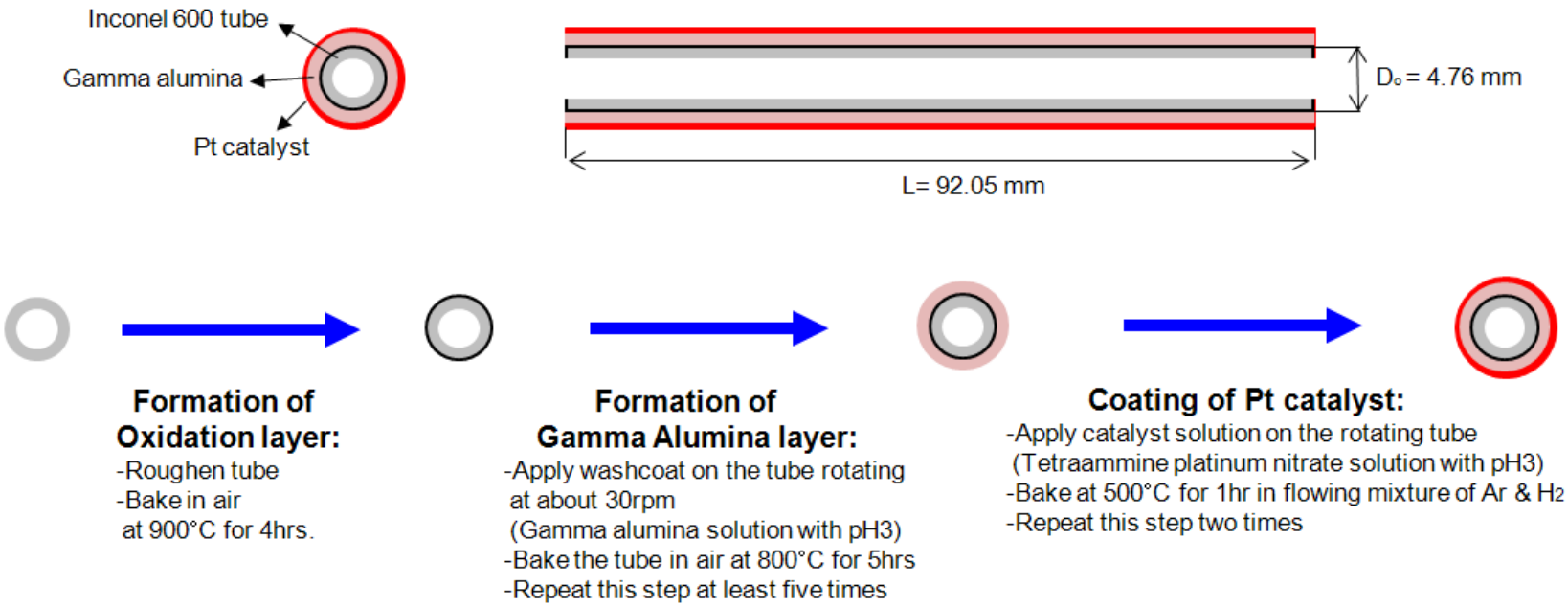

Figure 2.24: Catalyst coating procedure

while the tube is rotating at 30rpm. The tube is then baked in an oven at 500°C for one hour in a flowing mixture of 96% argon and 4% hydrogen for reduction.

An attempt to use the above procedure in our laboratory gave uncertain results. Experiments using methanol with a catalyst coated tube we fabricated (see Figure 2.25 (a)) as discussed above gave irregular and unstable product flow rate as shown in Figure 2.25 (b). The catalytic tube appears active generating considerable product gases up to approximately 7 L/min in the FIBOR as represented by red line between 600°C and 900°C (while black line is product flow rate due to catalyst activity above liquid reactant pool). Hysteresis and significant fluctuations were observed in that temperature range. The instability in flow rate is considered to be caused by the irregular catalyst loading along the tube. Consequently, even though a considerable effort had been made to fabricate the catalyst coated tube, we decided to enlist the help of an expert to fabricate catalyst coatings which would hopefully result in more uniform and well characterized results. Catacel Corporation (Garrettsville, OH) provided two professionally fabricated catalytic tubes which have a precise uniform catalyst coating in black as shown in Figure 2.26 (b). These tubes were fabricated by a process similar to that given above.

Specifications are presented for the catalytic tubes in Table 2.3. The first catalyst coated tube (CT#1) is an Inconel 600 tube with an alumina oxide (Al_2O_3) layer impregnated with 55% by wt. platinum black (Pt) catalyst, while the second catalyst coated tube (CT#2) had 38% by wt. Pt. In this study, CT#1 was used for methanol and CT#2 was used for ethylene glycol. Since bare tubes do not have a catalyst, chemical reaction in the FIBOR occurs by thermal decomposition (pyrolysis). It should be noted that no attempt was made to systematically vary catalyst property. Rather, the intent was merely to show the extent to which a catalyst could prompt reactions at a lower temperature than a bare tube.

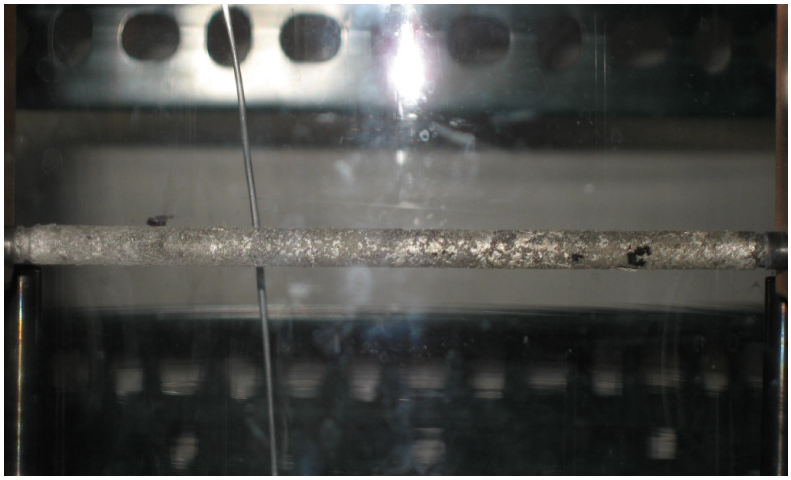

(a)

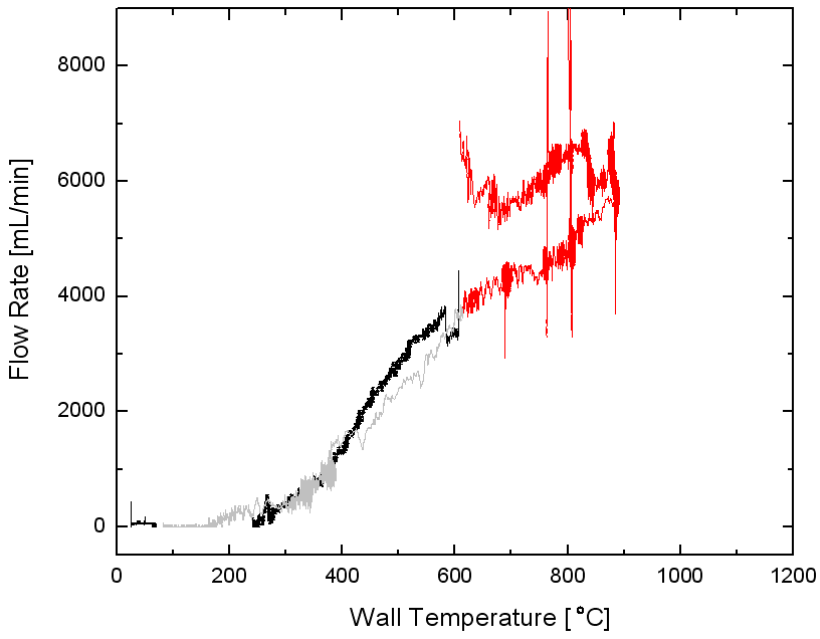

(b)

Figure 2.25: (a) Self-fabricated Pt catalytic tube and (b) the experimental result

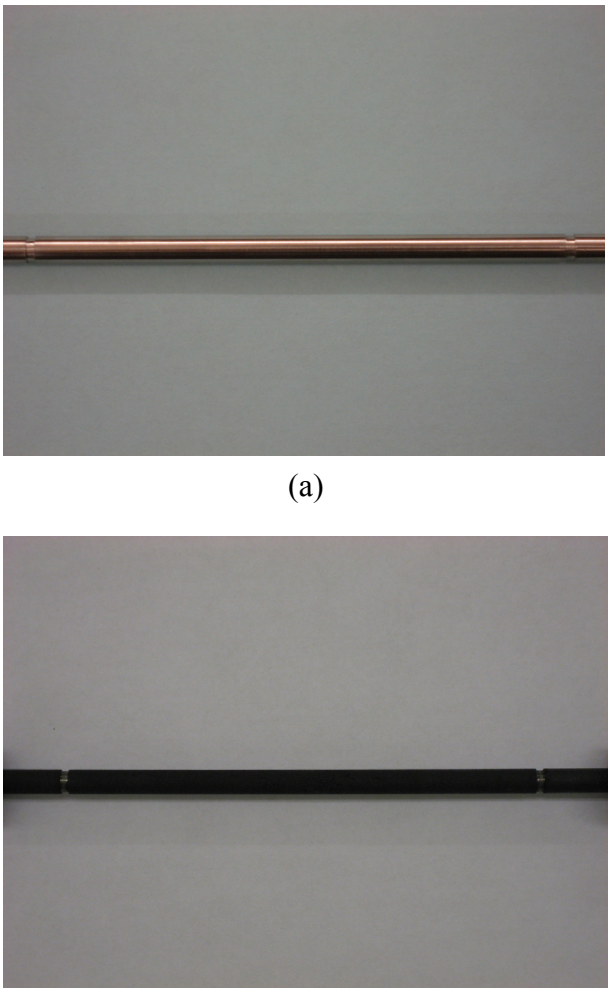

(a)

(b)

Figure 2.26: (a) Bare tube and (b) catalyst coated tube provided by Catacel Corp.

Table 2.3: Specification of test tubes

	Alumina [g]	Pt [g]	wt. % of Pt	Total wt. [g] (Before / After use)	Thickness of alumina [mm]
1. Catalytic tube #1 (used for methanol)	0.045	0.054	55%	0.099 / 0.118	0.008
2. Catalytic tube #2 (used for ethylene glycol)	0.047	0.029	38%	0.076 / 0.087	0.009
3. Bare tube	0	0	-	-	-

2.4 Procedure for Developing Film Boiling

The procedure for establishing film boiling is critical to success for creating the FIBOR. Especially for tubes coated with a catalyst, it is important that film boiling be established with no liquid coming into contact with the catalyst as this could deactivate it (this is not a concern for bare tubes for which thermal decomposition is the reaction mechanism). As a result, film boiling of catalyst-coated tubes cannot be established in the more traditional manner of immersion, power increase, and transition from nucleate boiling to critical heat flux (CHF) and then to film boiling following the red dot line in Figure 2.27 (a). Furthermore, immersion prior to increasing power will be problematic for the power-controlled procedure used here as the temperature excursion on transitioning from CHF to film boiling will typically occur far too fast to avoid burnout or severe damage to the tube.

A solution to these problems was developed that facilitated power adjustment during the wall temperature excursion and which also mitigated the catalyst deactivation problem. The procedure also facilitated assessing the efficacy of the catalyst to promote reaction prior to carrying out a complete experiment to determine if the catalyst was viable. Figure 2.27 schematically illustrates the procedure for establishing film boiling. The procedure is as follows.

1. A flow of nitrogen gas (10-20psi, ~100ccm) is first maintained in the chamber to prevent potential ignition of reactant vapors prior to immersion (the presence of nitrogen does of course show up in the GC trace of the output gases as described later).
2. The tube is pre-heated to about 600K in an empty chamber. This prevents any unintentional liquid/surface contact (inadvertent bubbling/splashing due to air pockets in feedstock line) as the reactant liquid enters the chamber.

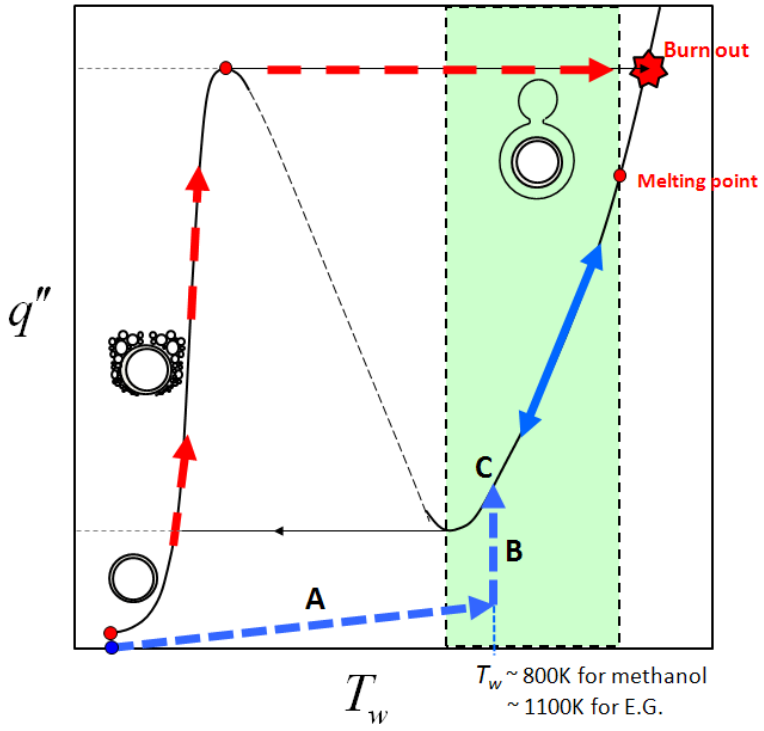

(a)

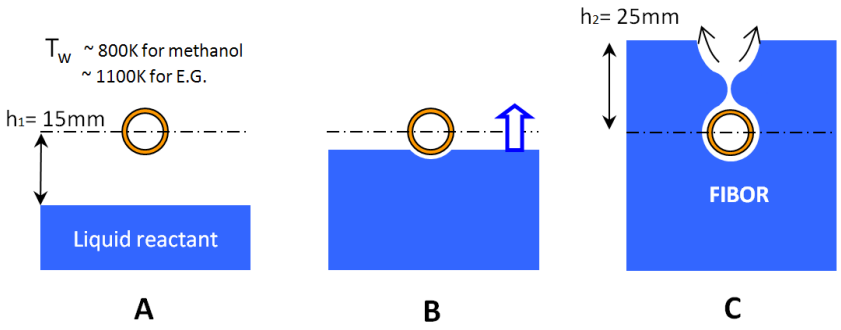

(b)

Figure 2.27: Quenching Method

3. Reactants are drawn from the bottom to a level of about 15mm below the heater ('A' in Figure 2.27).
4. The bulk pool reactant temperature is then increased to its saturation point by four immersion heaters installed in the chamber.
5. The temperature of the tube surface is then raised to about 800K for methanol (or 1100K for ethylene glycol). This temperature is chosen based on several trial and error attempts until a high enough temperature was found. Theoretically, the initial heater temperature should only need to be above the Leidenfrost, or minimum film boiling temperature. During this period, vapors are produced and the activity of the catalyst is assessed by monitoring both the flow meter and GC output (chemical reaction occurs on the surface of the tube as the vaporized reactant flows around the hot tube).
6. The liquid level is then raised around the tube. Quenching effects are coordinated with increasing the heat input to the tube ('B' in Figure 2.27). The process is similar to that described by Ede and Siviour et al. (1975). The liquid level starting from 'A' is raised slowly at a rate of approximately 0.5 millimeters per second. As the liquid level appears to touch the bottom of the tube, power is simultaneously increased to attempt to maintain the wall temperature at 800K for methanol and at 1100K for ethylene glycol. Successful immersions with no liquid contact were consistently attained by quickly raising the power setting by a factor of about 4 for a bare tube while by a factor of 9 for a catalyst coated tube. Although this method has not been developed or analyzed theoretically, it is experimentally proven to be an effective and consistent means to achieve film boiling. Once film boiling is attained, the liquid level is kept 25 mm above the tube ('C' in Figure 2.27). It

is noted that this rather elaborate process is unnecessary for bare tubes where surface deactivation is not an issue.

7. Experimental data are collected by traversing the film boiling curve through adjusting the power input into the tube within the FIBOR operational domain. Power (or voltage) is increased or decreased by increments of 0.02V, allowing 2-3 minutes for the heater temperature to reach steady state at each point. Data outputs include thermocouple temperatures, flow rates, current, voltage, power and time. They are displayed on the LabVIEW interface (Fig.2.17) and automatically stored as column data in the folder of C:\experiment in PC.

CHAPTER 3

EXPERIMENTAL RESULTS AND DISCUSSION

The rate of chemical reaction, k, has an exponential dependence on temperature, T, evidenced by the common Arrhenius Equation where E_a is the activation energy, R is the universal gas constant and A is a pre-exponential factor (Arrhenius 1889).

$$k = Ae^{\frac{-E_a}{RT}} \tag{3.1}$$

Coating the heater's surface with a suitable catalyst lowers the activation energy by opening up new pathways for chemical reaction, thereby increasing the rate of chemical reaction (Oxtoby et al. 2002). It follows that selecting a suitable catalyst can promote higher product flow rates at lower temperatures.

Platinum (Pt) was selected as a catalyst material because it is widely used. However, Pt may be susceptible to deactivation at high operating temperatures in the FIBOR. Generally, catalyst performance may degrade during operation due to fusion of the catalyst crystal structure at high temperatures, otherwise known as sintering (Baird 1973). The catalyst surface can also become fouled with carbon deposits through the chemistry of equations 2.7 through 2.9, known as "coking" (Xun 2009). Lastly, the catalyst surface can detach or delaminate from the heater surface due to differential thermal expansion of Inconel 600 (heater material) and adhesion material of the catalyst. The catalyst deactivation is further discussed in Section 3.5 with experimental evidences.

Experiments in this research mainly consist of four combinations of two reactant substances (methanol and ethylene glycol) and two chemical modes (catalytic

reaction and thermal decomposition). Experiments are repeated twice to check repeatability resulting in a total of eight experimental results. In the experiments with a catalytic tube, a noticeable product flow rate decrease was observed between the first and second experiments (the repeatability test) implying catalyst deactivation (A bare tube does not involve this issue). This observation motivated two separate endurance tests of the catalytic tubes with methanol and ethylene glycol under prolonged operating conditions.

A conversion efficiency is defined because it is natural to evaluate a chemical reactor's efficiency. The FIBOR's conversion cannot be directly measured from experiments unlike conventional chemical reactors due to its unique physical mechanism. Operating parameters, namely reactant flow, is estimated through an energy balance around the FIBOR.

3.1 Boiling Curve

Figures 3.1 and 3.2 show boiling curves for bare tubes, CT#1 and CT#2 for methanol and ethylene glycol respectively, at the indicated sub-cooling. The nucleate boiling portion of the boiling curve for methanol is shown only for the bare tube, as the catalyst would deactivate by liquid contact as noted previously. The differences between the bare tube and catalytic tube are marked at five different temperatures in the Figures. It is noticed that the difference increases with temperature because of more active chemical reaction at a higher temperature. Interestingly, for methanol, the difference between the bare tube and catalyst tube in Figure 3.1 is very close to the heat of reaction (ΔH°_{rxn}) for methanol decomposition (Eq.1.1) of 91 kJ/mol (Imai 1986). The heat of reaction (ΔH°_{rxn}) can be expressed as

$$\frac{\Delta q'' \cdot A_o}{\dot{N}_P / v}.$$

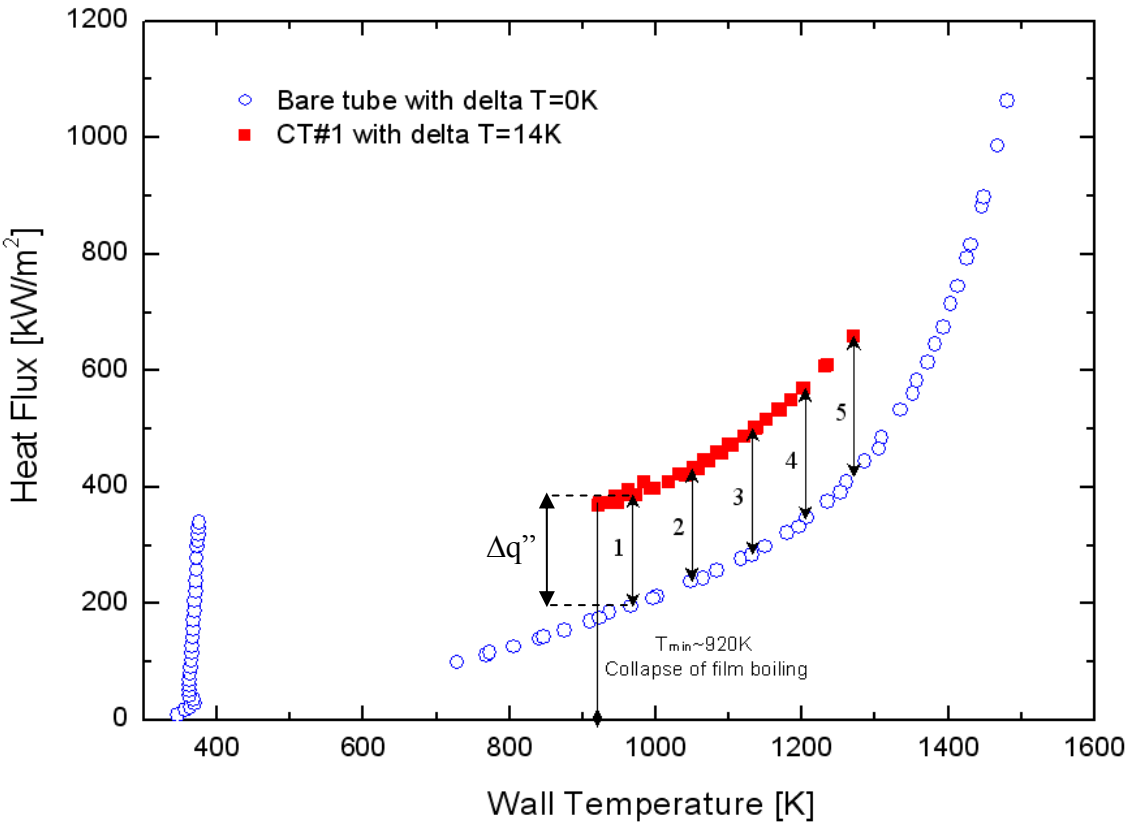

Figure 3.1: Boiling curve for methanol

Since the summation of stoichiometric coefficients (v) for the products of Eq.1.1 is 3, the estimated heat of reaction is 94 kJ/mol. This fact suggests that the influence of the secondary reactions (e.g. that may produce carbon dioxide, methane, or carbon (coke)) are not contributing to the overall energy balance for methanol. This difference is representative of catalytic conversion because the boiling curve of methanol on a bare tube does not have any contribution from thermal decomposition which occurs at higher temperatures as discussed later.

The boiling curve for ethylene glycol (Figure 3.2) exhibits similar features to methanol, but the interpretation is more complicated for several reasons. We found that ethylene glycol is reacting by both thermal decomposition and catalytic means for both tube conditions examined, especially at the higher temperatures of Figure 3.2 (to be discussed later). The reaction chemistry of ethylene glycol is more complicated than methanol so that the difference between the bare and catalyst tubes is not entirely the heat of reaction of Eq. 1.2. The more complex chemical mechanism is supported by GC traces as presented in Section 3.3 which showed species such as CH_4, C_2H_2 and C_2H_4, and GC/MS analysis of the liquid sample which detected seven condensable species in the bulk liquid of ethylene glycol after a long exposure to FIBOR operation. Maintaining the bulk liquid temperature near its boiling temperature is more challenging for ethylene glycol because ethylene glycol has a higher boiling temperature (197.3 °C) than methanol (64.7 °C). The sub-cooling is therefore larger than for methanol in our system and more heat is needed to compensate for the heat loss resulting in higher fluxes in film boiling for ethylene glycol compared to methanol (cf, Figures 3.1 and 3.2).

The effect of sub-cooling can be explained with respect to Figure 1.4. The applied heat ($\dot{Q}_{app}$) due to I^2R heating goes to maintenance of film boiling ($\dot{Q}_{fb}$), endothermic chemical reaction ($\dot{Q}_{rxn}$), and heat loss to sub-cooled bulk liquid ($\dot{Q}_{sub}$):

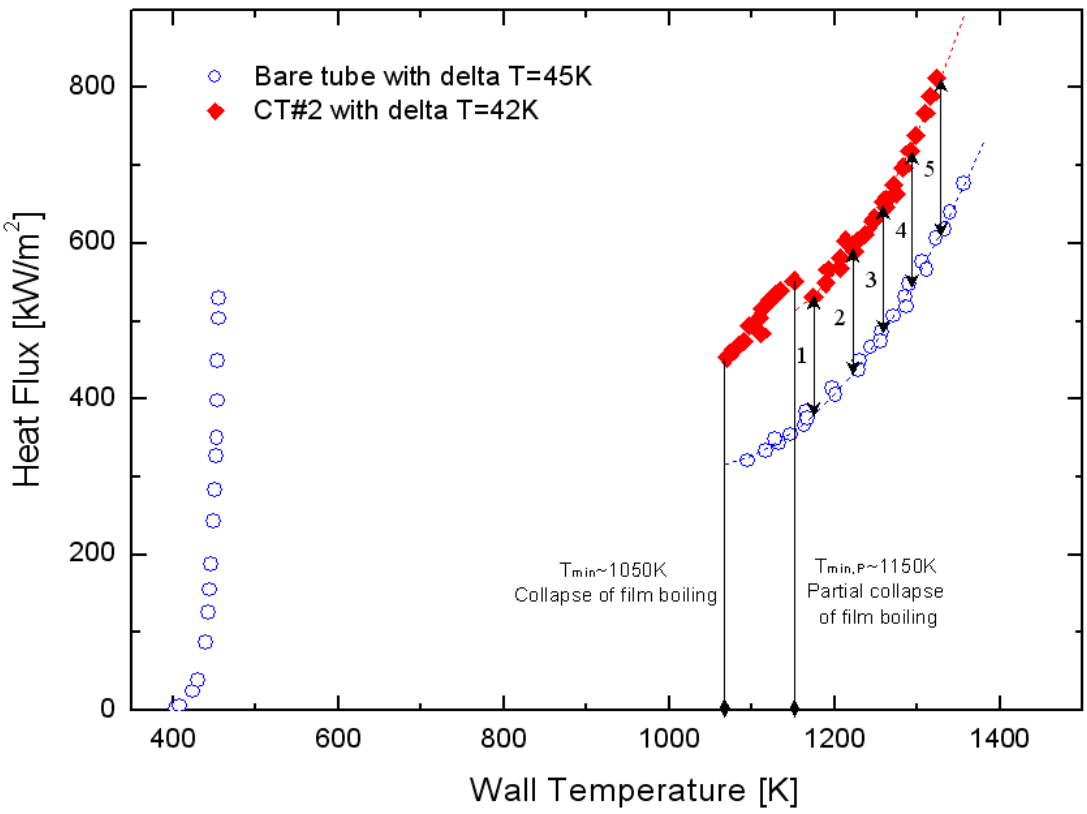

Figure 3.2: Boiling curve for ethylene glycol

$\dot{Q}_{app} = \dot{Q}_{fb} + \dot{Q}_{rxn} + \dot{Q}_{sub}$. Provided that the sub-cooling of the bulk liquid increases, the amount of heat for chemical reaction and maintenance of film boiling decreases resulting in lower product yields and higher film boiling instability respectively.

There is a noticeable upward shift of the heat flux below about 1150K in Figure 3.2. This effect is believed to be caused by destabilization of film boiling due to higher sub-cooling. This conjecture was confirmed by visual observations of nucleate boiling near the ends of the tube where it was clamped to the electrodes. With destabilization, the heat flux increases for a given temperature because of the effective nucleate boiling to transfer heat by bubble action compared to film boiling. If the wall temperature decreases further, nucleate boiling spreads along the heater tube leading to film boiling collapse on the "front" spreads as shown in Figure 3.3.

3.2 Catalytic Reaction and Thermal Decomposition of Methanol

For methanol, the immersion heaters were kept off because the heater tube continues to supply heat high enough to maintain the bulk liquid near its boiling point. On the other hand, the immersion heaters should be at a higher power (around 1,000 Watt) during ethylene glycol's experiments to keep the bulk liquid near its higher boiling temperature (197.3°C). Considerable amount of heat seems to be lost from the FIBOR chamber's boundary (the chamber glass and top and bottom plates) to the atmosphere due to the significant temperature difference.

3.2.1 Catalytic Reaction of Methanol

Figure 3.4 shows the variation of product gas flow rates with wall temperature for CT#1 in methanol with 14K sub-cooling. The numbers signify the sequence of power adjustments. It is important to re-emphasize that the flow rates shown in Figure 3.4 are essentially only due to product gases, which for methanol are non-condensable

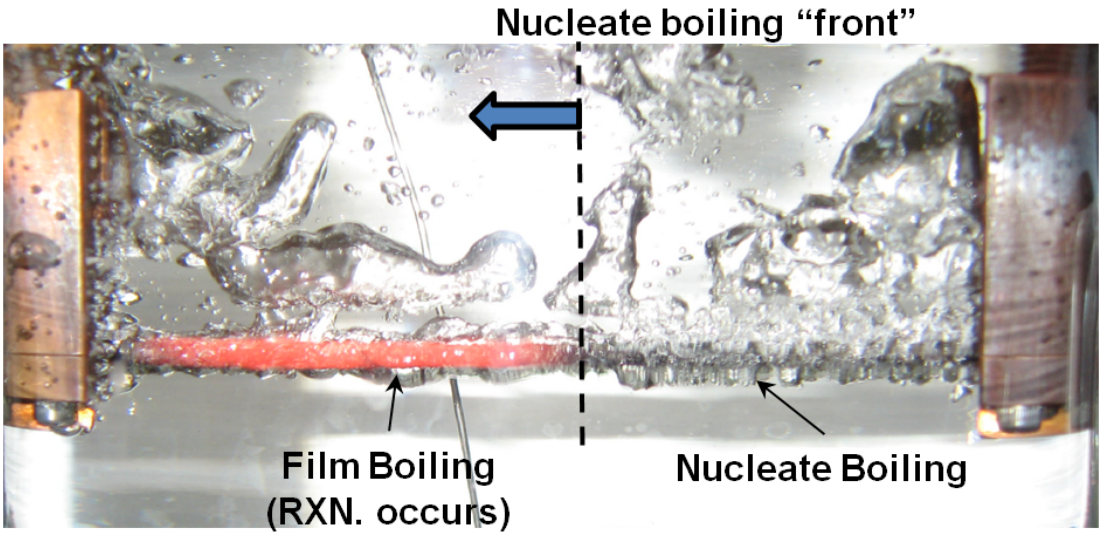

Figure 3.3: FIBOR collapse

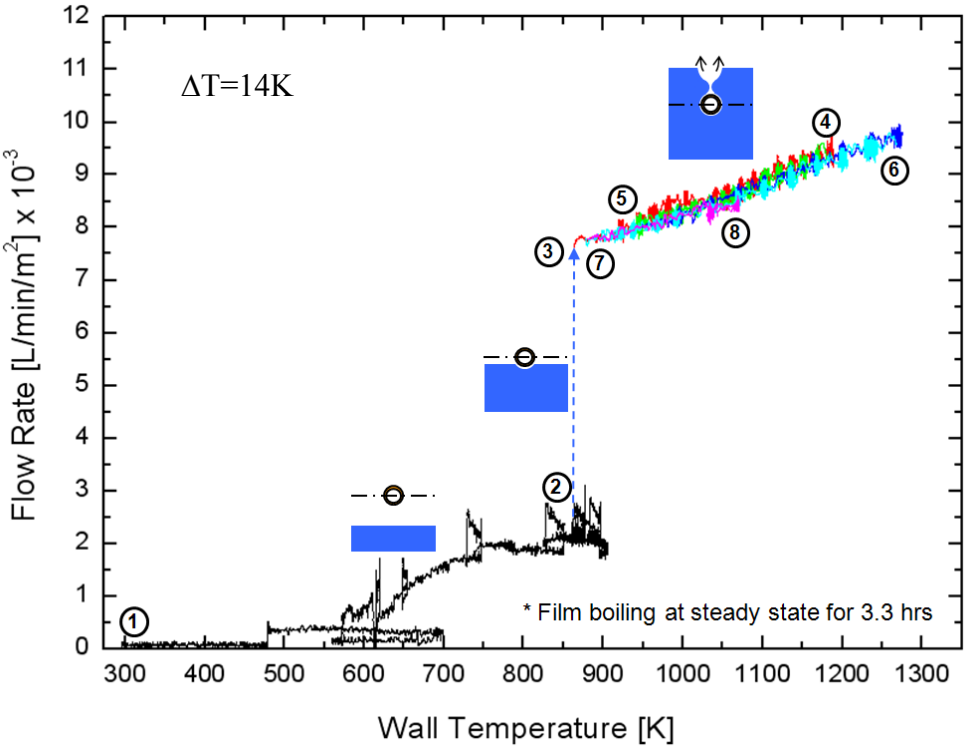

Figure 3.4: Flow rate of product gas (synthetic gas) vs. wall temperature for CT#1 and methanol.

as evidenced by GC analysis and that the methanol temperature did not change over time (see Section 3.6 for ethylene glycol).

Starting with the tube positioned as "A" in Figure 2.27, power was increased from "1" and the first evidence of reaction is observed at about 600K in Figure 3.4. That the flow rate was not zero at 600K signified that we could proceed toward full immersion to create the FIBOR. A temperature of 850K ("2") was chosen as being sufficiently high that the process of immersion and power increase could be coordinated to avoid liquid/solid contact during the transition from Figure 2.27-"B" to 2.27-"C". Again, liquid/solid contact is not a concern for a bare tube where the reaction process occurs by thermal decomposition.

Upon full immersion ("3"), the power was varied to move along the film boiling portion of the boiling curves ("3" to "8"). Yields increased significantly from "2" to "3" and "3" to "4". The corresponding flow rates ranged from 7.8 to 9.4 $L/min/m^2 \times 10^3$. At "4", power was decreased to 940K "5". Power was increased again to "6" at 1270K, then decreased to 920K at "7" and increased again to 1070K at "8" to further assess the efficacy of the film boiling process to promote chemical change of methanol. Figure 3.5 (a) and (b) are photographs of the FIBOR at the wall temperatures of 1033K and 1393K respectively for CT#1 and methanol showing turbulent bubbles agitating the bulk liquid.

Figure 3.6 (a) is a GC trace of methanol obtained at 1018K for CT #1. The peaks are indicated as CO (34%), H_2 (62%), CH_4 (3.1%) and N_2 (0.93%). N_2 was introduced into the gas above the methanol pool to prevent the possibility of ignition in the quenching step for film boiling establishment as noted before. The proportion of these species is close to the theoretical composition based on Eq. 1.1 of 33% CO and 67% H_2 which further indicates that Eq.1.1 is likely the controlling decomposition reaction. The presence of small amounts of CH_4 suggests the relevance of Eq. 1.4 and

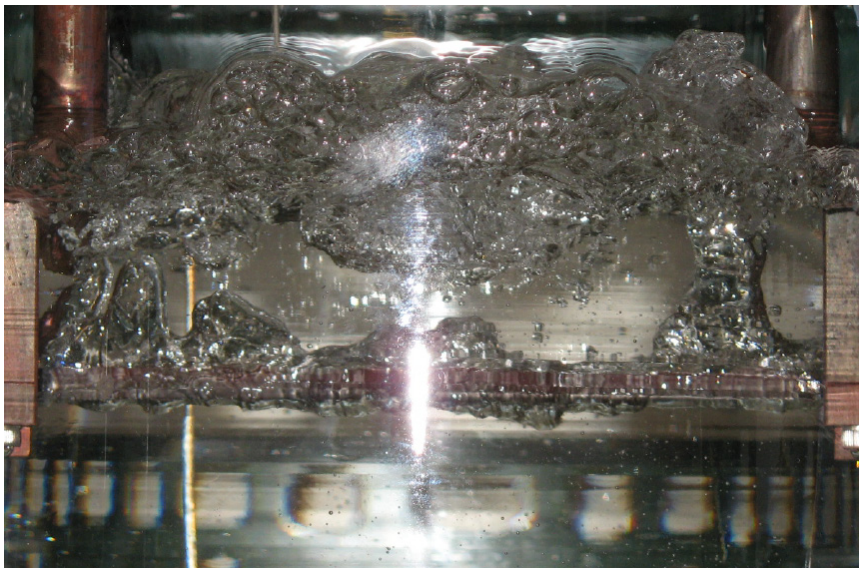

(a)

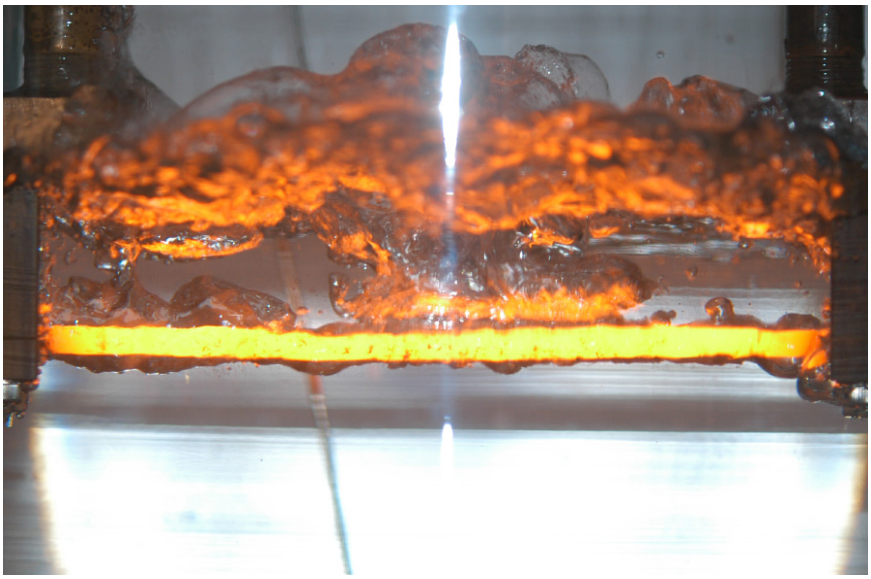

(b)

Figure 3.5: Pictures of FIBOR of methanol

for (a) CT#1 (@T_w=1033K) and (b) bare tube (@T_w=1393K)

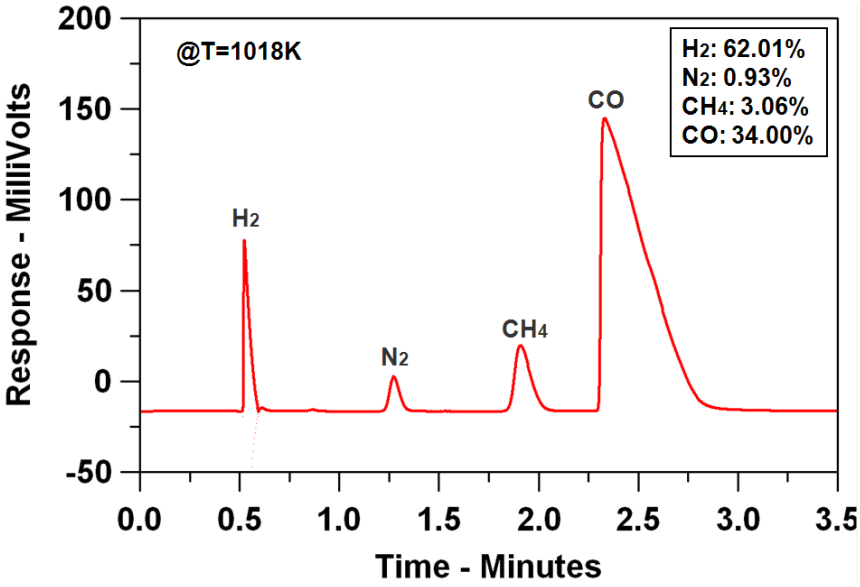

(a)

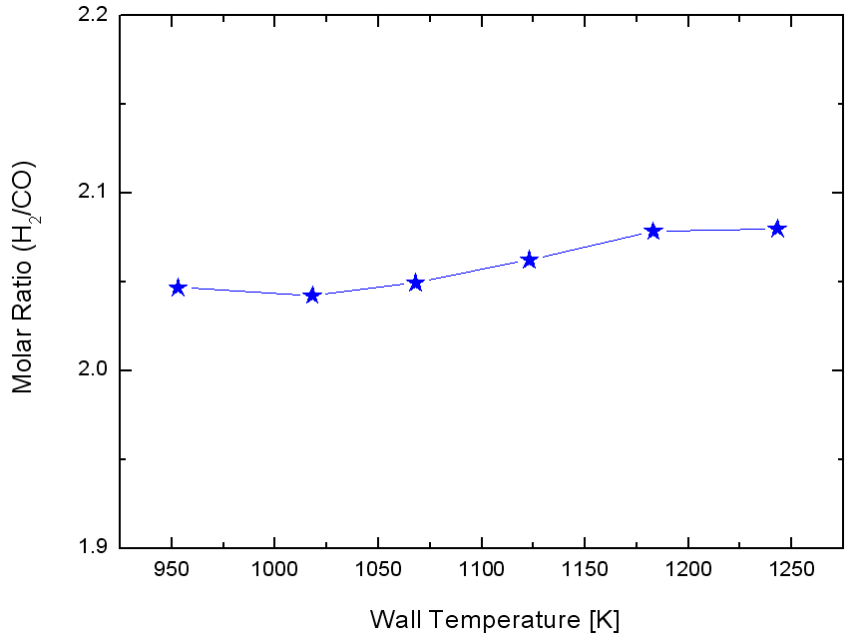

(b)

Figure 3.6: (a) GC trace of the product gas at 1018K and (b) molar ratio change of hydrogen to carbon monoxide with wall temperature for CT#1 and methanol.

therefore the prospect of carbon formation as discussed later. Carbon formation is suggested by the SEMs in Section 3.5. While the carbon formation reactions are exothermic (Xun et al. 2009), the difference between the bare and catalyst tube film boiling heat fluxes (Figure 3.1) is essentially the heat of reaction of Eq. 1.1. This suggests that the potential for energy enhancements by the exothermic formation of carbon to increase the tube wall temperatures does not appear to have been realized. Product gas was measured by GC at different seven temperatures and Figure 3.6 (b) shows the measured molar ratio of hydrogen to carbon monoxide. It suggests that the overall chemical reaction rarely changes with wall temperature in the investigated temperature range.

Figure 3.7 shows additional measurements for CT#1 at a sub-cooling of 14K for two developments of the FIBOR obtained one week apart (blue triangle data were obtained after red circle data) to check the repeatability of the experimental results. A small decrease in product flow rates is observed in the second development of the FIBOR. The difference in flow rates for the same tube temperature suggests that the catalyst has undergone changes between the two sets of data (this result motivated an endurance test to be discussed in Section 3.5). Though the emphasis of the present study is film boiling with reaction, we also investigated some qualitative effects associated with prolonged operation. These include an endurance test to examine the potential for catalyst deactivation (Section 3.5). Again recall that the data in Figure 3.7 will be adjacent averaged values from raw data (see Appendix E) that filters out artificial noise and scatter in the data to provide easier analysis and a cleaner presentation of results.

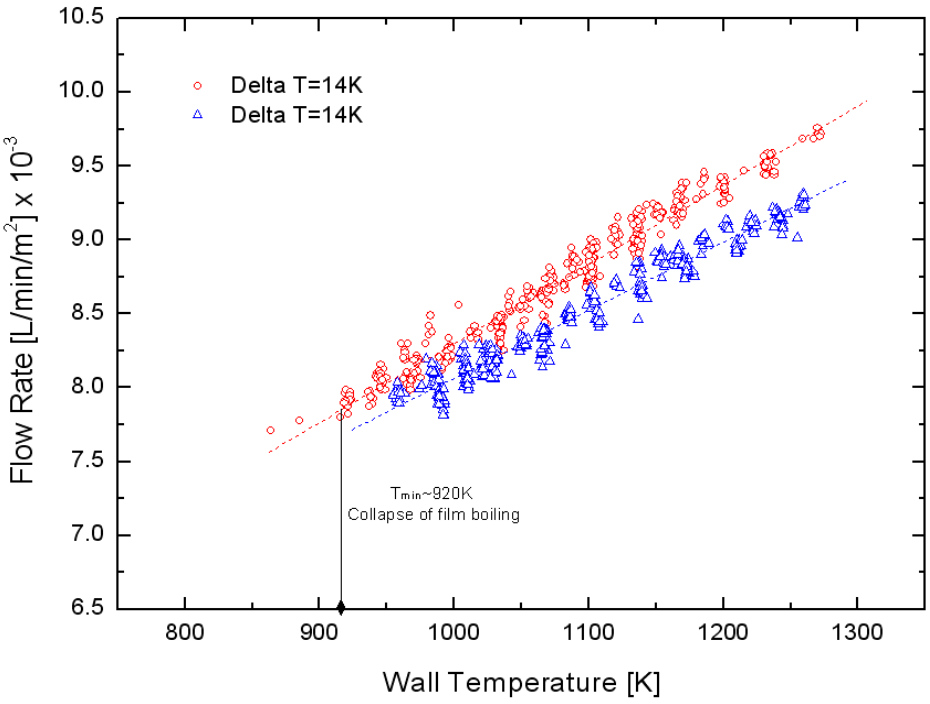

Figure 3.7: Repeatability test for CT#1 and methanol

3.2.2 Thermal Decomposition of Methanol

The reaction mechanism for thermal decomposition was determined by developing a FIBOR around a bare tube because for a bare tube the only reaction possible is thermal decomposition. Figure 3.8 shows product yields for methanol at saturation (zero sub-cooling) and Figure 3.9 (a) and (b) show a corresponding GC analysis at 1423K and the measured molar ratios of hydrogen to carbon monoxide at different four temperatures respectively. The species produced are essentially the same as for CT#1 (Figure 3.6) though the molar ratio change with wall temperature is noticeable which suggests a possible change of chemical reaction mechanism with temperature. Below about 1250K, the yields are essentially zero. This confirms that the flow rates in Figure 3.4, being developed at a tube wall temperature below 1250K, were generated by catalytic reaction only. Without a catalyst, the flow rates shown in Figure 3.8 were quite repeatable for two different experimental runs while the flow rates in figure 3.7 showed differences. This indicates the influence of a changing surface condition on product yields. In figure 3.7, the differences are almost certainly the result of morphological change on the catalyst over prolonged operation.

All flow rate data for catalytic and thermal decomposition of methanol were generated based on the calibration gas #1 (see Section 2.2.4.2). The selection of the calibration gas #1 can be justified because it has a concentration (H_2 66.66% and CO 33.34%) which is very close to the product gases of the FIBOR as shown in Figure 3.6 and 3.9.

3.3 Catalytic Reaction and Thermal Decomposition of Ethylene Glycol

3.3.1 Catalytic Reaction of Ethylene Glycol

Experiments with ethylene glycol showed similar results to methanol. Figure 3.10 shows product flow rates for CT #2 at two sub-coolings taken one week apart.

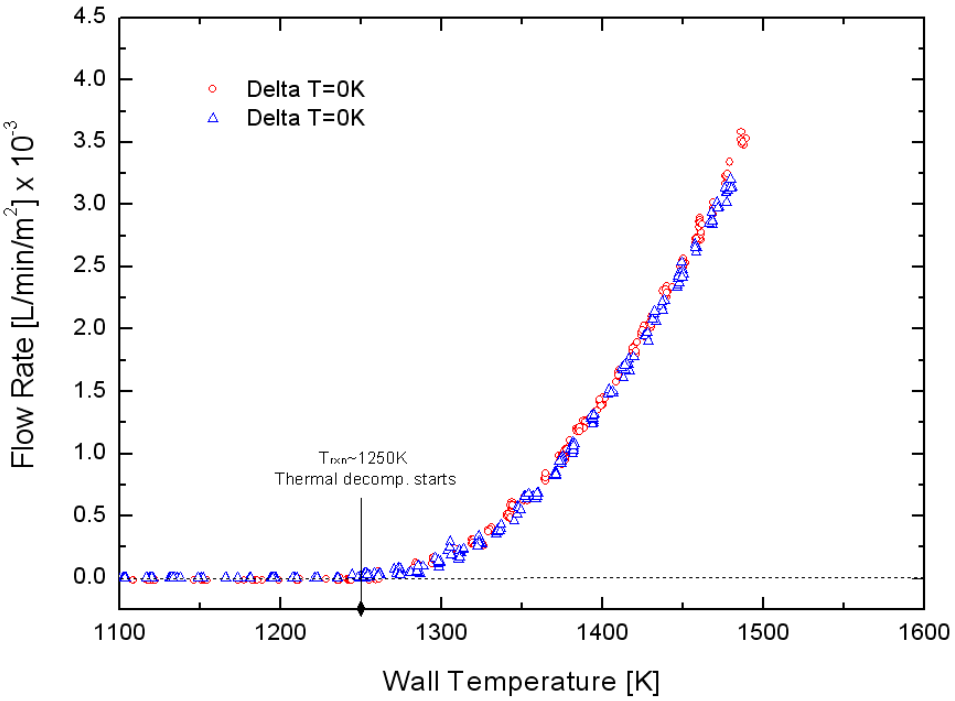

Figure 3.8: Repeatability test for bare tube and methanol.

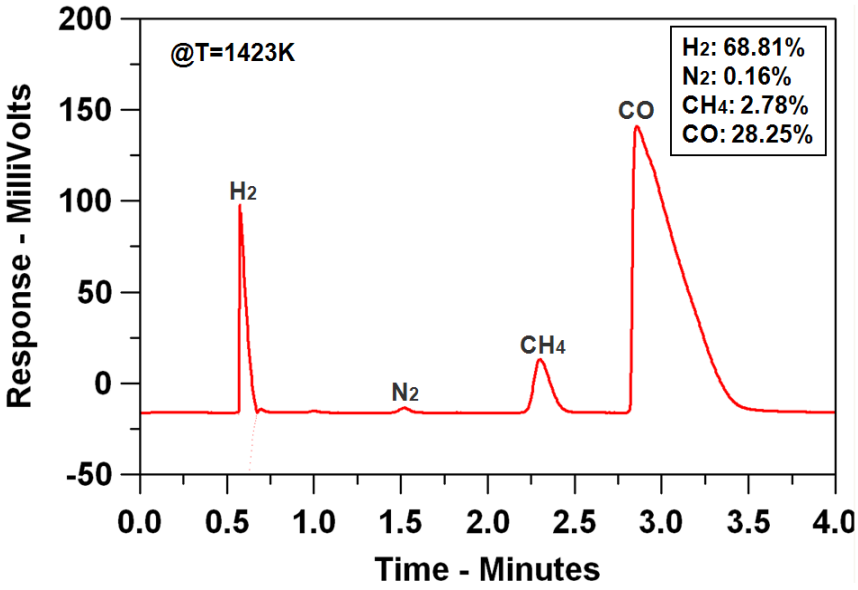

(a)

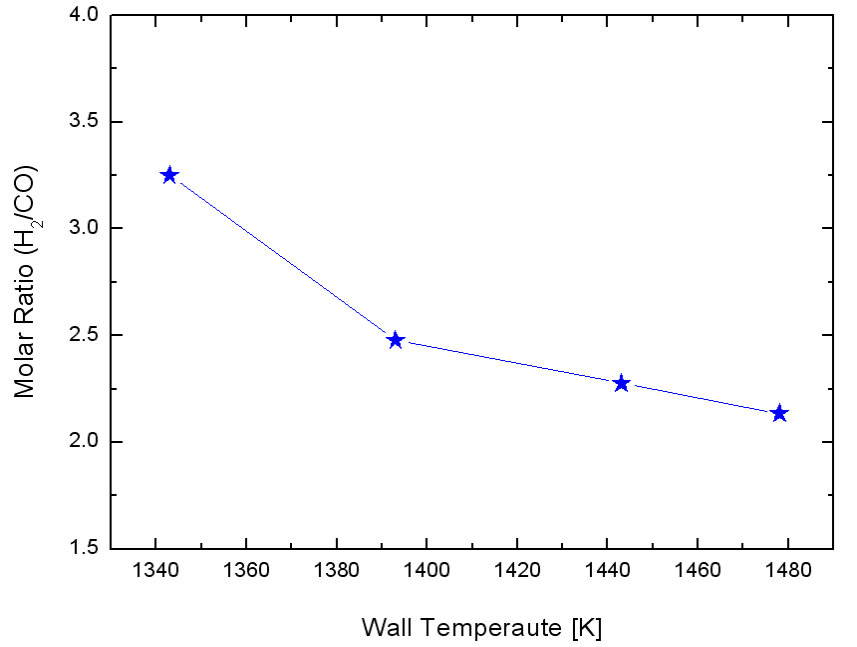

(b)

Figure 3.9: (a) GC trace of the product gas at 1423K and (b) molar ratio change of hydrogen to carbon monoxide with wall temperature for bare tube and methanol.

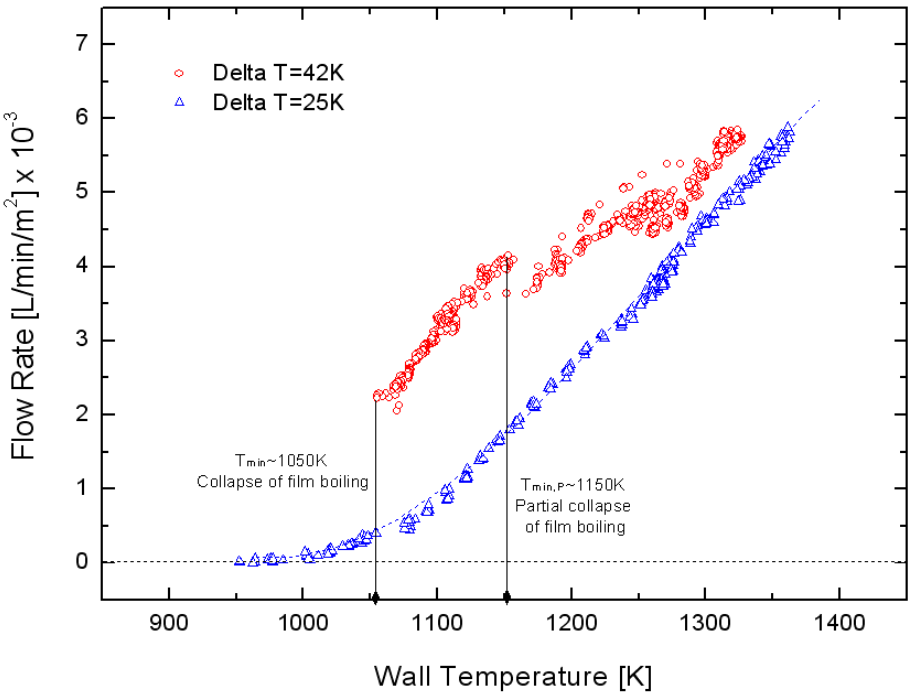

Figure 3.10: Repeatability test for CT#2 and ethylene glycol

The higher sub-cooling data were obtained first, on a newly coated tube. In these experiments the nitrogen gas flow was turned off after establishing film boiling to enhance the accuracy of results. The higher sub-cooling produced considerably higher yields but a more instable vapor film. This result is counterintuitive because we should expect the opposite - product yields should decrease with higher sub-coolings as discussed with regard to Figure 1.4, since less energy is available to support the primary endothermic chemical reaction at higher sub-cooling. We speculate that the ethylene glycol catalyst degraded - producing lower yields - between the two tests in Figure 3.10, and that it dominates over the sub-cooling effect. This trend is consistent with the methanol results shown in Figure 3.7, where a degraded catalyst gave lower yields for the same sub-cooling.

The shift in the yields at around $4x10^3$ L/min/m^2 shown in Figure 3.10 to lower temperatures at a sub-cooling of 42K is, as noted previously in connection with the ethylene glycol boiling curve (see Figures 3.2 and 3.3), a result of partial collapse of the vapor film.

A representative GC trace for ethylene glycol on CT#2 is shown in Figure 3.11 at 1233K. Though trace amounts of CH_4, C_2H_2 (acetylene) and C_2H_4 (ethylene) are found, the dominant gaseous species are CO and H_2, which are close to the stoichiometric ratio prescribed by Eq. 1.2. Carbon deposits also form and the GC trace shows methane as a prominent peak thus indicating that Eq. 1.4 may be operative. Besides the product species measured by GC, several condensable species were detected in the bulk ethylene glycol suggesting a more complex chemical reaction mechanism as discussed in Sec. 3.6.

3.3.2 Thermal Decomposition of Ethylene Glycol

As shown in Figure 3.12, the decomposition reaction for ethylene glycol in the

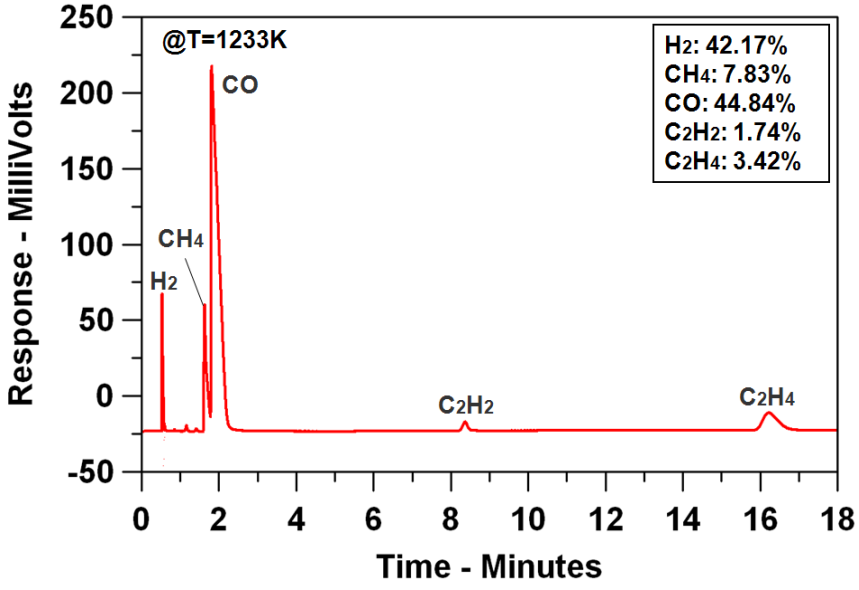

Figure 3.11: GC trace of the product gas for CT#2 and ethylene glycol

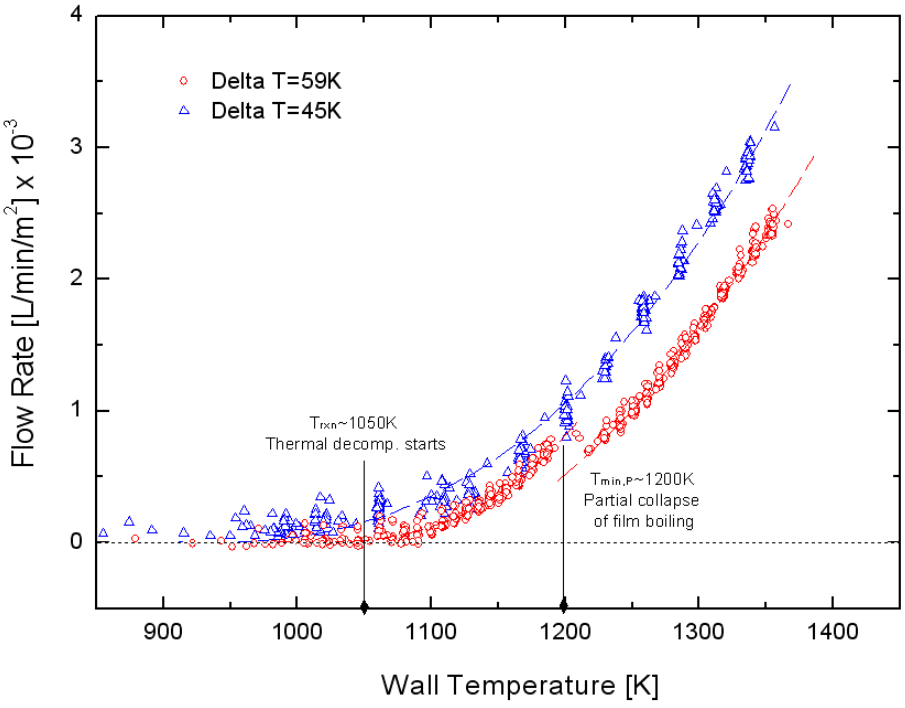

Figure 3.12: Repeatability test for bare tube and ethylene glycol.

FIBOR appears to begin at around 1050K. The corresponding yields at this temperature are considerably lower than for the catalyst tube (Figure 3.10). From this fact we infer that the conversion process in Figure 3.10 is by catalytic means at the lower temperatures shown and that as the tube wall temperature increases, thermal decomposition begins to exert an influence. When compared to the catalytic yields of Figure 3.10, the data in Figure 3.12 now suggest that a combination of thermal decomposition and catalytic conversion is responsible for product formation at the upper temperature ranges for CT#2 in Figure 3.10. This observation contrasts to methanol (cf, Figures 3.7 and 3.8) where conversion is primarily by catalytic means in Figure 3.7.

The abrupt shift to lower temperatures at around 1200K shown in Figure 3.12 is caused by film destabilization near the end of the tube near where it is clamped to the electrodes, as was also observed for CT#2 in Figure 3.10. Such collapse and instability seem to be a characteristic of high sub-cooling where films are less stable. In contrast to CT#2 (Figure 3.10), the higher sub-cooling for the bare tube produces lower yields. This trend is consistent with the assumption that increasing the sub-cooling reduces the heat available to drive the reaction for a given heat input (See Section 3.1) and maybe a consequence of the great film stability for thermal decomposition compared to film boiling on a catalyst surface.

Figure 3.13 shows a representative GC trace for thermal decomposition of ethylene glycol at a tube temperature of 1313K. In comparison to product gas concentrations for catalytic conversion (Figure 3.11) the hydrogen concentration was reduced by a factor of two while the methane concentration doubled and the ethylene concentration nearly tripled. The presence of these species in greater amounts for thermal decomposition, and also in comparison with methanol (Figures 3.6 and 3.9),

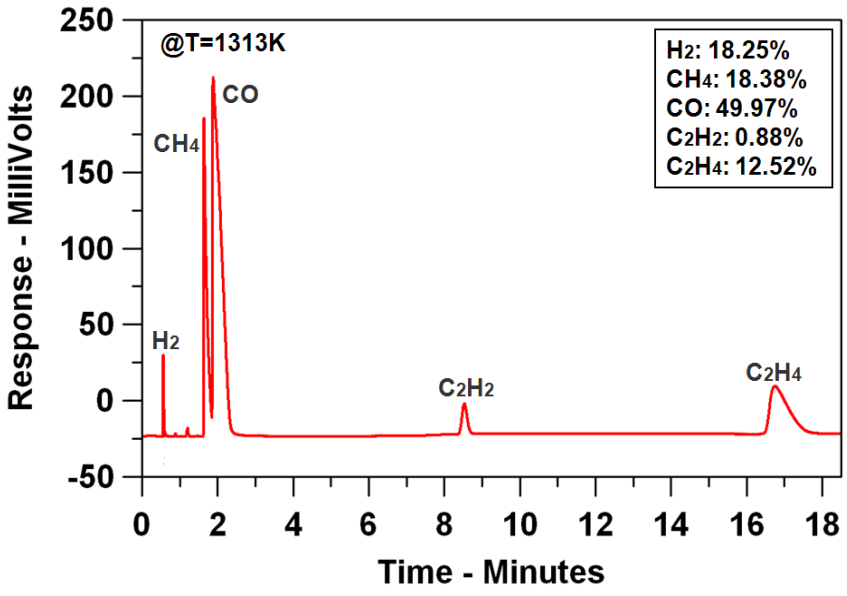

Figure 3.13: GC trace of the product gas for bare tube and ethylene glycol

suggest a stronger influence of reactions to produce carbon for ethylene glycol (Eqs. 1.4 - 1.7) compared to methanol.

Again, Figure 3.11 and 3.13 shows that the product concentrations of the FIBOR with ethylene glycol (for both the CT#2 and a bare tube) are quite different than methanol. This suggests a need to use two different calibration gases for the flow rate calibration of ethylene glycol as mentioned in Section 2.2.4.2.

Figure 3.14 (a) and (b) show photographs of the FIBOR with ethylene glycol for the CT#2 and a bare tube respectively.

3.4 Conversion in a Film Boiling Reactor

It is typical to specify the performance of any reactor in terms of an appropriately defined operational efficiency. For the FIBOR, this effort is complicated by several factors. No actual work is produced by the conversion process so that the thermodynamic efficiency is an irrelevant measure of performance.

Since we measure the product gas flow rate we define a "conversion", X, as

$$X \equiv \frac{\text{Molar flow rate of A converted}}{\text{Molar flow rate of A supplied}} \qquad 3.2$$

where "A" designates the reactant (i.e. methanol or ethylene glycol) and $X \leq 1$.

For the FIBOR as configured in this study, the molar flow rate of supplied reactant A (denominator in Eq. 3.2) cannot be measured while the molar flow rate of reacted A (numerator in the Eq. 3.2) is directly measured by the flow meter (Figure 2.1). The supplied reactant is attributed to evaporation for our version of the FIBOR.

An energy balance around the vapor film allows approximating the molar flow rate of supplied reactant. Figure 1.3 shows a control volume for a balance to determine the reactant flow rate.

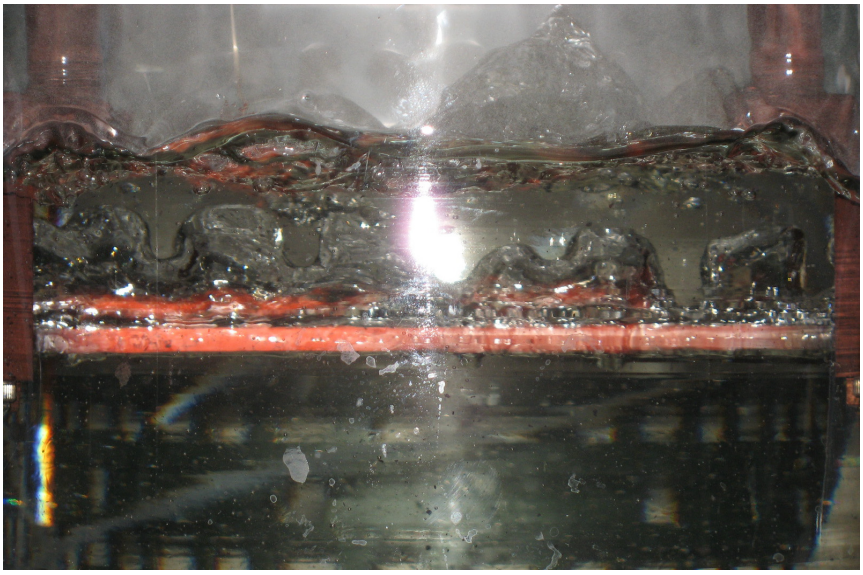

(a)

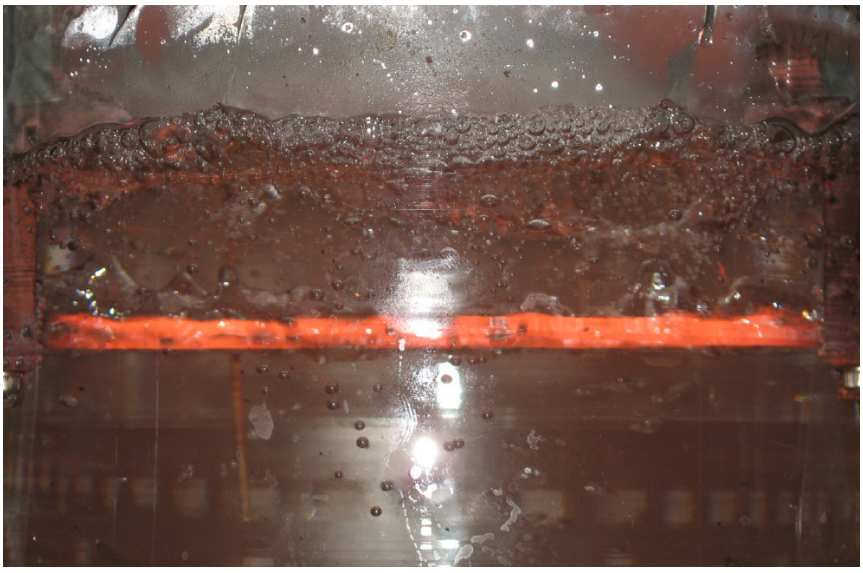

(b)

Figure 3.14: Pictures of FIBOR of ethylene glycol
for (a) CT#2 (@T_w=1271K) and (b) bare tube (@T_w=1288K)

In terms of the flow rates (see Nomenclature), Eq. 3.2 can be expressed as

$$\mathrm{X} \equiv \frac{\dot{N}_{R,in} - \dot{N}_{R,out}}{\dot{N}_{R,in}} \tag{3.3}$$

If chemical reactions in the FIBOR are generalized by a single step unimolecular decomposition, then $\mathrm{A} \rightarrow \sum_i \alpha_i \mathrm{B}_i$ where $\sum_i \alpha_i \equiv \nu$. The numerator in Eq. 3.3 is then $\sum_i \dot{N}_{\mathrm{B}_i,out} \Big/ \nu$ (Williams 1965) so that

$$\dot{N}_{R,in} - \dot{N}_{R,out} = \sum_i \dot{N}_{\mathrm{B}_i,out} \Big/ \nu . \tag{3.4a}$$

Since $\dot{N}_{P,out} \equiv \sum_i \dot{N}_{\mathrm{B}_i,out}$, Eq. 3.3 becomes

$$\mathrm{X} = \frac{\dot{N}_{P,out} \Big/ \nu}{\dot{N}_{R,in}} . \tag{3.4}$$

$\dot{N}_{R,in}$ is obtained from an energy balance on a control volume around the tube (Figure 1.3) such

$$\dot{Q} = h_{R,out}\dot{N}_{R,out} + h_{P,out}\dot{N}_{P,out} - h_{R,in}\dot{N}_{R,in} + \dot{Q}_{sub} \tag{3.5}$$

From Eq.3.4a, Eq.3.5 can be organized resulting in

$$\dot{Q} = \left(h_{R,out} - h_{R,in}\right)\dot{N}_{R,in} + \left(\nu h_{P,out} - h_{R,out}\right)\left(\dot{N}_{P,out} \Big/ \nu\right) + \dot{Q}_{sub} . \tag{3.6}$$

Incorporating the specific heat (C_P), heat of vaporization (ΔH_{fg}), and heat of reaction (ΔH_{rxn}), and taking $T_{in} = T_{sat}$, Eq.3.6 becomes

$$\dot{Q} = \left(\int_{T_{sat}}^{T_{out}} C_{P,R}\, dT\right)\dot{N}_{R,in} + \Delta H_{fg,R}\dot{N}_{R,in} + \Delta H_{rxn,out}\left(\dot{N}_{P,out} \Big/ \nu\right) + \dot{Q}_{sub} \tag{3.7}$$

where $T_{out} \equiv \frac{T_{wall} + T_{sat}}{2}$ since the temperature profile in vapor film is linear (Urban et al. 2006). Terms on the right hand side of Eq. 3.7 come from the heat to raise the

vapor temperature to T_{sat}, the heat of evaporation of reactant, the heat of reaction, and heat loss from the liquid/vapor interface to the bulk by sub-cooling, respectively. This last term can be expressed as

$$\dot{Q}_{sub} = A_o \bar{h} \left(T_{sat} - T_\infty \right) \tag{3.8}$$

where $\bar{h}$ is the average heat transfer coefficient around the vapor film. Combining Eqs. 3.7 and 3.8 and solving for $\dot{N}_{R,in}$ gives

$$\dot{N}_{R,in} = \frac{\dot{Q} - A_o \bar{h} \left(T_{sat} - T_\infty \right) - \Delta H_{rxn,out} \left(\dot{N}_{P,out} / v \right)}{\int_{T_{sat}}^{T_{out}} C_{P,R} dT + \Delta H_{fg,R}}. \tag{3.9}$$

Finally, substituting Eq. 3.9 into Eq. 3.4 relates X to parameters as

$$\mathrm{X} = \frac{\dot{N}_{P,out} / v}{\left(\frac{\dot{Q} - A_o \bar{h} \left(T_{sat} - T_\infty \right) - \Delta H_{rxn,out} \left(\dot{N}_{P,out} / v \right)}{\int_{T_{sat}}^{T_{out}} C_{P,R} dT + \Delta H_{fg,R}} \right)}. \tag{3.10}$$

To proceed further, we need a correlation for the average heat transfer coefficient around the vapor film. Unfortunately, no correlation for $\bar{h}$ exists that incorporates heat transfer from liquid/vapor interface to bulk liquid. To simplify the calculation, we used a free convection correlation around a horizontal cylinder (Churchill and Chu, 1975) with an effective diameter of $d_o + 2\delta$ and assumed $\delta \ll d_o$ to give

$$\bar{h} \simeq \frac{k}{d_o} \left\{ 0.6 + \frac{0.387 \mathrm{Ra}_{d_o}^{1/6}}{\left[1 + \left(0.559 / \mathrm{Pr} \right)^{9/16} \right]^{8/27}} \right\}^2. \tag{3.11}$$

In this regard, X must be considered a defined quantity based on this correlation. Also, another assumption in computing X, namely the one step reaction, influences quantitative values of X but not the overall trends.

Appendix D.5 lists the MATLAB codes to estimate X. The computer program gives the conversion and the heat rates (four terms on the right hand side of Eq.3.7) as output results while it imports the ASCII data files of the experimentally measured $\dot{N}_{P,out}$, T_{wall}, T_{∞}, and $\dot{Q}$. Table 3.1 shows the physical properties of all substances to run the program. The further details of the code are described in Appendix F.5.

Figures 3.15 and 3.16 show the computed variation of X with wall temperature (T_w) for methanol and ethylene glycol, respectively, using the measured product flow rates for these chemicals. Both catalytic (for methanol with 14K subcooling and ethylene glycol with 42K subcooling) and thermal decomposition results are shown. The conversions consider gaseous species in the definition of X that were detected in the product gas analysis by GC. Actual conversion for ethylene glycol should be higher than the calculated conversion because the produced condensable species were not taken into account to estimate the conversion efficiency (see Section 3.6). The results show that up to 40% methanol and 27% ethylene glycol is converted. It should be noted that the FIBOR is not a once-through system (e.g., as it is for a tubular flow reactor). If unconverted reactant can be completely condensed, the reactant will be continuously recycled (evaporated) back into the FIBOR. Ultimately, all of the reactant could be converted by maintaining the FIBOR for prolonged periods as the liquid boils away.

For a FIBOR on a catalyst-coated tube the methanol conversion process occurs only by catalytic action. This fact was previously shown in connection with Figures 3.7 and 3.8. For $T_w < 1250K$, the temperature is too low for methanol to be thermally decomposed (see Figure 3.8) while for a catalyst coated tube (Figure 3.7) significant

Table 3.1: Physical properties of all substances to calculate conversion (Beaton and Hewitt 1989)

	CH_4O	$C_2H_6O_2$	H_2	CO	CH_4	C_2H_2	C_2H_4
Heat of vaporization (ΔH_{fg}, J mol^{-1})	35,255	49,661	-	-	-	-	-
Enthalpy of formation (h_f, J mol^{-1})	-200,670	-394,400	0	-110,530	-74,850	226,730	52,280
Boiling point (T_{sat}, K)	337.8	470	-	-	-	-	-
Thermal conductivity of liquid (k_l, W m^{-1} K^{-1})	0.193 @T_{sat}	0.252 @T_{sat}	-	-	-	-	-
Expansion coefficient of liquid ($\beta_{e,l}$, K^{-1})	0.42×10^{-3}@T_{sat}	0.65×10^{-3}@T_{sat}	-	-	-	-	-
Viscosity of liquid (μ_l, kg m^{-1} s^{-1})	39.6×10^{-5}@T_{sat}	85.9×10^{-5}@T_{sat}	-	-	-	-	-
Density of vapor (ρ_v, kg m^{-3})	1.222 @T_{sat}	2.196 @T_{sat}	-	-	-	-	-
Density of liquid (ρ_l, kg m^{-3})	765 @T_{sat}	1,016 @T_{sat}	-	-	-	-	-
Specific heat of liquid ($c_{p,l}$, J kg^{-1} K^{-1})	2,680 @T_{sat}	2,940 @T_{sat}	-	-	-	-	-
Molar specific heat of gas ($\overline{c}_{p,v}$, J mol^{-1} K^{-1}) = a + bT + cT^2 + dT^3	a=19 $b=9.152\times10^{-2}$ $c=-1.22\times10^{-5}$ $d=-8.039\times10^{-9}$	a=35.7 $b=24.83\times10^{-2}$ $c=-14.97\times10^{-5}$ $d=30.1\times10^{-9}$	a=29.11 $b=-0.1916\times10^{-2}$ $c=0.4003\times10^{-5}$ $d=-0.8704\times10^{-9}$	a=28.16 $b=0.1675\times10^{-2}$ $c=0.5372\times10^{-5}$ $d=-2.222\times10^{-9}$	a=19.89 $b=5.024\times10^{-2}$ $c=1.269\times10^{-5}$ $d=-11.01\times10^{-9}$	a=21.8 $b=9.2143\times10^{-2}$ $c=-6.527\times10^{-5}$ $d=18.21\times10^{-9}$	a=3.95 $b=15.64\times10^{-2}$ $c=-8.344\times10^{-5}$ $d=17.67\times10^{-9}$

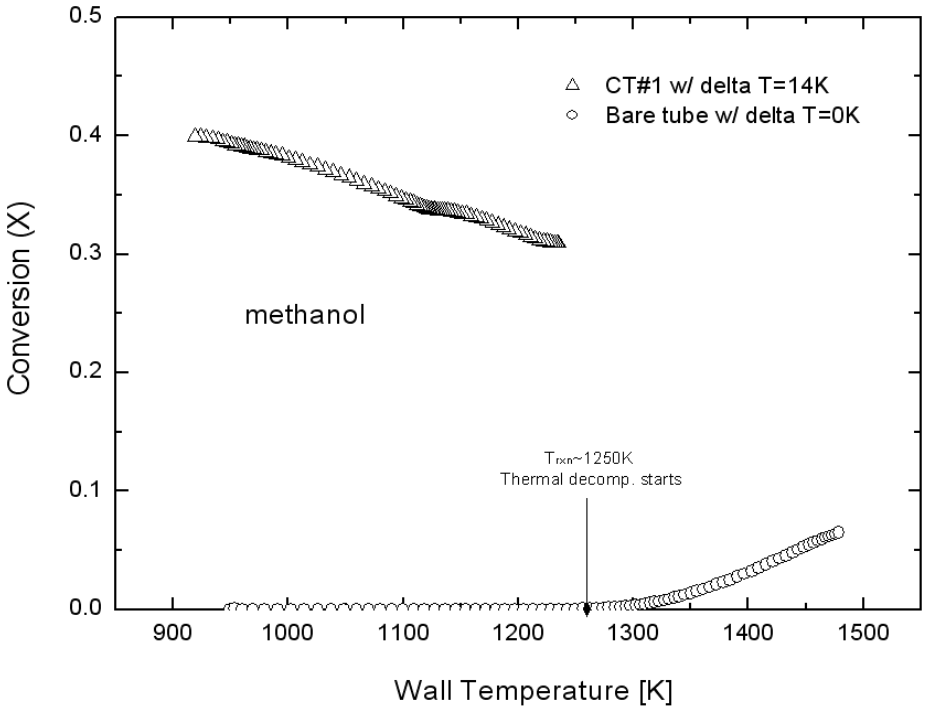

Figure 3.15: Conversion for methanol with CT#1 (14K sub-cooling) and a bare tube (0K sub-cooling)

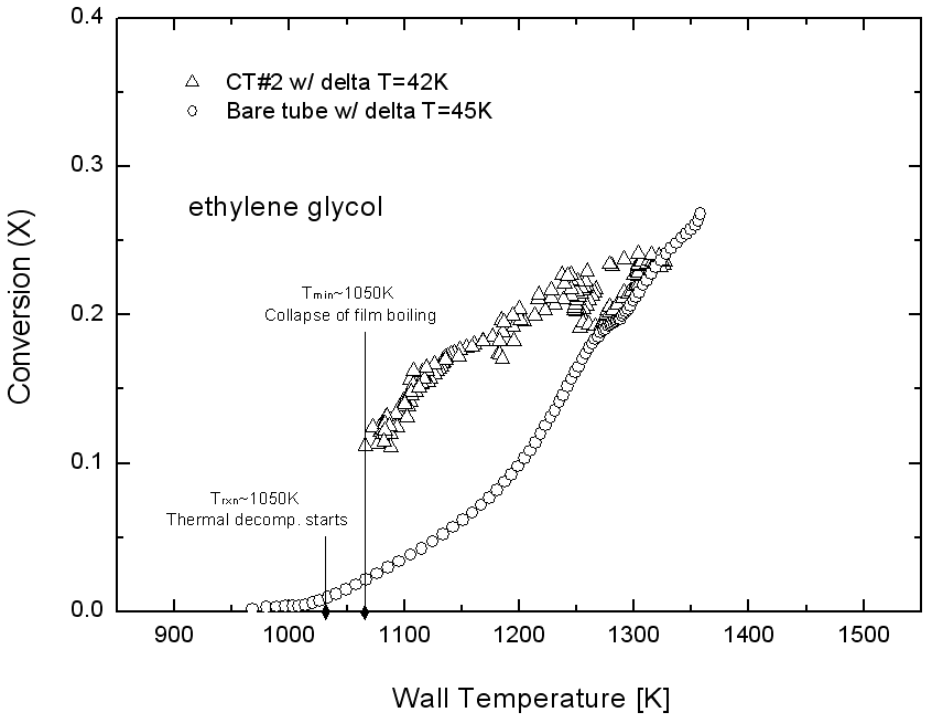

Figure 3.16: Conversion for ethylene glycol with CT#2 (42K sub-cooling) and a bare tube (45K sub-cooling)

catalytic activity is realized. The conversion follows this trend in Figure 3.15. Below 1250K, X=0 for thermal decomposition (open circles in Figure 3.15) while X is significant in this temperature range for the catalyst coated tube (open triangle in Figure 3.15). As such, catalytic reaction is the only route to convert methanol at $T_w <$ 1250K.

Ethylene glycol (Figure 3.16) shows a more complex reaction process. As previously noted in connection with Figures 3.10 and 3.12, thermal decomposition begins for ethylene glycol at approximately T_w = 1050K. At the same time, the FIBOR can only be developed for catalytic reaction in ethylene glycol for $T_w > 1050$K because of issues of film boiling destabilization at lower temperatures. Furthermore, at lower wall temperatures a FIBOR cannot be created for ethylene glycol without deactivating the catalyst. Thus, for wall temperatures where both the vapor film is maintained and film boiling itself can be created by avoiding solid/liquid contact (as per the procedure in Figure 2.27), both reaction mechanisms occur simultaneously for the catalyst tube in Figure 3.16.

Perhaps more interesting is that the methanol conversion decreases with T_w while the ethylene glycol conversion increases with T_w in the investigated temperature range. These opposite trends was a consequence of the ethylene glycol conversion process occurring by two routes as noted above - thermal decomposition and catalytic conversion - while for methanol only catalytic conversion is operative for the range of T_w values in Figure 3.15. As shown in Figure 3.16, thermal decomposition conversion (for the FIBOR on a bare tube) is substantial at $T_w > 1050$K. For methanol, conversion is only by catalytic means in the temperature range below 1250K (Figure 3.15). As the wall temperature increases, the evaporation rate increases as well and so does the supply of reactant to the FIBOR. For methanol, with only one conversion route operative the supply rate of methanol may saturate the catalyst and thereby

reduce the conversion as temperature increase. On the other hand, X for ethylene glycol increases with T_w for the temperature range shown in Figure 3.16. Since two conversion routes are possible for ethylene glycol in the temperature range investigated, the combination of these two mechanisms may be sufficient to meet the evaporative supply of ethylene glycol that increases with T_w. The result is that X increases with T_w.

With the reasoning above we may expect that X would eventually increase even if it decreases at low T_w (Figure 3.15) as the wall temperature enters a regime where thermal decomposition occurs. However, imposing higher temperatures is problematic because of materials considerations as the melting point of the tube material is approached, as well as compromises of the adhesion and structure of the catalyst coating at these high temperatures.

In the process of the conversion calculation, each element of energy flow from the wall can also be estimated by Eq. 3.7. Figure 3.17 and 3.18 show the computed results of energy pathway for methanol and ethylene glycol respectively. In more detail, the results are represented separately for the catalytic tubes (Figure 3.17 (a) and 3.18 (a)) and bare tubes (Figure 3.17 (b) and 3.18 (b)). Examining the heat transfer elements provides further insights into the overall trends of conversion. Specifically the heat transfer for evaporation (blue circle) scales with the denominator in Eq. 3.2 while the heat transfer for chemical reaction (red triangle) scales with the numerator. The results also show that the heat loss to sub-cooled liquid (violet diamond) is comparably smaller to the other heats, which is consistent with the small effects of sub-cooling at regions of high temperatures that Lee (1998) found in film boiling experiments with methanol.

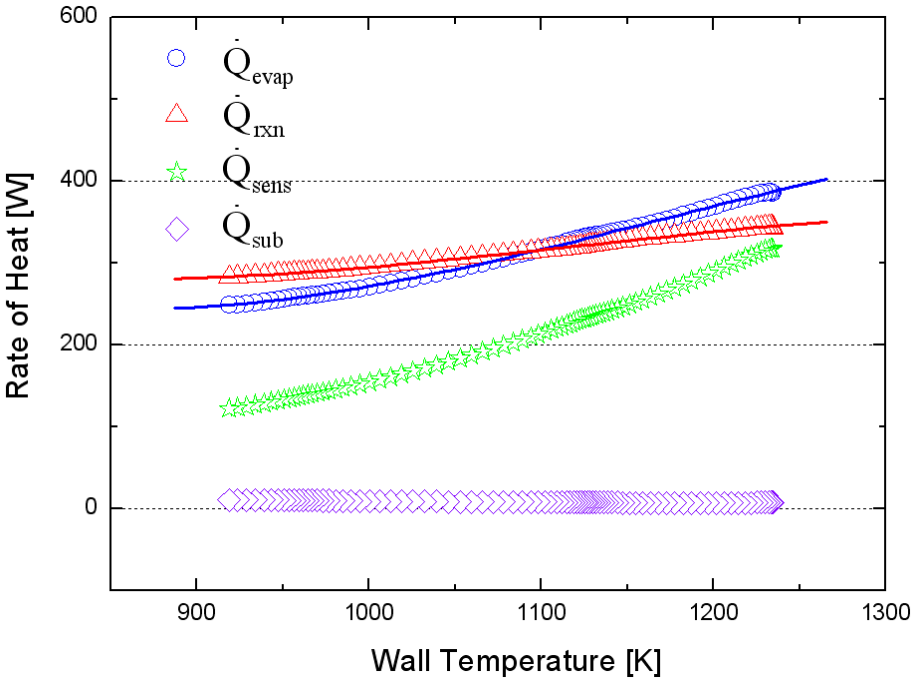

(a)

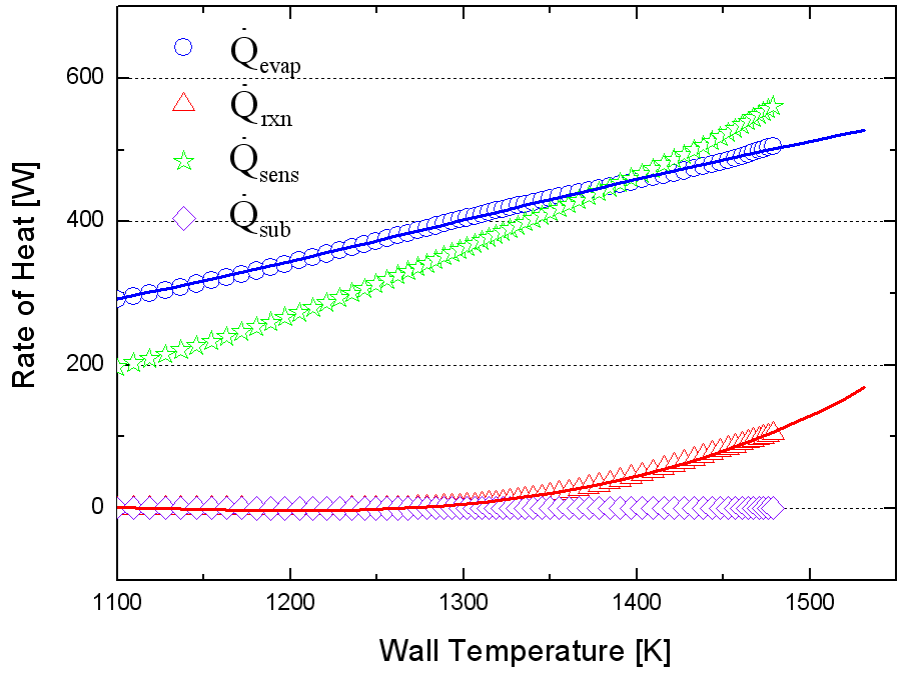

(b)

Figure 3.17: Energy pathways in FIBOR for methanol with (a) CT#1 (14K sub-cooling) and (b) a bare tube (0K sub-cooling)

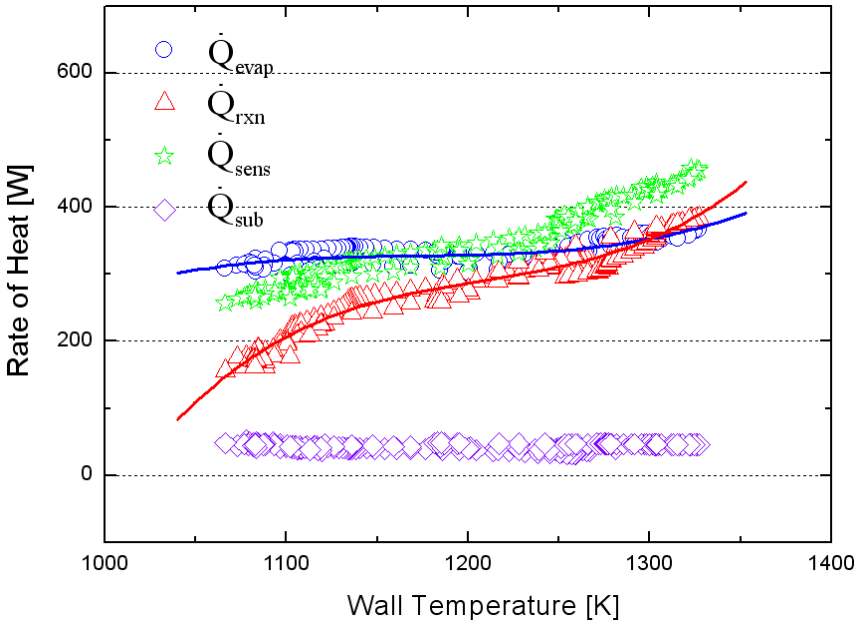

(a)

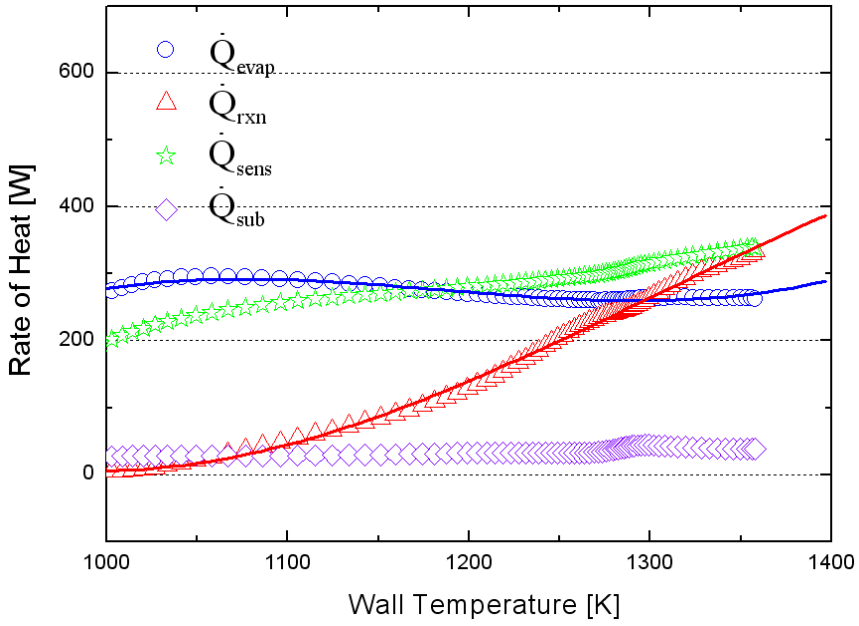

(b)

Figure 3.18: Energy pathways in FIBOR for ethylene glycol with (a) CT#2 (42K sub-cooling) and (b) a bare tube (45K sub-cooling)

3.5 Catalyst Degradation

The difference in flow rates of the two repeated experiments with the same catalytic tube (Section 3.2.1 and 3.3.1) suggests that the catalyst has been degraded after prolonged operation in the FIBOR. Though the present study focuses on film boiling with reaction, it is inevitable that catalyst quality exerts an important influence on the results.

It is known that one of the most insidious problems in catalysis is the loss of catalyst activity that occurs as chemical reactions progress. A wide variety of mechanisms have been proposed (e.g. see Butt and Petersen 1988), to explain and model catalyst deactivation. The three most common mechanisms include carbon deposits (coking) from coke formation reactions (Eqs. 1.5-1.7); sintering as a result of exposure to high operating temperatures, particularly in the presence of hydrogen, in which the pores would tend to fuse (Baird 1973); and catalyst de-lamination or detachment which could be caused by extreme changes in surface temperature during the quenching procedure or during the normal course of exposure to high temperatures and the cool-down period associated with the termination of an experiment.

To examine if prolonged operation of a FIBOR could degrade the catalyst, CT#1 was maintained at a given temperature for a specified period of time and the yields were measured. The test time of total 7.8 hours was determined by the available amount of coolant (dry-ice/acetone mixture). Figure 3.19 (a) shows the near uniform tube wall temperatures selected for these tests – 993K and 1193K - and Figure 3.19 (b) the corresponding product gas flow rates. At 993K, a slight decrease in product flow rate is observed while at 1193K the decay rate is more pronounced (i.e., 0.43 L/min/m^2 per min or 4.83% x 10^{-3} per min at 993K and 1.05 L/min/m^2 per min or 13.67% x 10^{-3} per min at 1193K). This yield reduction is qualitatively consistent with the sintering decay law by Fogler (2006) which estimates a higher sintering decay rate

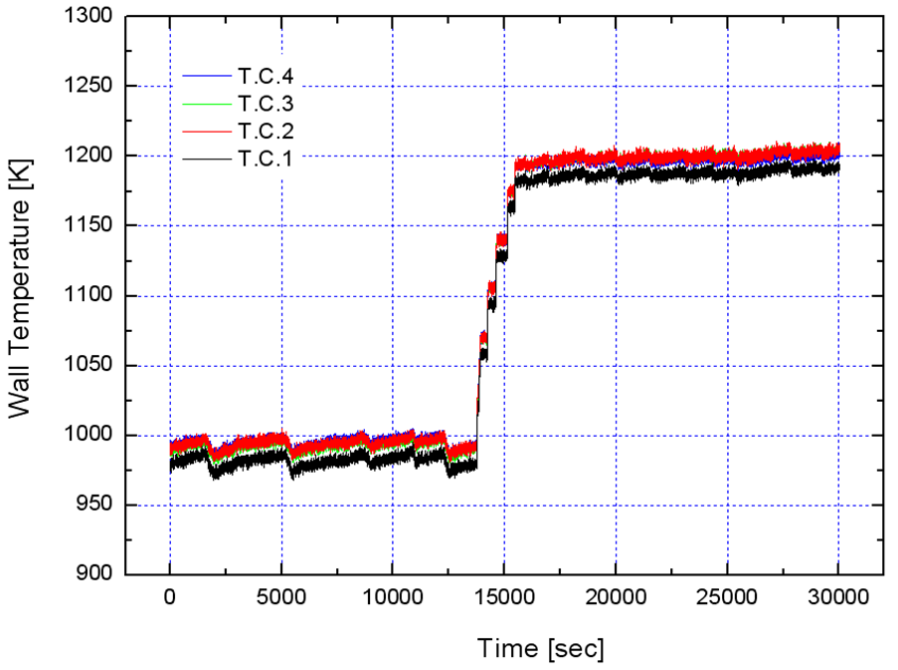

(a)

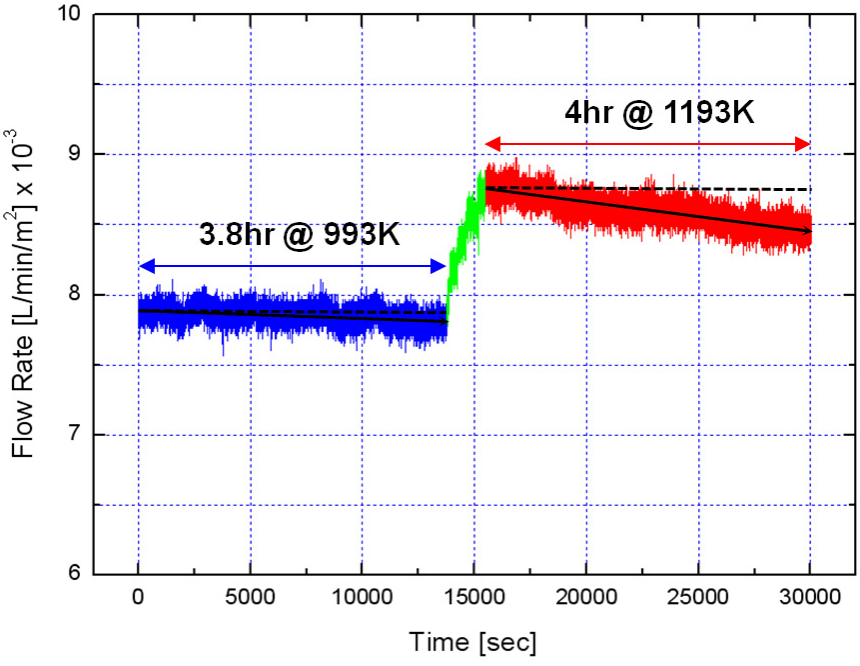

(b)

Figure 3.19: Endurance test for CT#1 and methanol

at a higher temperature.

Scanning Electron Microscope (SEM) photos in Figure 3.20 (x410) and 3.21 (x1100) suggest formation of carbon deposits on catalyst surface by comparing the catalyst structures (a) before and (b) after the endurance test (Figure 3.19). The bright clusters are considered to be Pt catalyst while dark ones be carbon which is likely to be generated by carbon formation reactions (Eq. 1.5 – 1.7). The increase in tube weight shown in Table 2.3 after the endurance test of CT#1 also supports the possible carbon formation.

The possibly deposited carbon on the catalyst structure was removed by a burning-off process between 100 to 250 °C for 10 minutes (in the presence of air) giving a possibility to recycle a catalytic heater tube. Figure 3.22 shows that the weight of the CT#1 decreases as a result of the carbon burn-off. Most deposited carbon on CT#1 seems to be removed after 3 burn-off processes.

3.6 Unique Features of Ethylene Glycol Experiment

An endurance test was also conducted for CT#2 to examine the potential for catalyst degradation for ethylene glycol. Figure 3.23 shows that both wall temperature and product gas flow rate decrease with time over the approximately 3.6 hour duration of the test. This result suggests that something different from the methanol experiment is taking place for the long operation of the FIBOR with ethylene glycol.

If additional secondary reactions (which are not included in Eqs.1.1-1.7) produce condensable by-products in a FIBOR, the bulk liquid concentration changes over the course of an experiment as a result of by-products accumulating inside the chamber (Zhukov 2003) as illustrated in Section 2.2.3. The concentration change then results in bulk liquid's temperature change because boiling temperatures of the by-products are different from the pure reactant. The result of the endurance test with

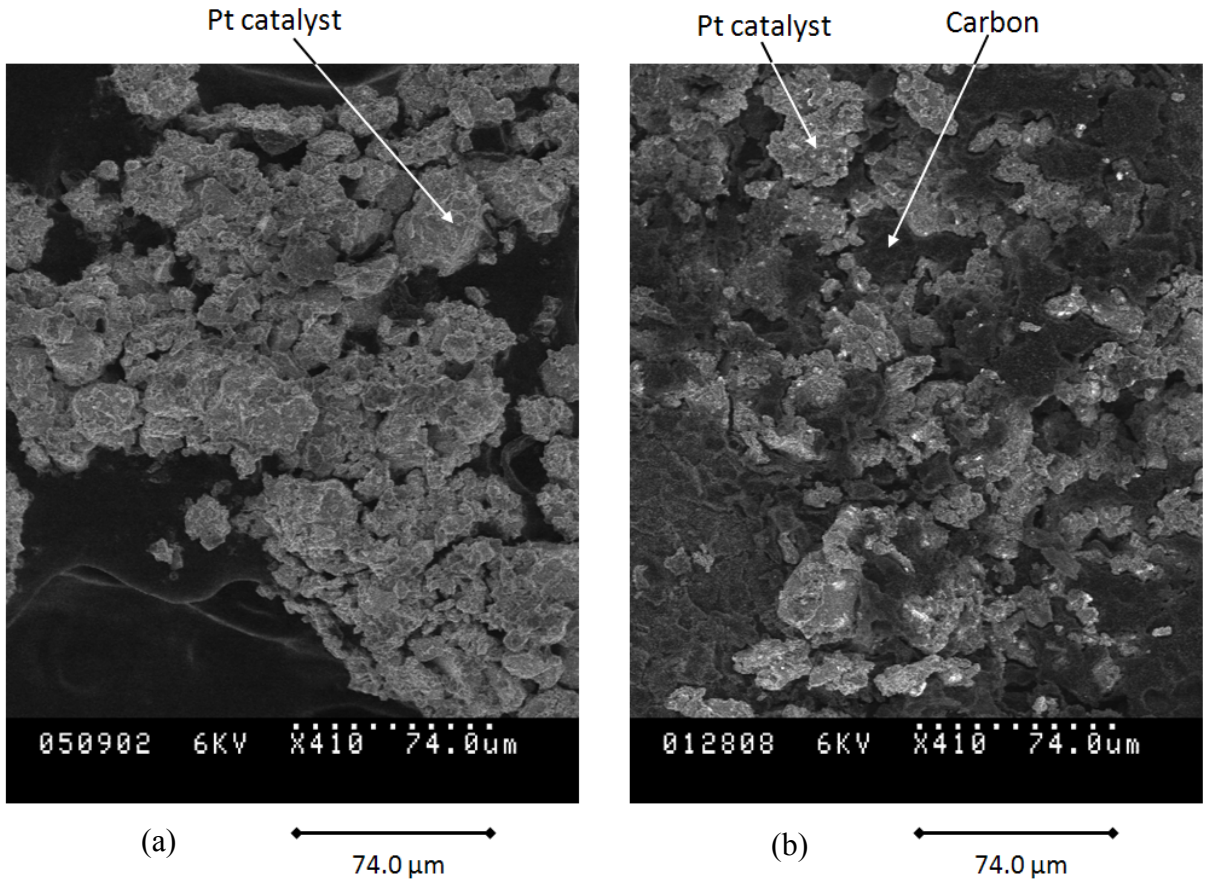

Figure 3.20: SEM pictures (X410) before (a) and after (b) experiments of CT#1 and methanol

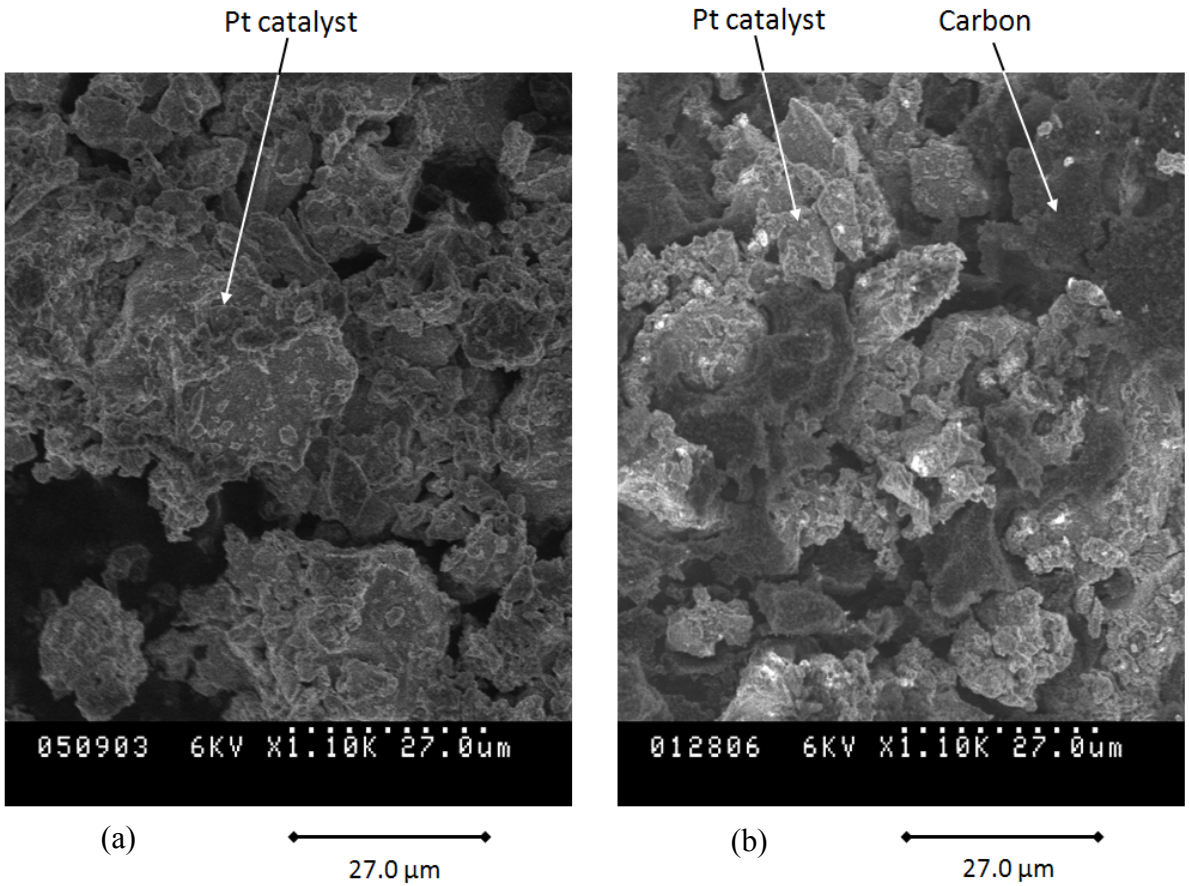

Figure 3.21: SEM pictures (X1100) before (a) and after (b) experiments of CT#1 and methanol

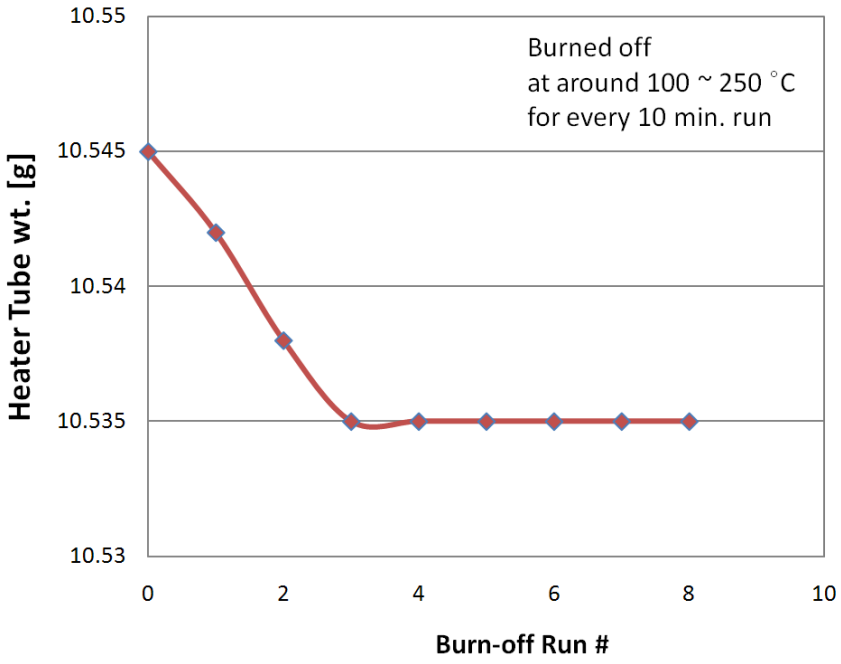

Figure 3.22: Baking of the heater tube to burn off carbon

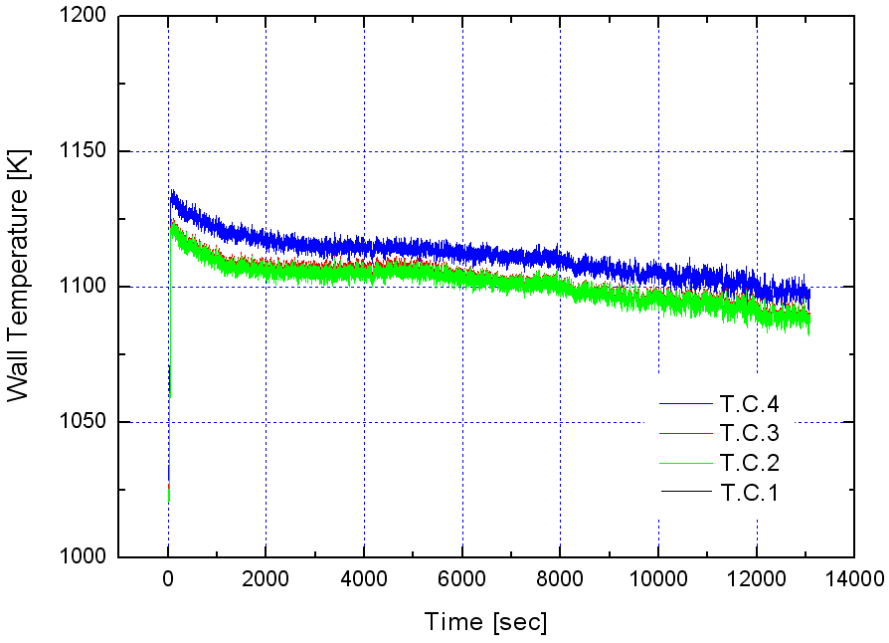

(a)

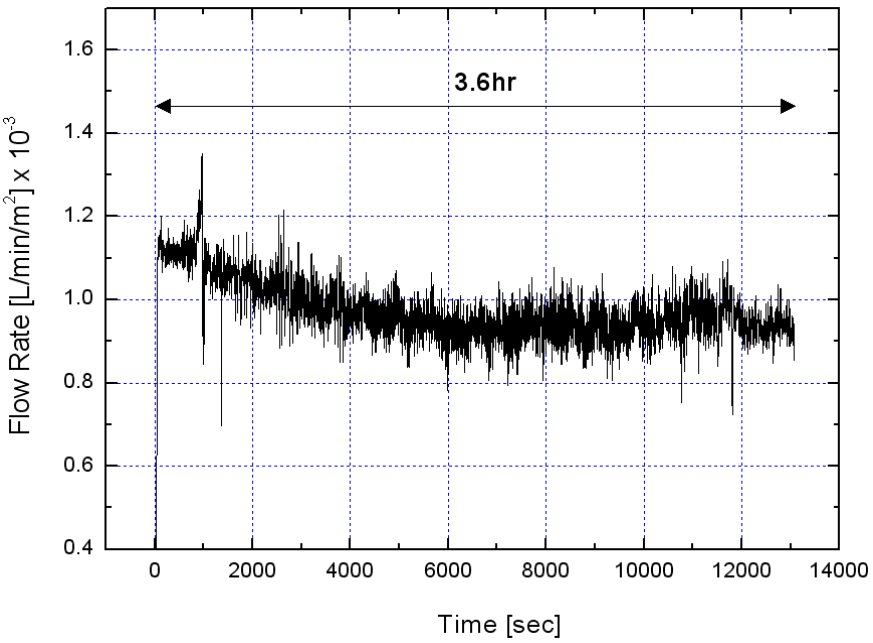

(b)

Figure 3.23: Endurance test for CT#2 and ethylene glycol

ethylene glycol (Figure 3.24) shows the obvious temperature decrease implying the concentration change of the bulk liquid. The exact nature of the temperature change involves complex vapor-liquid equilibrium phenomena owing to the unsteady development of a multi-component reactant mixture. GC-MS analysis (Agilent Technologies 6890N/5973 High Performance combination) of a liquid sample was carried out after the endurance test. The results are shown in Figure 3.25 and Table 3.2. The bulk liquid contains nearly 15% (molar) contaminants (various alcohols, ketone, and heterocyclic acetals). Components with a lower boiling temperature than ethylene glycol account for approximately 5% of the liquid after 3.6 hours, while components with higher boiling temperatures account for approximately 10%. The closer analysis of the individual component boiling temperatures suggests that the decreasing temperature trend could be the result of an azeotrope.

In addition to the contamination of liquid reactant, another unique feature of the FIBOR with ethylene glycol was observed in the experiments with bare tubes. Figure 3.26 shows the formation of black flakes around a bare tube after prolonged operation in the FIBOR. The flakes appear to be detached segments from the bare tube (Inconel 600) and seem to be generated through unknown chemical reactions between the tube material and ethylene glycol at a higher surface temperature above 1100°C. The flakes were not found in the experiments of the catalyst coated tube because the alumina layer and catalyst around the heater tube prevents the unknown chemical reactions from taking place. Furthermore, the flakes are attributed to ethylene glycol since they were not found in the methanol experiments. The outer surface of the flakes is black while the inner surface appears metallic.

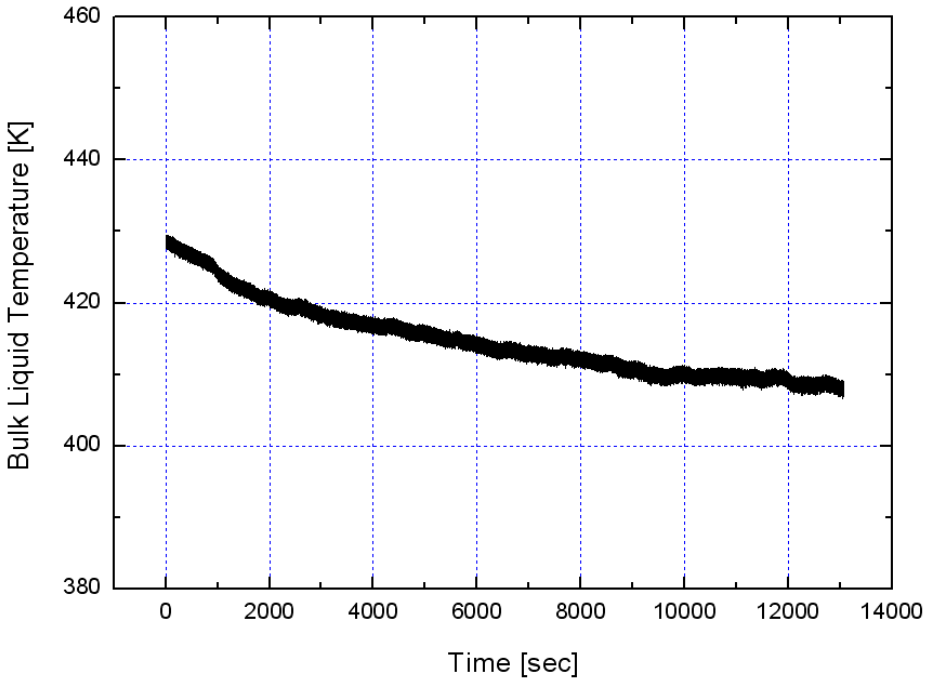

Figure 3.24: Bulk liquid temperature change in the endurance test for CT#2 and ethylene glycol

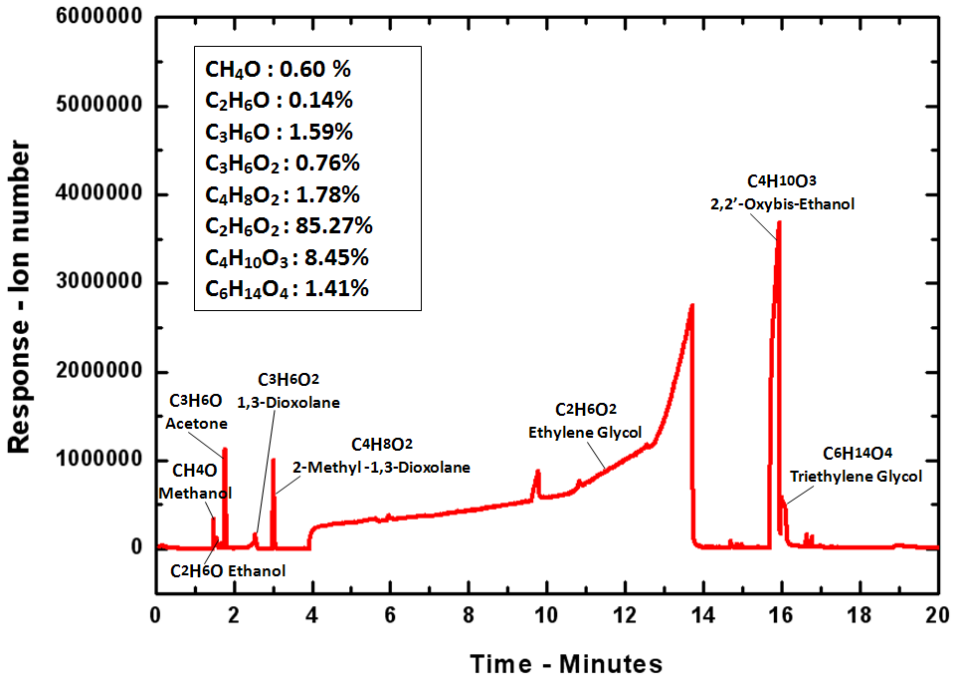

Figure 3.25: GC-MS trace of contaminated bulk liquid in the endurance test for CT#2 and ethylene glycol

Table 3.2: Physical properties of contaminants in the endurance test for CT#2 and ethylene glycol

	Methanol	Ethanol	Acetone	1,3-dioxolane	2-methyl-1,3-dioxolane	Ethylene glycol	2,2'-oxybis-Ethanol	Triethylene glycol
Chemical structure	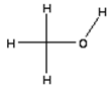				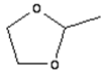	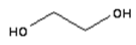	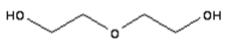	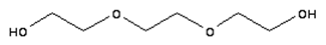
Boling point [°C]	64.8	78.5	56.3	75	81.7	197.5	246	267
Molecular wt. [g/mol]	32.04	46.07	58.08	74.1	88.11	62.07	106.12	150.17
Molar concentration [%]	0.60	0.14	1.59	0.76	1.78	85.27	8.45	1.41

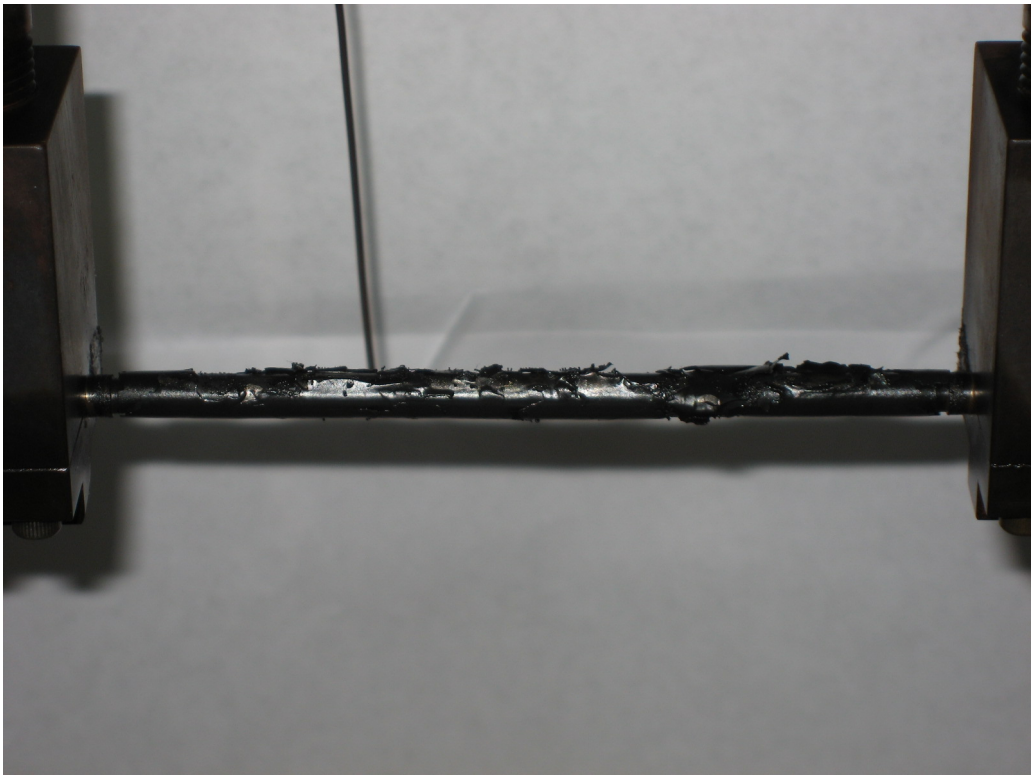

Figure 3.26: Flake formation around a bare tube

after an experiment of ethylene glycol

Evangelista (2010) has determined using X-ray Dispersion Spectroscopy (EDS) that the black color of the outer surface is due to carbon deposits on the flake though the flake material is still under investigation.

CHAPTER 4

CONCLUDING REMARKS

1. A laboratory scale platform to convert organic liquids has been constructed based on film boiling. The platform allows for control of parameters (wall temperature or power) and measurement of products yields and concentrations.

2. The experimental results show the efficacy of film boiling to affect chemical change as a chemical reactor. Specifically, it has been demonstrated that methanol and ethylene glycol can be decomposed into synthesis gas by means of both catalytic and thermal decomposition.

3. The procedure for immersion of the heated tube into the reactant pool ("quenching") is critical to achieve film boiling without burnout of a heater tube and to further avoid liquid to catalyst surface contact which possibly causes the catalyst degradation.

4. Differences in the catalyst coating quality (e.g., thickness, uniformity, catalyst loading) could vary the product yield. A home-made catalyst coated tube produced a significant amount of product yield, though was not repeatable in the product gas flow rates. Professionally fabricated catalyst coated tubes showed stable flow rates with much less scatter.

5. Obvious differences of heat flux between boiling curves of catalytic and bare heater tubes is considered to be due to the endothermic nature of the catalytic reaction of methanol and ethylene glycol.

6. The sub-cooling effect of the bulk liquid reactant causes instability and low product yields of the FIBOR because of significant heat to the bulk liquid.

7. Thermal decomposition starts at a higher temperature than catalytic conversion with a rapid increase in flow-rate. Methanol starts to decompose at approximately 1250K, while ethylene glycol starts at approximately 1050K.

8. Gas chromatography analysis shows that the product concentrations of methanol (for catalytic and thermal decomposition) are very close to the stoichiometry of the primary reaction of methanol decomposition. On the other hand, the chemical mechanism of ethylene glycol in the FIBOR is more complicated, being accompanied by secondary reactions which result in various species in both the gas and liquid phases.

9. A conversion efficiency was calculated and showed that it increases for ethylene glycol and decreases for methanol with wall temperature. The different trends were considered to be due to thermal decomposition occurring in conjunction with catalytic conversion for ethylene glycol compared to methanol.

10. Catalyst degradation was noted during long operating times. Evidence of possible causes of deactivation includes SEM images and differences in weights of the tubes before and after experiments.

11. The continuous decrease in bulk liquid temperature was measured during prolonged operation with pure ethylene glycol, which consequently decreases wall temperature and product yields. GC-MS analysis confirms that the bulk liquid temperature decrease was caused by the continuous change in the bulk liquid's concentration. A variety of condensable by-products such as alcohols, ketone, and heterocyclic acetals were generated by the complicated secondary reactions, and they continue accumulating in the FIBOR liquid chamber.

12. A long operation of the FIBOR with pure ethylene glycol produces black flakes around a bare tube (Inconel 600) which starts to appear approximately at 1373K. The flakes were not observed around the catalytic tube suggesting that the coating layer (alumina and Pt) prevents a chemical reaction between ethylene glycol and Inconel 600 surface which possibly produces the flakes.

APPENDIX A

MECHANICAL DRAWINGS

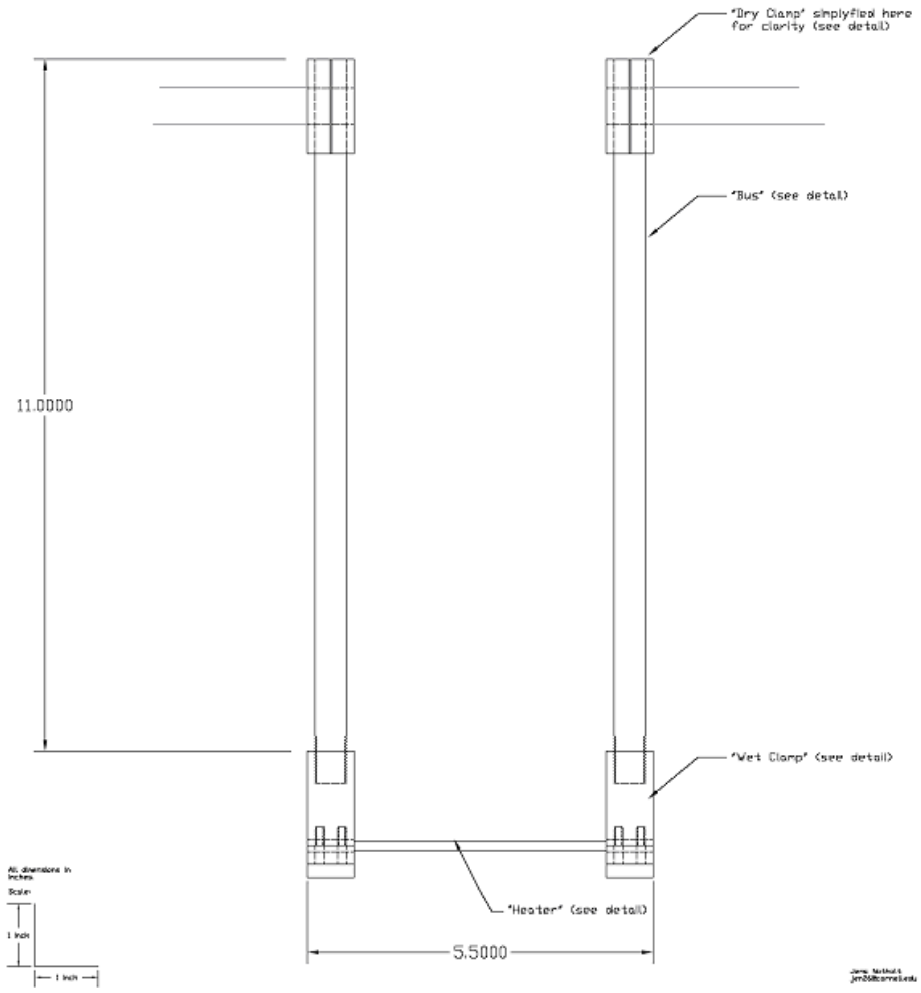

Figure A.1 Heater assembly

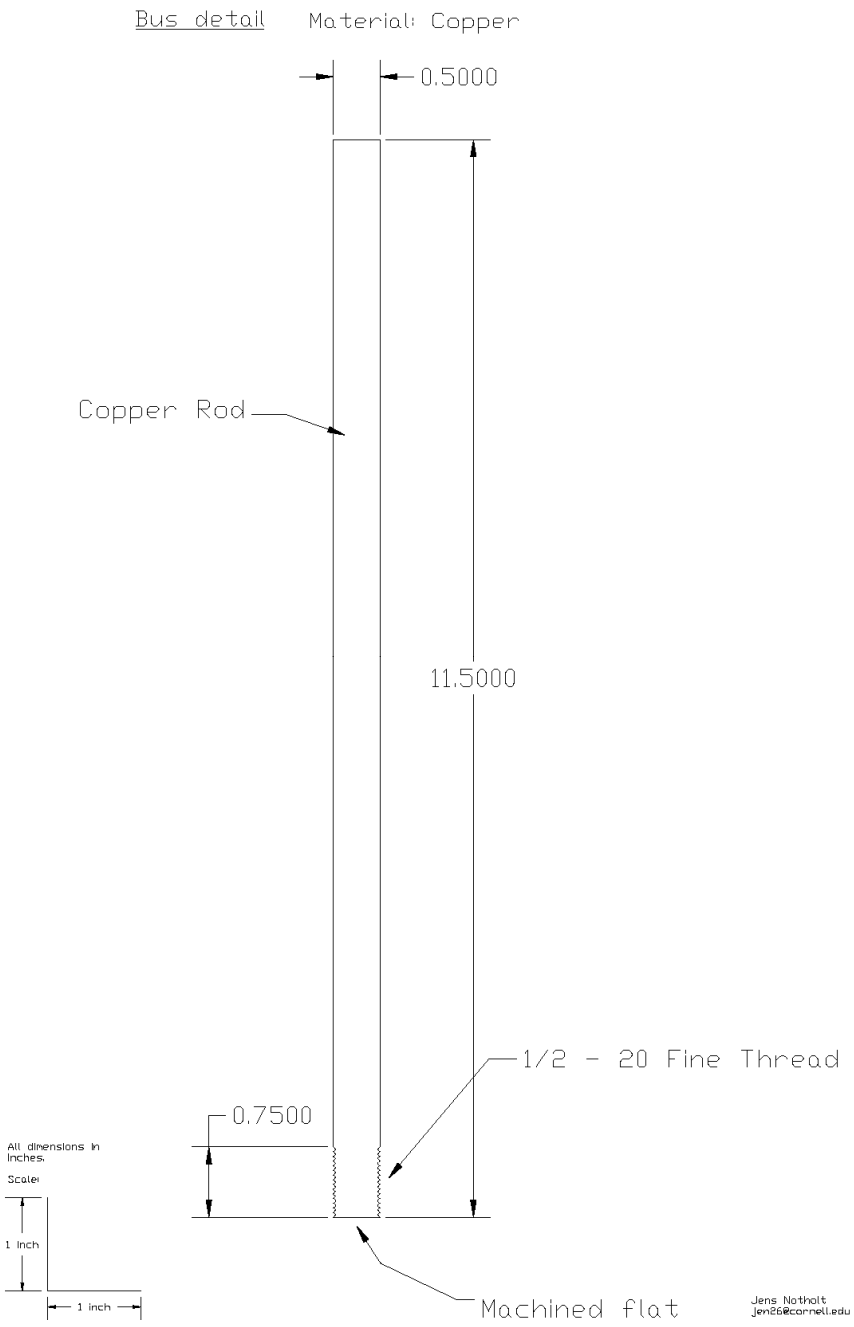

Figure A.2 Electrode copper bus

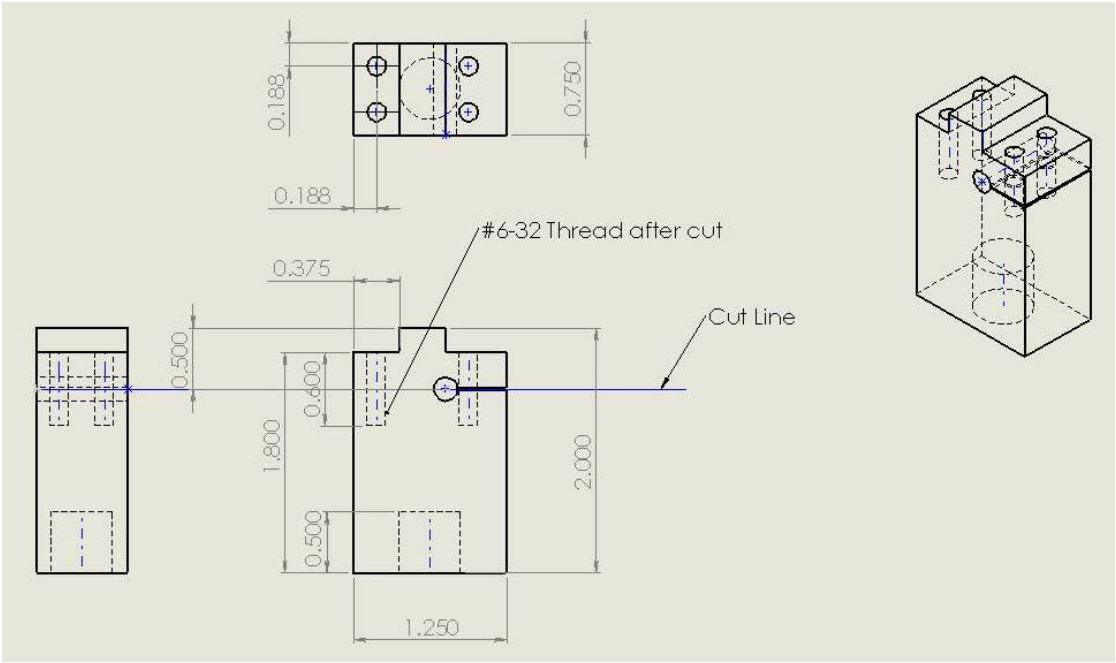

Figure A.3 Electrode wet clamp

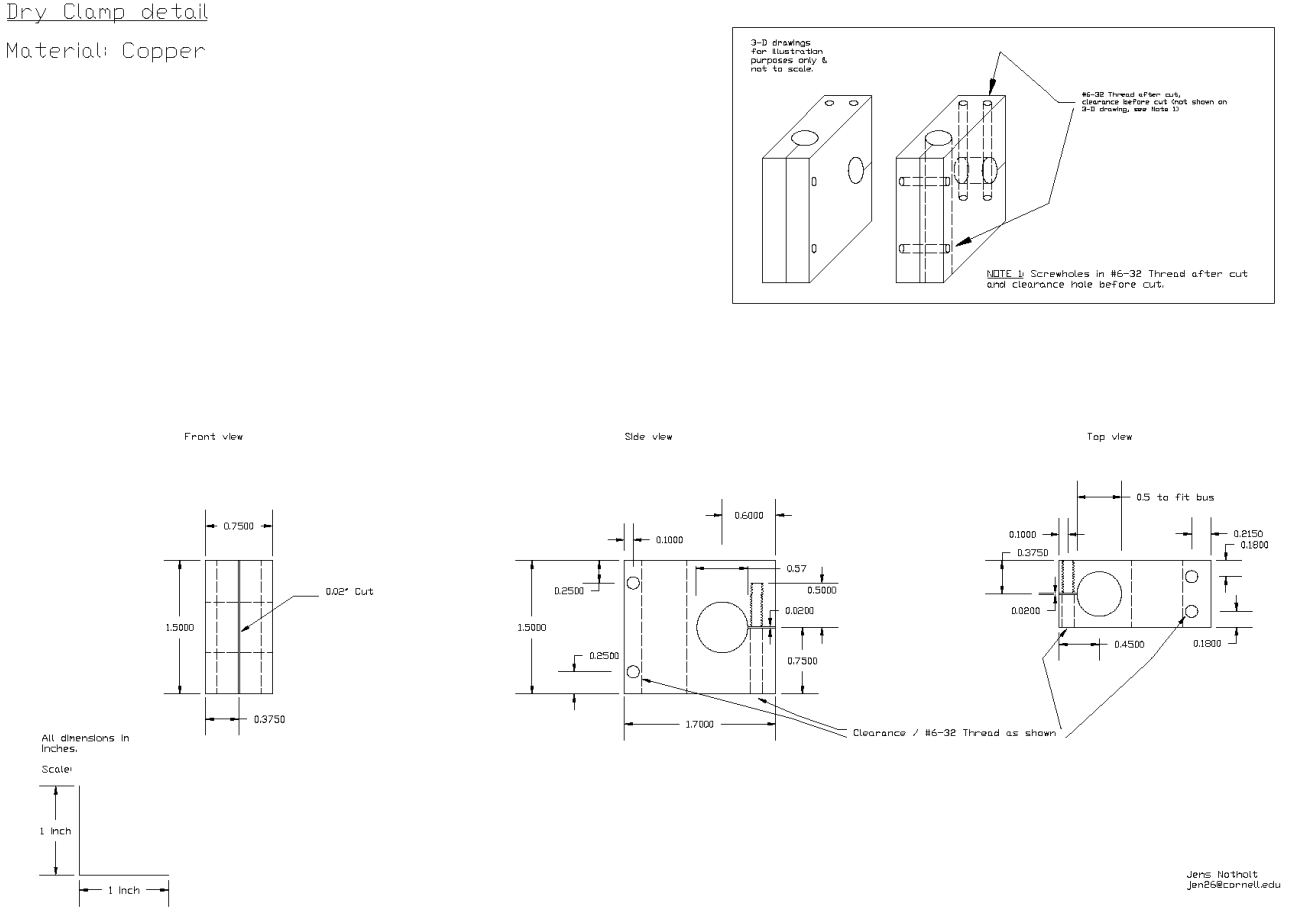

Figure A.4 Electrode dry clamp

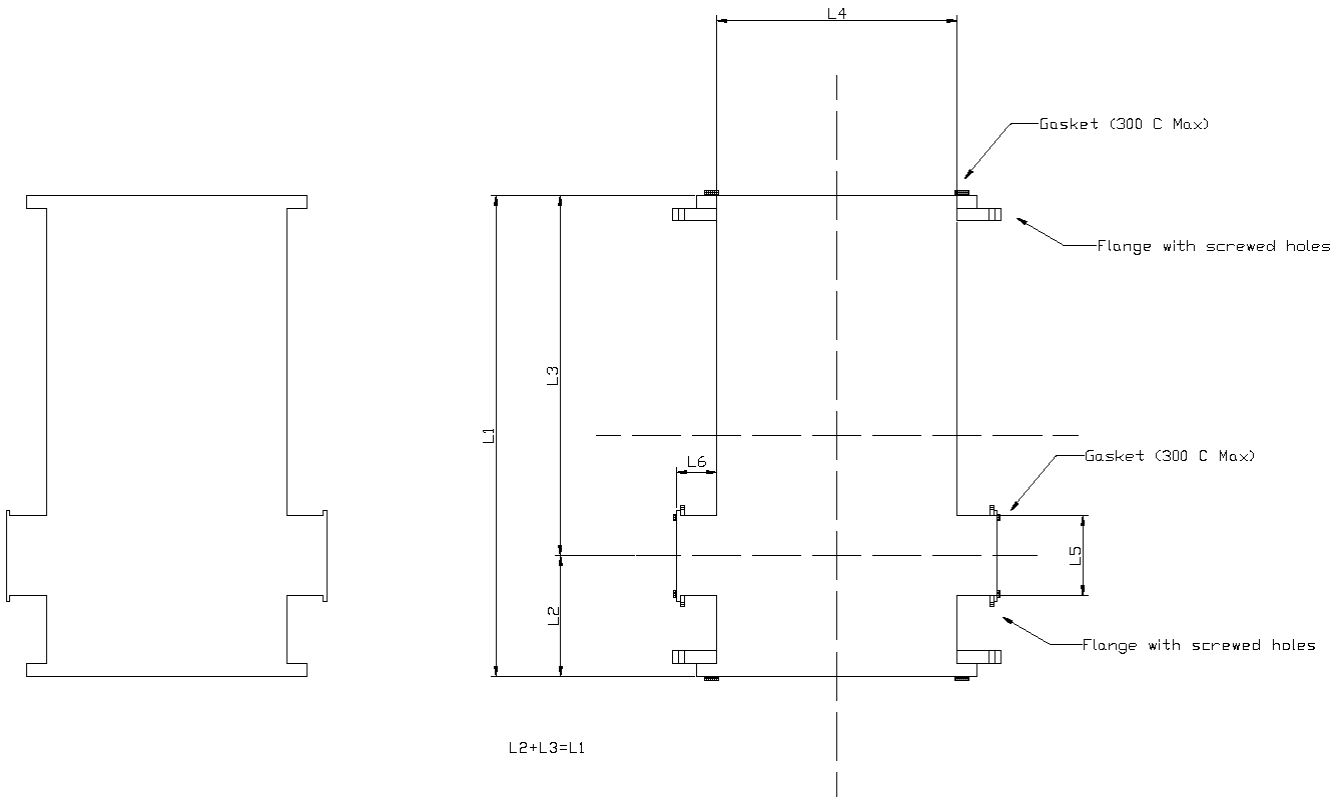

Figure A.5 Glass middle chamber

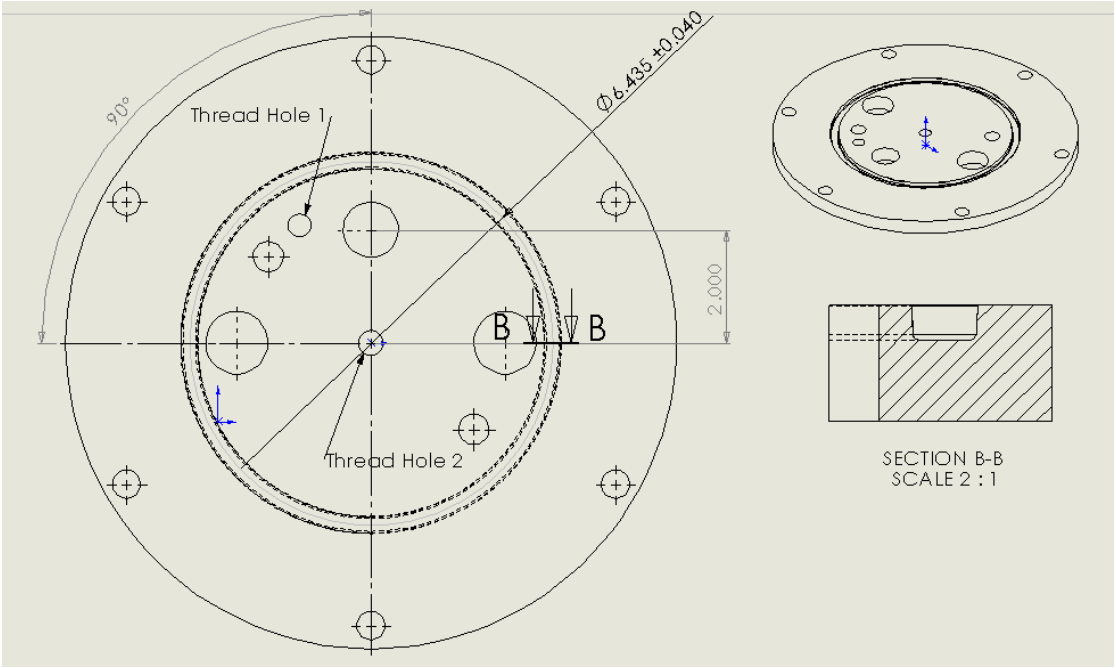

Figure A.6 Aluminum top plate

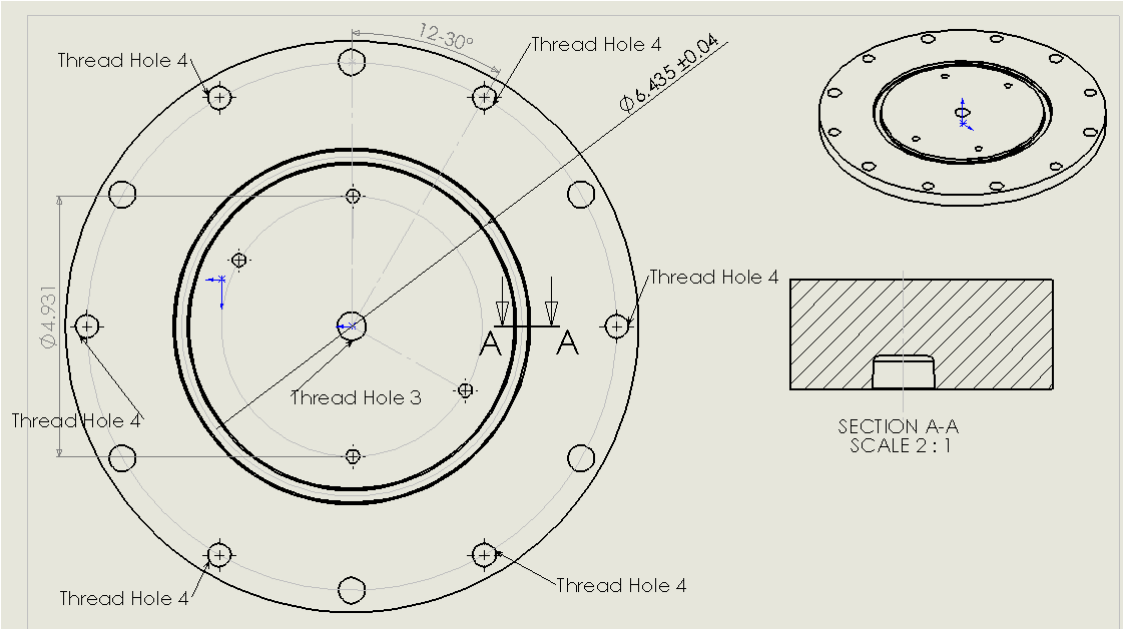

Figure A.7 Aluminum bottom plate

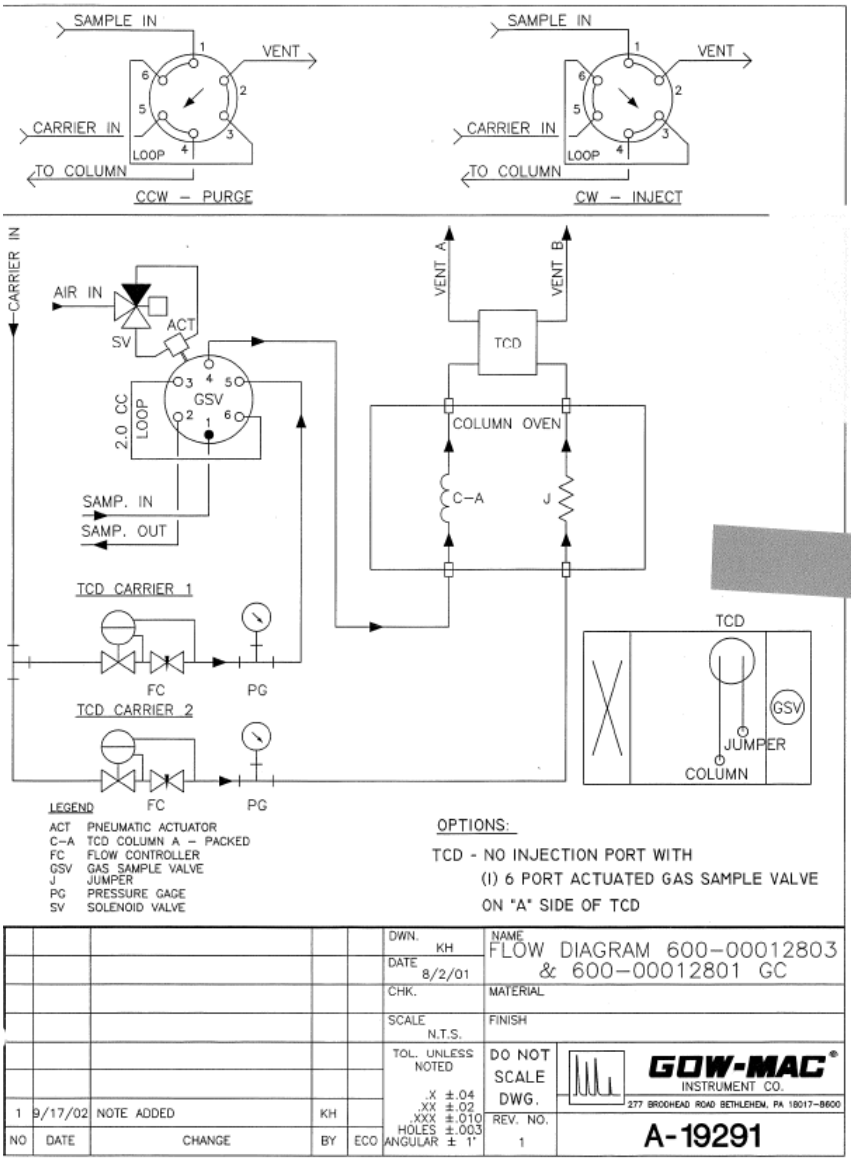

Figure A.8 The first version Gas Chromatograph

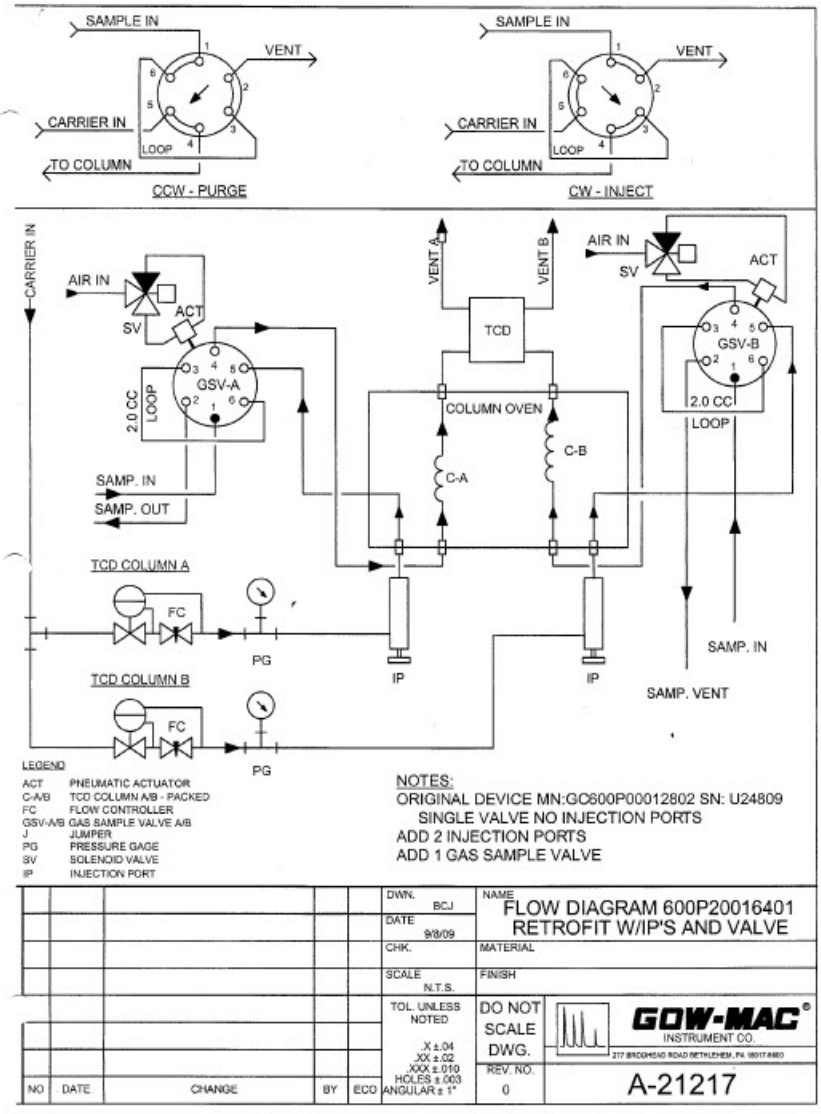

Figure A.9 The second version Gas Chromatograph

APPENDIX B

DESIGN CALCULATIONS

This section is assigned to detailed design calculations of the heater tube, immersion heaters, condensers and flow meter.

B.1 Design of Heater Tube

The FIBOR module was designed to film boiling of water because water parameters were believed to bracket organic liquid parameters. The power supply (Agilent #6681A) rating voltage and current, 0-8V and 0-580A, were sufficient for this purpose. Water is chosen as a reference substance because it has a higher critical heat flux than methanol and ethylene glycol and its boiling curve is well known. Figure 2.8 shows the boiling curve of water (Collier et al. 1996). The critical heat flux is approximately 100W/cm^2 and heat fluxes corresponding to a temperature range from 250°C (the minimum temp.) to 1400°C (the tube melting point) are 20W/cm^2 and 126W/cm^2 respectively. The heater and associated equipment were designed to these specifications.

Heat from the tube is generated by Joule heating (ohmic heating).

$$q'' = \frac{P}{A_o} = \frac{I^2 R}{A_o}. \qquad \text{B.1}$$

In terms of current (I), Eq. B.1 becomes

$$I = \sqrt{\frac{q'' A_o}{R}} \qquad \text{B.2}$$

and $R = \rho \cdot \frac{L}{A_c}$: tube electrical resistance. B.3

Inserting Eq. B.3 into Eq. B.2 and organizing, the current results in

$$I = \sqrt{\frac{q''\pi^2 d_o \left(d_o^{\,2} - d_i^{\,2}\right)}{4\rho}}\,. \tag{B.4}$$

The voltage between the tube ends is (Fig. 2.7)

$$V = I \cdot R\,. \tag{B.5}$$

Inserting Eq. B.3 and Eq. B.4 into Eq. B.5 gives

$$V = \sqrt{\frac{q''\pi^2 d_o \left(d_o^{\,2} - d_i^{\,2}\right)}{4\rho}} \cdot \rho \frac{L}{A_c} = 2L\sqrt{\frac{q''\rho d_o}{d_o^{\,2} - d_i^{\,2}}} \tag{B.6}$$

Eq. B.4 and B.6 show that current is dependent on only tube diameters while voltage is dependent on both diameters and length. This guides the design of the tube dimensions to be compatible with the power supply specification.

B.2 Design of Immersion Heater

In order to heat a 2L volume of water from room temperature (18°C) to its boiling temperature (100°C) in ten minutes (a time chosen somewhat arbitrarily), the required minimum power is

$$\dot{Q}_{\min} = \rho V_{\text{chamber}} \cdot c \cdot \frac{T_{sat} - T_{room}}{\Delta t} = 1058\text{W} \tag{B.7}$$

B.3 Design of Condensers

Cooling rate, $\dot{Q}_{\text{Cond}}$, of the condenser is expressed as

$$\dot{Q}_{\text{Cond}} = \bar{h}A\left(T_{sat} - T_s\right) \qquad \text{B.8}$$

where

$\bar{h}$: average heat transfer coefficient, A : condenser surface area, T_{sat} : saturation temperature of reactant liquid, and T_s : condenser surface temperature.

The condenser surface area is then (with Eq. 2.1)

$$A \geq \frac{\left(\dot{Q}_{\text{FIBOR}} + \dot{Q}_{\text{IH}}\right)}{\bar{h}\left(T_{sat} - T_s\right)} \qquad \text{B.9}$$

The maximum values of $\dot{Q}_{\text{FIBOR}}$ and $\dot{Q}_{\text{IH}}$ can be conservatively estimated based on boiling curve data for ethylene glycol $q''_{CHF} \sim 1\times10^6$ W/m^2 (Lienhard et al. 1973) and the four immersion heaters' specification (300 W each) such that

$\dot{Q}_{FIBOR} = q''_{CHF} \cdot \left(\pi \cdot l \cdot d\right) = 1\times10^6 \cdot (3.14\times0.0918\times4.76\times10^{-3}) = 1373$ W and

$\dot{Q}_{IH} = 4$ x 300 W $= 1200$ W

The design task is now to find a reasonable estimate of the average heat transfer coefficient, $\bar{h}$. Correlations of $\bar{h}$ for condensation are available in references (Incropera et al 5$^{\text{th}}$ ed.).

To proceed further, the following assumptions are made regarding the condenser design: laminar film condensation; for a conservative estimate, ethylene glycol is considered as a "design fluid" because of its comparatively lower liquid thermal conductivity (0.252 W/m·K) and higher critical heat flux (~ 1×10^6 W/m^2) than water and methanol respectively; non-condensable gases are present and reduce the rate of heat transfer by a factor of 10 (Rohsenow 1998); the condensate film thickness is small relative to the cylinder diameter; the ice water coolant as a constant surface

temperature (T_s) at 0°C; and acetone/dry ice coolant provides a constant surface temperature (T_s) of -78°C.

The Condenser S (Figure B.1) is a cross flow heat exchanger using cold water flow while the Condenser L (Figure B.1) uses dry-ice/acetone as a coolant. Output gases from the FIBOR chamber are cooled down at the rate of $\dot{Q}_{C1}$ as they pass through the first condenser assembly: the two sub-condensers count $\dot{Q}_{C1,L}$ and $\dot{Q}_{C1,S}$ respectively. That is, $\dot{Q}_{C1} = \dot{Q}_{C1,L} + \dot{Q}_{C1,S}$. For a conservative estimate, the cooling capacity of the smaller condenser, Condenser S, is assumed to be zero leading to

$$\dot{Q}_{C1} = \dot{Q}_{C1,L} . \qquad \text{B.10}$$

The selection of the commercial condensers was determined due to several reasons. A main reason is that they have adequate shape and size to be installed in the total FIBOR system of this study and sufficient surface area to condense. In order to evaluate whether the first condenser assembly provided an appropriate reflux (or condensation), from Eq. 2.1 and Eq. B.10

$$\dot{Q}_{FIBOR} + \dot{Q}_{IH} \le \dot{Q}_{C1,L} . \qquad \text{B.11}$$

Eq.B.11 concerns Condenser L. This condenser has a shape of vertical cylinder that is 74.5 mm diameter (D) and 209 mm tall (L) as shown in Figure B.1. Combining Eq. B.11 & Eq. B.8 gives

$$D \ge \frac{\dot{Q}_{\mathrm{FIBOR}} + \dot{Q}_{\mathrm{IH}}}{\pi L \bar{h}_{C1} \left(T_{sat} - T_s \right)} . \qquad \text{B.12}$$

For laminar film condensation on a vertical surface,

$$\bar{h} = 0.943 \left[\frac{g \rho_l \left(\rho_l - \rho_v \right) k_l^{\,3} h_{fg}{}' }{\mu_l \left(T_{sat} - T_s \right) L} \right]^{1/4} \qquad \text{(Incropera et al. p618)} \qquad \text{B.13}$$

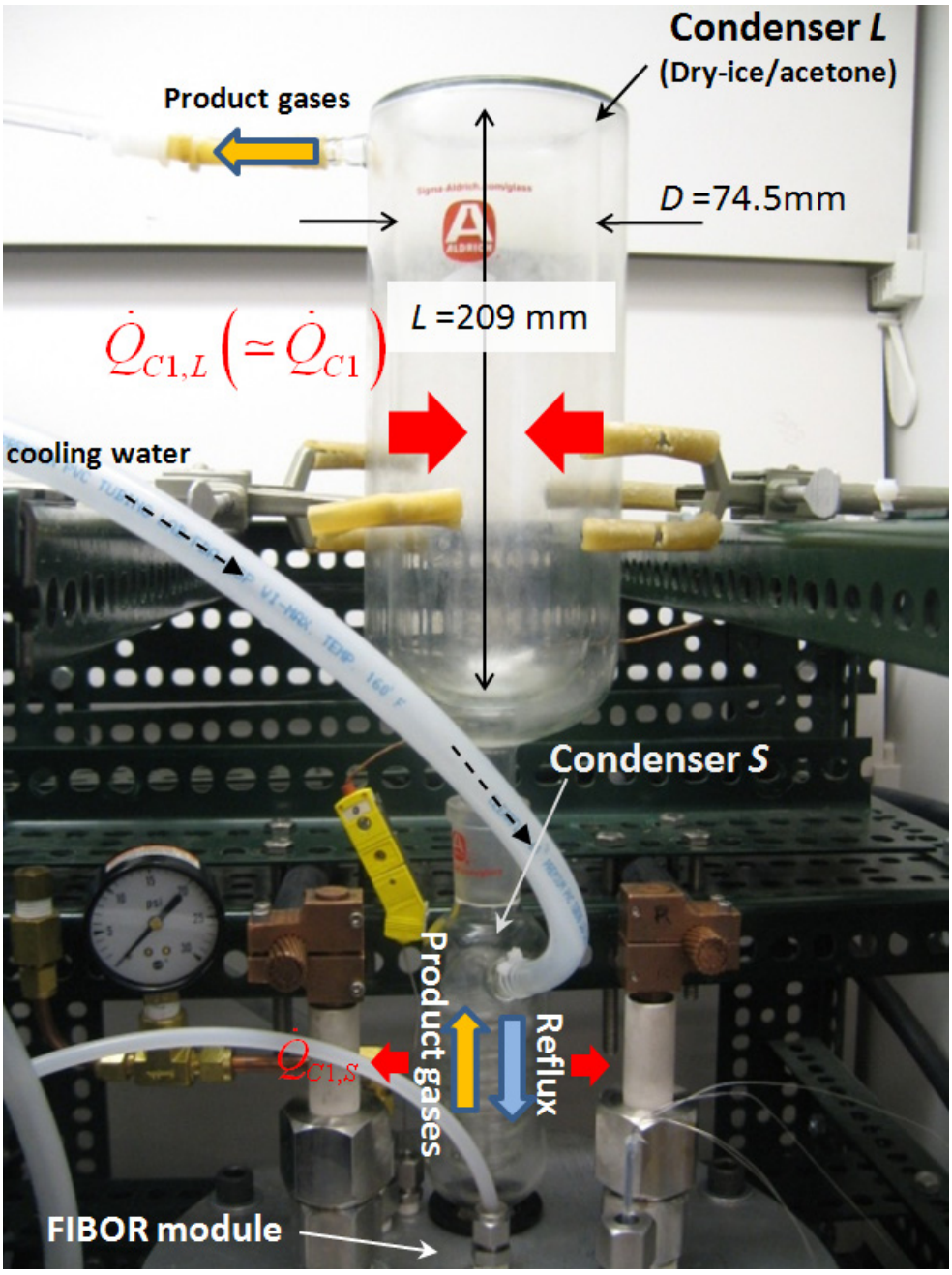

Figure B.1: The first condenser assembly

where $h_{fg}' = h_{fg}\left(1+0.68Ja\right)$. We estimate that $h_{fg}' \simeq 1355.97$ kJ/kg with

$$Ja = \frac{c_{p,l}\left(T_{sat}-T_s\right)}{h_{fg}} = 1.022$$

where T_{sat} =197.3°C and T_s =-78.5°C.

Using methanol properties (see Table 3.1), Eq. B.13 gives $\overline{h}$ = 1365.1 W/m^2·K. As remarked earlier, however, this value is reduced by a factor of 10 as non-condensable gases are present in the out gas of the FIBOR module (Rohsenow 1998). Thus $\overline{h}_{C1} = 136.5$ W/m^2·K.

Based on the above, a minimum diameter of the condenser is then

$$D_{\min} = \frac{\dot{Q}_{\text{FIBOR}} + \dot{Q}_{\text{IH}}}{\pi L \overline{h}_{C1}\left(T_{sat}-T_s\right)} = 103.3 \text{ mm}$$

A coiled-type condenser (Figure B.2) was selected as the second condenser assembly to provide greater cooling surface area that was used in a prior study (Purdy 1987). The diameter (d_i) of the coiled tube is fixed at 9.7mm and the length of the coil (L) is the design parameter. The coolant is water-ice for the coiled-type condenser.

In order to determine the length of the coil, Eq. B.9 is rearranged to

$$L \geq \frac{\left(\dot{Q}_{\text{FIBOR}} + \dot{Q}_{\text{IH}} - \dot{Q}_{\text{C1}}\right)}{\pi d_i \overline{h}_{C2}\left(T_{sat}-T_s\right)} \qquad \text{B.14}$$

where $\dot{Q}_{\text{C1}}$, the cooling rate of the first condenser assembly, is subtracted because the coiled condenser is located at the downstream of the first condenser assembly.

$\dot{Q}_{\text{C1}}$ is estimated by using the previous calculation, $\dot{Q}_{\text{C1}} = A_{\text{C1}}\overline{h}_{\text{C1}}\left(T_{sat}-T_s\right) = 1856.2$ W where $\overline{h}_{\text{C1}}$ = 136.5 W/m^2·K, A_{C1} =0.0489m^2, and T_s = -78.5°C.

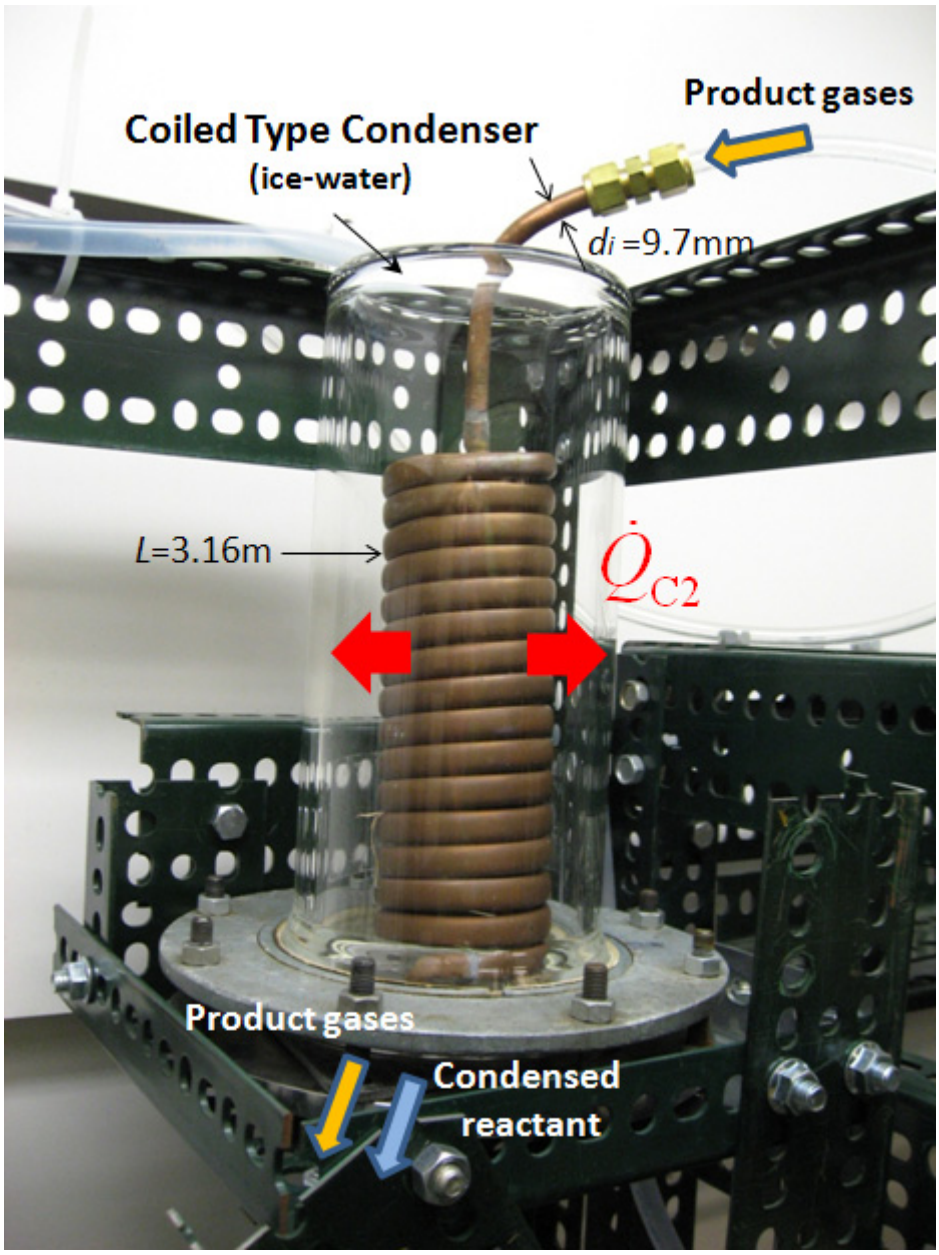

Figure B.2: The second condenser assembly (Coiled type condenser)

Then the average heat transfer coefficient of the coiled type condenser ($\overline{h}_{C2}$) is calculated. Having assumed condensate flow in a horizontal tube (Chato 1962), it follows that

$$\overline{h} = 0.555\left[\frac{g\rho_l\left(\rho_l-\rho_v\right)k_l^{\,3}h_{fg}{}'}{\mu_l\left(T_{sat}-T_s\right)d_i}\right]^{1/4} \qquad \text{B.15}$$

with the modified latent heat $h_{fg}{}' \equiv h_{fg}+\frac{3}{8}c_{p,l}\left(T_{sat}-T_s\right)=$ 1020.5 kJ/kg where T_{sat} =197.3°C, T_s = 0°C.

Again, being divided by 10 due to the non-condensable gases' presence (Rohsenow 1998) $\overline{h}_{C2}$ = 175.0 W/m^2·K. From Eq. B.14, $L_{\min}$ = 0.672m. If the second coiled condenser with 9.7mm diameter and 3.16m length (Fig. B.2) is filled with ice-water coolant, it now provides enough capacity to condense the vaporized ethylene glycol at a maximum power condition when coupled with the first condenser assembly.

Two cold traps were placed after the second condenser assembly (i.e. the coiled-type condenser) to assure more complete screening of reactant and condensable contaminants before entering the flow meter. Figure B.3 shows the cold trap arrangement.

B.4 Design of Flow Meter

The selection of the gas flow rate range (0-10 SLM) was determined based on the FIBOR analysis for methanol by Avedisian et al. (2008) and the selected tube size (L: 140mm, D: 4.76mm).

Total volumetric flow rate of product gases ($\dot{V}_{\mathrm{Tot}}$) can be calculated as

$$\dot{V}_{\mathrm{Tot}} = \overline{v}\cdot\left(N^*_{\mathrm{H_2}}+N^*_{\mathrm{CO}}\right)\cdot A_o\,. \qquad \text{B.16}$$

By stoichiometry of Eq. 1.1, Eq. B.16 becomes

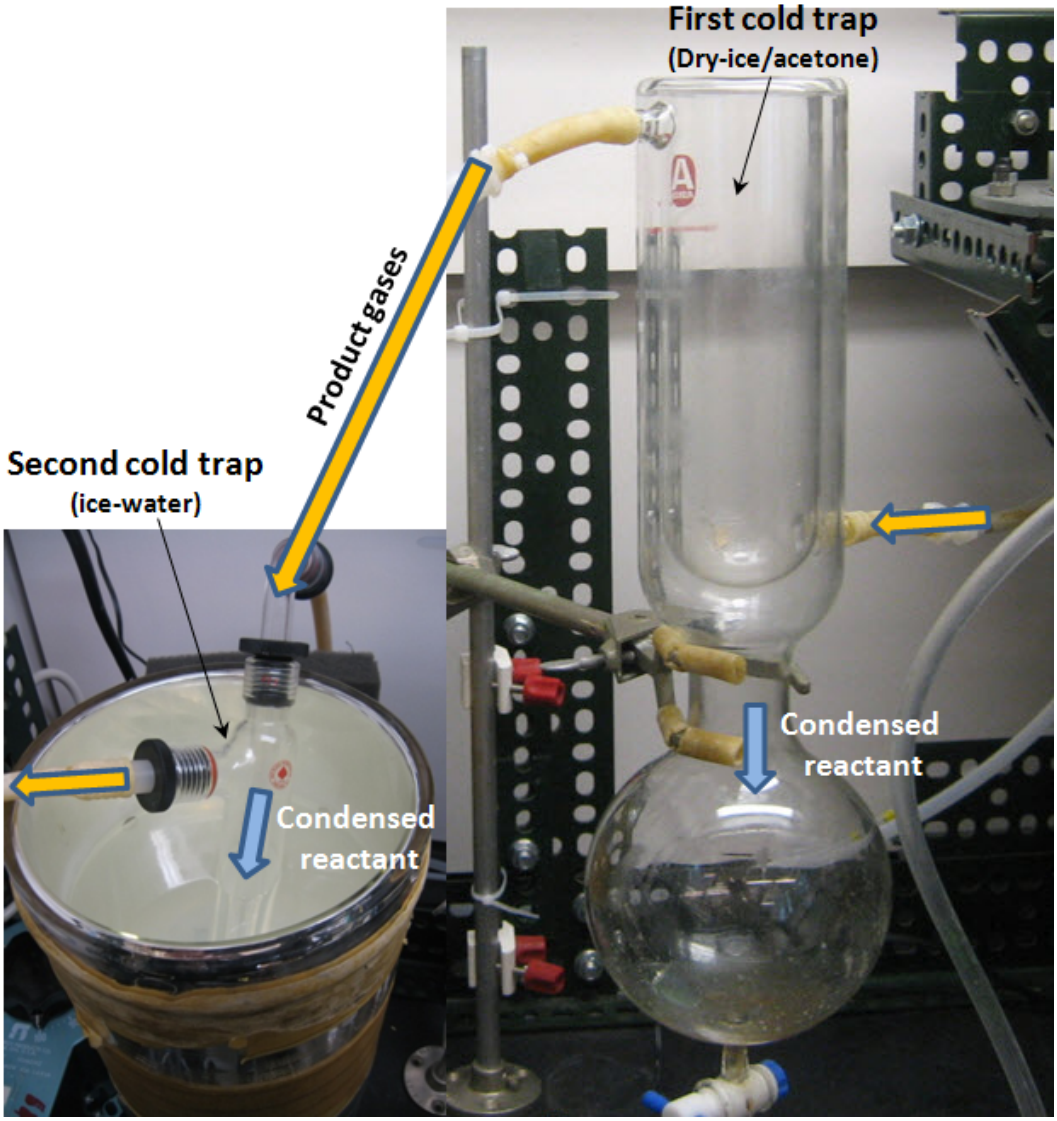

Figure B.3: Cold traps

$$\dot{V}_{\text{Tot}} = \overline{v} \cdot \frac{3}{2} N^{*}_{\text{H}_2} \cdot A_o \qquad \text{B.17}$$

According to the analysis by Avedisian et al. (2008), hydrogen throughput is produced to be approximately $1.5 \text{x} 10^4$mol/hr/m^2 at 1200K for a 5mm diameter tube (including radiation effect) and the rate values incorporated. The chemical reaction surface area of the selected tube is 1376 x10^{-6} m^2 from $A_o = \pi \cdot d_o \cdot l$. Molar specific volume is 22.4 L/mol assuming that product gases are ideal. Thus, $\dot{V}_{\text{Tot}}$ =11.6L/min. A flow meter with 1-10 L/min range was selected taking account of the estimated flow rate rage and measurement accuracy. The manufacturer's accuracy is stated to be 1% of the total.

APPENDIX C

EXPERIMENTAL PROCEDURE

This section deals with the assembly and setup of all aforementioned components. In addition, a general experimental procedure for creating film boiling is presented. Before discussing details of executing FIBOR experiments, we briefly provide some overall perspective as it relates to how experiments are run and what information exactly is desired. In the broadest sense, the underlying purpose of every experiment is to demonstrate the extent that a FIBOR can promote chemical conversion. The objectives are a set of more specific tasks to be carried out during the experiment. They provide the building blocks, or data sets, for further analysis. Critical data sets include: 1) flow rates with respect to wall temperature to give the simplest proof of chemical reaction and its sensitivity to temperature (provided that products do not dissolve in the reactant pool liquid); 2) GC analysis to identify individual product species and their concentrations; and 3) boiling curve data to show the FIBOR operational domain and to reveal the heat required to support the endothermic nature of the chemical reaction mechanism postulated in Section 1.2.3.

C.1 FIBOR Chamber Set-up

Preparation for an experiment starts with the heater tube. If using a catalyst coated tube, the surface is first characterized through Scanning Electron Microscope (SEM) images. A Hitachi S-900 SEM in CCMR (Cornell Center for Materials Research) at Cornell University was used to analyze the catalytic tubes in this study. The SEM is a Field Emission Gun Scanning Electron Microscope (FEGSEM) of "in-lens" design capable of 0.8 nm resolution at 30 kV and 3-4 nm resolution at 1 kV. Magnification ranges from 100X to 800,000X. The "in-lens" design imposes a sample

size limit of ~ 5 mm W × 10 mm L × 2.5 mm H. Digital images are acquired via an analog-to-digital converter / PCI system. This instrument provides only a qualitative analysis and cannot provide precise surface composition results.

Following SEM characterization, four thermocouples (Omega, KMQXL-010G-18) are mounted inside of the heater tube at locations shown in Figure 2.4. Thermocouples are spaced equidistantly between the electrode clamps to verify an axially symmetric temperature profile. Silicone sealant is used at the ends of the heater tube (Dow Corning, RTV 736) and on the electrode clamps to prevent liquid penetration. The FIBOR chamber is assembled with an air-tight seal through use of packing gland (Conax, PG2-125-AT) feedthroughs for thermocouples and an o-ring (Viton, no. 362) between the glass chamber and heater tube mount. Once the FIBOR module is assembled properly as Figure 2.2, it is moved into a fume hood and installed. The installation includes connections of power cables, chemical waste line, immersion heater power terminals, thermocouples, nitrogen gas line.

C.2 Condenser Module Set-up

The assembled condenser module (Figure 2.13) is checked thoroughly for leaks before each experiment by inspecting each connection as nitrogen flows (10-20psi, ~0.1LPM) through the system. An initial leak check includes comparing the readings of the flow regulator at the compressed cylinder and that of the digital flow meter; they should match within 0.05 LPM. Sealant (DuPont, Krytox) is used at all connections to ensure a proper vacuum seal is achieved and to also allow for ease of disassembly. For a thorough check, inspect each connection with Snoop Liquid Leak Detector (Swagelok).

For safety with the heater tube at high temperature positioned above the bulk liquid reactant, nitrogen is passed through the system (0.1 LPM) to eliminate the

possibility of ignition. After the heater tube is submerged and film boiling ensues, the nitrogen is recommended to be turned off so that the measured gas flow includes only product species as a result of chemical reaction in the FIBOR.

C.3 Data Acquisition Testing and GC Set-up

A detailed step by step procedure is given in a later sub-section for setting up and launching the LabVIEW program that controls the operating parameters of an experiment. Here, the general steps are outlined as follows: connect all thermocouples (4 or 7 heater tube TC's and 1 bulk liquid TC); power on DAQ (National Instruments, NI SCXI-1102C); power on Power Supply (Agilent, 6681A); open Agilent Connection Expert in PC, refresh all connections; open, start and stop Power Initiation LabVIEW Program (Power.vi); open User Interface LabVIEW Program (FIBOR Control Interface.vi); set "cutoff temperature" to 1300 °C (~ tube melting point), set "divide voltage by" to 1.3 and set "current" to 580 A; start the program by clicking arrow on main toolbar at top of screen ; the time should begin to scroll by giving 5 TC (or 8 TC) readings. The bulk liquid TC should be slightly lower (1-2 degrees) than the four (or seven) heater TC readings that are enclosed inside of the tube; and apply a small voltage (.1-.2V) to observe heater TC response.

If thermocouples are mounted according to Figure 2.4 (a), a symmetrical temperature profile should be displayed. For instance, in the case of 7 TCs mounting, the temperatures of TC#2 and #6 should be within 1-2 degrees, while the temperatures of TC#3 and #5 should also be within 1-2 degrees. Due to conductions losses to the electrode wet clamps, the temperature reading of TC#1 and #7 should be lower than TC#2 and #6. A voltage of approximately 0.5V is sufficient to raise the temperature of the tube and test for a symmetrical profile along the tube.

The GC is pre-programmed and configured to minimize setup time during an experiment as discussed in Section 2.2.5.2. Details regarding additional information of the GC running can be found in the Series 600 Gas Chromatograph User's Manual (GOW-MAC, 2006). Three separate gas flows must first be connected to the GC (see Figures 2.20 or 2.22 and Figure C.6 for additional details). The actuator gas (compressed Nitrogen, 20-30psi) serves to pressurize the solenoid inside of the GC which physically controls the injection of the sample gas into the column(s). The carrier gas (compressed Helium, 40-50psi, 30CCM) provides a constant flow through the column(s) and carries the product species of interest with it. The sample gas consists of either the actual FIBOR product gas or a calibration gas. The FIBOR gas sample is extracted from the actual product gas flow during an experiment through the mini-pump arrangement described previously (see Figures 2.20 or 2.22, and 2.21). After an experiment is complete, the direction of the two-way valve (Figures 2.20 or 2.22 and C.6) is changed so that a calibration gas (10psi/30CCM) with a known composition can be analyzed for comparative analysis. Once all three gas lines are connected, the GC is powered on.

The GC settings are adjusted from the keypad on the front of the instrument. Figure C.5 (a) is a depiction of the "Home Page" that the GC displays by default after it powers on and also from which all commands start from. The GC automatically heats the column oven to 60°C and the TCD to 95°C which is programmed into a "method file" (for isothermal mode: Fig.2.23 (a)) and is activated from the keypad. Detailed steps are described in a later part of this section. The GC is also equipped with Chrom Perfect data acquisition software that provides automated user control of the GC during an experiment along with chromatogram retrieval and analysis tools. Detailed steps for opening and setting up the software are also included in the later part. Once the column oven and TCD are heated to the temperatures specified in the

method file, the GC is ready to inject and analyze a sample. Samples are injected on command by the user through the Chrom Perfect Software: For the upgraded GC, the first sample is injected into Column A. After five minutes, a second sample is injected automatically into column B. The chromatogram is automatically displayed and saved to the hard drive of PC (the folder of C:\Cornell 600GC) once the run is complete (after ~10min).

C.4 Detailed Steps for Experimental Procedure

Setting up for an experiment using a new heater tube requires at least two days for proper mounting and time for sealants to cure. The end-state is shown in Figure 2.3 (a) that depicts the bulk liquid reactant chamber top mount. The heater tube is properly mounted with installed thermocouples. The actual experiment occupies the third (final) day. A detailed, step-by-step description follows that is organized first by the first two set-up days, followed by the actual experimental procedure on the third day.

C.4.1 Construction of Heater Assembly (Day 1-2)

a. If using a bare heater tube, rinse the inside and outside with ethanol and allow to dry. Plastic gloves are recommended whenever handling the heater tube, especially if coated with a catalyst.

b. If a catalyst coated heater tube is used, the surface should first be characterized with Scanning Electron Microscope (SEM) images. Analysis in this study uses a Hitachi S-900 SEM in CCMR (Cornell Center for Materials Research) at Cornell University.

c. Thoroughly clean the contact surfaces of the copper electrode clamp components (Figure 2.5) to remove any built up oxidation residue. Brake cleaner (CRC Brakleen)

works sufficiently well, evaporates quickly and does not leave a residue. Battery terminal cleaner (Lynx Battery Cleaner) can be used to remove more difficult residue build up. Figure 2.5 shows cleaned, disassembled electrode clamps that include two top wet-clamps, two bottom wet-clamps and eight 1/8" (#6-32 thread) hex screws, ceramic tube insert and the heater tube. Heater tubes are manufactured and cut to length by Microgroup, Inc. (Microgroup, 600F10188X028SL) Details of the heater tube to include dimensions and material characteristics are listed in Table 2.2. Cut a ceramic insert tube (Omega, ORX-11618) to 137mm using a Dremel Tool with a specialty blade designed for cutting ceramics (Dremel 545 Diamond Wheel).

d. Apply a coating of heat resistant silicon sealant (Dow Corning, RTV 736) on the left end of the heater tube prepared in 'c' to secure the inside of the heater tube. Allow to dry for 24 hours.

e. Place the bulk liquid reactant chamber top mount on a workbench as shown in Figure C.1 (a).

f. Connect the two top wet-clamps to the electrode copper buses. Assemble the heater tube prepared in 'd' and the left hand side top and bottom wet-clamps. Then, fasten them by four hex screws. Using an Allen Wrench, fasten the hex screws in an opposite manner to ensure even pressure so achieve optimum electrical and thermal contact between the wet-clamp components and heater tube. See Figure C.1 (a).

g. Cut a 200mm piece of Teflon tubing (Sigma-Aldrich, Z515337-1PAK, Chemflour Tubing, PTFE, I.D. 1/16in., O.D. 1/8in.). Insert the Teflon tubing through packing gland (CONAX, PG2-125-AT: 'k' in Figure 2.2) using a Teflon packing gland seal

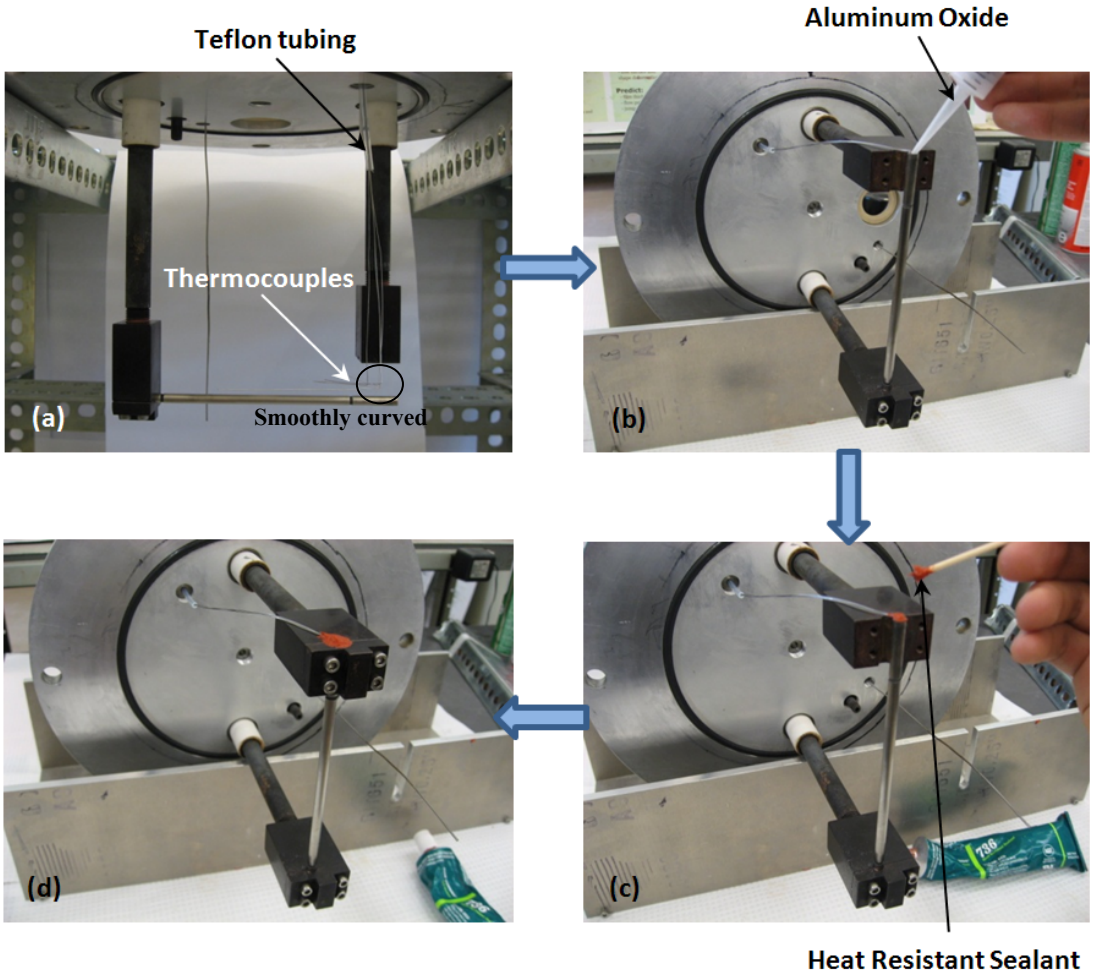

Figure C.1: Procedure of heater assembly construction

(CONAX, RS-PG2-125-T). Assemble gland components but do not tighten. See Figure C.1 (a).

h. Insert 4 thermocouples (Omega, KMQXL-010G-18) through Teflon tubing as shown in Figure C.1 (a). If new thermocouples are being used, label the thermocouples (TC) #1-4.

i. From the end of TC#1, measure 24 mm and place a mark on the TC wire using a black permanent marker. In the same manner, from the end of TC#2, measure and mark 39.3 mm. For TC#3, measure and mark 54.6 mm and for TC#4 measure and mark 69.9 mm. Accurate measurements and markings are critical as they will affect the assumption of a symmetrical temperature profile across the length of the heater tube. See Figure 2.4.

j. Move the bulk liquid reactant chamber top mount from the workbench and lay it on another workbench as shown in Figure C.1. (b).

k. Insert the ceramic insert into the heater tube.

l. Insert TC's #1 to #4 into the right hand side of the heater tube assembly. Ensure the markings on the TC's align exactly with the end of the ceramic insert/heater tube. Figure 2.4 depicts the proper spacing of thermocouples inside of the heater tube/ceramic insert assembly.

m. Fill up the empty space of the heater tube with alumina (aluminum oxide) powder. A slight intermittent hitting of the heater tube allows the space to be tightly packed with the powder. See Figure C.1 (b).

n. Apply a coating of heat resistant silicon sealant (Dow Corning, RTV 736) on the right end of the heater tube to secure the TC's and ceramic insert inside of the heater tube. Allow to dry for 12 hours. See Figure C.1 (c).

o. Assemble the right hand side top and bottom wet-clamps with the heater tube and fasten the hex screws hand-tight. Using an Allen Wrench, fasten the hex screws in the same manner as in step 'f'. See Figure C.1 (d).

p. Gently move and place the heater tube assembly at an appropriate position while adjusting the TC's through the Teflon tube and packing gland. Fasten the feed-throughs for copper buses ('j' in Figure 2.2) by hand-tight.

q. Move the bulk liquid reactant chamber top mount back to the original work bench as shown in Figure 2.3. (a).

r. Apply a second coat of heat resistant silicon sealant (Dow Corning, RTV 736) on the both ends of the heater assembly. Apply a generous coat to prevent liquid penetration inside of the tube or between the electrode clamps.

s. Apply a coat of clear silicon sealant (GE, RTV 108) around the adjoining wet-clamps to prevent liquid penetration.

t. Apply a coat of clear silicon sealant (GE, RTV 108) to the top and bottom of the Teflon tube to prevent escape of vapors/product gases. See Figure 2.3 (a). Allow to dry for 12 hours.

u. If using new thermocouples, apply a coat of varnish (GC Electronics, 10-9002) at the junction of the TC wire and the yellow electrical connector. This will strengthen this connection as it is easy to break over the course of experiments. Allow to dry for 24 hours.

C.4.2 Experiment (Day 3)

Once the sealants on the heater tube have cured, one or multiple experiments can be run with the same heater tube. On the day of an experiment, the following supplies must be acquired and readily available before proceeding to further steps: feedstock (e.g. methanol or ethylene glycol) prepared; ground dry ice (fill 3-gallon cooler); 1 L Acetone; crushed ice (fill 3-gallon cooler); ensure adequate compressed nitrogen on-hand for both safety feed (Figure 2.1) and GC actuator gas (Figure 2.20 or 2.22); ensure adequate compressed helium on-hand for GC carrier gas (Figure 2.20 or 2.22).

C.4.2.1 Mount FIBOR into Fume Hood

a. The heater assembly (Figure 2.3 (a)) is inserted inside of the reactant chamber assembly (Figure 2.3 (b)) with an o-ring and a rubber gasket, and fastened forming an air tight seal. Tighten six hex bolts in an opposite manner while ensuring that the top of the reactant chamber is centered on the chamber o-ring for a proper sealing. See Figure 2.2.

b. Insert the FIBOR module (Figure 2.2) into the hood. Align and fasten copper electrode terminals (power cable connection) and chemical waste line. See Figure C.2.

c. Connect immersion heater power terminals. When connecting, ensure a positive (red) and ground (black) is connected to each immersion heater line. See Figure C.2.

d. Connect thermocouples, ensuring proper connections for respective numbering. See Figure C.2.

e. Connect Nitrogen gas line; fasten fitting tightly to prevent any leakage. See Figure C.2.

f. Before going further, it is recommended to test thermocouples in LabVIEW to ensure all data acquisition is working properly.

C.4.2.2 Data Acquisition Testing

a. Turn on the temperature DAQ (National Instruments SCXI-1000). See Figure 2.14.

b. Turn on Power Supply (Agilent 6681A). See Figure 2.14.

c. Open Agilent Connection Expert in PC (Figure C.3 (a)) and click 'Refresh All'.

d. Establish a new folder on the hard drive (c-drive). Establish a sub-folder containing the LabVIEW programs (Power.vi, FIBOR Control Interface.vi). If more or less heater thermocouples are used, the block diagrams (Appendix D) for these programs

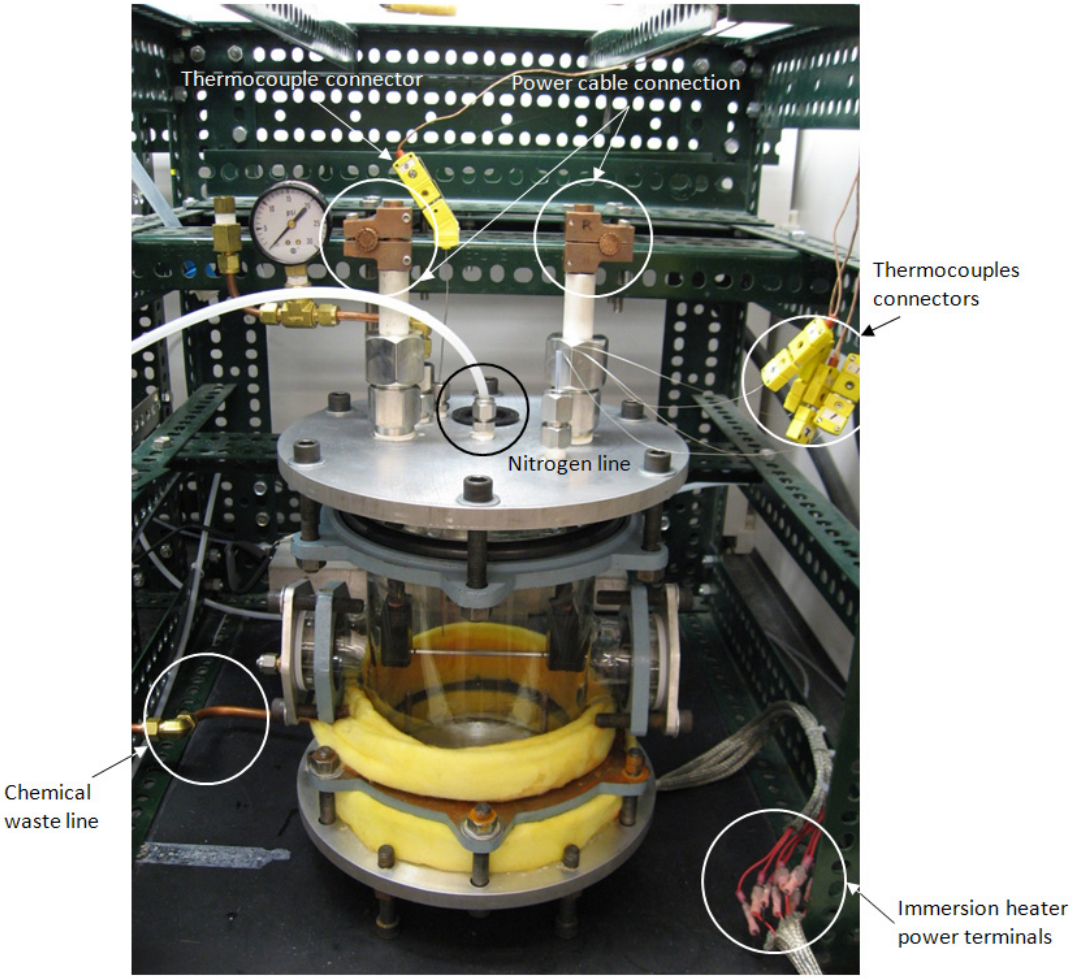

Figure C.2: FIBOR chamber set-up

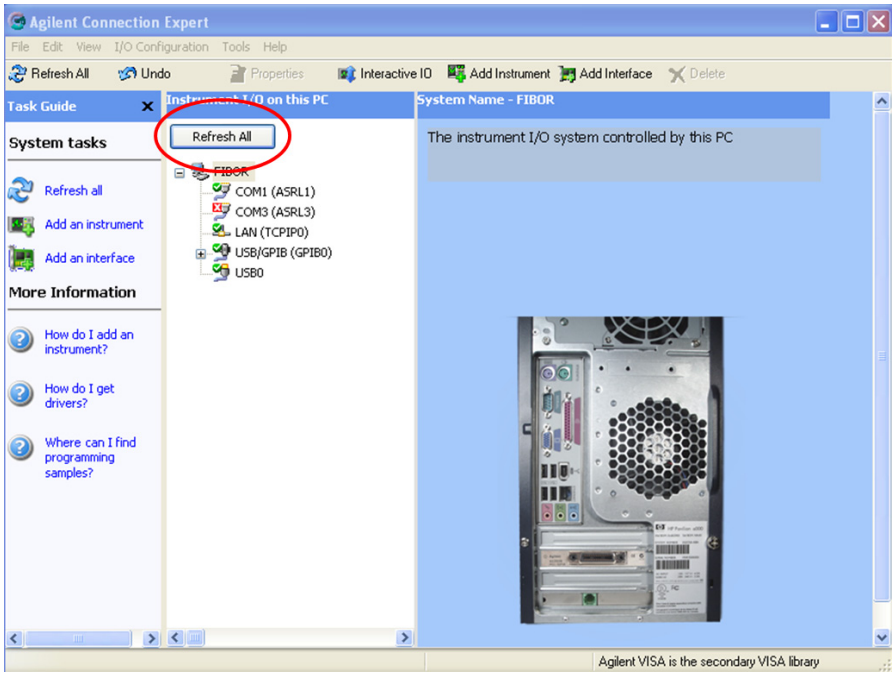

(a)

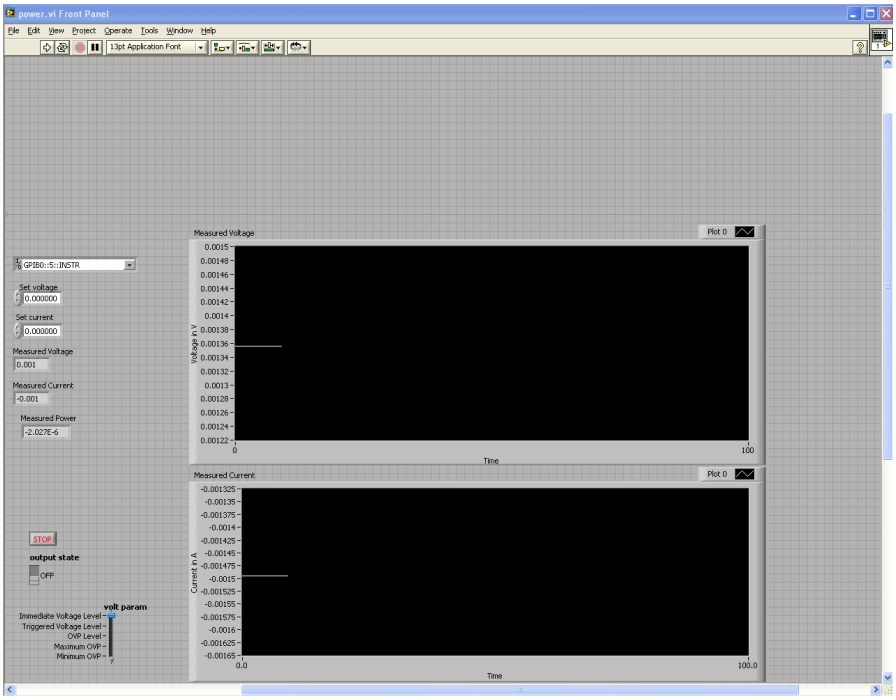

(b)

Figure C.3: (a) Agilent Connection Expert

and (b) LabVIEW Power Initiation Interface (Power.vi)

must be modified. Also establish necessary subfolders to place copies of column data and Chromatograms.

e. Open “Power.vi”. Select GPIBO::5::INSTR under the I/O control selector. Click the “run” arrow button at the top of the screen. Once a power reading is observed, click the red “stop” button. A captured view of this software program is provided in Figure C.3 (b).

f. Open “FIBOR Control Interface.vi”. Set “CUTOFF-TEMP” to 1300, set “Divide Voltage by?” to 1.3 and set “Set current” to 580. Click the “run” arrow button at the top of the screen. A captured view of this software program is provided in Figure 2.17.

g. Three plots are provided. The first depicts a scrolling time reading of the 5 TC’s. The second is a scrolling time reading of the power output from the power supply. The third display is a scrolling flow reading from the flow meter. Additionally the actual numerical values of the voltage (V), power (W) and current (A) are digitally displayed. See Figure 2.17.

h. The experiment is controlled by the user inputting the voltage under “Set Voltage.” The corresponding power and current are automatically adjusted. In order to apply power to the tube, click “output state” to “on.” Apply a small voltage (.1-.2V) to observe heater TC response. See Figure 2.17 for a depiction of the LabVIEW program and Appendix C.3 for further discussion regarding a typical TC response during DAQ testing.

C.4.2.3 Condenser Assembly and Leak Test

a. The assembled condenser module is shown in Figure C.4. Install the first condenser (Sigma-Aldrich, Z517232) by first applying sealant (DuPont, Krytox) to both the male and female connections. The condenser is named 'Condenser S' in Figure C.4. Insert the male end into the rubber fitting at the top of the FIBOR (Figure 2.10). Insert fully to ensure an adequate seal. Connect the water lines and slowly pressurize with running cold tap water which runs through its coil design.

b. Install the second and primary condenser (Sigma-Aldrich, Z164038) by applying necessary sealant (DuPont, Krytox) and inserting the male fitting into the female fitting of the first condenser. The condenser is named 'Condenser L' in Figure C.4. Fill the dry finger (inside portion of condenser) ¾ full with dry ice. Slowly poor acetone until a boiling slurry is made. Continue to slowly combine dry ice and acetone until the cold finger is full. CAUTION: Always wear gloves when handling dry ice to avoid freezer burns. Also ensure acetone is added slowly as it is easy to boil over.

c. Connect gas line from the Condenser L in the first condenser assembly to the second condenser assembly (See Figure 2.13). Fill the second condenser assembly with ice-water (50% crushed ice and 50% tap water).

d. Connect gas line from the second condenser assembly to the first cold trap (Sigma-Aldrich, Z422347). Fill the cold trap with dry-ice/acetone slurry in the same manner of the step 'b'. See Figure 2.13.

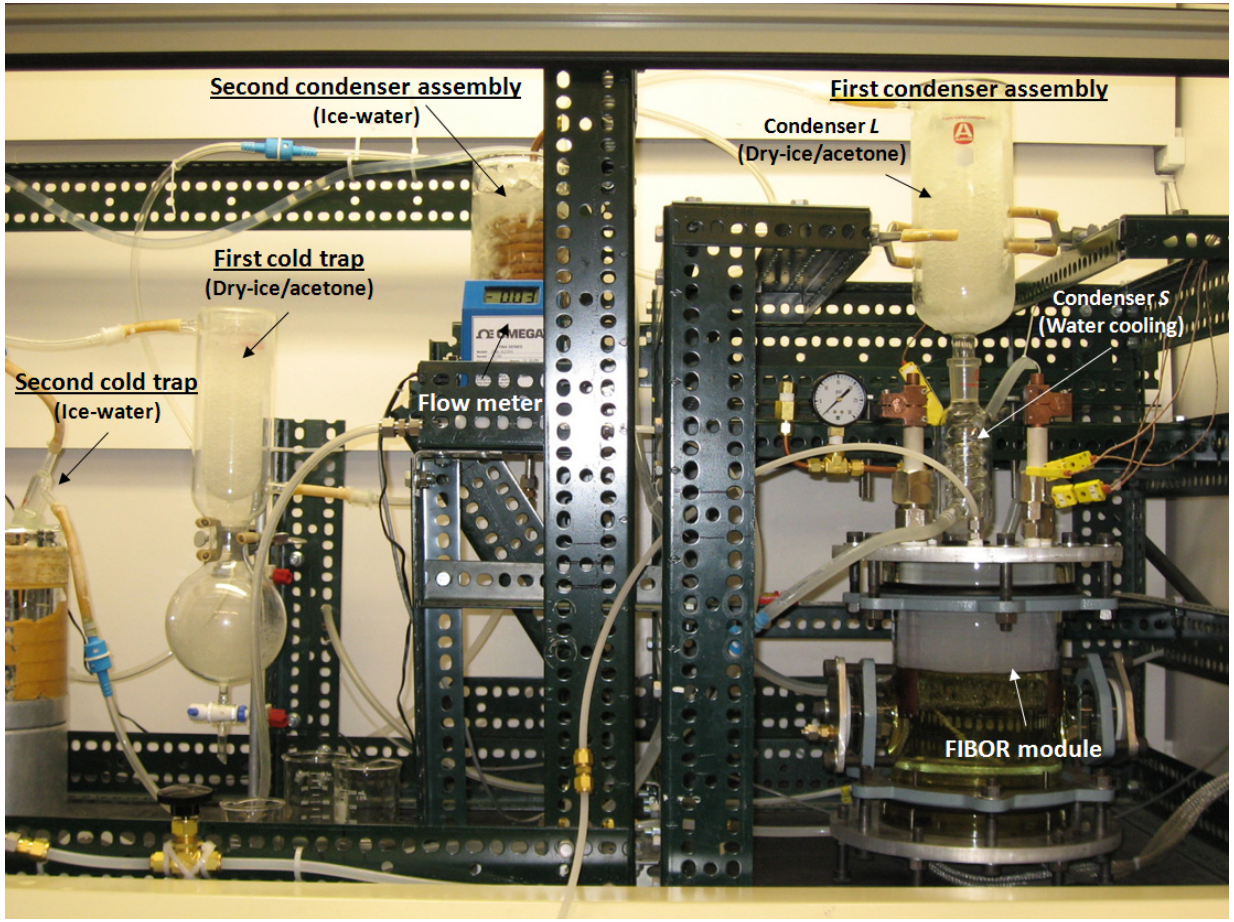

Figure C.4: FIBOR and Condenser Modules Setup

e. Connect gas line from the first cold trap to the second cold trap (Ace Vacuum Trap, Aldrich Z256870). Place the cold trap in an insulated container immersed in ice water. See Figure 2.13.

f. Connect gas line from the second cold trap to the flow meter.

g. Open safety Nitrogen feed line (Figure 2.13) and pressurize the system to test for leaks. The system should be sealed from outside air if all components are installed properly. To check for leaks, the first step is to set the flow of the Nitrogen and turn on the flow meter. The flow rates should be within +/- 0.05 LPM. Next, use liquid leak detector (Snoop, Swagelok) at each fitting in the system. The presence of tiny bubbles forming indicates a leak. Fix leaks as necessary by adjusting or tightening fittings.

C.4.2.4 GC Setup

The last step before filling the bulk liquid reactant chamber and establishing a FIBOR is to configure the GC so that product gas samples can be extracted and analyzed once chemical reaction is detected by a flow reading on the flow meter. The GC is pre-programmed and configured to minimize setup time during an experiment. This section describes the GC setup procedure in detail for the isothermal mode of the upgraded GC (Figure 2.23).

Once all three gas lines are connected according to Figure 2.22, the following steps are executed in order before powering on the GC:

a. Open carrier gas flow-compressed Helium, 40-50psi, ~30CCM.

b. Open actuator gas-compressed Nitrogen, 20-30psi.

c. On the back of the GC, turn the power switch to “on”.

Figure C.5 (a) is a depiction of the “Home Page” that the GC displays by default after it powers on and also from which all commands start from. Pressing the “Home” button on the key pad always returns to this display. The first step to program the GC for use during an experiment involves retrieving a pre-programmed “method.” This requires pressing the following keys:

d. Edit>Retrieve>QCTEST1>Return

e. “Method Retrieved Successfully” should be displayed

f. Press “Home”

The GC is equipped with Chrom Perfect data acquisition software that provides automated user control of the GC during experiments along with chromatogram retrieval and analysis tools. The software is opened through the following steps:

g. Open Chrom Perfect Software (Figure C.5 (b))

h. Click Data Acquisition Button

i. Click the yellow “Claim” button under the Selection Tab

(a)

(b)

Figure C.5: (a) GOW-MAC Series 600 GC Key Pad and (b) Chrom Perfect Software

j. The Instrument Control Button should be highlighted in color under the Status Tab and the word “Ready” should be displayed next to it

The remaining steps conclude setting up the GC for an experiment since all control after is from the Chrom Perfect Software. Going back to the key pad on the front of the GC, press:

k. Action>Heat On

l. Press “Home”

As the GC heats, the words “Not Ready” will be displayed on the Home Page in the upper left corner. The actual temperature of the column oven and TCD can be viewed by pressing “Status.” Once the word “Ready” appears in the top left corner, press:

m. Control>Filament>On

n. The GC is now ready to detect a sample. During an experiment, ensure the mini-pump (Figure 2.21) is turned on and the flow reads approximately 30CCM. For a calibration gas, set the gas regulator on top of the cylinder to 10psi and the flow regulator to 30CCM (Figure C.6 (a)). Figure C.6 (b) is an actual picture of the gas line configuration on the back of the GC that is drawn in Figure 2.22. In order to inject a sample, change the direction of the two-way valve (Figure C.6 (b)) to either the FIBOR gas (during an experiment) or the calibration gas.

(a)

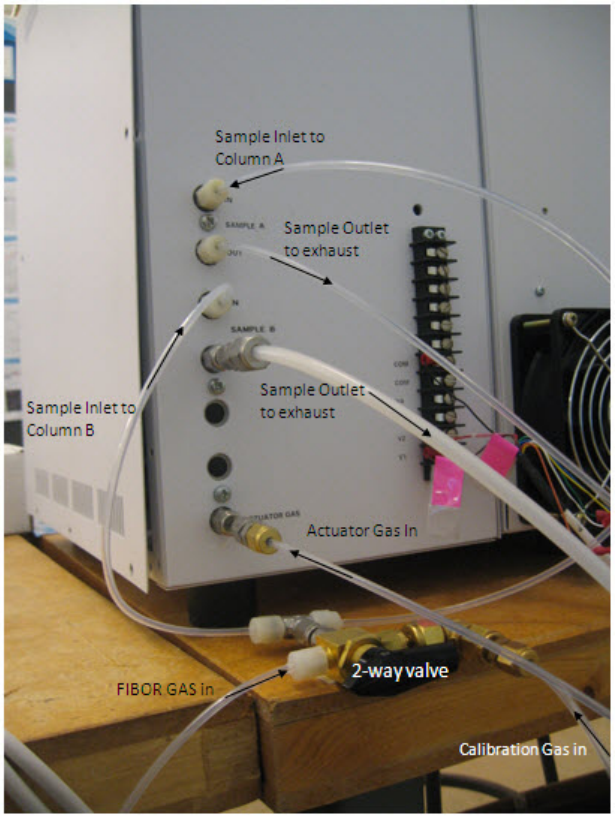

(b)

Figure C.6: (a) Calibration Gas Setup and (b) Back View of GC; Gas Line Configuration

o. Click the colored “Instrument Control” button in the Chrom Perfect status window. Press “Start Run” when ready to inject a sample. The first sample is injected into Column A. After five minutes, a second sample is injected automatically into column B. The chromatogram is automatically displayed and saved to the hard drive once the run is complete (after ~10min). It is important to not change any of the settings (power input) during an injection so that the conditions for the sample entering Column A are identical to the conditions for the sample entering Column B

OPTIONAL

The GC automatically heats the column oven to 60°C and the TCD to 95°C which is programmed into a method file (See Figure 2.23 (a) – Isothermal mode). There may be conditions where these settings should be changed such as overlapping detection peaks or insufficient retention time to detect a certain species. The general rule of thumb is that increasing the column temperature speeds up the retention time. However the TCD temperature must always be higher than the oven temperature. The Series 600 Gas Chromatograph User’s Manual (GOW-MAC, 2006) should always be reviewed prior to changing any settings on the GC or call GOW-MAC Technical Support (610-954-9000). To modify settings of the GC method press:

1) Edit>Chromatography Method 1>Do This
2) Select either Detector 1 or Column Oven by pressing the arrow key until it is next to it
3) Press “Do This”
4) Manually raise or lower the respective temperatures with up/down buttons
5) Press “Accept”
6) Press “Home”

C.4.2.5 Quenching Method and Data Collection

At this point in the experiment, an assistant is recommended. The heater temperature should first be raised to the reactant's saturation temperature (65°C for methanol and 197°C for ethylene glycol). For safety reasons, the first step is activating Nitrogen flow through the system:

a. Set Nitrogen flow to 10-20psi and ~0.1LPM

b. To start the data acquisition, follow the same steps in Section C.4.2.2.

c. Electrically heat the tube to at least 197°C by increasing the voltage in increments of 0.1V

d. Open the bulk feedstock reservoir valve (Figure C.7 (a)). The peristaltic pump is not necessary when using methanol and ethylene glycol because the viscosity is low enough to allow sufficient flow as a result of gravity alone. Processing more viscous liquids however such as glycerol require additional pumping.

e. Figure C.7 (b) is a picture of liquid lines and valves that control flow in and out of the FIBOR chamber. Heating tape is installed yet is unnecessary for methanol and ethylene glycol. This component is intended to enhance the flow of liquids with a sensitive viscosity dependence on temperature (e.g. glycerol). Ensure the 3-way valve (Figure C.7 (b)) is set to the appropriate direction. The two-way valve (Figure C.7 (b)) is now the means to control the level of the bulk liquid reactant. Ensure it is open.

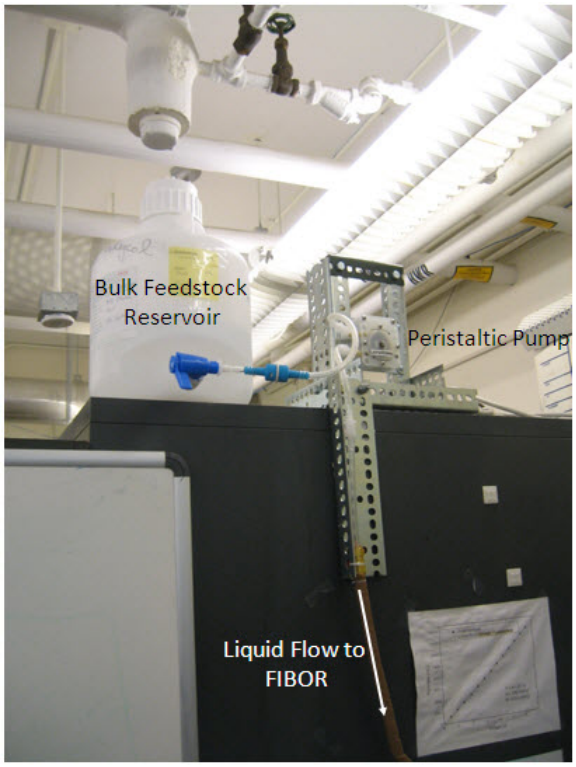

(a)

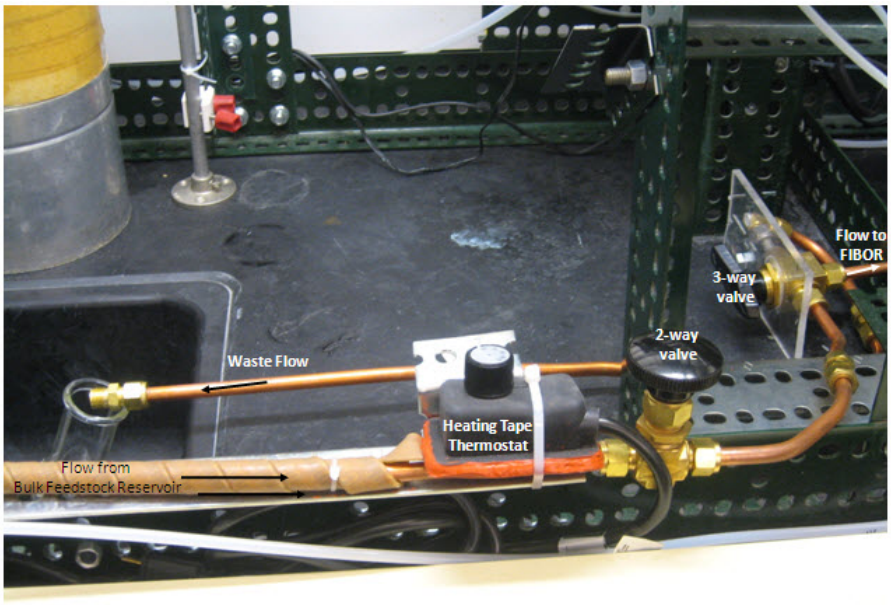

(b)

Figure C.7: (a) Bulk feedstock reservoir and (b) Liquid line configuration

f. Visually inspect as the bulk liquid reactant chamber is filled. Fill to the bottom of the wet-clamps and close the two way valve.

g. Turn on immersion heaters to maximum power.

h. Wait until liquid temperature reaches its saturation point. The bulk liquid reactant TC is the lowest on the LabVIEW TC display (Figure 2.17). The liquid should be visibly boiling when quenching the heater tube to prevent any heat losses to sub-cooling and stable achieve film boiling.

i. Heat the tube to a minimum of 873K (600ºC) for methanol or 1073K (800ºC) for ethylene glycol.

j. Bring the liquid level approximately 15mm below the heater tube (See Figure 2.27 (b)-A). Allow the bulk liquid to reach saturation.

k. For a bare tube, take voltage in step i and double it. For a catalyst coated tube, triple the voltage. Enter this voltage into LabVIEW, however DO NOT PRESS ENTER.

l. It is best to have the assistant control the two way valve. Slowly open the two way valve and closely monitor the temperature of the tube in LabVIEW. As soon as the temperature begins to drop (the liquid level is reaching the tube) the ENTER button is simultaneously pressed to either double the voltage (4x power) for the bare tube or triple the voltage for the catalyst tube (9x power). This technique has been experimentally proven to provide the necessary surge in heat to support film boiling

yet is not high enough to melt the tube. The additional heat for the catalyst coated tube is necessary to offset the heat that is consumed by the endothermic chemical reaction.

m. Once film boiling is achieved, traverse the film boiling curve by increasing/decreasing the voltage in increments of 0.02V. Between each increment allow approximately two minutes for the tube's temperature to reach steady state. A change of 0.02V changes the tube's temperature by approximately 10 degrees. Ensure the Nitrogen is TURNED OFF once film boiling is achieved to prevent erroneous (over-estimate) flow rate results.

C.4.2.6 Saving Data and Removing Heater From Liquid

Once the necessary amount of data has been acquired from the film boiling curve, the data must first be saved. The tube is then removed from the liquid in the reverse fashion of the quenching method. It is also recommended to have an assistant during this part of the experiment.

a. Stop the experiment at a temperature that is not at risk of film boiling collapsing. A temperature of 1173K (900ºC) is suitable. Press the two "stop" buttons on the LabVIEW interface (See Figure 2.17). This temporarily stops data from being stored however the power settings remain on.

b. Navigate to the hard drive (c:\experiment)

c. Locate six relevant data files: current.lvm, flowrates.lvm, POWER.lvm, TEMPERATURES.lvm, time.lvm and voltage.lvm. One at a time, right click, select

"open with," select "notepad," and save files into the folder created in step C.4.2.2.d above.

d. Once all files are saved, click the "run" arrow button in LabVIEW. The LabVIEW program resumes yet also erases all data in the files from the previous step (c:\experiment) and begins storing new data. It is therefore crucial that all data is verified to have saved properly in the separate folder established in C.4.2.2.d since it could easily be lost once the LabVIEW program resumes.

e. Enter a voltage of 1V into LabVIEW, however DO NOT PRESS "ENTER."

f. Turn off immersion heaters if they are on.

g. Open the Nitrogen feed line for safety.

h. Have the assistant place a waste beaker at the end of the waste line and change the direction of the 3-way valve so that the bulk liquid in the chamber begins to empty. See Figure C.7 (b). CAUTION: This liquid is scolding hot and protective gloves should be worn.

i. As soon as the bulk liquid level reaches the level of the heater tube, the temperature in LabVIEW will begin to rapidly rise. The temperature increases rapidly because the heat transfer coefficient is abruptly decreased in quiescent air compared to the conditions of film boiling. Simultaneously press "ENTER." This lowers the power input, and therefore the temperature of the heater tube. This prevents liquid from contacting the surface and also inadvertently melting the tube.

j. Gradually continue to decrease the temperature of the tube and safely dispose the waste liquid.

k. Safely shut down the experiment by following these remaining steps:

1) Shut Down LabVIEW program
2) Turn off power supply
3) Turn off DAQ
4) Shut down the GC by pressing Action>Shutdown on the keypad. The GC column oven must cool before safely turning the power off. The word "OFF" will be displayed in the top left corner of the keypad display when it is safe to power off. See Figure C.5 (a).
5) Turn off all gas flow (Nitrogen, Carrier, Actuator). Carrier gas must be turned off after TCD and oven temperature cool down to avoid the TCD filament burnout.
6) Allow dry ice to evaporate before removing condensers (allow 24 hours)
7) Ensure bulk feedstock reservoir valve is closed.

APPENDIX D

LabVIEW PROGRAM FOR EXPERIMENTS

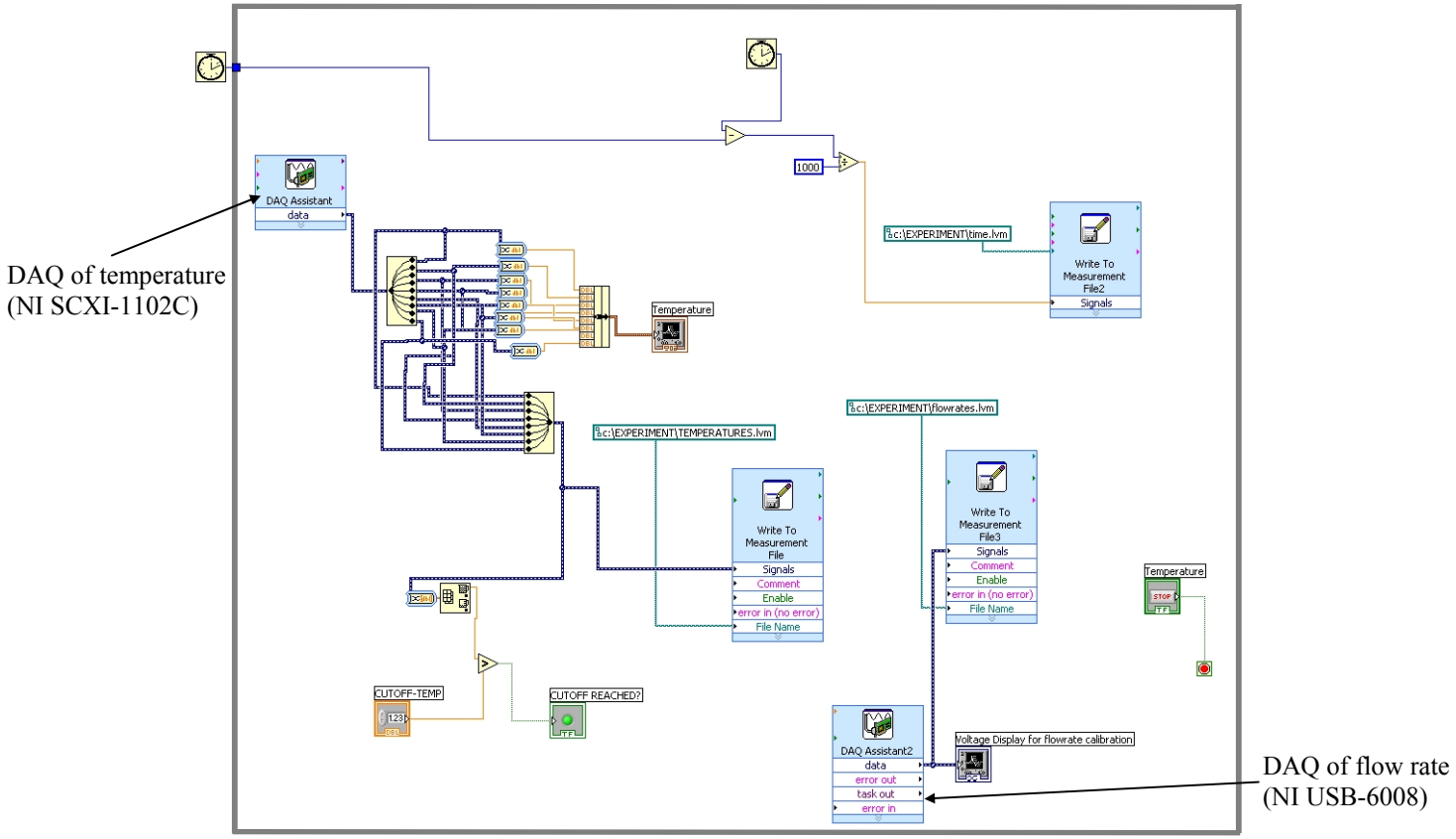

Figure D.1 Block diagram for temperature and flow rate measurement

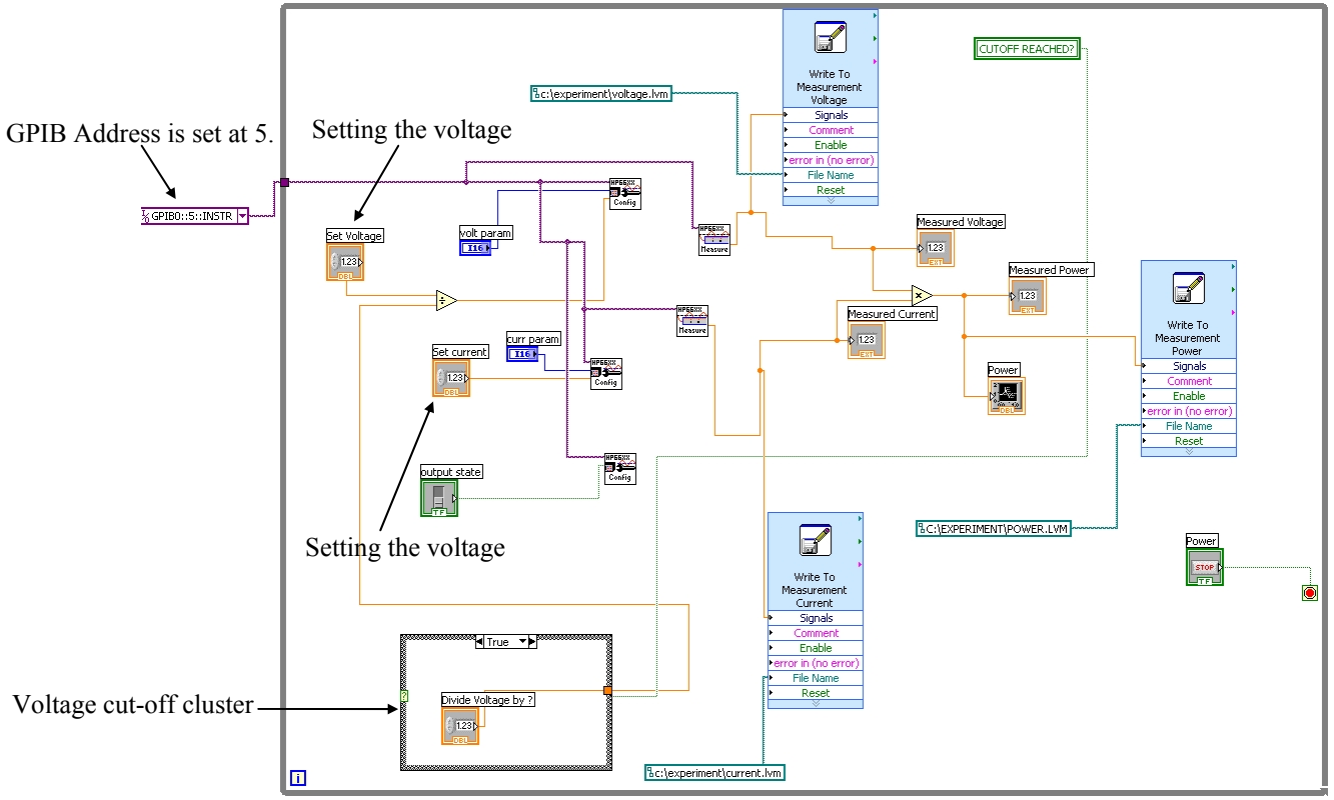

Figure D.2 Block diagram for voltage and current control

APPENDIX E

DATA ORGANIZATION AND ANALYSIS

The raw data collected during the experiments is used to generate three figures that, with further analysis, can measure the extent of chemical conversion in the FIBOR: the volumetric flow rate of product species with respect to wall temperature, or the "flow rate curve"; the applied heat flux with respect to wall temperature, or the so-called "boiling curve" (see Figure 1.1) which depicts the operational domain of the FIBOR and also provides insight into the chemical mechanism's endothermicity; and the chromatogram which is a result of GC analysis.

The chromatogram's peaks reveal the presence of individual chemical species, and the integrated area under the peak is related to its concentration. Chromatograms generated from analyzing a FIBOR gas sample are compared to chromatograms from a calibration gas sample. This analysis serves to verify both the presence and concentration of individual species in the FIBOR gas stream.

The organization and analysis of raw data requires significant computation in Matlab and Excel, advanced data plotting and statistical analysis in OriginPro and chromatogram analysis with the ChromPerfect software. The remainder of this section describes the detailed steps of organizing raw data and analyzing the extent that the FIBOR can promote chemical conversion.

E.1 Data Organization (Correlating Temperature and Power Time Scales)

The time increments over which temperature, flow rate data and power setting data are obtained are different. Temperature and flow rate data are acquired and stored simultaneously with corresponding time data approximately every 0.01 seconds (100Hz). Power data (voltage, current and power) however is stored at a different

time interval of approximately every 0.13 seconds due to different DAQ sampling rates: the NI temperature and flow rate DAQs provide 100Hz sampling rates while the Agilent USB-GPIB provides 7.7Hz. A common time scale synchronizing temperature, flow rate and power setting data must be found.

Raw data files (TEMPERATURES.lvm, time.lvm, flowrates.lvm, voltage.lvm, POWER.lvm and current.lvm) are stored on the workstation PC and saved to a separate folder after an experiment. (See Appendix C.4.2.6) Data files are first opened with Notepad++ software then copied into OriginPro 7. Notepad++ is useful because of its capability to handle large volumes of data that can be conveniently selected, copied and pasted. OriginPro is also used because of its ability to handle large volumes of data, yet also provides advanced plotting and statistical analysis tools.

Data organization starts with plotting raw temperature (TEMPERATURES.lvm) data versus time (time.lvm) data and power data vs. row number. The following steps cover inserting row number data along with steps to create general plots in OriginPro:

1) right click raw data (.lvm) file and select “edit with Notepad++”;
2) right click column, select “select all,” right click again and select “copy”;
3) open OriginPro, right click the first cell of desired column to place data in, and select “paste”;
4) to create a new column, right click the top of the column (gray cell) and select “insert” (a new column is created to the right of the column selected);
5) before plotting data, ensure the respective column is designated as “X” for x-axis and “Y” for y-axis by double clicking the top of the column (gray cell);
6) select the columns by clicking the top of the column (gray cell), right click, then select plot (several options are given e.g. line, scatter etc.);

7) to create row number data, select the cell after the last corresponding data point, right click and select "Set as End";
8) select the entire column, right click and select "Fill Column with Row Numbers".

Figure E.1 is a sample data set that shows raw power versus row number (a) and temperature data plotted against time (b). In order to create a corresponding time scale for the power data, known reference points (x_1, y_1, x_2, y_2) are identified. At this moment during the experiment, the power is instantaneously surged with a corresponding abrupt increase in temperature. With the four known points depicted in Figure E.1, the following two equations can be readily solved for the linear parameters, a and b, which further allows time data to be created from linear interpolation.

$$y_1 = ax_1 + b \quad \text{E.1}$$

$$y_2 = ax_2 + b \quad \text{E.2}$$

With a and b solved, time data are created through the computational Matlab code found in Appendix F.1 and further used to plot corresponding power setting data (power, current and voltage).

E.2 Boiling Curve

a. Radial and axial heat fluxes (q_r'' and q_x'')

The heat flux depicted by the boiling curve for the case of a cylindrical FIBOR represents heat transfer via radial conduction from the heater surface into the vapor film. Figure E.2 is a drawing (not to scale) that shows the various heat transfer paths. The black bold dotted line of Figure E.2 (a) represents the control volume used for an energy balance analysis to calculate the heat flux. Also shown is a cross sectional

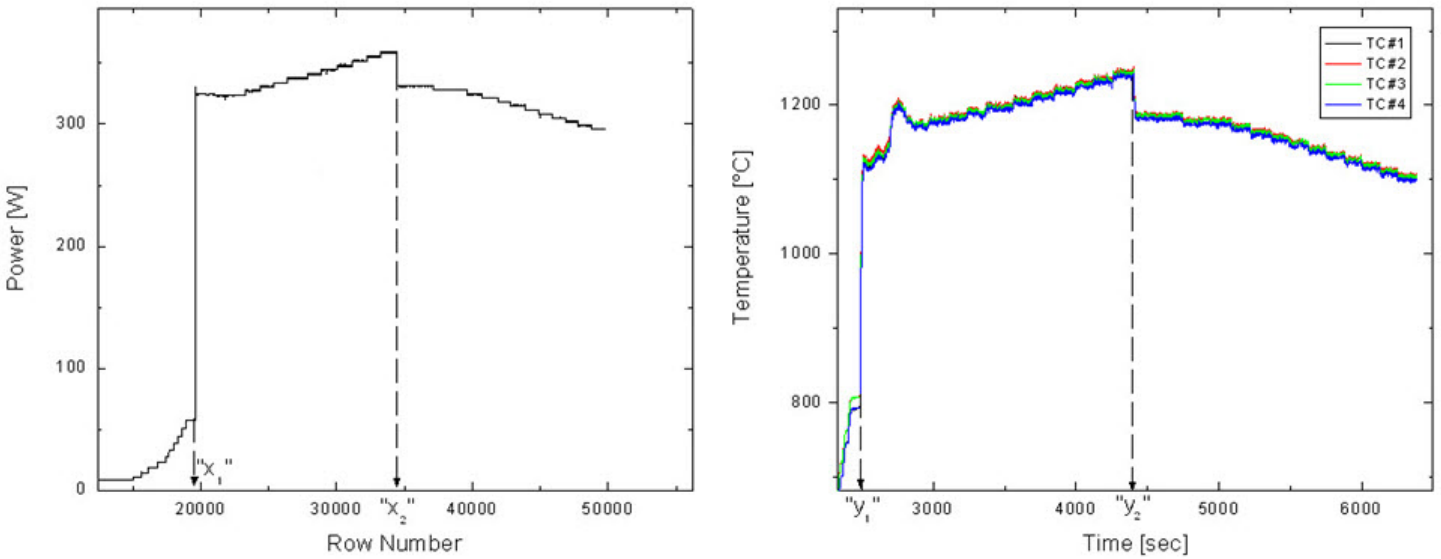

(a) (b)

Figure E.1: Correlating (a) Temperature and (b) Power Time Scales

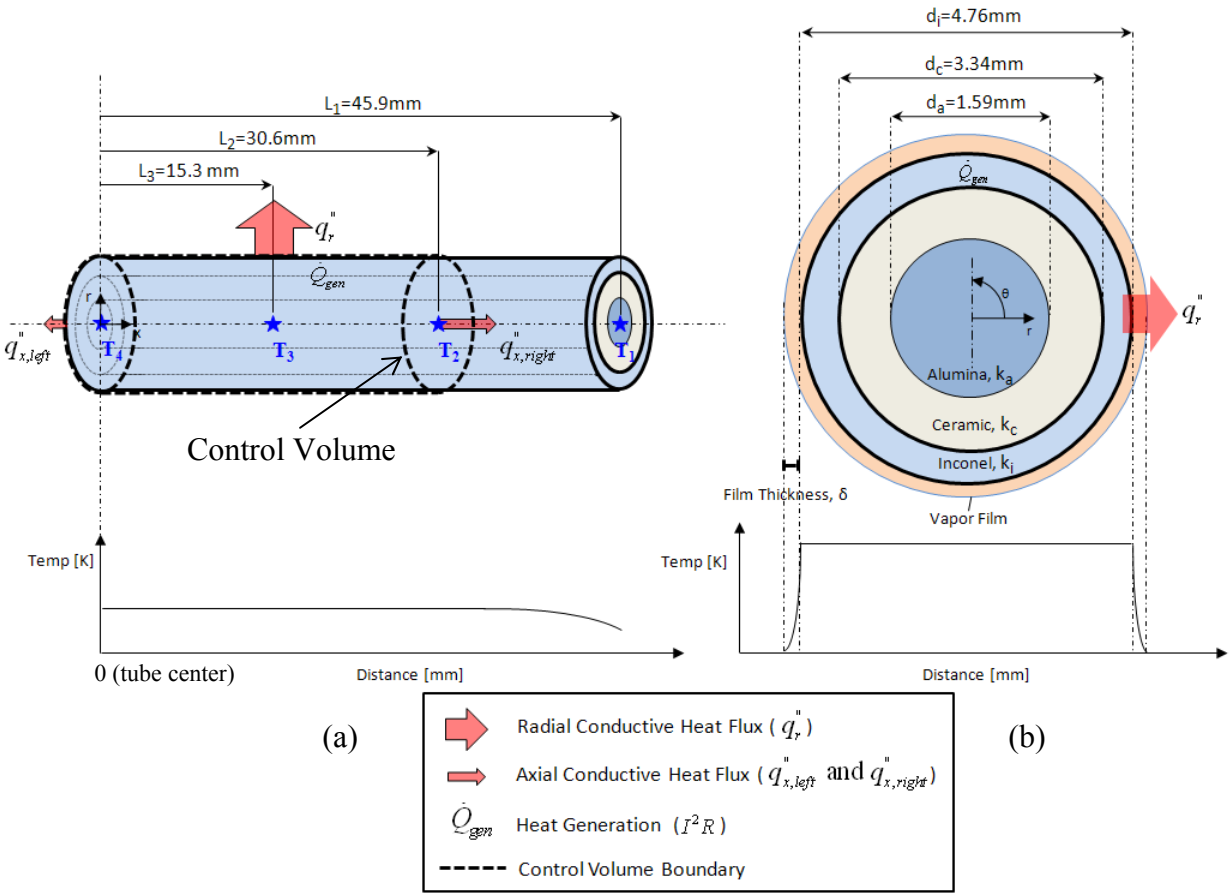

Figure E.2: Energy balance to calculate radial heat flux

view (right). Below each drawing is a qualitative sketch of the temperature profile. Through scale analysis (or even inspection), one can determine that axial conduction is much smaller, even negligible, compared to radial conduction for temperature distributions like those shown in Figure E.2. The problem of determining the heat flux could therefore be simplified significantly by just dividing the power input (measured and recorded by the power supply) by the heater surface area. We proceed however with a more rigorous treatment of the problem, considering both axial and radial conduction.

In order to make the boiling curve data as accurate as possible, the radial heat flux is found through an energy balance which considers axial conduction. Analysis starts with a steady state energy balance on the control volume over T.C.2 to T.C.4 over which the temperature is uniform (see Figure 2.4 (b))

$$\dot{Q}_{gen} = \dot{Q}_r + \dot{Q}_{x,left} + \dot{Q}_{x,right} \tag{E.3}$$

where $\dot{Q}_{gen}$, $\dot{Q}_r$, $\dot{Q}_{x,left}$ and $\dot{Q}_{x,right}$ represent the rate of heat generation, radial heat transfer, leftward and rightward axial heat transfers respectively.

Inserting the geometric parameters in Figure E.2,

$$\dot{Q}_{gen} = q_r^{"}\pi d_i L_2 + \frac{\pi d_i^2}{4}\left(q_{x,left}^{"} + q_{x,right}^{"}\right) \tag{E.4}$$

where L_2 is the distance from T.C.2 to T.C.4 and d_i is the heater's outer diameter.

The heat generated by the heater is

$$\begin{aligned}\dot{Q}_{gen} &= I^2 R \\ &= I^2 \rho \frac{4L_2}{\pi\left(d_i^2 - d_c^2\right)}\end{aligned} \tag{E.5}$$

where I is the experimentally measured current and ρ is Inconel's electrical resistivity which is a function of temperature.

By invoking Fourier's Law of heat conduction and considering the temperature reading of each thermocouple, T_2-T_4 (See Figure 2.34),

$$q''_{x,left} = k\frac{dT}{dx} \simeq k\left(\frac{T_3 - T_4}{L_3}\right) \quad \text{E.6}$$

$$q''_{x,right} = k\frac{dT}{dx} \simeq k\left(\frac{T_3 - T_2}{L_3}\right) \quad \text{E.7}$$

along with each material cross section and substituting Equations E.5-E.7, Eq. E.4 becomes,

$$\frac{4\rho L_2 I^2}{\pi\left(d_i^2 - d_c^2\right)} = q''_r \pi d_i L_2 + \pi\left[k_i\left(d_i^2 - d_c^2\right) + k_c\left(d_c^2 - d_a^2\right) + k_a d_a^2\right]\left(\frac{T_3 - T_4}{L_3} + \frac{T_3 - T_2}{L_3}\right) \quad \text{E.8}$$

where d_a and d_c are the outer diameters of the alumina space and the ceramic tube respectively, and $L_2 = 2L_3$ (See Figure E.2).

Simplifying and solving for q''_r gives

$$q''_r = \frac{4\rho I^2}{\pi^2 d_i\left(d_i^2 - d_c^2\right)} - \frac{\left[k_i\left(d_i^2 - d_c^2\right) + k_c\left(d_c^2 - d_a^2\right) + k_a d_a^2\right](2T_3 - T_2 - T_4)}{2d_i {L_3}^2} \quad \text{E.9}$$

The heat flux for the boiling curve can now readily be solved. All information on the right hand side of Equation E.9 is known. The current (I) and corresponding temperatures (T_2-T_4) are raw data outputs retrieved from the experiment (See Appendix E.1, TEMPERAURES.lvm and current.lvm). The geometry (d_i, d_c, d_a, L_3)

is of course known and remains unchanged for each experiment. The resistivity (ρ) however is dependent on temperature. A 6th order polynomial is used to determine the resistivity which is based on material data for Inonel 600 (see Table 2.2 or Figure 2.9, Special Metals, 2008),

$$\rho(T) = 0.4763 + 5.27E(-3)T - 1.95E(-5)T^2 + 3.56E(-8)T^3 \\ -3.23E(-11)*T^4 + 1.35E(-14)T^5 - 1.89E(-18)T^6 \quad \text{E.10}$$

where the temperature (T) is the average of T_2-T_4 [K]. The heat flux (E.9) is plotted versus the average wall temperature (T_2-T_4) to attain the boiling curve. Appendix F.4 provides details regarding the computation of the boiling curve using Excel software.

It turns out that the added complexity of considering axial conduction losses (the second term on the right hand side of Eq. E.9) could be actually neglected for the thermocouple spacing and data used in this study which on average accounts for just under 0.2% of the total heat flux (See Appendix F.4). That is,

$$q_r'' \gg q_{x,left}'' \quad \text{and} \quad q_r'' \gg q_{x,right}'' \quad \text{E.11}$$

This fact can be also confirmed simply by scale analysis.

b. Radial and axial temperature distributions

At steady state, the temperature within the heater assembly (r < 3.34mm, ceramic insert and alumina) is uniform in the radial direction as shown by Figure E.2 (b). This can be readily shown by solving the Laplace equation (2.45) which applies to a steady-state situation without heat sources.

$$\nabla^2 T = 0 \quad \text{E.12}$$

In cylindrical coordinates, Eq. E.12 can be expressed as

$$\frac{1}{r}\frac{\partial}{\partial r}\left(r\frac{\partial T}{\partial r}\right)+\frac{1}{r^2}\frac{\partial^2 T}{\partial \theta^2}+\frac{\partial^2 T}{\partial x^2}=0 \qquad \text{E.13}$$

The second and third terms are zero because the angular change doesn't exist and the axial heat conduction is much smaller than the radial heat conduction as proved above. Thus,

$$\frac{1}{r}\frac{\partial}{\partial r}\left(r\frac{\partial T}{\partial r}\right)=0 \qquad \text{E.14}$$

After integrating, the general solution is

$$T(r)=C_1\ln r+C_2 \qquad \text{E.15}$$

At r = 0, the solution must be bounded. Therefore $C_1 = 0$ and the temperature in the radial direction inside of the heater tube is shown to be constant. Furthermore, the temperature across the heater material (Inconel) in the radial direction can be proved to be almost constant due to Inconel's high thermal conductivity (23.9 W/m·K) and considerably thin tube's thickness (0.71×10^{-3} mm) even though there is energy generation. Therefore, the temperature reading monitored by the thermocouple inside of the heater assembly can be considered to be a reasonable measurement of the actual surface temperature.

E.3 GC Analysis Procedure

Chromatograms are automatically saved (see Appendix C.3) and are analyzed using Chrom Perfect software. The Chrom Perfect compares experimental chromatograms with a calibration chromatogram in order to determine the actual species and their concentrations. The residence time for each species is proportional to its molecular weight so that peaks appear in the order from lightest to heaviest.

Since the composition of the calibration is known, each species can be readily identified based on the order they appear and their respective molecular weight. When comparing to experimental chromatograms, overlapping peaks allow the identification of individual species.

Determining the specie concentrations however is more complex since integration of the peaks is required. Chrom Perfect software is able to perform this integration and compare the integrating results with that of the calibration chromatograms, and then reports the final composition results. For calibration in methanol, a gas mixture of 33.34% CO and 66.66% H_2 (Airgas Inc., with the uncertainty of +/- 1.0%) was selected. This calibration gas was also used to calibrate the flow meter. This mixture concentration was chosen as a "guess" of the actual composition based on methanol decomposition (Equation 1.1). On the other hand, a self-mixed calibration gas composed of 11.11% CO, 22.22% H_2, 33.33% CH_4, 0.17% C_2H_2, 33.17% C_2H_4 was used to analyze the product gases for ethylene glycol. This calibration gas initially used for concentration analysis was not used for the product flow rates of ethylene glycol experiments in order to get accurate flow rate results.

- *Procedure to Create a Calibration File and Determine Product Gas Concentration*

    1) Acquire a chromatogram by analyzing a calibration gas sample in the same manner as analyzing an experimental sample (see Appendix C.3)

    2) Open raw data file created in the previous step with the Chrom Perfect software and select "Analysis" button (see Figure C.5 (b))

    3) Open a separate window by selecting the "File Editor" button (See Figure C.5 (b))

4) Select “New Calibration File” and the blank file will appear as shown in Figure E.3.

5) Activate the “Analysis” window and right click on the GC trace. Select “peak properties.” Click anywhere on the first peak (H_2) and a window will appear with information related to the peak (See Figure E.4)

6) Activate the “New Calibration File” window and fill in the name (e.g. H2), retention time (“retention time” value from peak properties), window width (“width” from peak properties), level 1 amount (actual concentration), and level 1 response (“area” from peak properties).

7) Repeat the previous step for each peak by selecting “insert comp.” The final result for the calibration file should look like Figure E.5. Name and save the file.

8) Open an experimental chromatogram of interest by selecting “Analysis” (see Figure C.5 (b)) and open the raw data file of interest. Select file>Calibration. Navigate to the calibration file created in the previous step.

9) Select Report>Fixed Long Form. Concentrations are displayed for each species (See example in Figure E.6) under the “Amt %” column.

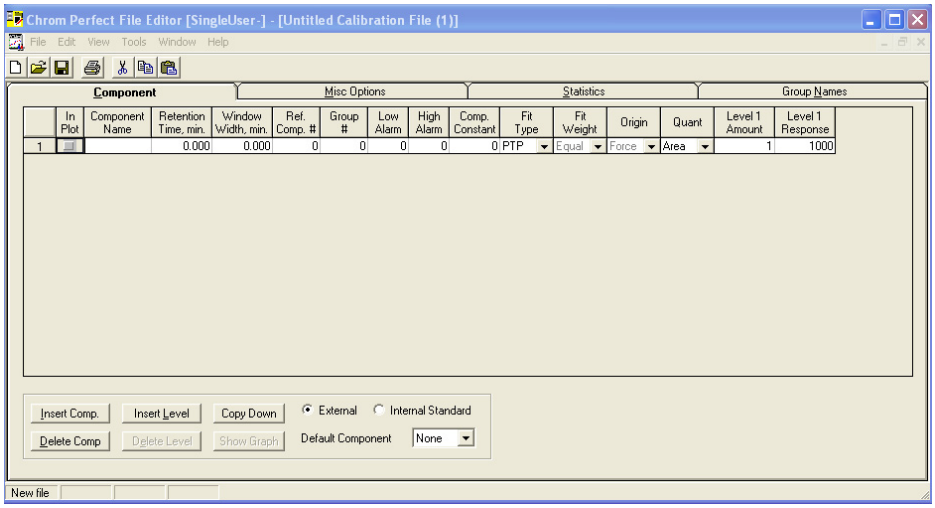

Figure E.3: New Calibration File

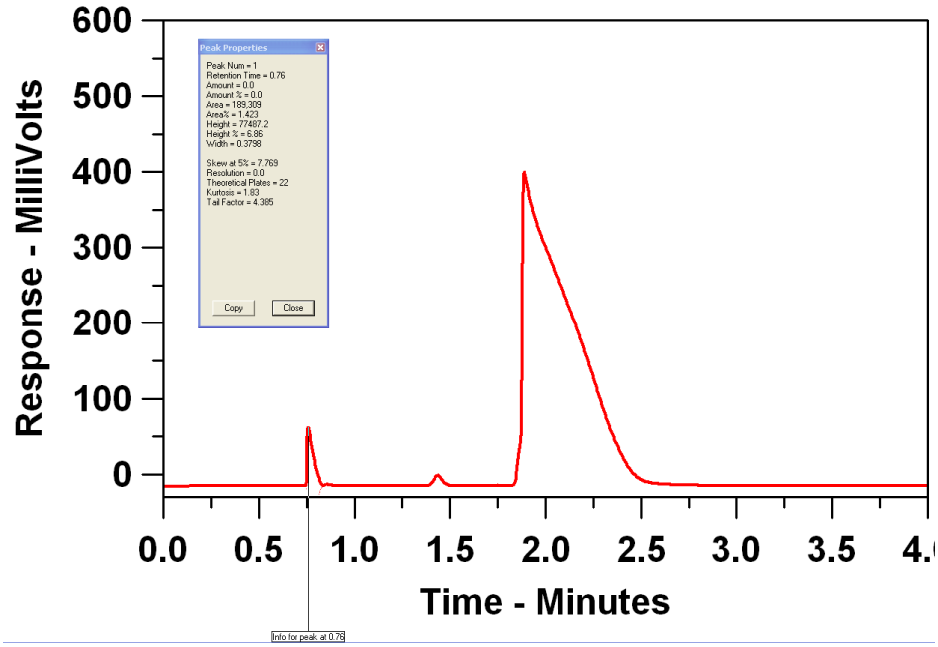

Figure E.4: Peak Properties

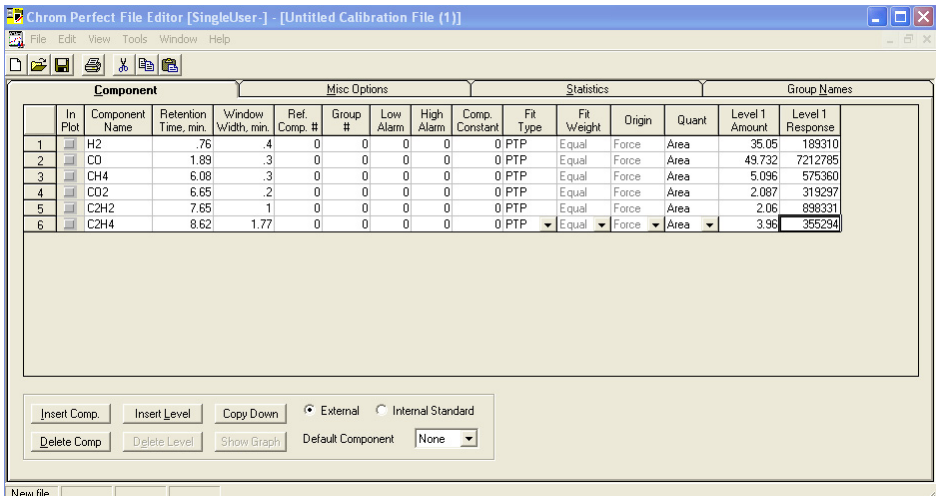

Figure E.5: Final Calibration File

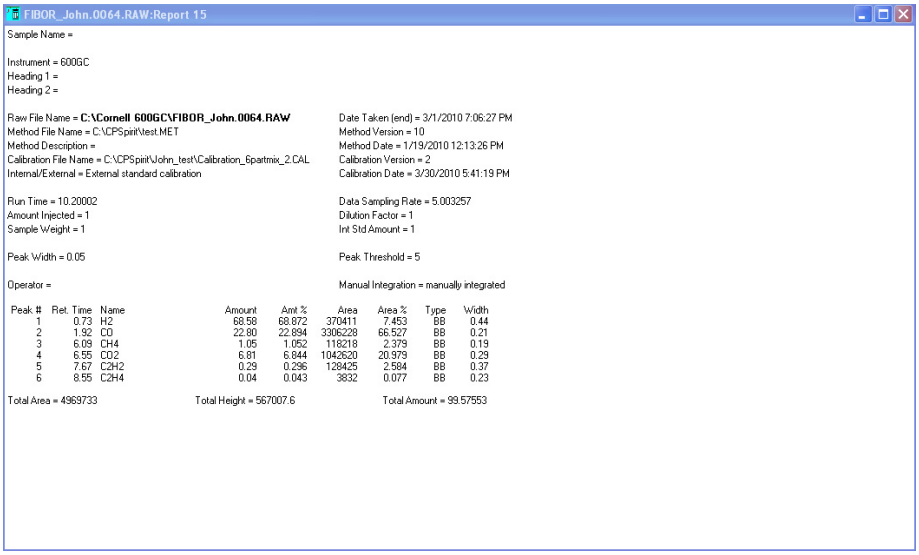

Figure E.6: Sample Composition Results Using a Calibration File

APPENDIX F

MATLAB CODES AND EXCEL FILE

FOR DATA ORGANIZATION AND ANALYSIS

F.1 Synchronizing Temperature and Power Data

With a and b solved from E.1 and E.2 in Appendix E, synchronized time data are created through this computational Matlab code and further used to plot corresponding power setting data (power, current and voltage). See Appendix E.1 for detail.

```
%Orignal Matlab Code Written by Sung Ryel Choi, Cornell University
2010
%Modified by John Evangelista,Cornell University 2010
%Computes:
%time data for corresponding power data points through linear
interpolation

i=1; %initialize counter
a=0.1284; %linear parameter solved by Equations E.1 and E.2
b=117.48; %linear parameter solved by Equations E.1 and E.2

%Establish empty column, number of rows must match the rows of power
data
TimeG = zeros(183535,1);
%Fill column with linearly interpolated time data
while i <= 183535
    TimeG(i,1) = a*i+b;
    i = i + 1;
end
TimeG;

%Write column data to file in working directory to be retrieved for
%plotting power setting data (power, current, voltage)
dlmwrite('TimeG.txt',TimeG)
```

F.2 Calibrate and Normalize Flow Rate Data

A flow rate curve (flow rate vs. wall temperature) can be generated from raw data files. The raw data files (TEMPERATURES.lvm, flowrates.lvm and time.lvm) are first copied and pasted into the Matlab working directory. This Matlab code is then run to retrieve the actual flow rate data normalized by the heater surface area. It is convenient to first plot the flow rate versus time in order to easily identify the portion of data to be analyzed. For example, data that is recorded before immersion and when the nitrogen supply is turned on should be neglected.

```
%Orignal Matlab Code Written by Sung Ryel Choi, Cornell
University2010
%Modified by John Evangelista,Cornell University 2010
%Computes:
%actual flow rate normalized by heater surface area

TEMP = dlmread('TEMPERATURES.lvm','\t'); %read in raw temp column
data
flowrates = dlmread('flowrates.lvm'); %read in raw flowrate column
data
time = dlmread('time.lvm'); %read in time data
d=.00476; %Heater tube outside diameter, meters
l=.0918; %Heater tube length, where reaction occurs, meters
i=1; %initialize counter

%Establish empty column, number of rows must match the rows of time
data
CFR_real= zeros(720731,1);
%Fill column with actual flow rate normalized by heater surface area
while i <= 720731
    FS = flowrates(i,1);
    % calibration & compensation of omega flow meter L/min/m^2*10^-3
    CFR_real(i,1) = (2352.84813*FS-
169.95803+94)/(3.14159265*d*l*1000000); % flow rate calibration
equation such as Eq.2.2 to 2.4
    i = i + 1;
end
CFR_real;
%Write column data to file in working directory to be retrieved for
%plotting flow rate curve
dlmwrite('CFR_real.txt',CFR_real)
```

F.3 Average Thermocouple Temperature and Convert to Kelvin

Temperature data is averaged based on the assumption of a constant axial temperature (Figure 2.4) and converted to Kelvin with this Matlab code. The raw data files (TEMPERATURES.lvm) are first copied and pasted into the Matlab working directory. The resulting exported flow rate in Appendix F.2 and average temperature data is then plotted to generate the flow rate curve.

```
%Orignal Matlab Code Written by Sung Ryel Choi,
%Modified by John Evangelista,Cornell University 2010
%Computes:
%average heater tube thermocouple temperature and converts to Kelvin
scale
TEMP = dlmread('TEMPERATURES.lvm','\t'); %read in raw temp column
data

i=1; %initialize counter

%Establish empty column, number of rows must match the rows of time
data
TEMP_AVG = zeros(720731,1);

%Fill column with average temperature, Kelvin
while i <= 720731
    TEMPERATURE =
((TEMP(i,2)+273.15)+(TEMP(i,3)+273.15)+(TEMP(i,4)+273.15)+(TEMP(i,5)+
273.15))/4;
    TEMP_AVG(i,1) = TEMPERATURE;
    i = i + 1;
end
TEMP_AVG;

%Write column data to file in working directory to be retrieved for
%plotting flow rate curve
dlmwrite('TEMP_AVG_Kelvin.txt',TEMP_AVG)
```

F.4 Boiling Curve

The heat flux for the boiling curve is calculated by this Excel file. All information on the right hand side of Equation E.9 is given. The current (I) and corresponding temperatures (T_2-T_4) are raw data outputs retrieved from the experiment (See Appendix E.1, TEMPERAURES.lvm and current.lvm). The geometry (d_i, d_c, d_a, L) is of course known and remains unchanged for each experiment. The resistivity (ρ) however is dependent on temperature. A 6th order polynomial is used to determine the resistivity which is based on material data for Inonel 600 (see Table 2.2 or Figure 2.9, Special Metals, 2008),

	A	B	C	D	E	F	G	H
1	**Radial Heat Flux Calculatior**							
2	Heater outer diameter, di [m]					0.00476		
3	Ceramic insert outer diameter, dc [m]					0.00334		
4	Alumina packing space diameter, da [m]					0.00159		
5	Inconel 600 thermal conductivity, ki [W/m·K]					23.9		
6	Ceramic (Al2O3) thermal conductivity, kc [W/m·K]					18		
7	Alumina (Al2O3) thermal conductivity, ka [W/m·K]					18		
8	Length of a small segment, L3 [m]					0.0153		
9	Current[A]	Resistivity [m	T4 [°C]	T3 [°C]	T2 [°C]	T_avg [°C]	Radial Heat Flux (w/o Axial Conduction) [W/m^2]	Radial Heat Flux (w/ Axial Conduction) [W/m^2]
10	214.534	1.139562	885.492	884.704	873.545	881.247	387444.9217	386894.0661
11	217.896	1.14514552	900.53	899.25	888.47	896.0833	401641.8407	401137.2483
12	221.258	1.15069151	912.81	911.9	899.81	908.1733	416137.2832	415543.4576
13	224.46	1.15756543	924.93	923.79	913.78	920.8333	430827.3053	430356.1754
14	227.662	1.1666483	938.32	938.07	928.45	934.9467	446684.4132	446186.7258
15	230.7	1.177771	953.57	951.76	943.26	949.53	463058.4326	462703.0933
16	233.746	1.1889057	966.27	964.26	955.74	962.09	479861.0908	479515.3122
17	237.108	1.20190434	979.06	977.04	968.67	974.9233	499162.6392	498825.359
18	240.15	1.22010629	993.734	991.91	985.92	990.5213	519807.573	519586.296
19	244.473	1.3441268	1063.91	1063.07	1058.54	1061.84	593446.8077	593250.8133
20	247.675	1.38086981	1079.54	1078.76	1072.79	1077.03	625744.1998	625468.5329
21	250.717	1.42206727	1095.15	1091.88	1089.84	1092.29	660339.7762	660405.1076
22	247.675	1.39239143	1083.69	1081.98	1078.73	1081.467	630965.244	630883.4469
23	244.473	1.36020423	1069.92	1069.92	1066.25	1068.697	600545.1717	600350.2397

C10: Thermocouple #4, Raw Data from Experiment (TEMPERATURES.LVM)

D10: Thermocouple #3, Raw Data from Experiment (TEMPERATURES.LVM)

E10: Thermocouple #2, Raw Data from Experiment (TEMPERATURES.LVM)

F10: Average wall temperature = (C10+D10+E10)/3

G10: Radial heat flux (w/o Axial conduction)

=4*(A10)^2*B10*10^(-6)/(3.14159^2*F2*(F2^2-F3^2))

H10: Radial heat flux (w/o Axial conduction)

=4*(A10)^2*B10*10^(-6)/(3.14159^2*F2*(F2^2-F3^2))-(2*D10-C10-E10)*((F2^2-F3^2)*F5+ (F3^2-F4^2)*F6+F4^2*F7)/(2*F2*F8^2)

→ Column H (Heat Flux [W/m^2], y-axis) is plotted with respect to Column F (Average Wall Temperature [°C], x-axis) to attain the boiling curve.

F.5 Conversion Calculations

F.5.1 Methanol Conversion

A main scrip file 'Frame.m' calls the two function files of 'HeatRXN.m' and 'Qbalance.m'. Then 'HeatRXN.m' calls the sub-function files of 'HeatCapCO.m', 'HeatCapH2.m', 'HeatCapCH4.m' and 'HeatCapMe.m' to calculate the heat of reaction of methanol decomposition. On the other hand, 'Qbalance.m' calls 'Qe.m', 'Qsens.m', 'Qr.m' and 'Qconv.m' to balance the heat transfer terms in Eq. 3.7.

a. Catalytic Reaction (CT#1)

Frame.m

```
%Main scrip to get Conversion (X) and the rates of heat in Eq.3.7 for
methanol
%Orignal Matlab Code Written by Sung Ryel Choi, Cornell University
2010

global Tw Tinf Power Np

n=83; %the number of data nodes

% Import input variables
Twall=load('Twall.txt'); %Wall temperature [K]
Tinfinite=load('Tinfinite.txt'); %Bulk temperature [K]
PowerQ=load('Power.txt'); %Total supplied power [W]
Productrate=load('Productrate.txt');  %Product molar flowrate
[mol/sec]

global hfg coeff Tavg Tsat A h hrxn

% Initialize output variables
Conversion=zeros(n,1); %Conversion
QEvap=zeros(n,1); %Heat for evaporation [J/sec]
QSens=zeros(n,1); %Sensible heat [J/sec]
QRxn=zeros(n,1); %Heat fot chemical reaction [J/sec]
QConv=zeros(n,1); %Convective heat [J/sec]
TotalQ=zeros(n,1); %Total Heat

for i=1:n
    Tw=Twall(i); %Wall temperature [K]
    Tinf=Tinfinite(i); %Bulk temperature [K]
    Power=PowerQ(i); %Total power [W]
    Np=Productrate(i); %Product molar flowrate [mol/sec]
```

```
hfg=35255; %heat of vaporiztion of methanol
[J/mol](1100[J/g]*32.05[g/mol])
coeff=2.6734; %chemical reaction coefficient for methanol
decomposition reaction
% Cpr=61.43; %Heat capacity of reactant [J/mol/K](@100~223 degC)
% Cpp=28.93; %Heat capacity of product [J/mol/K] (H2 and CO average)
Tsat=337.8; %Saturation temperature of methanol [K]
Tavg=(Tw+Tsat)/2;
%hrxn=90600; %heat of reaction (methanol decomposition)[J/mol]
hrxn=HeatRXN; %heat of reaction (methanol decomposition): Function of
temperature [J/mol]
d=0.00476; %heater diameter [m]
L=0.09205; %heater length [m]
A=d*pi*L; %Surface area [m^2]
k=0.193; %liquid thermal conductivity of methanoal[W/m/K]@Tsat(=
about 50 degC)"C.F. Beaton"
g=9.8; %gravity constant[m/sec^2]
beta=0.42*10^(-3); %expansion coefficient of liquid methanol
[1/K]@Tsat "C.F. Beaton"
mu=39.6*10^(-5); %dynamic viscosity [Pa*Sec] @Tsat(= about 50
degC)"C.F. Beaton"
roh=765; %density of liquid methanol [kg/m^3] @Tsat(= about 50 degC)
v=mu/roh;  %5.18*10^(-7); %kinematic viscosity of liquid methanol
[m^2/sec] @Tsat(= about 50 degC)
Cp=2680; %heat capacity of liquid methanol [J/kg/K] @Tsat(= about 50
degC)
alpha=k/(roh*Cp); %thermal diffusivity of liquid methnoal [m^2/sec]
Ra=g*beta*(Tsat-Tinf)*(d^3)/(v*alpha); %Rayleigh number
Pr=v/alpha; %Prandtl number

       if Ra>=10^12
         fprintf('Ra is over range')
          break
       end

Nu=(0.6+(0.387*Ra^(1/6))/((1+(0.559/Pr)^(9/16))^(8/27)))^2; % Nusselt
number
h=k*Nu/d; %Convective heat transfer coefficient


x=fzero('Qbalance',1);  %Nonlinear algebraic equation's solution <--
Energy Balance (Eq.3.7)
Nr1=x; % Molar flow rate of reactant drawn into FIBOR

Conversion(i,1)=(Np/coeff)/Nr1;
QEvap(i,1)=Qe(Nr1);
QSens(i,1)=Qsens(Nr1);
QRxn(i,1)=Qr;
QConv(i,1)=Qconv;
TotalQ(i,1)=Qe(Nr1)+Qsens(Nr1)+Qr+Qconv;

end

dlmwrite('Conversion.txt',Conversion)
```

```
dlmwrite('QEvap.txt',QEvap)
dlmwrite('QSens.txt',QSens)
dlmwrite('QRxn.txt',QRxn)
dlmwrite('QConv.txt',QConv)
dlmwrite('TotalQ.txt',TotalQ)
```

HeatRXN.m

```
%Heat of reaction of methanol decomposition: function of temperature
%Orignal Matlab Code Written by Sung Ryel Choi, Cornell University
2010
function hrxn=HeatRXN

global Tavg

Tr=298; %Reference Temperature[K] (25[degC])

hfMe=-200670; %Enthalpy of formation of Methanol(gas) @ 25degC & 1atm
[KJ/Kmol]
hfH2=0; %Enthalpy of formation of hydrogen @ 25degC & 1atm [KJ/Kmol]
hfCO=-110530; %Enthalpy of formation of carbon monoxide @ 25degC &
1atm [KJ/Kmol]
hfCH4=-74850; %Enthalpy of formation of Methane(gas) @ 25degC & 1atm
[KJ/Kmol]

SenHeatMe=quad('HeatCapMe',Tr,Tavg); %Sensible heat of Methanol
[J/mol]
SenHeatH2=quad('HeatCapH2',Tr,Tavg); %Sensible heat of Hydrogen
[J/mol]
SenHeatCO=quad('HeatCapCO',Tr,Tavg); %Sensible heat of CO [J/mol]
SenHeatCH4=quad('HeatCapCH4',Tr,Tavg); %Sensible heat of Methane
[J/mol]

hrxn=(1.6734.*hfH2+0.9175.*hfCO+0.0825.*hfCH4-
hfMe)+1.6734.*SenHeatH2+0.9175.*SenHeatCO+0.0825.*SenHeatCH4-
SenHeatMe;
```

HeatCapCO.m

```
%Heat capacity of of carbon monoxide [J/mol/K] (Temperature rage:
%273~1800[K])
%Orignal Matlab Code Written by Sung Ryel Choi, Cornell University
2010
function y=HeatCapCO(x)

a=28.16;
b=0.1675.*10.^(-2);
c=0.5372.*10.^(-5);
d=-2.222.*10.^(-9);

y=a+b.*x+c.*x.^2+d.*x.^3;
```

HeatCapH2.m

```
%Heat capacity of of hydrogen [J/mol/K] (Temperature rage:
273~1800[K])
%Orignal Matlab Code Written by Sung Ryel Choi, Cornell University
2010
function y=HeatCapH2(x)

a=29.11;
b=-0.1916.*10.^(-2);
c=0.4003.*10.^(-5);
d=-0.8704.*10.^(-9);

y=a+b.*x+c.*x.^2+d.*x.^3;
```

HeatCapCH4.m

```
%Heat capacity of of methane gas [J/mol/K] (Temperature rage:
273~1000[K])
%Orignal Matlab Code Written by Sung Ryel Choi, Cornell University
2010
function y=HeatCapCH4(x)

a=19.89;
b=5.024.*10.^(-2);
c=1.269.*10.^(-5);
d=-11.01.*10.^(-9);

y=a+b.*x+c.*x.^2+d.*x.^3;
```

HeatCapMe.m

```
%Heat capacity of of methanol gas [J/mol/K] (Temperature rage:
273~1000[K])
%Orignal Matlab Code Written by Sung Ryel Choi, Cornell University
2010
function y=HeatCapMe(x)

a=19;
b=9.152.*10.^(-2);
c=-1.22.*10.^(-5);
d=-8.039.*10.^(-9);

y=a+b.*x+c.*x.^2+d.*x.^3;
```

Qbalance.m

```
%Energy Balance of Eq.3.7 (function file)
%Orignal Matlab Code Written by Sung Ryel Choi, Cornell University
2010
function f=Qbalance(x)

global Power

f=Qe(x)+Qsens(x)+Qr+Qconv-Power;
```

Qe.m

```
%Heat of vaporization (latent heat)[J/sec]
%Orignal Matlab Code Written by Sung Ryel Choi, Cornell University
2010
function Qlatent=Qe(x)

global hfg

Qlatent=hfg*x;
```

Qsens.m

```
%Heat for temperature increase (sensible heat) [J/sec]
%Orignal Matlab Code Written by Sung Ryel Choi, Cornell University
2010
function Qsensible=Qsens(x)

global Tsat Tavg

Qsensible=(quad('HeatCapMe',Tsat,Tavg))*x;
```

Qr.m

```
%Heat for chemical reaction [J/sec]
%Orignal Matlab Code Written by Sung Ryel Choi, Cornell University
2010
function Qchemical=Qr

global hrxn Np coeff

Qchemical=hrxn*(Np/coeff);
```

Qconv.m

```
%Convective heat transfer(loss) into bulk liquid [J/sec]
%Orignal Matlab Code Written by Sung Ryel Choi, Cornell University
2010
function Qsubcool=Qconv
```

```
global A h Tinf Tsat

Qsubcool=A*h*(Tsat-Tinf);
```

b. Thermal decomposition (a bare tube)

Frame.m

```
%Main scrip to get Conversion (X) and the rates of heat in Eq.3.7 for
methanol
%Orignal Matlab Code Written by Sung Ryel Choi, Cornell University
2010

global Tw Tinf Power Np

n=82; %the number of data nodes

% Import input variables
Twall=load('Twall.txt'); %Wall temperature [K]
Tinfinite=load('Tinfinite.txt'); %Bulk temperature [K]
PowerQ=load('Power.txt'); %Total supplied power [W]
Productrate=load('Productrate.txt');  %Product molar flowrate
[mol/sec]

global hfg coeff Tavg Tsat A h hrxn

% Initialize output variables
Conversion=zeros(n,1); %Conversion
QEvap=zeros(n,1); %Heat for evaporation [J/sec]
QSens=zeros(n,1); %Sensible heat [J/sec]
QRxn=zeros(n,1); %Heat fot chemical reaction [J/sec]
QConv=zeros(n,1); %Convective heat [J/sec]
TotalQ=zeros(n,1); %Total Heat

for i=1:n
    Tw=Twall(i); %Wall temperature [K]
    Tinf=Tinfinite(i); %Bulk temperature [K]
    Power=PowerQ(i); %Total power [W]
    Np=Productrate(i); %Product molar flowrate [mol/sec]


hfg=35255; %heat of vaporiztion of methanol
[J/mol](1100[J/g]*32.05[g/mol])
coeff=3.2173; %chemical reaction coefficient for methanol
decomposition reaction
% Cpr=61.43; %Heat capacity of reactant [J/mol/K](@100~223 degC)
% Cpp=28.93; %Heat capacity of product [J/mol/K] (H2 and CO average)
Tsat=337.8; %Saturation temperature of methanol [K]
Tavg=(Tw+Tsat)/2;
%hrxn=90600; %heat of reaction (methanol decomposition)[J/mol]
```

```
hrxn=HeatRXN; %heat of reaction (methanol decomposition): Function of
temperature [J/mol]
d=0.00476; %heater diameter [m]
L=0.09205; %heater length [m]
A=d*pi*L; %Surface area [m^2]
k=0.193; %liquid thermal conductivity of methanoal[W/m/K]@Tsat(=
about 50 degC)"C.F. Beaton"
g=9.8; %gravity constant[m/sec^2]
beta=0.42*10^(-3); %expansion coefficient of liquid methanol
[1/K]@Tsat "C.F. Beaton"
mu=39.6*10^(-5); %dynamic viscosity [Pa*Sec] @Tsat(= about 50
degC)"C.F. Beaton"
roh=765; %density of liquid methanol [kg/m^3] @Tsat(= about 50 degC)
v=mu/roh;  %5.18*10^(-7); %kinematic viscosity of liquid methanol
[m^2/sec] @Tsat(= about 50 degC)
Cp=2680; %heat capacity of liquid methanol [J/kg/K] @Tsat(= about 50
degC)
alpha=k/(roh*Cp); %thermal diffusivity of liquid methnoal [m^2/sec]
Ra=g*beta*(Tsat-Tinf)*(d^3)/(v*alpha); %Rayleigh number
Pr=v/alpha; %Prandtl number

       if Ra>=10^12
         fprintf('Ra is over range')
          break
       end

Nu=(0.6+(0.387*Ra^(1/6))/((1+(0.559/Pr)^(9/16))^(8/27)))^2; % Nusselt
number
h=k*Nu/d; %Convective heat transfer coefficient


x=fzero('Qbalance',1);  %Nonlinear algebraic equation's solution <--
Energy Balance (Eq.3.7)
Nr1=x; % Molar flow rate of reactant drawn into FIBOR

Conversion(i,1)=(Np/coeff)/Nr1;
QEvap(i,1)=Qe(Nr1);
QSens(i,1)=Qsens(Nr1);
QRxn(i,1)=Qr;
QConv(i,1)=Qconv;
TotalQ(i,1)=Qe(Nr1)+Qsens(Nr1)+Qr+Qconv;

end

dlmwrite('Conversion.txt',Conversion)
dlmwrite('QEvap.txt',QEvap)
dlmwrite('QSens.txt',QSens)
dlmwrite('QRxn.txt',QRxn)
dlmwrite('QConv.txt',QConv)
dlmwrite('TotalQ.txt',TotalQ)
```

HeatRXN.m:

```
%Heat of reaction of methanol decomposition: function of temperature
%Orignal Matlab Code Written by Sung Ryel Choi, Cornell University
2010
function hrxn=HeatRXN

global Tavg

Tr=298; %Reference Temperature[K] (25[degC])

hfMe=-200670; %Enthalpy of formation of Methanol(gas) @ 25degC & 1atm
[KJ/Kmol]
hfH2=0; %Enthalpy of formation of hydrogen @ 25degC & 1atm [KJ/Kmol]
hfCO=-110530; %Enthalpy of formation of carbon monoxide @ 25degC &
1atm [KJ/Kmol]
hfCH4=-74850; %Enthalpy of formation of Methane(gas) @ 25degC & 1atm
[KJ/Kmol]

SenHeatMe=quad('HeatCapMe',Tr,Tavg); %Sensible heat of Methanol
[J/mol]
SenHeatH2=quad('HeatCapH2',Tr,Tavg); %Sensible heat of Hydrogen
[J/mol]
SenHeatCO=quad('HeatCapCO',Tr,Tavg); %Sensible heat of CO [J/mol]
SenHeatCH4=quad('HeatCapCH4',Tr,Tavg); %Sensible heat of Methane
[J/mol]

hrxn=(2.2173.*hfH2+0.9113.*hfCO+0.0887.*hfCH4-
hfMe)+2.2173.*SenHeatH2+0.9113.*SenHeatCO+0.0887.*SenHeatCH4-
SenHeatMe;
```

HeatCapCO.m: same as the Catalytic Reaction (CT#1) code

HeatCapH2.m: same as the Catalytic Reaction (CT#1) code

HeatCapCH4.m: same as the Catalytic Reaction (CT#1) code

HeatCapMe.m: same as the Catalytic Reaction (CT#1) code

Qbalance.m: same as the Catalytic Reaction (CT#1) code

Qe.m: same as the Catalytic Reaction (CT#1) code

Qsens.m: same as the Catalytic Reaction (CT#1) code

Qr.m: same as the Catalytic Reaction (CT#1) code

Qconv.m: same as the Catalytic Reaction (CT#1) code

F.5.2 Ethylene Glycol Conversion

A main scrip file 'Frame.m' calls the two function files of 'HeatRXN.m' and 'Qbalance.m'. Then 'HeatRXN.m' calls the sub-function files of 'HeatCapCO.m', 'HeatCapH2.m', 'HeatCapCH4.m', 'HeatCapC2H2.m', 'HeatCapC2H4.m' and 'HeatCapEG.m' to calculate the heat of reaction of ethylene glycol decomposition. On the other hand, 'Qbalance.m' calls 'Qe.m', 'Qsens.m', 'Qr.m' and 'Qconv.m' to balance the heat transfer terms in Eq. 3.7.

a. Catalytic Reaction (CT#2)

Frame.m

```
%Main scrip to get Conversion (X) and the rates of heat in Eq.3.7 for
ethylene glycol
%Orignal Matlab Code Written by Sung Ryel Choi, Cornell University
2010

global Tw Tinf Power Np

n=368; %the number of data nodes

% Import input variables
Twall=load('Twall.txt'); %Wall temperature [K]
Tinfinite=load('Tinfinite.txt'); %Bulk temperature [K]
PowerQ=load('Power.txt'); %Total supplied power [W]
Productrate=load('Productrate.txt');  %Product molar flowrate
[mol/sec]

global hfg coeff Tavg Tsat A h hrxn

% Initialize output variables
```

```
Conversion=zeros(n,1); %Conversion
QEvap=zeros(n,1); %Heat for evaporation [J/sec]
QSens=zeros(n,1); %Sensible heat [J/sec]
QRxn=zeros(n,1); %Heat fot chemical reaction [J/sec]
QConv=zeros(n,1); %Convective heat [J/sec]
TotalQ=zeros(n,1); %Total Heat

for i=1:n
    Tw=Twall(i); %Wall temperature [K]
    Tinf=Tinfinite(i); %Bulk temperature [K]
    Power=PowerQ(i); %Total power [W]
    Np=Productrate(i); %Product molar flowrate [mol/sec]


hfg=49661; %heat of vaporiztion of EG
[J/mol](800.1[J/g]*62.068[g/mol])
coeff=3.1750; %chemical reaction coefficient for EG decomposition
reaction

Tsat=470; %Saturation temperature of EG [K]
Tavg=(Tw+Tsat)/2;

hrxn=HeatRXN; %heat of reaction (EG decomposition): Function of
temperature [J/mol]
d=0.00476; %heater diameter [m]
L=0.09205; %heater length [m]
A=d*pi*L; %Surface area [m^2]
k=0.252; %liquid thermal conductivity of EG [W/m/K]@Tsat(= about 155
degC)
g=9.8; %gravity constant[m/sec^2]
beta=65*10^(-5); %expansion coefficient of liquid EG [1/K] Ref.
Incropera "Heat and Mass Transfer"
mu=85.9*10^(-5); %dynamic viscosity of liq EG [Pa*Sec] @Tsat(= about
155 degC) Ref. C.F. Beaton "Physical properties..."
roh=1016; %density of liquid EG [kg/m^3] @Tsat(= about 155 degC)
v=mu/roh;  %kinematic viscosity of liquid EG [m^2/sec] @Tsat(= about
155 degC)
Cp=2940; %heat capacity of liquid EG [J/kg/K] @Tsat(= about 155 degC)
alpha=k/(roh*Cp); %thermal diffusivity of liquid EG [m^2/sec]
Ra=g*beta*(Tsat-Tinf)*(d^3)/(v*alpha); %Rayleigh number
Pr=v/alpha; %Prandtl number

       if Ra>=10^12
         fprintf('Ra is over range')
          break
       end

Nu=(0.6+(0.387*Ra^(1/6))/((1+(0.559/Pr)^(9/16))^(8/27)))^2; % Nusselt
number
h=k*Nu/d; %Convective heat transfer coefficient

x=fzero('Qbalance',1);  %Nonlinear algebraic equation's solution  <--
Energy Balance (Eq.3.7)
Nr1=x; % Molar flow rate of reactant drawn into FIBOR
```

```
Conversion(i,1)=(Np/coeff)/Nr1;
QEvap(i,1)=Qe(Nr1);
QSens(i,1)=Qsens(Nr1);
QRxn(i,1)=Qr;
QConv(i,1)=Qconv;
TotalQ(i,1)=Qe(Nr1)+Qsens(Nr1)+Qr+Qconv;

end

dlmwrite('Conversion.txt',Conversion)
dlmwrite('QEvap.txt',QEvap)
dlmwrite('QSens.txt',QSens)
dlmwrite('QRxn.txt',QRxn)
dlmwrite('QConv.txt',QConv)
dlmwrite('TotalQ.txt',TotalQ)
```

HeatRXN.m

```
%Heat of reaction of ethylene glycol decomposition: function of
temperature
%Orignal Matlab Code Written by Sung Ryel Choi, Cornell University
2010
function hrxn=HeatRXN   %Heat of reaction: function of temperature

global Tavg

Tr=298; %Reference Temperature[K] (25[degC])

hfEG=-394400; %Enthalpy of formation of EG(gas) @ 25degC & 1atm
[KJ/Kmol]   Ref. Knauth and Sabbah, 1989
hfH2=0; %Enthalpy of formation of hydrogen @ 25degC & 1atm [KJ/Kmol]
hfCO=-110530; %Enthalpy of formation of carbon monoxide @ 25degC &
1atm [KJ/Kmol]
hfCH4=-74850; %Enthalpy of formation of methane @ 25degC & 1atm
[KJ/Kmol]
hfC2H2=226730; %Enthalpy of formation of acetylene @ 25degC & 1atm
[KJ/Kmol]
hfC2H4=52280; %Enthalpy of formation of ethylene @ 25degC & 1atm
[KJ/Kmol]

SenHeatEG=quad('HeatCapEG',Tr,Tavg); %Sensible heat of EG [J/mol]
SenHeatH2=quad('HeatCapH2',Tr,Tavg); %Sensible heat of Hydrogen
[J/mol]
SenHeatCO=quad('HeatCapCO',Tr,Tavg); %Sensible heat of CO [J/mol]
SenHeatCH4=quad('HeatCapCH4',Tr,Tavg); %Sensible heat of CH4 [J/mol]
SenHeatC2H2=quad('HeatCapC2H2',Tr,Tavg); %Sensible heat of C2H2
[J/mol]
SenHeatC2H4=quad('HeatCapC2H4',Tr,Tavg); %Sensible heat of C2H4
[J/mol]
```

```
hrxn=(1.3389.*hfH2+1.4236.*hfCO+0.2486.*hfCH4+0.0553.*hfC2H2+0.1086.*
hfC2H4-
hfEG)+1.3389.*SenHeatH2+1.4236.*SenHeatCO+0.2486.*SenHeatCH4+0.0553.*
SenHeatC2H2+0.1086.*SenHeatC2H4-SenHeatEG;
```

Qbalance.m: same as the Catalytic Reaction (CT#1) code

HeatCapCO.m: same as the Catalytic Reaction (CT#1) code

HeatCapH2.m: same as the Catalytic Reaction (CT#1) code

HeatCapCH4.m: same as the Catalytic Reaction (CT#1) code

HeatCapC2H2.m

```
%Heat capacity of of acetylene gas [J/mol/K] (Temperature rage:
273~1000[K])
%Orignal Matlab Code Written by Sung Ryel Choi, Cornell University
2010
function y=HeatCapC2H2(x)

a=21.8;
b=9.2143.*10.^(-2);
c=-6.527.*10.^(-5);
d=18.21.*10.^(-9);

y=a+b.*x+c.*x.^2+d.*x.^3;
```

HeatCapC2H4.m

```
%Heat capacity of of Ethylene gas [J/mol/K] (Temperature rage:
273~1000[K])
%Orignal Matlab Code Written by Sung Ryel Choi, Cornell University
2010
function y=HeatCapC2H4(x)

a=3.95;
b=15.64.*10.^(-2);
c=-8.344.*10.^(-5);
d=17.67.*10.^(-9);

y=a+b.*x+c.*x.^2+d.*x.^3;
```

HeatCapEG.m

```
%Heat capacity of of Ethylene Glycol gas [J/mol/K] (Temperature rage:
273~? [K]) Ref. Robert C. Reid "The properties of gases & liquids"
%Orignal Matlab Code Written by Sung Ryel Choi, Cornell University
2010
function y=HeatCapEG(x)

a=35.7;
b=24.83.*10.^(-2);
c=-14.97.*10.^(-5);
d=30.1.*10.^(-9);

y=a+b.*x+c.*x.^2+d.*x.^3;
```

Qe.m: same as the Catalytic Reaction (CT#1) code

Qsens.m

```
%Heat for temperature increase (sensible heat) [J/sec]
%Orignal Matlab Code Written by Sung Ryel Choi, Cornell University
2010
function Qsensible=Qsens(x)

global Tsat Tavg

Qsensible=(quad('HeatCapEG',Tsat,Tavg))*x;
```

Qr.m: same as the Catalytic Reaction (CT#1) code

Qconv.m: same as the Catalytic Reaction (CT#1) code

b. Thermal decomposition (a bare tube)

Frame.m

```
%Main scrip to get Conversion (X) and the rates of heat in Eq.3.7 for
ethylene glycol
%Orignal Matlab Code Written by Sung Ryel Choi, Cornell University
2010
```

```
global Tw Tinf Power Np

n=82; %the number of data nodes

% Import input variables
Twall=load('Twall.txt'); %Wall temperature [K]
Tinfinite=load('Tinfinite.txt'); %Bulk temperature [K]
PowerQ=load('Power.txt'); %Total supplied power [W]
Productrate=load('Productrate.txt');  %Product molar flowrate
[mol/sec]

global hfg coeff Tavg Tsat A h hrxn

% Initialize output variables
Conversion=zeros(n,1); %Conversion
QEvap=zeros(n,1); %Heat for evaporation [J/sec]
QSens=zeros(n,1); %Sensible heat [J/sec]
QRxn=zeros(n,1); %Heat fot chemical reaction [J/sec]
QConv=zeros(n,1); %Convective heat [J/sec]
TotalQ=zeros(n,1); %Total Heat

for i=1:n
    Tw=Twall(i); %Wall temperature [K]
    Tinf=Tinfinite(i); %Bulk temperature [K]
    Power=PowerQ(i); %Total power [W]
    Np=Productrate(i); %Product molar flowrate [mol/sec]


hfg=49661; %heat of vaporiztion of EG
[J/mol](800.1[J/g]*62.068[g/mol])
coeff=2.102; %chemical reaction coefficient for EG decomposition
reaction

Tsat=470; %Saturation temperature of EG [K]
Tavg=(Tw+Tsat)/2;

hrxn=HeatRXN; %heat of reaction (EG decomposition): Function of
temperature [J/mol]
d=0.00476; %heater diameter [m]
L=0.09205; %heater length [m]
A=d*pi*L; %Surface area [m^2]
k=0.252; %liquid thermal conductivity of EG [W/m/K]@Tsat(= about 155
degC)
g=9.8; %gravity constant[m/sec^2]
beta=65*10^(-5); %expansion coefficient of liquid EG [1/K] Ref.
Incropera "Heat and Mass Transfer"
mu=85.9*10^(-5); %dynamic viscosity of liq EG [Pa*Sec] @Tsat(= about
155 degC) Ref. C.F. Beaton "Physical properties..."
roh=1016; %density of liquid EG [kg/m^3] @Tsat(= about 155 degC)
v=mu/roh;  %kinematic viscosity of liquid EG [m^2/sec] @Tsat(= about
155 degC)
Cp=2940; %heat capacity of liquid EG [J/kg/K] @Tsat(= about 155 degC)
```

```
alpha=k/(roh*Cp); %thermal diffusivity of liquid EG [m^2/sec]
Ra=g*beta*(Tsat-Tinf)*(d^3)/(v*alpha); %Rayleigh number
Pr=v/alpha; %Prandtl number

       if Ra>=10^12
         fprintf('Ra is over range')
          break
       end

Nu=(0.6+(0.387*Ra^(1/6))/((1+(0.559/Pr)^(9/16))^(8/27)))^2; % Nusselt
number
h=k*Nu/d; %Convective heat transfer coefficient

x=fzero('Qbalance',1);  %Nonlinear algebraic equation's solution  <--
Energy Balance (Eq.3.7)
Nr1=x; % Molar flow rate of reactant drawn into FIBOR

Conversion(i,1)=(Np/coeff)/Nr1;
QEvap(i,1)=Qe(Nr1);
QSens(i,1)=Qsens(Nr1);
QRxn(i,1)=Qr;
QConv(i,1)=Qconv;
TotalQ(i,1)=Qe(Nr1)+Qsens(Nr1)+Qr+Qconv;

end

dlmwrite('Conversion.txt',Conversion)
dlmwrite('QEvap.txt',QEvap)
dlmwrite('QSens.txt',QSens)
dlmwrite('QRxn.txt',QRxn)
dlmwrite('QConv.txt',QConv)
dlmwrite('TotalQ.txt',TotalQ)
```

HeatRXN.m

```
%Heat of reaction of ethylene glycol decomposition: function of
temperature
%Orignal Matlab Code Written by Sung Ryel Choi, Cornell University
2010
function hrxn=HeatRXN   %Heat of reaction: function of temperature

global Tavg

Tr=298; %Reference Temperature[K] (25[degC])

hfEG=-394400; %Enthalpy of formation of EG(gas) @ 25degC & 1atm
[KJ/Kmol]   Ref. Knauth and Sabbah, 1989
hfH2=0; %Enthalpy of formation of hydrogen @ 25degC & 1atm [KJ/Kmol]
hfCO=-110530; %Enthalpy of formation of carbon monoxide @ 25degC &
1atm [KJ/Kmol]
hfCH4=-74850; %Enthalpy of formation of methane @ 25degC & 1atm
[KJ/Kmol]
```

```
hfC2H2=226730; %Enthalpy of formation of acetylene @ 25degC & 1atm
[KJ/Kmol]
hfC2H4=52280; %Enthalpy of formation of ethylene @ 25degC & 1atm
[KJ/Kmol]

SenHeatEG=quad('HeatCapEG',Tr,Tavg); %Sensible heat of EG [J/mol]
SenHeatH2=quad('HeatCapH2',Tr,Tavg); %Sensible heat of Hydrogen
[J/mol]
SenHeatCO=quad('HeatCapCO',Tr,Tavg); %Sensible heat of CO [J/mol]
SenHeatCH4=quad('HeatCapCH4',Tr,Tavg); %Sensible heat of CH4 [J/mol]
SenHeatC2H2=quad('HeatCapC2H2',Tr,Tavg); %Sensible heat of C2H2
[J/mol]
SenHeatC2H4=quad('HeatCapC2H4',Tr,Tavg); %Sensible heat of C2H4
[J/mol]

hrxn=(0.3836.*hfH2+1.0504.*hfCO+0.3863.*hfCH4+0.0185.*hfC2H2+0.2632.*
hfC2H4-
hfEG)+0.3836.*SenHeatH2+1.0504.*SenHeatCO+0.3863.*SenHeatCH4+0.0185.*
SenHeatC2H2+0.2632.*SenHeatC2H4-SenHeatEG;
```

Qbalance.m: same as the Catalytic Reaction (CT#1) code

HeatCapCO.m: same as the Catalytic Reaction (CT#1) code

HeatCapH2.m: same as the Catalytic Reaction (CT#1) code

HeatCapCH4.m: same as the Catalytic Reaction (CT#1) code

HeatCapC2H2.m: same as the Catalytic Reaction (CT#2) code

HeatCapC2H4.m: same as the Catalytic Reaction (CT#2) code

HeatCapEG.m: same as the Catalytic Reaction (CT#2) code

Qe.m: same as the Catalytic Reaction (CT#1) code

Qsens.m: same as the Catalytic Reaction (CT#2) code

Qr.m: same as the Catalytic Reaction (CT#1) code

Qconv.m: same as the Catalytic Reaction (CT#1) code

APPENDIX G

FLOW RATE CURVE DATA

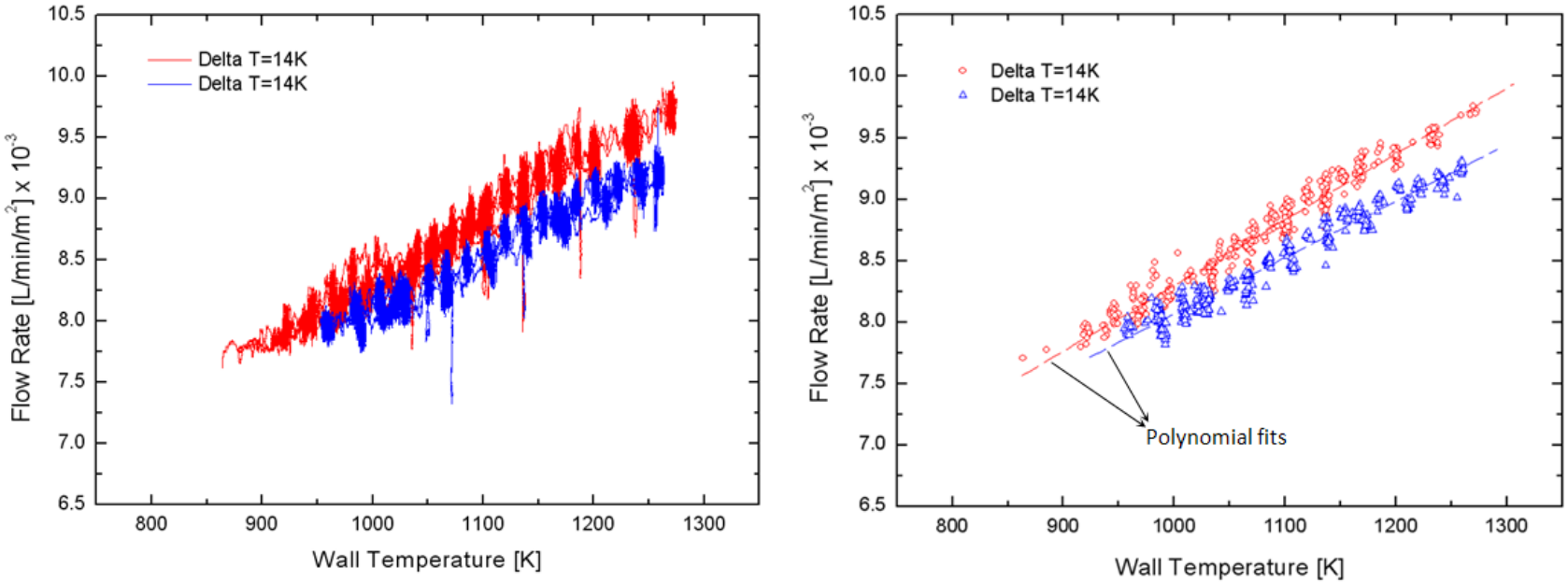

(a) (b)

Figure G.1: Methanol converted with CT#1 (a) raw data product flow rate and (b) corresponding Adjacent Average plot with polynomial fits

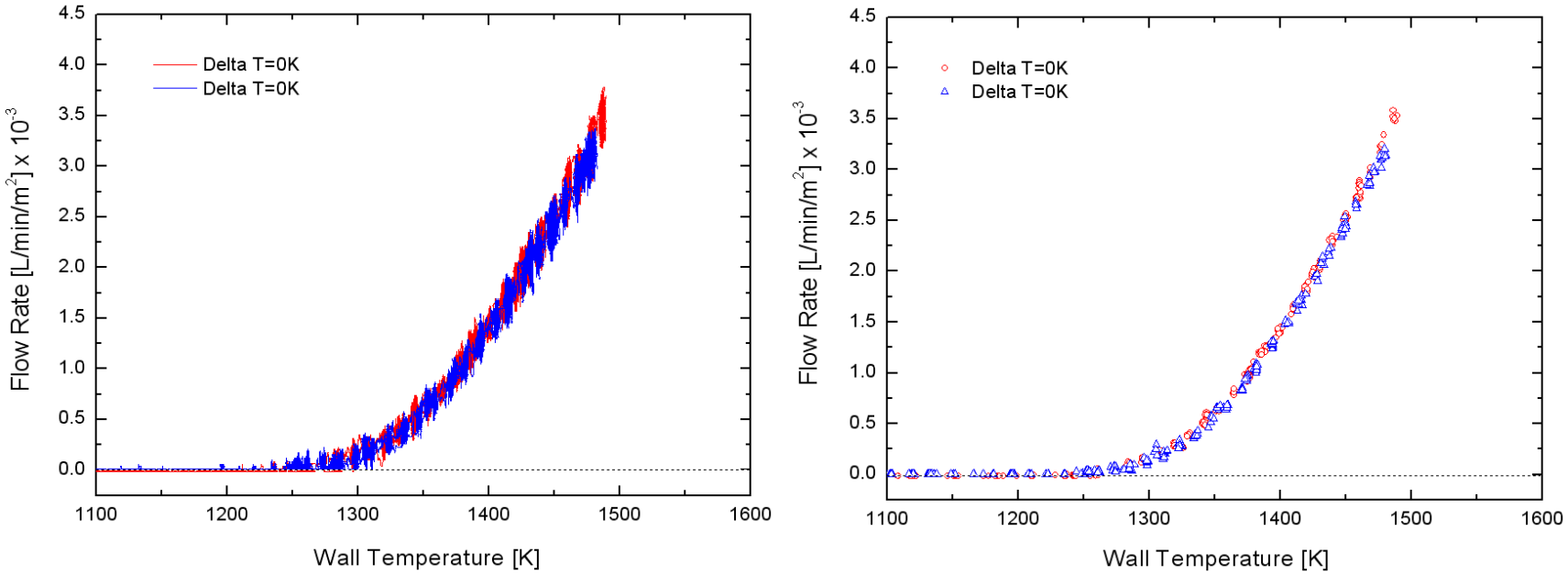

Figure G.2: Methanol converted with a bare tube (a) raw data product flow rate and (b) corresponding Adjacent Average plot

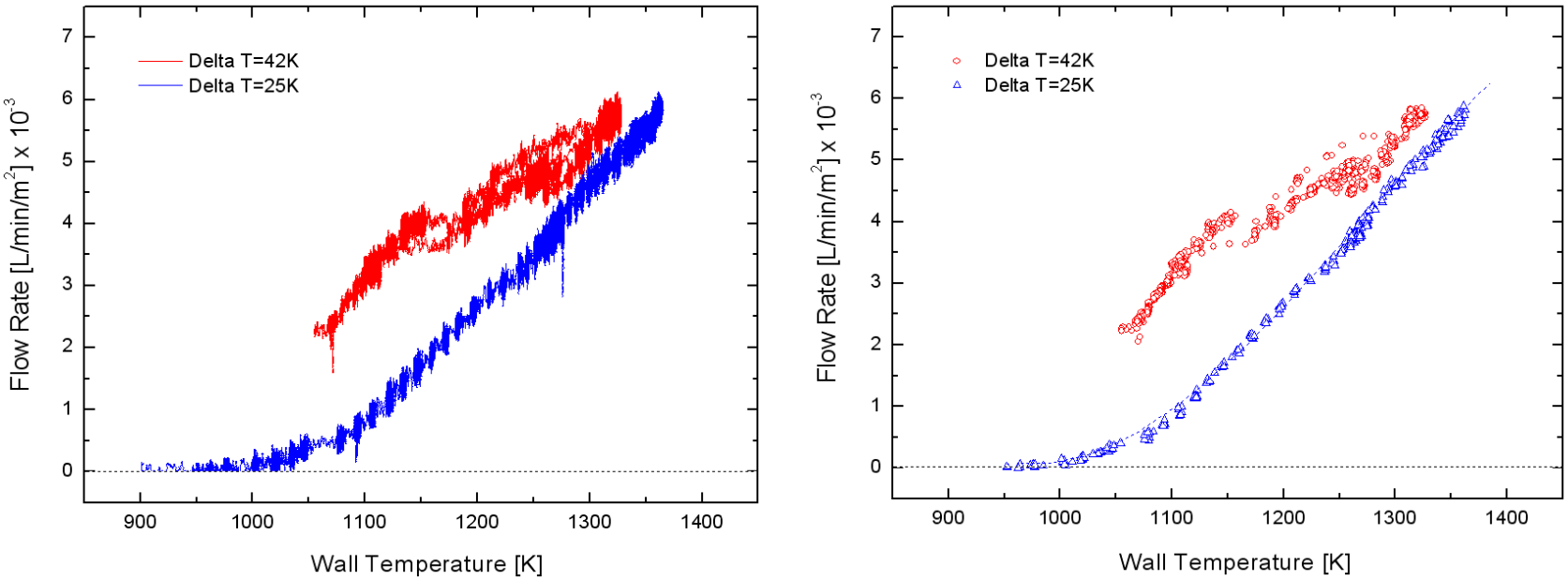

Figure G.3: Ethylene glycol converted with CT#2 (a) raw data product flow rate and (b) corresponding Adjacent Average plot

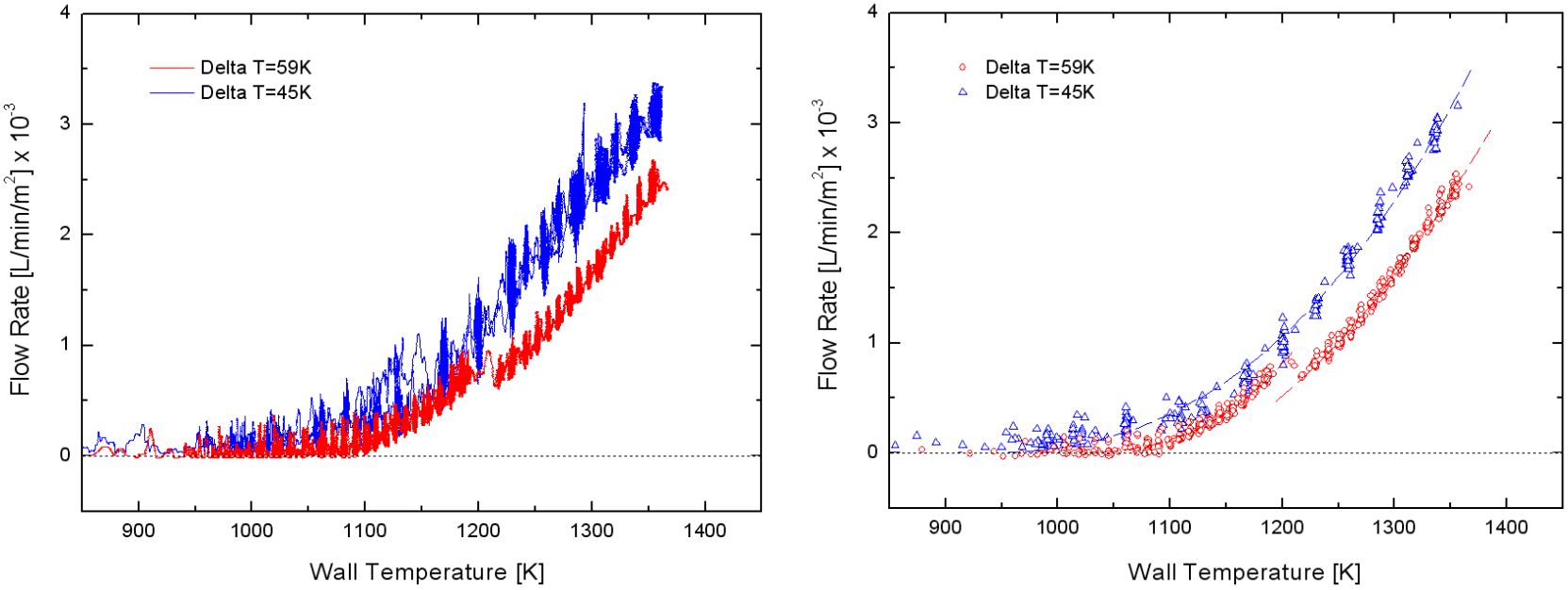

Figure G.4: Ethylene glycol converted with a bare tube (a) raw data product flow rate and (b) corresponding Adjacent Average plot with polynomial fit

APPENDIX H

VENDORS CONTACT LIST

Aluminum end plates (flanges), Cramps, and Copper buses

Company: Tim Brock – Machinist in Cornell University

Address: Hollister Hall in Cornell University

Contact: teb4@cornell.edu, (607) 255-4201

Cable and connectors to and from power supply

Model #: 1/C 250 mcm 600v cable - PC#112-24-2431

Company: The Okonite Company

Address: 169 South River Road, Bedford, NH 03110

Contact: www.okonite.com, Hartford@okonite.com, (603) 625-1900

Calibration and Carrier gases

Model #: Calibration gases in Sec.2.2.4.2, Helium carrier gas (99.999%)

Company: Airgas

Address: 27 Northwestern Drive, Salem, NH 03079

Contact: www.airgas.com, Robin, (607) 733-6527

Catalyst coating fabrication

Model #: See Table 2.3

Company: Catacel Corporation

Address: 7998 Gotham Rd., Garrettsville, OH 44231-9749

Contact: Dr. William B Retallick, (330) 527-0731, www.catacel.com

Ceramic insulators

Model #: ORX-11618 (OD 3.175mm, ID 1.588mm)

Company: Omega Engineering, Inc.

Address: One Omega Drive Box 4047, Stamford, CT 06907-0047

Contact: www.omega.com, (800)-872-9436

Computer

Model #: HP DC5000

Company: Hewlett Packard

Address: 3000 Hanover Street, Palo Alto, CA 94304-1185

Contact: www.hp.com, (650) 857-1501

Condensers & cold traps

Model #: Z517232, Z164038 (condensers), and Z422347, Z256870 (cold traps)

Company: Sigma-Aldrich

Address: St. Louis, MO, USA

Contact: www.sigmaaldrich.com, (314) 771-5765

Data acquisition unit

Model #: PCI-6220 (DAQ card), SCXI-1102C (Signal Conditioning Module), SCXI-1303 (Isothermal Terminal Block) for temperature and USB-6008 for flow rate

Company: National Instruments

Address: 11500 N Mopac Expwy, Austin, TX 78759-3504

Contact: www.ni.com, (800) 531-5066

Feed-through gland for thermocouples

Model #: MFT-040-3, T-FER-1/16

Company: Omega Engineering, Inc.

Address: One Omega Drive Box 4047, Stamford, CT 06907-0047

Contact: www.omega.com, (800)-872-9436

Feed-through glands for cooper buses

Model #: EG-500-A-12-T

Company: Conax Buffalo Tech. Inc.

Address: 2300 Walden Avenue, Buffalo, New York 14225

Contact: www.conaxbuffalo.com, (800) 223-2389, (716) 684-4500

Fittings

Company: Swagelok

Address: 29500 Solon Road, Solon OH 44139

Contact: www.cambridgevalve.com, default.aspx

Flow meter

Model #: FMA-A2309

Company: Omega Engineering, Inc.

Address: One Omega Drive Box 4047, Stamford, CT 06907-0047

Contact: www.omega.com, (800)-872-9436

Flow meter for calibration

Model #: Drycal Definer 220

Company: Bios International

Address: 10 Park Place, Butler, NJ 07405

Contact: www.biosint.com, (800) 663-4977

GC

Model #: GC600P00012801

Company: Gow-Mac

Address: 277 Brodhead Road, Bethlehem, PA 18017

Contact: www.gow-mac.com, (610) 954-9000, sales@gow-mac.com

Glass chamber (cross)

Model #: Special Item: Glass Cross Pipe DN 150, with sides DN50

Company: Goel Scientific Glass Works P.Ltd.

Address: C31/ A, Sardar Estate, Ajwa Road, Baroda - 390 019, Gujarat, India

Contact: www.goelscientific.com, Mr. Anshul Goel,

Email: anshul@goelscientific.com, Phone: 0091-265-2561595

Heater tube

Model #: 600F10188X028SL - 0.188" OD x 0.028",

Wall Annealed Inconel 600 tube

Company: MicroGroup Inc.

Address: 7 Industrial Park Road, Medway, MA 020553-1732

Contact: www.microgroup.com, Ms. Erin Bates,

Email: ebates@microgroup.com, Phone: 1-800-ALL-TUBE

Immersion heater

Model #: WC20303001 300W 120V 0.25"D x 3"L

Company: WATTCO

Contact: www.wattco.com, 800-4-WATTCO or (800) 492-8826

Mini-pump

Model #: VMP1624MM-6-60

Company: Virtual industries, Inc.

Address: 2130 Victor Place, Colorado Springs, Colorado 80915

Contact: http://virtual-ii.com/index.php, (719) 572-5566, info@virtual-ii.com

O-ring

Model #: Parker AS-362 70-DURO NITRILE

Company: Sealing Devices, Inc.

Address: 4400 Walden Ave. Lancaster, NY 14086

Contact: www.sealingdevices.com, (716) 684-7600, seals@sealingdevices.com

Power supply and GPIB

Model #: 6681A - DC Power supply, 82357A - USB/GPIB Interface converter

Company: Agilent Technologies, Inc.

Address: PO Box 4026, Englewood, CO 80155-4026

Contact: www.agilent.com, Karen Nyholm,

Karen_nyholm@agilent.com, (631) 454-4645

Thermocouples and Thermocouple extensions

Model #: KMQXL-010G-18 (wall temperature), GKMQSS-040G-12 (bulk temperature), GECK10-9 (extension)

Company: Omega Engineering, Inc.

Address: One Omega Drive Box 4047, Stamford, CT 06907-0047

Contact: www.omega.com, (800) 872-9436

REFERENCES

Anderson, M.H.; Meekunnasombat, P.; Corradini, M.L. Experimental Behavior of Molten SnxLiy When Impacted by a Vertical Column of Water. Fusion Technology. 2001;39: 965-969.

Avedisian, C.T. Bubble growth in superheated liquid droplets. In: Encyclopedia of Fluid Mechanics. Houston, TX: Gulf Publishing; 1986:131-153.

Avedisian, C.T. Sullivan JR. A generalized corresponding states method for predicting the limits of superheat of mixtures: Application to the normal alcohols. Chem Eng Sci. 1984;39:1033-1042.

Avedisian, C.T.; Tsang, W.; Davidovits, T.; Allaben, J.R. Influence of Radiation on Product Yields in a Film Boiling Reactor. AIChE Journal 2008;54:575-581.

Baird, T.; Paal, Z.; Thomson, S.J. Sintering Studies on Platinum Black Catalysts. J.Chem.Soc. Faraday Trans 1, 1973: 69: 50-55.

Baker, L; Just, LC. Studies of Metal-Water Reactions at High Temperatures. III. Experimental and Theoretical Studies of the Zirconium-Water Reaction. 17th Edition. AEC Research and Development Report, TID-4500, ANL-6548. Argonne, IL: Argonne National Laboratory, U.S. Department of Energy; May 1962.

Beaton, C. F. & Hewitt, G.F. Physical Property Data for the Chemical and Mechanical Engineer. Hemisphere Publishing Corporation; 1989.

Behura, J.; Batzle, M.; Hofmann, R.; Dorgan, J. Heavy oil: their shear story. Vol. 27, No. 8. Geophysics, Vol. 72 No. 5 (September-October 2007), p.E175-E183.

Beychok, M.R. Process and environmental technology for producing SNG and liquid fuels, U.S. EPA report EPA-660/2-75-011, May 1975.

Breen, B. P.; Westwater, J.W. Effect of diameter of horizontal tubes on film boiling heat transfer. Chem. Eng. Prog. July 1962; Vol. 58, no. 7, 67-73.

Bromley, L.A. Heat transfer in stable film boiling. Chem. Eng. Prog. 46, 221, 1950.

Bruneton, E.; Narch, B.; Oberlin, A. Carbon-carbon composites prepared by a rapid densification process II: Structural and textural characterizations. 1997 Carbon, 35, 1593.

Butt, J.B.; Petersen, E.E. Activation, deactivation and poisoning of catalysts, New York: Academic Press, 95-97, 1988.

Carey, V.P. Liquid-Vapor Phase-Change Phenomena. Hemisphere Publishing Corp. 1992; 275-279.

Chato, J.C. Laminar condensation inside horizontal and inclined tubes, J.ASHRAE, 4, 52, 1962.

Choi, S.R.; Avedisian, C.T.; Tsang, W. A film boiling reactor for chemical processing, 2008 ASME Conference, October 2008, Boston, Massachusetts, U.S.A.

Churchill, S.W.; Chu, H.H.S. Correlating Equations for Laminar and Turbulent Free Convection from a Horizontal Cylinder. Int. J. Heat Mass Transfer, 18, 1049, 1975.

Collier, J. G.; Thorne, J. R. Convective Boiling and Condensation 3rd edition (Oxford University Press), 1996.

Corma, A.; Huber, GW.; Sauvanaud, L.; O'Connor, P. Biomass to chemicals: Catalytic conversion of glycerol/water mixtures into acrolein, reaction network. Journal of Catalysis, v 257, n 1, p 163-171, July 1, 2008.
Corma, A.; Huber, GW.; Sauvanaud, L.; O'Connor, P. Processing biomass-derived oxygenates in the oil refinery: Catalytic cracking (FCC) reaction pathways and role of catalyst. Journal of Catalysis, v 247, n 2, p 307-327, April 25, 2007.

Crooks, RC; Hershall, PG; Sorgenti, HA; Lemmon, AW; Filbert, RB. Studies Relating to the Reaction between Zirconium and Water at High Temperatures. Report BMI-1154. Columbus, OH: Batelle Memorial Institute; May 1962.

Cussler, E.L. Diffusion mass transfer in fluid systems. 2nd ed. Cambridge University Press. 2005: 371-426.

Davidovits, T. Master's of Engineering Project Report. An Investigation of the Effects of Liquid Motion and Subcooling in the Analytical Film Boiling Reactor Model. Cornell University. 2008.

Ede, A.J.; Siviour, J.B. Sub-cooled film boiling on horizontal cylinders. Int. J. Heat and Mass Transfer, 1975; 18:737-742.

Epstein, M.; Leung, JC.; Hauser, GM; Henry, RE. Film boiling on a reactive surface. Int J Heat Mass Transfer. 1984;27:1365-1378.

Evangelista, J. Experimental demonstration of converting organic liquids and their aqueous solutions in a film boiling reactor. Thesis, 2010: Cornell University.

Fogler, H. Scott. Elements of Chemical Reaction Engineering, 4th ed. Westford Massachusetts: Pearson Publishing, 2006: 709-716.

Higgins, HM. A Study of the Reaction of Metals and Water. AECD-3664. Richland, WA: Hanford Atomic Products Operation; 1955.

Huang, Ziyan. The Film Boiling Reactor-LabVIEW Data Acquisition. MAE429 senior design report, Cornell. 2006.

Huber, GW.; Corma, A. Synergies between bio- and oil refineries for the production of fuels from biomass. Angewandte Chemie - International Edition, v 46, n 38, p 7184-7201, 2007.

Imai, T. Gasification of Methanol, Catalyst (in Japanese), Vol. 28, No. 3, 1986; p 221

Incropera F.P.; DeWitt D.P. Fundamental of Heat and Mass Transfer, 5th ed. Wiley, 2002: 593-640

Koh, J.C. Analysis of film boiling on vertical surfaces. ASME J Heat Transfer. 1962;84:55-62.

Lee, D.J. Two-mode boiling on a horizontal heating wire: effects of liquid subcoolings. Int. J. Heat and Mass Transfer, 1998; 41:2925-2928.

Lee, S.G. Isaac. Master's of Engineering Project Report. A study of chemical kinetics in FIBOR process by a comparison between the experimental result and analytical model. Cornell University. 2010.

Lienhard, J.H. 1987 A Heat Transfer Texbook, 2nd Edition, Prentice Hall, Englewood Cliffs, pp. 414, 415, 432,437-439.

Lienhard, J.H.; Dhir, V.K.; Riherd, D.M. Peak pool boiling heat-flux measurements on finite horizontal flat plates. Journal of Heat Transfer, v 95 Ser C, n 4, p 477-482, Nov 1973.

Lienhard, J.H.; Karimi, A. Homogeneous nucleation and the spinodal line. ASME J Heat Transfer. 1981;103:61-64.

Lustman, B. Zirconium–Water Reactions. Report WAPD-137. Pittsburgh, PA: Bettis Atomic Power Laboratory; December 1955.

Naydich, Alexander. Derivation of a Resistivity-Temperature Relationship and Film Boiling Curves for an Inconel 600 Tube in the FIBOR. MAE project report at Cornell, 2008.

Nilles, D. Combating the Glycerine Glut, in Biodiesel Magazine, September, 2006, 38-40.

Nukiyama, S. The maximum and minimum values of heat transmitted from metal to boiling water under atmospheric pressure. J. Janpan Soc. Mech. Eng. 37, 367, 1934 (Translation: Int. J. Heat Mass Transfer, 9, 1419, 1966).

Nusselt, W. Die Oberflachenkondensation des Wasserdampfes, Z.Ver.Deut.Ing., 60, 541, 1916.

Ohtake, H.; Koizumi, Y. Study on propagative collapse of a vapor film in film boiling (mechanism of vapor-film collapse at wall temperature above the thermodynamic limit of liquid superheat). Int J Heat Mass Transfer. 2004;47:1965-1977.

Okuno, H.; Trinquecoste, M.; Derre, A.; Monthious, M.; Delhaes, P. Catalytic effects on carbon/carbon composites fabricated by a film boiling chemical vapor infiltration process. J. Mat. Res. 2002; 17: 1904-1913.

Okuyama, K.; Iida, Y. Film-boiling heat transfer with a catalytic decomposition reaction. JSME International Journal. Ser. B. 1994; 37:123-131.

Oxtoby; Gillis; Nachtrieb. Modern Chemistry. The 5th ed. Thomson 2002; 458-462.

Perkins, A.S.; Westwater, J.W. Measurements of bubbles formed in boiling methanol. AIChE Journal. 1956; Vol.2: 471-476.

Rohsenow, W.; Hartnett, J.; Cho, Y. Handbook of Heat Transfer. The 3rd ed. McGraw Hill. 1998.

Rovillain, D.; Trinquecoste, M.; Bruneton, E.; Derre´, A.; David, P.; Delhae`s, P. Film boiling chemical vapor infiltration: An experimental study on carbon/carbon composite materials. 2001 Carbon, 39, 1355-1365.

Ruebsamen, WC; Shon, FJ; Chrisney, JB. Chemical Reaction between Water and Rapidly Heated Metals. Report NAA-SR-197. Los Angeles, CA: North American Aviation; October 1952.

Sakurai, A; Shiotsu, M; Hata, K. A general correlation for pool film boiling heat transfer from a horizontal cylinder to subcooled liquid: Part I. A theoretical pool film boiling heat transfer model including radiation contributions and its analytical solution. J Heat Transfer. 1990;112:430-440.

Sarma, PK; Subrahmanyam, T; Rao, VD; Bergles, AE. Turbulent film boiling on a horizontal cylinder. Int J Heat Mass Transfer. 2001;44: 207-214.

Shabaker, J.W.; Huber, G.W.; Davda, R.R.; Cortright, R.D.; Dumesic, J.A. Aqueous-phase reforming of ethylene glycol over supported platinum catalysts. Catalysis Letters. 2003; 88:1-8.

Sinha, J; Hochreiter, LE. Cheung FB. Effects of surface roughness, oxidation level, and liquid subcooling on the minimum film boiling temperature. Exp Heat Transfer. 2003;16:45-60.

Szepe, S.; Levenspiel, O. Optimum temperature policies for reactors subject to catalyst deactivation. I. Batch reactor. Chem. Eng. Sci., 23, 881-894, 1968.

Turkenburg, Wim C. et al. Chap.7-Renewable energy technologies, World energy assessment: energy and the challenge of sustainability. United Nations Development Programme. 2001: 220-272.

Urban, B.J.; Avedisian, C.T.; Tsang, W. The Film Boiling Reactor: A New Environment for Chemical Processing. AIChE Journal. 2006;52:2582-2595.

Xun, Hu; Gongxuan, Lu. Investigation of the steam reforming of a series of model compounds derived from bio-oil for hydrogen production. Applied Catalysis B: Environmental. 2009; 88:376-385.

Yaws, Carl L. Yaws' Handbook of Thermodynamic and Physical Properties of Chemical Compounds. Knovel: 2003. Online database available at: http://knovel.com.

Zhang, Y.F.; Gamo, M.N.; Xiao, C.Y.; Ando, T. Liquid phase synthesis of carbon nanotubes. Physica B. Condensed Matter. October 2002. v 323, n 1-4, p 293-295.

Zhang, Yafei1; N.-Gamo, Mikka1; Nakagawa, Kiyoharu1; Ando, Toshihiro1 Source. Synthesis of aligned carbon nanotubes in organic liquids. Journal of Materials Research. September 2002. v 17, n 9, p 2457-2464.

Zhukov, S.A.; Rafeev, V.A.; Afanas'ev, S. Yu.; Echmaev, S.B.; Korsunskii, B.L. Singularities of realization of film boiling on wire heaters. Organic liquids. High Temperature, vol. 41; No. 2, 2003; 243-251.